VOLUME 27 (1961) No. 3

NUCLEAR PHYSICS

JOURNAL DEVOTED TO THE EXPERIMENTAL AND THEORETICAL STUDY OF THE FUNDAMENTAL CONSTITUENTS OF MATTER AND THEIR INTERACTIONS

EDITOR: L. ROSENFELD - COPENHAGEN

F. M. PIPKIN, G. E. BRADLEY and R. E. SIMPSON, Beta decay matrix elements in As^{76} 353

M. A. MARKOV and I. M. ZHELEZNYKH, On high energy neutrino physics in cosmic rays 385

R. J. BLIN-STOYLE and HERMAN FESHBACH, Effects of parity non-conserving inter-nucleon potentials on the photoeffect in H^2 and H^3. 395

H. S. GREEN, Proton-proton scattering at relativistic energies. 405

C. CARTER-WASCHEK and B. LINDER, An isomeric state of Y^{90}. 415

E. M. FRIEDLÄNDER and M. E. MAYER, An estimation of the spectrum of true multiplicities in antinucleon annihilations 418

W. E. WILSON, R. L. WALTER and D. B. FOSSAN, Differential cross sections for the T(p, n)He^3 reaction 421

A. B. CLEGG and G. R. SATCHLER, Gamma-rays from inelastic scattering of high energy nucleons. 431

E. A. DAVIS, F. GABBARD, T.W. BONNER and R. BASS, The disintegration of B^{10} and F^{19} by fast neutrons 448

D. M. VAN PATTER, R. RIKMENSPOEL and P. N. TREHAN, The (p, p'γ) reaction in even isotopes of Zn, Ge and Se. 467

H. D. SCOTT, The application of distorted wave Born approximation calculations to the analysis of some(d, p) angular distributions 490

M. S. EL-NESR and R. OTHAZ, A study of beta-gamma directional correlation in the decay of Au^{199} 507

P. G. HANSEN, O. J. JENSEN and K. WILSKY, Decay of Er^{172} and Tm^{172}. 516

October 1961

NORTH-HOLLAND PUBLISHING COMPANY - AMSTERDAM

EDITORIAL BOARD

AUSTRALIA & NEW ZEALAND:	H. Messel (Sydney), M. L. Oliphant (Canberra)
AUSTRIA:	B. Karlik (Vienna), H. Thirring (Vienna)
BELGIUM:	M. de Hemptinne (Louvain), J. Verhaeghe (Ghent)
CANADA:	G. Volkoff (Vancouver)
DENMARK:	C. Møller (Copenhagen), S. Rozental (Copenhagen), G. E. Brown (Copenhagen)
FINLAND:	L. Simons (Helsinki)
FRANCE:	A. Berthelot (Saclay), S. Gorodetzky (Strasbourg)
GERMANY (DEM. REP.):	G. Hertz (Leipzig)
GERMANY (FED. REP.):	W. Gentner (Freiburg i. B.), J. H. D. Jensen (Heidelberg)
GREAT BRITAIN:	W. E. Burcham (Birmingham)
HUNGARY:	L. Janossy (Budapest)
INDIA:	H. Bhabha (Bombay), R. Ramanna (Trombay)
IRISH REPUBLIC:	J. McConnell (Maynooth)
ISRAEL:	G. Racah (Jerusalem)
ITALY:	E. Amaldi (Rome)
JAPAN:	S. Kikuchi (Tokay), S. Tomonaga (Tokyo)
MEXICO:	M. Moshinsky (Mexico)
NETHERLANDS:	H. Brinkman (Groningen), S. R. de Groot (Leiden)
NORWAY:	E. Hylleraas (Oslo), A. Lundby (Oslo), H. Wergeland (Trondheim)
POLAND:	L. Infeld (Warsaw), J. Werle (Warsaw)
PORTUGAL:	J. M. Araújo (Porto), J. R. de Almeida Santos (Coimbra)
SOUTH AMERICA:	G. Beck (Rio de Janeiro), J. Leite Lopes (Rio de Janeiro)
SPAIN:	J. M. Otero (Madrid), C. Sanchez del Rio (Madrid)
SWEDEN:	O. Klein (Stockholm), K. Siegbahn (Uppsala), I. Waller (Uppsala)
SWITZERLAND:	P. Huber (Basel), P. Scherrer (Zürich)
U.A.R. & ARAB COUNTRIES:	F. El Bedewi (Cairo), M. G. Nooh (Cairo)
U.S.A.:	H. H. Barschall (Madison, Wisconsin), S. Devons (New York)
U.S.S.R.:	M. A. Markov (Moscow), I. S. Shapiro (Moscow), D. V. Skobeltzyn (Moscow)
YUGOSLAVIA:	I. Supek (Zagreb)

CONTRIBUTIONS may be sent to the Editor, Professor L. Rosenfeld, NORDITA, Blegdamsvej 17, Copenhagen Ø, either directly, or preferably through the intermediary of one of the members of the Editorial Board of the country or region in which the author is working. They may be written in English, French or German.

NUCLEAR PHYSICS is published in fortnightly issues. The subscription price per volume of 700 pages is fl 57.00; 114s; $ 15.00. Post-free.

SUBSCRIPTIONS should be sent to the publishers, NORTH-HOLLAND PUBLISHING COMPANY P.O. Box 103, Amsterdam or to any subscription-agent.

BOOKS FOR REVIEW should be sent to Professor Rosenfeld.

No part of this issue may be reproduced in any form, by print, photoprint, microfilm or any other means without permission from the publisher.

Printed in the Netherlands

4.C

Nuclear Physics **27** (1961) 353—384; © *North-Holland Publishing Co., Amsterdam*

Not to be reproduced by photoprint or microfilm without written permission from the publisher

BETA DECAY MATRIX ELEMENTS IN As^{76}

F. M. PIPKIN †, G. E. BRADLEY †† and R. E. SIMPSON †††

Lyman Laboratory, Harvard University, Cambridge, Massachusetts ‡

Received 16 February 1961

Abstract: Dynamic nuclear orientation has been used to study the $2^- \leftrightarrow 2^+$ 2.41 MeV β-ray in the decay of As^{76}. The As^{76} was a substitutional donor atom in a silicon crystal and it was oriented by saturating each of the four $\Delta(m_J + m_I) = 0$ forbidden transitions. The angular distribution of the gamma rays following the 2.41 MeV β-ray was measured with two scintillation counters. The electron and nuclear relaxation times were determined by observing the rate of growth and decay of the anisotropy of the gamma rays. The electron ($\Delta m_J = \pm 1, \Delta m_I = 0$) relaxation time was (3.6 ± 0.7) min. The nuclear relaxation can be attributed to a modulation of the isotropic hyperfine interaction; the relaxation time for the nuclear polarization is $(3.1 \pm 1) \times 10^3$ min. An analogue computer was used to correct the initial orientation parameters for the effects of nuclear relaxation. From this orientation experiment restrictions can be placed on the angular momentum carried off by the 2.41 MeV β-ray. This result was analyzed in conjunction with β-γ angular correlation and β-γ circular polarization correlation experiments to determine the beta-decay matrix elements. The set which fits the data best is $V = -(0.9 \pm 0.2)$, $Y = -(0.9 \pm 0.2)$. It is not impossible to rule out the set $V = -(18 \pm 5)$, $Y = 0 \pm 4$.

1. Introduction

Now that the beta-decay interaction is known [1–3]), it can be used like the electromagnetic interaction to study nuclear structure. This makes it possible to determine a new class of transition matrix elements and consequently to study other facets of nuclear structure. These matrix elements are analogous to those which determine the relative probability of a magnetic dipole and an electric quadrupole gamma ray transition. The beta-interaction is, however, in general more complicated than its electromagnetic counterpart. Even for an allowed transition with no spin change, it takes two experiments to determine unambiguously the two nuclear matrix elements. Parity-non-conservation has simplified matters in that it furnishes several new experiments which were not thought relevant before. One of these is the correlation between the direction of emission of a β-ray and the circular polarization of a subsequent gamma ray.

† Alfred P. Sloan Research Fellow, 1959–61

†† Research performed while a National Science Foundation Faculty Fellow on leave from Western Michigan University

††† Now at University of Alaska, College, Alaska

‡ This research was supported by a grant from the National Science Foundation. A preliminary account of this work has been given [46]). This paper is in part based on a thesis submitted by one of the authors (R.E.S.) to Harvard University in partial fulfilment of the requirements for the degree of Doctor of Philosophy.

In this paper, we are concerned with a 2^- to 2^+ first-forbidden transition. There are six nuclear matrix elements describing processes which can contribute to such a transition; two processes which carry off no angular momentum; three which carry off one unit of angular momentum and one which carries off two units of angular momentum. Even though a great deal of work, both experimental and theoretical, has been done on these transitions, the complete set of matrix elements has not been determined for any transition of this type [4]).

This paper reports the use of the method of dynamic nuclear orientation [5, 6]) to study the 2^- to 2^+ first forbidden transition in As^{76}. The orientation experiments are simpler than the angular correlation experiments in that the matrix elements, which correspond to transfer of different units of angular momentum, do not interfere. From the orientation experiments, the fractions of the β-transition which carry off 0, 1 and 2 units of angular momentum can be determined. This information can then be used in conjunction with the angular correlation experiments to determine the various nuclear matrix elements.

2. Theory of the Experiment

The nuclear decay scheme for 26-h As^{76} has been investigated by many workers. One of the more recent investigations is that of Girgis, Ricci and Van

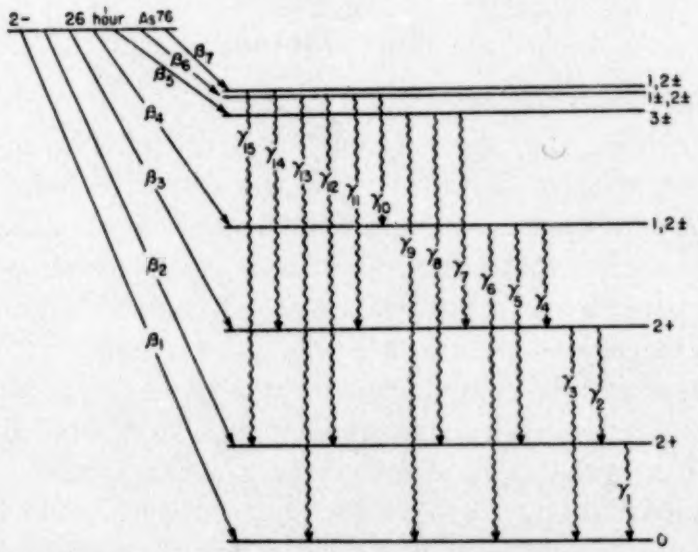

Fig. 1. Nuclear decay scheme of As^{76}.

Lieshout [7]). The decay scheme listed by the most recent nuclear data cards [8]) is shown in fig. 1. In tables 1 and 2, the energy and known characteristics of the various beta and gamma rays are summarized. An atomic beam experiment [9]) and a previous orientation experiment [5]) have shown that the spin of the ground

TABLE 1

Beta rays of As^{76}

Radiation	Energy in MeV	Intensity (per 100 decays)	Log ft
β_1	2.97	56.4	8.6
β_2	2.41	30.6	8.2
β_3	1.75	3.6	8.5
β_4	1.20	6.6	8.7
β_5	0.55	0.9	7.2
β_6	0.31	1.3	6.2
β_7	0.30	0.6	6.5

TABLE 2.

Gamma rays of As^{76}

Radiation	Energy in MeV	Intensity (per 100 decays)	Character
γ_1	0.559	39.2	EQ
γ_2	0.657	6.3	98% EQ, 2% MD
γ_3	1.216	4.3	EQ
γ_4	0.56	5.4	
γ_5	1.229	1.0	
γ_6	1.789	0.32	
γ_7	1.20	0.9	MD
γ_8	1.86	0.01	
γ_9	2.42	0.004	
γ_{10}	0.896	0.11	
γ_{11}	1.438	0.54	MD
γ_{12}	2.097	0.58	95% EQ, 5% MD
γ_{13}	2.656	0.034	
γ_{14}	1.454	0.24	MD
γ_{15}	2.112	0.33	95% EQ, 5% MD

state of As^{76} is 2. The 2.97 MeV β-ray has a unique first forbidden shape [10–13]; this confirms the assignment of spin 2 to the As^{76} ground state and shows that the parity of this state is negative. The spins and parities of the Se^{76} levels have been assigned from studies of the gamma-gamma and beta-gamma angular correlations [14–19]. The radiations γ_1 and γ_3 are pure electric quadrupole; the radiation γ_2 is a mixture of $(98\pm2)\%$ electric quadrupole and $(2\pm1)\%$, magnetic dipole radiation. The lifetime of the 550 keV state of Se^{76} has been measured by Coulomb excitations [20], by a coincidence method [21] and by observation of resonance fluorescence [22]. It is approximately 2×10^{-11} sec. Coulomb excitation studies have been made on both the first and second excited states [23, 24] of Se^{76}.

In this experiment, we are particularly concerned with the 2.41 MeV β-ray (β_2). This is a 2^- to 2^+ first forbidden transition. Its spectrum shape has been measured both by a coincidence method and by a subtraction technique [13]). It has an allowed shape in the experimentally accessible region. The β_2–γ_1 angular correlation has been measured as a function of energy [25, 26]). The data

TABLE 3

Angular correlarion data

$\frac{E}{(\text{MeV})}$	ε	$\frac{p^2}{W}$	$\varepsilon\frac{W}{p^2}$
1.42	0.037 ± 0.012	3.52	0.0104
1.69	0.042 ± 0.014	4.08	0.0104
2.00	0.049 ± 0.016	4.71	0.0105

The angular correlation is assumed to be expressed in the form $[1+\varepsilon P_2(\cos\theta)]$.

on the angular correlation are shown in table 3. These data are summarized in the equation

$$W(\theta) = 1+(0.0104\pm0.005)\frac{p^2}{W}P_2(\cos\theta), \tag{1}$$

where p is the momentum and W the total energy of the electron in $\hbar = m = c = 1$ units. The correlation between β_2 and the circular polarization of γ_1 has been found to be

$$W(\theta) = 1+(0.03\pm0.12)\frac{p}{W}\cos\theta \tag{2}$$

by one determination at one energy and one angle [27]). A measurement of the angular correlation of the direction of β_2 and the resonance fluorescence of γ_1 has been reported [28]). If this correlation is expressed in the form [29–31])

$$p^2qF(Z, W)\left[1-\alpha\frac{p\cos\theta}{Wg}(E+p\cos\theta)\right], \tag{3}$$

the experimental result is $\alpha = 0.9\pm1.1$.

In the experiments reported in this paper, orientation is produced in the As^{76} ground state and the angular distribution of γ_1 is observed. From the measured angular distribution of this γ-ray, the orientation of the 550 keV 2^+ state in Se^{76} is calculated. Thus the change in orientation due to the emission of β_2 is found. This is related to the angular momentum carried off by the electron-neutrino system.

The angular distribution of the electric quadrupole gamma ray γ_1 will be of the form [32])

$$W(\theta) = 1-\tfrac{10}{7}f_2B_2P_2(\cos\theta)-\tfrac{40}{3}f_4B_4P_4(\cos\theta), \tag{4}$$

where the Legendre polynomials are

$$\begin{aligned} P_2(\cos\theta) &= \tfrac{3}{2}(\cos^2\theta - \tfrac{1}{2}), \\ P_4(\cos\theta) &= \tfrac{35}{8}(\cos^4\theta - \tfrac{6}{7}\cos^2\theta + \tfrac{3}{35}) \end{aligned} \tag{5}$$

and the f parameters which describe the orientation in the As^{76} ground state are

$$\begin{aligned} f_2 &= \frac{1}{j_0^2}\left[\Sigma m_0^2\left(a_{m_0} - \frac{1}{2j_0+1}\right)\right], \\ f_4 &= \frac{1}{j_0^4}\left[\Sigma m_0^4\left(a_{m_0} - \frac{1}{2j_0+1}\right)\right. \\ &\quad \left. - \tfrac{1}{7}(6j_0^2+6j_0-5)\Sigma m_0^2\left(a_{m_0} - \frac{1}{2j_0+1}\right)\right]. \end{aligned} \tag{6}$$

The a_{m_0} are the populations of the As^{76} ground state normalised so that their sum is 1 and j_0 is the spin of this state; the parameters B_2 and B_4 depend upon the radiations emitted previous to the emission of γ_1. For those γ_1 which follow β_2 directly, B_2 and B_4 depend only upon the character of β_2. If it is assumed that β_2 is a typical first forbidden transition which carries off 0, 1 or 2 units of total angular momentum in the electron-neutrino field, an explicit expression can be given for B_2 and B_4. The transition probability for β_2 to occur with the emission of λ units of angular momentum into the electron-neutrino field is proportional to [33])

$$P_\lambda = \int_1^{W_0} S_\lambda(W)pW(W_0-W)^2F(Z,W)\mathrm{d}W, \tag{7}$$

where W is the total energy of the electron, W_0 is the total energy of the electron at the end point of the spectrum, p is the electron momentum ($p^2+1 = W^2$) and S_λ is the shape factor for the emission of λ units of angular momentum in the electron-neutrino field. The factor S_λ depends upon the nuclear matrix elements. The fraction of the decays which occurs with the emission of λ units of angular momentum is

$$\alpha_\lambda = \frac{P_\lambda}{\sum_{\lambda=0}^{2} P_\lambda} \tag{8}$$

In terms of the α, B_2 and B_4 are given by

$$B_2 = \alpha_0 + \tfrac{1}{2}\alpha_1 - \tfrac{3}{14}\alpha_2 = 1 - \tfrac{1}{2}\alpha_1 - \tfrac{17}{14}\alpha_2, \tag{9}$$

$$B_4 = \alpha_0 - \tfrac{2}{3}\alpha_1 + \tfrac{2}{7}\alpha_2 = 1 - \tfrac{5}{3}\alpha_1 - \tfrac{5}{7}\alpha_2. \tag{10}$$

To gain information about the beta decay from the nuclear orientation, we can use the measurements on γ_1 to determine (B_2f_2) and (B_4f_4). Then, if f_2 and f_4

where the Legendre polynomials are

$$\begin{aligned} P_2(\cos\theta) &= \tfrac{3}{2}(\cos^2\theta - \tfrac{1}{2}), \\ P_4(\cos\theta) &= \tfrac{35}{8}(\cos^4\theta - \tfrac{6}{7}\cos^2\theta + \tfrac{3}{35}) \end{aligned} \tag{5}$$

and the f parameters which describe the orientation in the As^{76} ground state are

$$\begin{aligned} f_2 &= \frac{1}{j_0^2}\left[\Sigma m_0^2\left(a_{m_0} - \frac{1}{2j_0+1}\right)\right], \\ f_4 &= \frac{1}{j_0^4}\left[\Sigma m_0^4\left(a_{m_0} - \frac{1}{2j_0+1}\right)\right. \\ &\quad \left. - \tfrac{1}{7}(6j_0^2+6j_0-5)\Sigma m_0^2\left(a_{m_0} - \frac{1}{2j_0+1}\right)\right]. \end{aligned} \tag{6}$$

The a_{m_0} are the populations of the As^{76} ground state normalised so that their sum is 1 and j_0 is the spin of this state; the parameters B_2 and B_4 depend upon the radiations emitted previous to the emission of γ_1. For those γ_1 which follow β_2 directly, B_2 and B_4 depend only upon the character of β_2. If it is assumed that β_2 is a typical first forbidden transition which carries off 0, 1 or 2 units of total angular momentum in the electron-neutrino field, an explicit expression can be given for B_2 and B_4. The transition probability for β_2 to occur with the emission of λ units of angular momentum into the electron-neutrino field is proportional to [33])

$$P_\lambda = \int_1^{W_0} S_\lambda(W) p W (W_0 - W)^2 F(Z, W)\,\mathrm{d}W, \tag{7}$$

where W is the total energy of the electron, W_0 is the total energy of the electron at the end point of the spectrum, p is the electron momentum ($p^2+1 = W^2$) and S_λ is the shape factor for the emission of λ units of angular momentum in the electron-neutrino field. The factor S_λ depends upon the nuclear matrix elements. The fraction of the decays which occurs with the emission of λ units of angular momentum is

$$\alpha_\lambda = \frac{P_\lambda}{\sum_{\lambda=0}^{2} P_\lambda} \tag{8}$$

In terms of the α, B_2 and B_4 are given by

$$B_2 = \alpha_0 + \tfrac{1}{2}\alpha_1 - \tfrac{3}{14}\alpha_2 = 1 - \tfrac{1}{2}\alpha_1 - \tfrac{17}{14}\alpha_2, \tag{9}$$

$$B_4 = \alpha_0 - \tfrac{2}{3}\alpha_1 + \tfrac{2}{7}\alpha_2 = 1 - \tfrac{5}{3}\alpha_1 - \tfrac{5}{7}\alpha_2. \tag{10}$$

To gain information about the beta decay from the nuclear orientation, we can use the measurements on γ_1 to determine $(B_2 f_2)$ and $(B_4 f_4)$. Then, if f_2 and f_4

levels into thermal equilibrium with the crystal lattice. The energy levels of an As^{76} donor atom in a large magnetic field ($\mu_0 H \gg A$) are shown in fig. 2. In the absence of the hyperfine interaction, the wave functions of the various magnetic substates are products of the form

$$\varphi(m_J, m_I) = \psi(\tfrac{1}{2}, m_J)\psi(I, m_I).$$

The hyperfine interaction mixes in a small component of the state with the same total ($m_I + m_J$) value; that is, the state ($\frac{1}{2}, m_I$) contains a small admixture of the state ($-\frac{1}{2}, m_I+1$). This admixture enables a radiofrequency field with a component along the direction of the static magnetic field to induce transitions between these two levels [6]). These transitions are forbidden in the sense that the transition probability for a resonant radiofrequency magnetic field is lower by a factor $(A/2\mu_0 H)^2$ for the $(\frac{1}{2}, m_I) \leftrightarrow (-\frac{1}{2}, m_I+1)$ transitions than for the $(\frac{1}{2}, m_I) \leftrightarrow (-\frac{1}{2}, m_I)$ transitions. The manner in which the saturation of a forbidden transition produces nuclear orientation is shown schematically in fig. 5. For As^{76} there are four forbidden transitions which can produce nuclear orientation. The following abbreviations will be used to designate the various transtions:

$$\begin{aligned}
\pi_l &\ (\tfrac{1}{2}, -2) \leftrightarrow (-\tfrac{1}{2}, -1),\\
\sigma_l &\ (\tfrac{1}{2}, -1) \leftrightarrow (-\tfrac{1}{2}, 0),\\
\sigma_u &\ (\tfrac{1}{2}, \ 0) \leftrightarrow (-\tfrac{1}{2}, 1),\\
\pi_u &\ (\tfrac{1}{2}, \ 1) \leftrightarrow (-\tfrac{1}{2}, 2).
\end{aligned}$$

These transitions are listed in the order in which they occur for a negative nuclear magnetic moment as the magnetic field is increased with a fixed klystron frequency. A diagram of four transitions is shown in fig. 3.

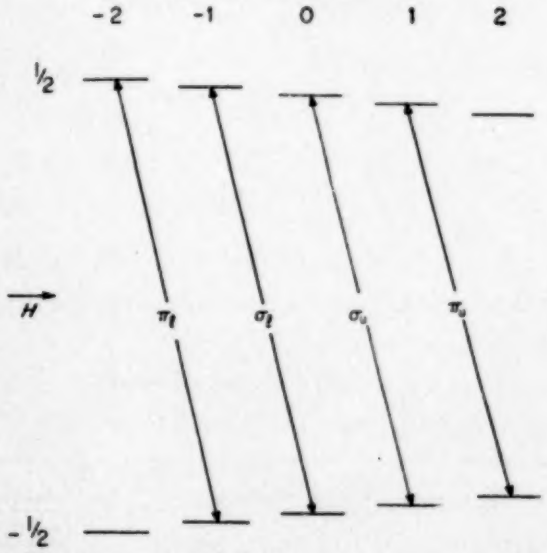

Fig. 3. The four forbidden transitions and the labels used in this paper.

The magnitude of the orientation depends not only upon which forbidden transition is saturated, but also upon the processes which restore the magnetic sublevels to thermal equilibrium. This is a complex problem which is not completely understood [35-38]. Here it will be assumed that the term in the Hamiltonian which produces the relaxation can be written in the form

$$\mathscr{H}(t) = -g_J\mu_0\mathbf{J}\cdot\mathbf{H}(t)+A(t)\mathbf{I}\cdot\mathbf{J}+\sum_{q=-2}^{2}(-1)^q Q_{-q}(\nabla E)_q(t). \tag{12}$$

In the transitions produced by this Hamiltonian, energy is exchanged between the lattice and the donor atom. The first term relaxes the electrons but does not affect the nuclei; the second term (modulation of the isotropic hyperfine interaction [38]) and the third term (nuclear electric quadrupole interaction [39]) produce nuclear-relaxation. For an atomic spin of $\frac{1}{2}$, the lattice-induced transition probabilities can be expressed in terms of the Clebsch-Gordan coefficients. They are:

(1)electron relaxation

$$W(m_J, m_I|m'_J, m'_I) = W_1\delta_{m_I, m'_I}(1-\delta_{m_J, m'_J}) \tag{13}$$

(2) modulation of isotropic hyperfine interaction

$$W(m_J, m_I|m'_J, m'_I) = W_2(I1m'_I\mu|I1Im_I)^2(1-\delta_{m_J, m'_J})\delta_{m_I+m_J, m'_I+m'_J}, \tag{14}$$

(3) nuclear quadrupole relaxation

$$W(m_J, m_I|m'_J, m'_I) = W_3(I2m'_I\mu|I2Im_I)^2\delta_{m'_J, m_J}(1-\delta_{m_I, m'_I}). \tag{15}$$

If $P(m_J, m_I)$ designates the occupation probabilities of the various substates of the donor atom normalized so that their sum is one, the change in time of the level populations is described by the equations

$$\dot{P}(m_J, m_I) = \sum_{\substack{m'_I \\ m'_J}} W(m_J, m_I|m'_J, m'_I) \left[e^{-\frac{\mu_0 H}{kT}(m_J-m'_J)}P(m'_J, m'_I)-e^{-\frac{\mu_0 H}{kT}(m'_J-m_J)}P(m_J, m_I)\right]. \tag{16}$$

For the calculation of the Boltzmann factors, the hyperfine contribution to the energy has been neglected. The three relaxation mechanisms are illustrated schematically in fig. 4.

Two important cases of this coupled set of equations can be easily solved. One is for the production of the orientation; the other is for the decay of the orientation. To simplify the problem, it is assumed that the nuclear relaxation time is much longer than the electron relaxation time and that the electron relaxation time is much longer than the time required to saturate the forbidden transition. For the production of the orientation only four

levels need to be considered; this is shown schematically in fig. 5. The orientation jumps up to one-half its final value soon after the radiofrequency field is turned on. It then increases exponentially with a time constant which

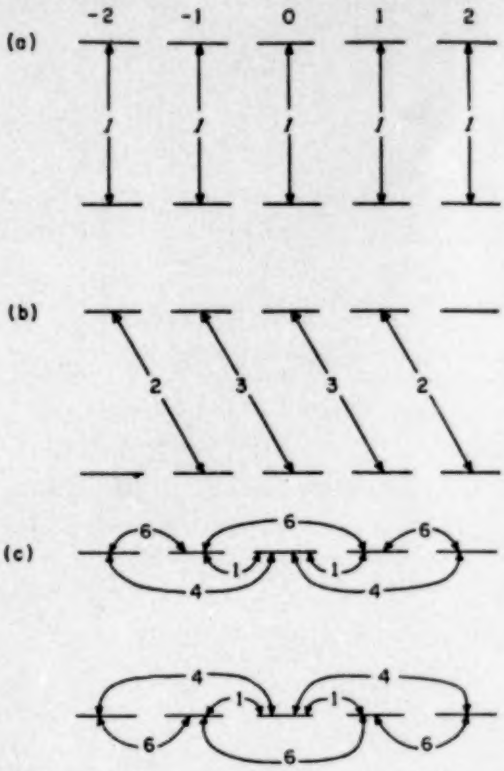

Fig. 4. Schematic representation of the various relaxation paths: (a) electron relaxation, (b) relaxation due to modulation of the isotropic hyperfine interaction, (c) relaxation due to quadrupole interaction.

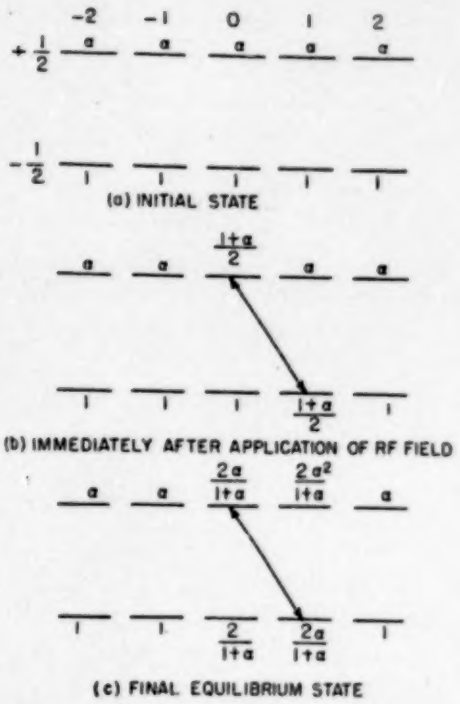

Fig. 5. Schematic representation of the saturation of the forbidden transition $(-\frac{1}{2}, 1) \leftrightarrow (\frac{1}{2}, 0)$. The numbers beside the levels represent the relative populations. The symbol α has been introduced for $\exp(-2\mu_0 H/kT)$; $\alpha = 0.4$ for 8500 G and 1.25° K. This transition increases the population of the nuclear $m = 0$ level at the expense of the $m = 1$ level. The nuclear relaxation time has been assumed to be much longer than the electron-only relaxation time.

depends upon the electron relaxation time until equilibrium is reached:

$$f_2(t) = f_2(\infty)(1-\tfrac{1}{2}e^{-\lambda_R t}),$$
$$f_4(t) = f_4(\infty)(1-\tfrac{1}{2}e^{-\lambda_R t}), \tag{17}$$

where

$$\lambda_R = W_1 \cosh \frac{\mu_0 H}{kT} = \frac{1}{2T_S}. \tag{18}$$

Here, T_S is the electron relaxation time as it is customarily defined [35]) and W_1 is the transition probability of eq. (13). In table 4 are summarized the equilibrium f_2 and f_4, which would be obtained if there were no nuclear relaxation.

TABLE 4

The f_2 and f_4 parameters for saturation of the four $\Delta(m_I+m_J) = 0$ transitions.

Transition	f_2	f_4
$(-\frac{1}{2}, -1) \leftrightarrow (\frac{1}{2}, -2)$	$\frac{3}{20}\,\mathrm{tgh}\,\frac{\mu_0 H}{kT}$	$\frac{3}{140}\,\mathrm{tgh}\,\frac{\mu_0 H}{kT}$
$(-\frac{1}{2}, 0) \leftrightarrow (\frac{1}{2}, -1)$	$\frac{1}{20}\,\mathrm{tgh}\,\frac{\mu_0 H}{kT}$	$-\frac{3}{70}\,\mathrm{tgh}\,\frac{\mu_0 H}{kT}$
$(-\frac{1}{2}, 1) \leftrightarrow (\frac{1}{2}, 0)$	$-\frac{1}{20}\,\mathrm{tgh}\,\frac{\mu_0 H}{kT}$	$\frac{3}{70}\,\mathrm{tgh}\,\frac{\mu_0 H}{kT}$
$(-\frac{1}{2}, 2) \leftrightarrow (\frac{1}{2}, 1)$	$-\frac{3}{20}\,\mathrm{tgh}\,\frac{\mu_0 H}{kT}$	$-\frac{3}{140}\,\mathrm{tgh}\,\frac{\mu_0 H}{kT}$

It has been assumed that there is no nuclear relaxation and that the time of application of the radiofrequency field is much longer than the electron relaxation time.

For the second case, which describes the decay of orientation after the radiofrequency field is turned off, it is advantageous to introduce the new variables

$$\begin{aligned} P^+(m) &= P(-\tfrac{1}{2}, m_I)+P(\tfrac{1}{2}, m_I), \\ P^-(m) &= \alpha P(-\tfrac{1}{2}, m_I)-P(\tfrac{1}{2}, m_I), \end{aligned} \tag{19}$$

where

$$\alpha = \mathrm{e}^{-\frac{2\mu_0 H}{kT}}$$

and m now refers to the nuclear substate. If it is assumed that

$$P^-(m) = 0,$$

the general relaxation equations (eq. (16)) reduce to the form

$$\dot{P}^+(m) = \sum_{m'} W(m|m')[P^+(m')-P^+(m)]. \tag{20}$$

For the two nuclear relaxation mechanisms of interest, the $W(m|m')$ are given by the following equations:

(1) for the isotropic hyperfine relaxation we have

$$W(m|m') = \frac{W_2}{2\cosh\frac{\mu_0 H}{kT}}\,(I1m'\mu|I1Im)^2(1-\delta_{m,m'}), \tag{21}$$

(2) for the nuclear quadrupole relaxation we have

$$W(m|m') = W_3(I2m'\mu|I2Im)^2(1-\delta_{m,m'}). \tag{22}$$

It is a consequence of this set of equations that

$$f_2(t) = f_2(0)\mathrm{e}^{-\lambda_2 t}, \qquad f_4(t) = f_4(0)\mathrm{e}^{-\lambda_4 t}, \tag{23}$$

where λ_2 and λ_4 depend upon the relaxation mechanism. For the isotropic hyperfine interaction we have

$$\lambda_2 = \frac{W_2}{4\cosh\dfrac{\mu_0 H}{kT}}, \tag{24}$$

$$\lambda_4 = \frac{5}{6}\frac{W_2}{\cosh\dfrac{\mu_0 H}{kT}}, \tag{25}$$

and, for the quadrupole relaxation †, we have

$$\lambda_2 = \tfrac{17}{14}W_3, \tag{26}$$

$$\lambda_4 = \tfrac{10}{14}W_3. \tag{27}$$

In the case of the quadrupole interaction, the f_2 decays faster, while in the case of the isotropic hyperfine interaction the f_4 decays more rapidly. This makes it possible to distinguish experimentally the two relaxation mechanisms.

In order to solve the general case, it is convenient to use an analogue computer. The relaxation equations also describe an electrical network of resistors and condensers. Each of the levels is replaced by a condenser; the charge on a condenser corresponds to the population of a particular level; the relaxation paths are replaced by the appropriate resistors. The ratio of the condensers representing the $m_J = +\frac{1}{2}$ levels, $C_{+\frac{1}{2}}$, and the condensers representing the $m_J = -\frac{1}{2}$ levels, $C_{-\frac{1}{2}}$, is made equal to the Boltzmann factor:

$$\frac{C_{+\frac{1}{2}}}{C_{-\frac{1}{2}}} = \mathrm{e}^{-\frac{2\mu_0 H}{kT}} = \alpha. \tag{28}$$

The analogue circuit for relaxation by modulation of the isotropic hyperfine interaction is shown in fig. 6(a); that for quadrupole relaxation in fig. 6(b). The similarity to the diagrams in fig. 4 is apparent. A battery arranged so that it equalizes the charge on a $C_{-\frac{1}{2}}$ and a $C_{+\frac{1}{2}}$ condenser is the analogue of the saturating radiofrequency field. This use of the battery is shown schematically in fig. 7. If the condensers are originally charged to a voltage V, the voltage V_B of the equalizing battery should be

$$V_B = \frac{1-\alpha^2}{2\alpha}V. \tag{29}$$

In terms of the circuit components in fig. 6, the orientation rise constant is

$$\lambda_R = \frac{1+\alpha}{2\alpha}\frac{1}{R_1 C}. \tag{30}$$

† In refs. [5, 35]) the quadrupole decay constants for f_2 and f_4 are interchanged.)

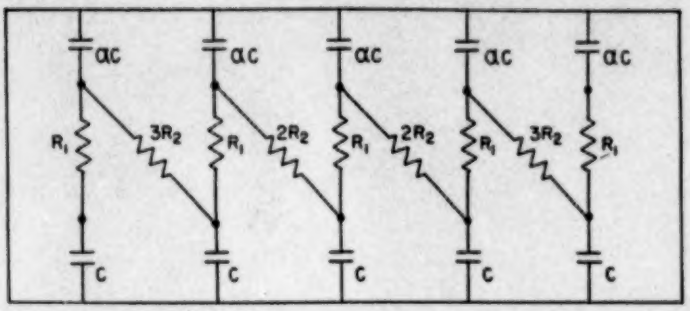

Fig. 6 (a) The analogue circuit for the electron relaxation plus modulation of the isotropic hyperfine interaction.

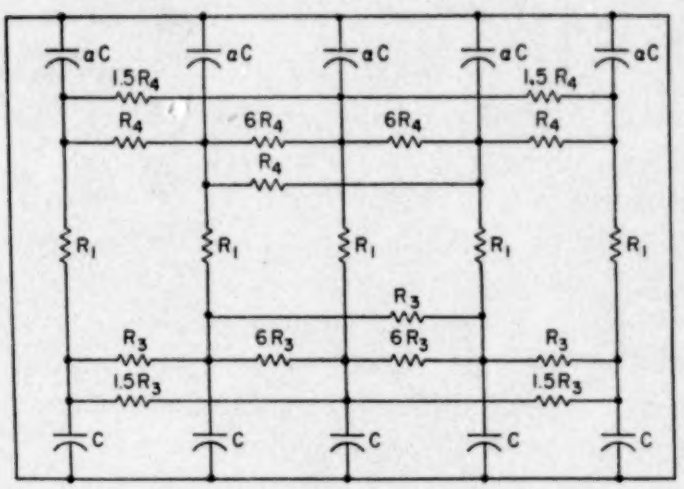

$\alpha R_4 = R_3$

Fig. 6 (b). The analogue circuit for the electron relaxation plus nuclear quadrupole relaxation.

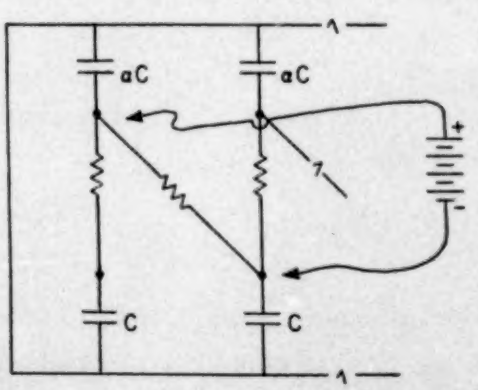

Fig. 7. The use of a battery to equalize the levels and thus simulate the effect of a saturating radiofrequency field.

The decay constants for the isotropic hyperfine relaxation are

$$\lambda_2 = \frac{1}{2}\,\frac{1}{1+\alpha}\,\frac{1}{R_2 C}, \tag{31}$$

$$\lambda_4 \doteq \frac{5}{3}\,\frac{1}{1+\alpha}\,\frac{1}{R_2 C}. \tag{32}$$

and those for the quadrupole relaxation

$$\lambda_2 = \frac{17}{6R_3 C}, \tag{33}$$

$$\lambda_4 = \frac{5}{3R_3 C}. \tag{34}$$

The circuits used to present the data from the analogue computer are described in the section on apparatus.

3. Apparatus

Most of the apparatus used in this experiment has been described in the previous papers [5, 40]) on As^{76} and Sb^{122}. The general arrangement of the two counters is shown in fig. 8. A regulator of the de Woord type [5]), which keeps

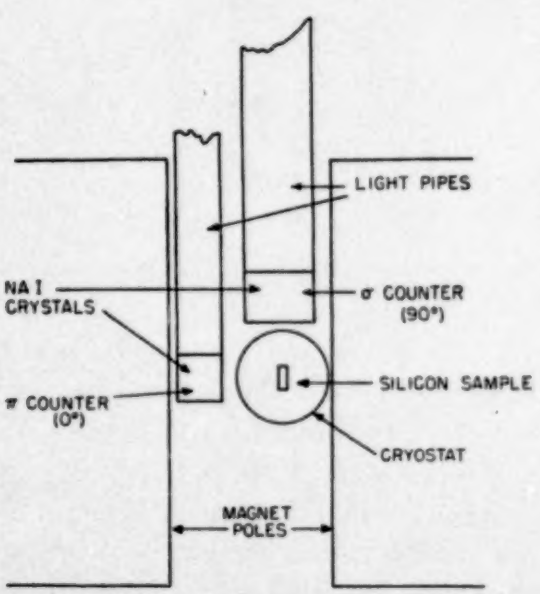

Fig. 8. Diagram showing the relative position of the two counters.

the As^{76} 550 keV photopeak at a constant voltage, was used for each counter. This made it possible to obtain the stability expected from the $\sqrt{N}$ counting law for counting periods giving as many 2×10^6 counts. Four integral dis-

criminators and four scalars were provided so that the number of gamma rays with energies both above and below the 550 keV photopeak could be recorded.

The metal dewar which was used in the previous orientation experiments developed a leak which only opened up when the helium was below the λ point. To cure this, the helium pot was rebuilt. The rebuilt dewar had a total capacity of 1.2 l helium. Even though the wave guide assembly was inserted after the dewar had been filled with helium, the helium lasted for as long as 20 hours after it was pumped down to a temperature of 1.2° K.

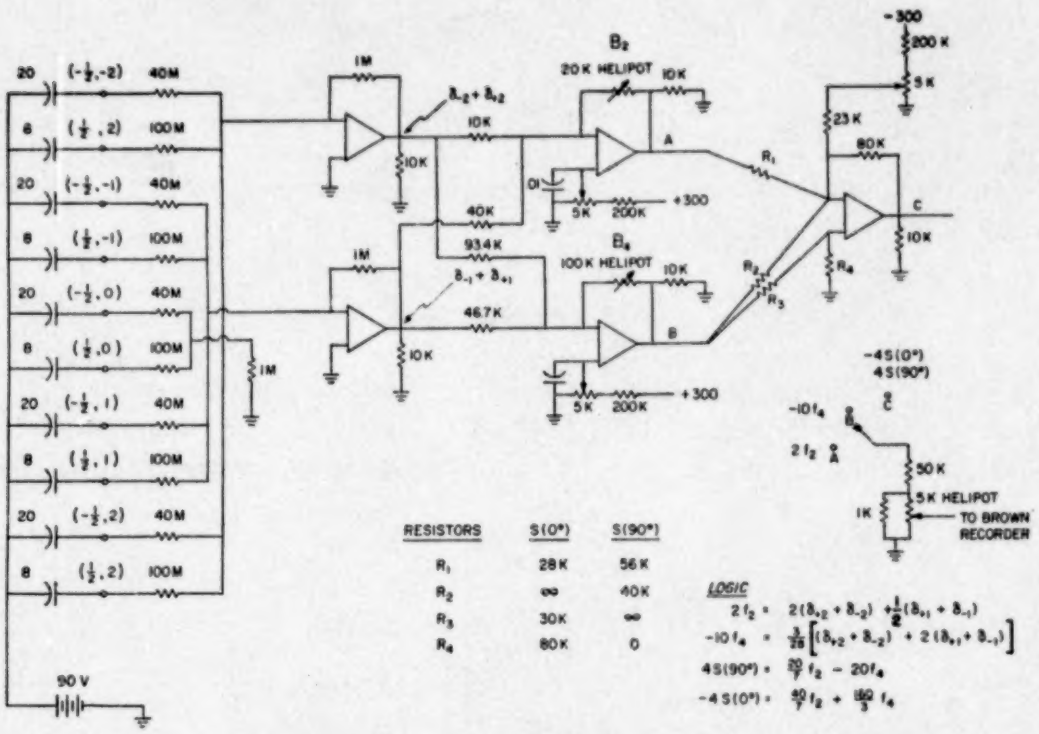

Fig. 9. The circuit for the analogue computer

The circuit for the analogue computer is shown in fig. 9. The condensers were low-leakage oil-filled condensers. They were measured with a bridge and then combinations selected to obtain the proper capacitance ratios to within 1 %. The amplifiers were Philbrick K-2W operational amplifiers. The resistors in the computer circuits were 1 % metal film; the resistors for the relaxation matrix were ordinary carbon resistors. Asmall Leeds and Northrup Wheatstone-bridge and a Brown null detector were used to measure and match these resistors to 1 %. The computer was built so that the points corresponding to the ten levels were readily accessible on the front panel, and the physical arrangement corresponded with that of the energy levels in fig. 2. Helipots were provided to set the B_2 and B_4 coefficients so as to reproduce the observed signals. The output of the computer was presented

on a Brown zero centre recorder with a 0.2 second time constant. Typical computer results are shown in fig. 10.

The arsenic doped silicon sample used in this experiment was part of a crystal obtained from the Raytheon Manufacturing Company. Pieces of the

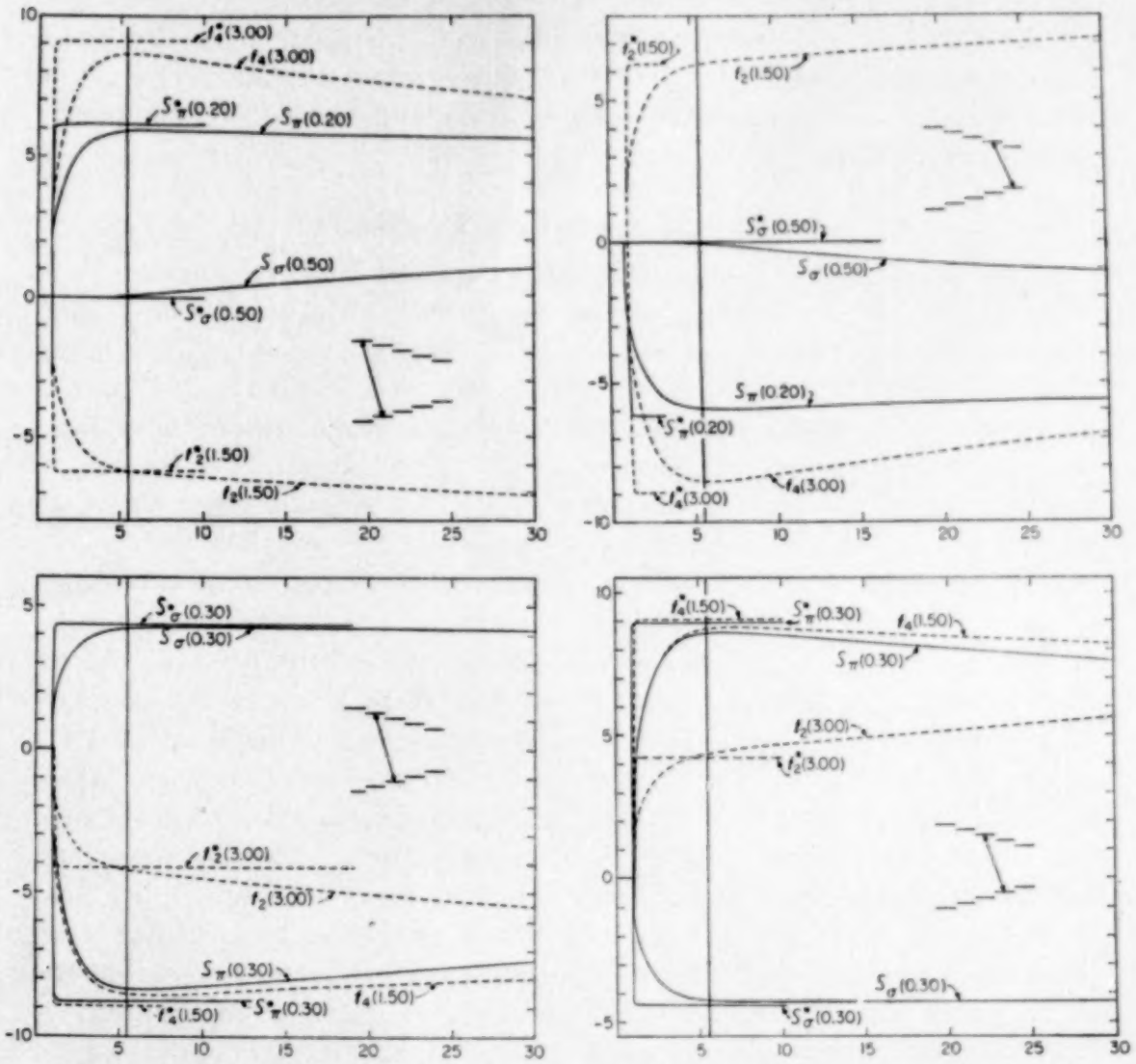

Fig. 10. A set of analogue computer data for each of the four forbidden transitions. The nuclear relaxation was assumed to be due to the modulation of the hyperfine interaction and the resistors were such that $\lambda_4/\lambda_R = 2.56 \times 10^{-2}$. The starred quantities are for the case of no nuclear relaxation and for a very short electron relaxation. The vertical line indicates the point corresponding to that at which the klystron was turned off in the experiment. The S_π denotes the fractional change in counting rate at 0^0 and the S_σ the fractional change in counting rate in 90^0. The full scale gain of the computor was 10 and the number in parenthesis gives the relative gain. The computor was constructed so that full scale corresponded to $-2f_2$, $10f_4$, $4S(0°)$ and $-4S(90°)$.

same crystal were used in the previous experiment on As^{76}. The sample consisted of two pieces of silicon 0.170 cm by 0.420 cm by 0.420 cm. The microwave cavity was made of rectangular copper wave guide of inside dimension 0.420

cm by 0.170 cm and the power was coupled in through an asymmetric iris which covered approximately half the wave guide cross-section. For this experiment two irradiations of the same sample were made at the Materials Testing Reactor at Arco, Idaho. The first (S–1) irradiation was for 24 h in a flux of 2×10^{14} thermal neutrons per cm^2 per sec and the second (S–2) was for a period of 48 h in a similar flux. Subsequently to their arrival in Cambridge, the crystals were cleaned in a $HF\text{-}HNO_3$ etch to remove radioactive surface contamination and then annealed for 4—6 h at a temperature of 1100—1200° C to heal radiation damage.

4. The Measurement Procedure

After the sample had been annealed, it was placed in the rectangular microwave cavity, and the wave guide assembly was inserted into the helium-filled dewar. The dewar was placed in the magnet; the four integral discriminator curves were run; and the discriminators were set. There were two integral discriminators for each channel; one was set in the valley below the 550 keV photopeak; the other was set just above the 550 keV photopeak. The He cryostat was then pumped down to a temperature of 1.2° K and a good cavity mode was located by adjusting the klystron frequency. The positions in magnetic field of the stable As^{75} electron resonances were measured, and the positions of the four forbidden transitions in As^{76} calculated. In order to establish a uniform state of the sample from which to start the experiments, the magnet was turned off and the field reduced to less than 1G by a pair of auxiliary coils on the magnet pole pieces. The relaxation times at low magnetic field are apparently very fast [37]). The klystron power was then attenuated so that no microwave power reached the cavity; the magnet was turned on, and the field was adjusted so that the frequency of one of the four forbidden transitions coincided with the resonant frequency of the cavity. The magnetic field was swept back and forth over an interval of 10 G so as to bring all parts of the As^{76} line into resonance and make the position of the magnetic field less critical. The separation between the As^{76} forbidden lines and the adjacent allowed transitions is 16.7 G. The counting rate in both the 0° and 90° counters was observed for a period of 30 to 40 min to determine the counting rates in the absence of nuclear orientation. The counter was automatically gated on for 180 sec and then off for 20 sec. During the 20 sec period, the observer would record the four scalar readings. The klystron power was turned on and the forbidden transition was saturated. The saturation was continued until the counting rates were no longer seen to change. This procedure was repeated with each of the forbidden transitions until the supply of helium was exhausted. During one filling of helium each of the transitions was observed at least once and sometimes twice. A typical set of data for each of the four transitions is shown in fig. 11.

It became apparent early in the experiment that the nuclear relaxation time was very long. In order to measure it a different procedure was used. First the $(-\frac{1}{2}, 0) \leftrightarrow (\frac{1}{2}, -1)$ transition was saturated and then the $(-\frac{1}{2}, 2) \leftrightarrow (\frac{1}{2}, 1)$ transition was saturated. This produced a change in counting rate equal to the sum of the two transitions. The klystron was turned off, and the

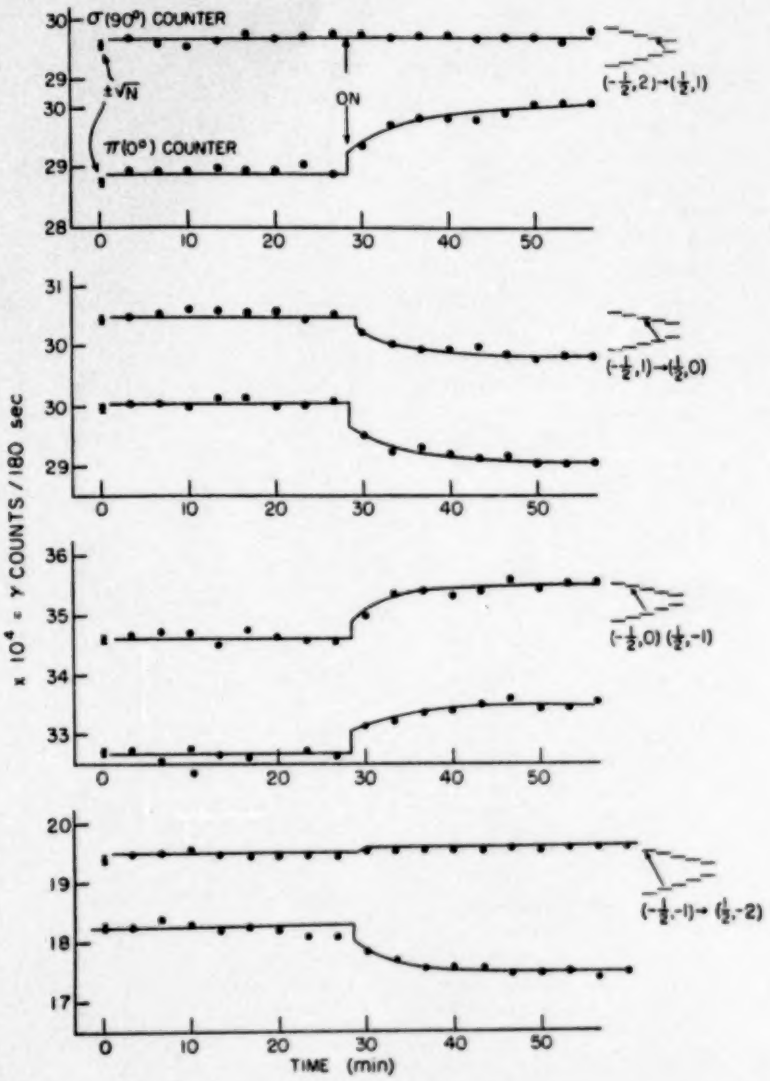

Fig. 11. Plot of counting rate versus time for the 0° and 90° positions for saturation of each of the four forbidden transitions.

decay was observed for several hours. At the end of the run the magnet was turned off and the field at the sample reduced to zero. The magnet was turned back on and the counting rates observed. Test observations indicated that, although the counting rates were different when the magnet was off than when it was on even when there was no nuclear orientation, the counting rate was the same when it was turned back on as before it was turned off. This procedure destroyed the remaining orientation and permitted observation of the amount of

TABLE 5

The observed counting rate changes for both sources and all forbidden transitions.

	Transition	Run	Counting rate changes in %			
			Low channel		High channel	
			$S(90°)$	$S(0°)$	$S(90°)$	$S(0°)$
A. Source S−1	π_u	3−142	+0.21	+4.21	+0.38	+2.97
		3−132	−0.01	+3.62	+0.41	+2.36
		4−16	−0.24	+4.05	+0.56	+2.55
		4−26	−0.04	+3.71	+0.86	+2.31
		Mean	−0.02	+3.90	+0.55	+2.55
	π_l	3−138	+0.49	−3.50	+0.98	−3.17
		3−146	+0.66	−3.92	+0.41	−3.40
		4−18	+0.31	−3.77	−0.35	−2.49
		4−8	+0.52	−4.21	+0.29	−3.82
		Mean	+0.50	−3.85	+0.33	−3.22
	σ_u	3−140	−2.30	−3.41	−1.09	−2.65
		3−130	−2.13	−3.75	−1.84	−3.91
		4−14	−2.01	−2.66	−0.33	−1.39
		4−24	−1.42	−2.62	−1.09	−2.65
		Mean	−1.97	−3.11	−1.09	−2.65
	σ_l	3−134	+2.62	+2.65	+1.48	+1.35
		3−144	+2.45	+2.13	+1.52	+1.18
		4−10	+2.52	+2.04	+1.52	+1.16
		4−22	+2.23	+2.63	+1.54	+1.02
		4−12	+2.43	+2.65	+1.52	+1.02
		Mean	+2.45	+2.42	+1.52	+1.18
B. Source S−2	π_u	4−70	−0.11	+3.32	−0.35	+2.09
		4−74	−0.11	+3.16	−0.38	+1.42
		Mean	−0.11	+3.24	−0.37	+1.76
	π_l	4−72	+0.49	−4.46	−0.33	−2.17
		4−78	+0.49	−4.83	−0.00	−2.60
		Mean	+0.49	−4.65	−0.17	−2.39
	σ_u	4−68	−1.47	−2.99	−1.32	−1.88
		4−80	−1.38	−3.80	−1.18	−2.08
		Mean	−1.43	−3.40	−1.25	−1.98
	σ_l	4−82	+1.88	+1.74	+1.23	+1.49
		4−66	+1.78	+2.41	+0.95	+1.45
		Mean	+1.83	+2.08	+1.09	+1.47

The data have been corrected for counting rate loss. The statistical error in a given measurement is smaller than the variation between successive runs. The run number corresponds to the page in the data book and gives its approximate chronological sequence.

orientation remaining after several hours' relaxation. A typical run is shown in fig. 12. Table 5 gives the data on the counting rate changes for all transitions and both sources.

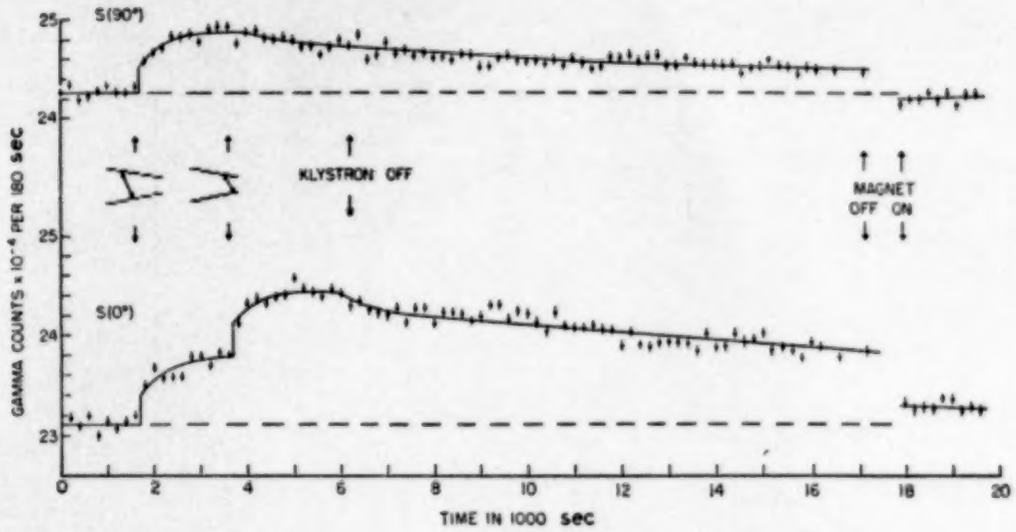

Fig. 12. Plot of counting rate versus time for one of the long runs which were used to determine the nuclear relaxation time.

5. Reduction of the Data

In order to determine the B_2f_2 and B_4f_4 parameters, which describe the orientation of the 550 keV state, we corrected for the presence of the extraneous gamma rays and the finite solid angle of the counters. To correct for the other γ rays, it was assumed that the As^{76} could be represented by

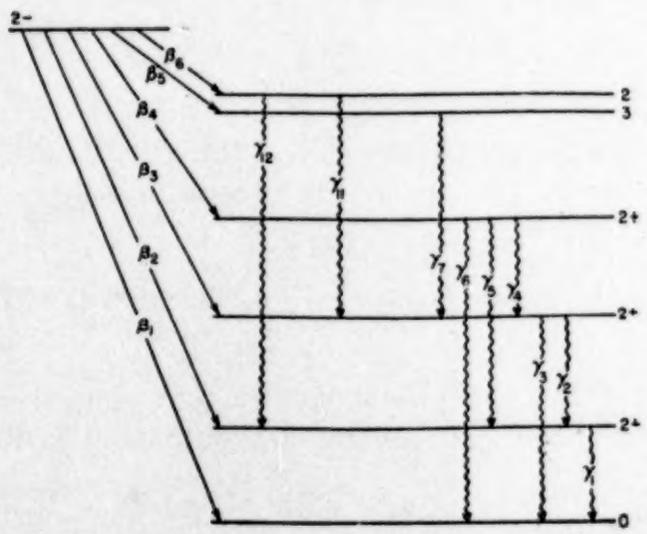

Fig. 13. The simplified As^{76} decay scheme which was used in calculating the corrections to the data.

the simplified decay scheme shown in fig. 13 and that all the β and γ rays were as described in tables 6 and 7. The parameters B_2 and B_4 characterize the change in orientation by the emission of γ_2, B'_2 and B'_4 the change by γ_3 and B''_2 and B''_4 the change by γ_4. The most critical part of this assumption

TABLE 6

The beta-rays assumed for As^{76} in the simplified decay scheme

Radiation	Occurrence per 100 decays	Change in orientation parameters	
		f_2	f_4
β_1	56.4		
β_2	38.6	B_2	B_4
β_3	3.6	B'_2	B'_4
β_4	6.6	B''_2	B''_2
β_5	0.9	$\frac{16}{21}$	$\frac{880}{1701}$
β_6	1.9	$\frac{1}{2}$	$-\frac{2}{3}$

TABLE 7

The gamma rays assumed for As^{76} in the simplified decay scheme

Radiation	Occurrence per 100 decays	Character
γ_1	39.2	EQ
γ_2	6.3	EQ
γ_3	4.3	EQ
γ_4	5.4	EQ
γ_5	1.0	EQ
γ_6	0.32	EQ
γ_7	0.9	Dipole
γ_{11}	0.78	Quadrupole
γ_{12}	0.91	Quadrupole

is the character of the mixed gamma rays. The angular distribution of a 2–2 mixed magnetic dipole and electric quadrupole transition is given by the expression [41]).

$$W(\theta) = 1+\tfrac{1}{21}\{-21a_1^2+126(\tfrac{5}{21})^{\frac{1}{2}}a_1a_2+\tfrac{45}{7}a_2^2\}f_2P_2(\cos\theta)-\tfrac{80}{21}a_2^2f_4P_4(\cos\theta). \quad (35)$$

In this equation, a_1 and a_2 are the reduced matrix elements for the magnetic dipole and electric quadrupole components normalized so that

$$a_1^2+a_2^2 = 1.$$

It was assumed that all the low energy gamma rays, γ_1, γ_2 and γ_4, were counted

with the same efficiency and that the high energy gamma rays were counted with 1.2 times this efficiency. This latter number is based on the observed γ-ray spectra and the setting of the discriminators. Under these circumstances the counting rate in the upper discriminator channel is proportional to

$$W(\theta) = 1-\tfrac{10}{7}(0.1650\ B'_2+0.0057\ B''_2-0.0454)f_2P_2(\cos\theta) \\ -\tfrac{40}{3}(0.1650\ B'_4+0.1357\ B''_4-0.0219)f_4P_4(\cos\theta), \quad (36)$$

and that in the low-energy channel is proportional to

$$W(\theta) = 1-\tfrac{10}{7}(0.5137\ B_2+0.0082\ B'_2-0.0095\ B''_2-0.0060)f_2P_2(\cos\theta) \\ -\tfrac{40}{3}(0.5137\ B_4+0.0451\ B'_4+0.0592\ B''_4-0.0326)f_4P_4(\cos\theta). \quad (37)$$

To make it possible to analyze the data, it was assumed that $B'_2 = B''_2$ and $B'_4 = B''_4$. Thus from the observation of the high-energy channel, we can find B'_2f_2 and B'_4f_4; these results can then be used together with the data from the low-energy channel to find B_2f_2 and B_4f_4.

A numerical integration was used to correct for the finite solid angle of the counters and the finite source size. These correction factors can be expressed as attenuation coefficients S_2 and S_4 in the angular distribution

$$W(\theta) = 1-\tfrac{10}{7}S_2B_2f_2P_2(\cos\theta)-\tfrac{40}{3}S_4B_4f_4P_4\ (\cos\theta). \quad (38)$$

The values for S_2 and S_4 for the two sources are shown in table 8. The measured

TABLE 8

Solid angle correction factors.

Source	Counter	S_2	S_4
October	0°	0.8841	0.6552
	90°	0.9213	0.8310
November	0°	0.9237	0.7628
	90°	0.8713	0.6214

resolving times of the scalars were used to correct for the counting rate loss. This correction was always less than 5 %.

To determine the electron relaxation time the rise of all the observed curves was fitted to an expression of the form

$$A-Be^{-\lambda t}, \quad (39)$$

by plotting the observed signals on semilog paper. The results of this analysis are shown in table 9. From these data we conclude that the rise constant is the same for all transitions. It is

$$\lambda_R = (2.3\pm0.5)\times10^{-3}\ \text{sec}^{-1}.$$

TABLE 9

Time constants for the rise of the orientation (in units of 10^{-3} sec^{-1})

	Transition	Run	0°	90°	Data quality
A. Source S—1	π_u	3—142	2.28		poor
		3—132	1.94		fair-good
		4—16	0.94		fair-good
		4—26	1.34		fair
		Mean	1.41		
	π_l	3—138	2.10		poor
		3—146	1.96		good
		4—18	1.58		poor
		4—8	1.73		fair-good
		Mean	1.84		
	σ_u	3—140	3.29	2.68	poor
		3—120	1.51	1.98	fair
		4—14	2.39	1.17	very poor
		4—24	3.16		very poor
		Mean	2.38	1.94	
	σ_l	3—148	2.98	2.44	fair
		3—144		0.33	poor
		4—10			
		4—22	1.19	1.58	poor
		4—12		2.49	very good
		Mean	2.38	2.17	
B. Source S—2	π_u	4—70	1.54		poor
		4—74	4.11		fair
		Mean	2.83		
	π_l	4—72	1.35	1.74	fair
		4—78	1.43		fair
		Mean	1.39	1.74	
	σ_u	4—68	3.44	2.36	fair
		4—80	2.35	1.69	fair
		Mean	2.90	2.03	
	σ_l	4—82	4.03	4.28	good
		4—66	3.50	2.46	fair-good
		Mean	3.87	3.37	

This corresponds to an electron relaxation time

$$T_S = (3.6 \pm 0.7) \text{ min.}$$

This result agrees with the value found in a previous experiment [35]).

To determine the nuclear relaxation time, the data from the long decay runs were analyzed into f_2 and f_4 components. Semilog plots were then made of the f_2 and f_4 and the decay constants were calculated. Three such runs were made. The plot of the f_4 for the second October run is shown in fig. 14.

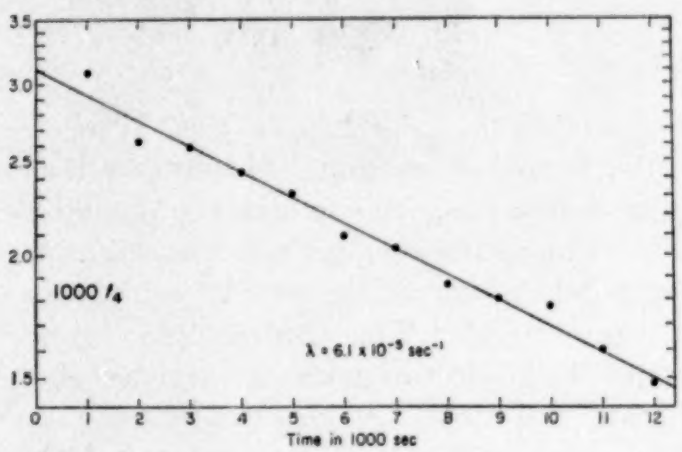

Fig. 14. Semilog plot of the f_4 versus time for the decay in fig. 12.

TABLE 10

Measured decay constants

Source	Run	$\lambda_2(\times 10^{-5}$ sec$^{-1})$	$\lambda_4(\times 10^{-5}$ sec$^{-1})$
October	3—148		3.76
October	4—2		6.10
November	4—94		6.36

The f_2 decayed so slowly that no decay constant could be assigned from the data. The results of the three runs for the f_4 decay constant are listed in table 10. From these data we conclude that

$$\lambda_4 = (5.4 \pm 2.0) \times 10^{-5} \text{ sec}^{-1},$$

$$\lambda_2 < \lambda_4,$$

and that the relaxation is due to a dipole rather than a quadrupole mechanism. This relaxation time agrees with that found in a previous experiment [35]). The corresponding relaxation time for the nuclear polarization can be computed from eq.(20). It is

$$T_N = \frac{1}{\lambda_1} = \frac{10}{\lambda_4} = (3.1 \pm 1.0) \times 10^3 \text{ min.} \qquad (40)$$

This time is not the same as the cross relaxation time used in ref. [35]). The cross relaxation time is

$$T_X = \frac{5\alpha}{(1+\alpha)^2}\frac{1}{\lambda_4} = (3.1\pm 1.0)\times 10^2 \text{ min.} \tag{41}$$

To compute the correction to the f_2 and f_4 parameters from the values given by the simple no nuclear relaxation theory, the computer was set up so as to approximate the ratio

$$\frac{\lambda_4}{\lambda_R} = 2.35\times 10^{-2}.$$

In the actual computation, the value 2.56 was used. It was assumed in setting up the computer that the only relaxation mechanism was the modulation of the isotropic hyperfine interaction. The following procedure was used. First, the computer was set up with the proper resistors and a run was made of f_2, f_4, $S(0°)$ and $S(90°)$. Before each run the recorder paper was moved backwards so that the initial points coincided. When these graphs were finished, the coupling resistors were removed, the electron relaxation resistors shorted out, and the runs of the f_2, f_4, $S(0)°$ and S(90°) were repeated with the same gain as before in each case. This gave a calibration with which to calculate the correction factors. If we designate f_i^* as the f_i value calculated using the simple theory which neglects nuclear relaxation we can write the actual f_i as

$$f_i = A_i f_i^*. \tag{42}$$

The correction factor A_i depends upon when the saturating radiofrequency field was turned off. This point was chosen to correspond to the time the klystron was turned off in the experiment. The set of computer data used to determine the corrections is shown in fig. 10. A similar procedure was used to measure the decay constant for the coupled system. Table 11 gives a

TABLE 11

A comparison between the decay constants determined by using the computer and those which would be calculated using the simple very fast electron relaxation model

	π_u	π_l	σ_u	σ_l	Decoupled theoretical
λ_2	0.00708	0.00790	0.00689	0.00737	0.00624
λ_4	0.0218	0.0208	0.0211	0.0217	0.0208
λ_2/λ_4	3.08	2.63	3.06	2.94	3.33

comparison between the measured decay constants and those calculated using the very fast electron relaxation theory. In table 12 are listed the correction factors calculated for the various transitions. They are never very large;

TABLE 12

The correction factors A_i which relate the actual f_2 and f_4 values in the presence of nuclear relaxation to those which would be calculated assuming the no nuclear relaxation model (table 4).

	π_u	π_l	σ_u	σ_l
f_2	1.010	0.995	1.007	1.029
f_4	0.963	0.944	0.962	0.961

nor does the relaxation introduce any large asymmetry into the orientation signals. These correction factors can be used to calculate the B_2 and B_4 parameters form the observed $B_2 f_2$ and $B_4 f_4$. The results are listed in table 13.

TABLE 13

The experimentally measured B_2 B_4, B'_2 and B'_4 parameters.

Parameter	Source 1				Source 2				Mean			
	π_u	π_l	σ_u	σ_l	π_u	π_l	σ_u	σ_l	π_u	π_l	σ_u	σ_l
B'_2	0.73	1.72	0.43	2.27	1.04	0.75	1.93	1.91	0.89	1.24	1.28	2.09
B'_4	1.24	0.81	0.93	0.75	0.42	0.96	0.83	0.70	0.83	0.89	0.88	0.73
B_2	0.45	0.46	0.35	0.93	0.33	0.54	0.35	1.04	0.39	0.51	0.34	0.98
B_4	0.29	0.25	0.30	0.35	0.35	0.31	0.29	0.29	0.32	0.29	0.29	0.32
B_2/B_4	1.55	1.84	1.17	2.66	0.94	1.74	1.21	3.60	1.22	1.76	1.17	3.06

The estimated error in B_2 and B_4 is about 10 to 15 %. The B'_2 and B'_4 have an uncertainty of about 40 to 50 %.

6. Interpretation of the Results

It is clear from table 13 that the same result for B_4 is obtained from all four of the transitions and for both sources. This is not true for B_2. The σ_l transition is particularly anomalous; also there is an asymmetry in the B_2 values which seems to grow worse as the sample is irradiated longer. In this regard, it should be noted that the B_2 is more sensitive to the corrections for other gamma rays, especially in the case where the $2^+ \leftrightarrow 2^+$ gamma rays have a large magnetic dipole admixture. The explanation for this behaviour is not known. With the analog computer we were unable to produce such an asymmetry. This asymmetry must be due to some interaction of the arsenic donors with other centres in the crystal. There are two possible situations. First, assume that all the arsenic atoms are in the donor sites. In this case, when a radiofrequency field at the frequency corresponding to the σ_l transition is applied to the sample, other transitions which can alter the nuclear orientation of the donor atoms and change f_2 but not the f_4 must be excited. The second possible situation is that all As atoms are not in the donor sites, but instead approximately 50 % of the arsenic atoms are in a state where there is no net electron spin. In this case when a radiofrequency field is applied, it can not only

orient the donor by saturation of the forbidden transition, but it can also orient the other arsenic atoms by dipolar coupling with other paramagnetic centres. This would in general produce a positive f_2 and a situation where $f_2 \gg f_4$. In each case, the change in the f_2 is due to the background paramagnetic centres. Such centres could be due to groups of atoms or to anomalous centres. Feher and Gere noted such a background line in their experiments on the relaxation times in P doped silicon [36]). The centre that they observed had a g factor of two and gave a very broad resonance.

To see what restrictions the B_2 and B_4 values impose on the β decay, it will be assumed that the B_2 and B_4 for the outer lines represent a measure of the B_2 and B_4 for a single isolated donor atom. In this case, we have

$$\frac{B_2}{B_4} = \frac{1-\frac{1}{2}\alpha_1-\frac{17}{14}\alpha_2}{1-\frac{5}{3}\alpha_1-\frac{5}{7}\alpha_2} = 1.5\pm 0.3. \tag{43}$$

This gives one linear relationship between α_1 and α_2. The two straight lines corresponding to the limits of error are plotted in fig. 15. A second relationship

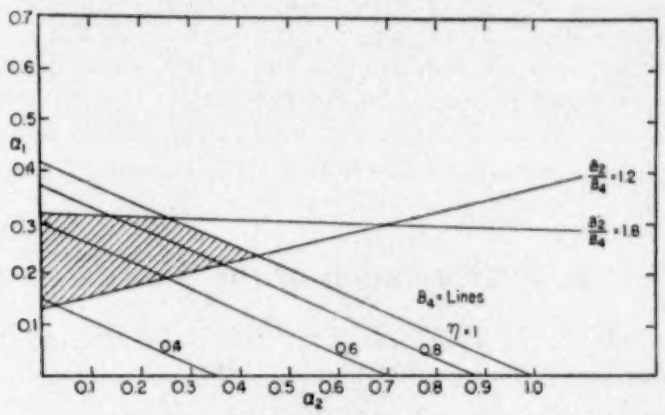

Fig. 15. A graphical representation of the relationship between α_0, α_1 and α_2 imposed by the observed B_2/B_4 and the B_4.

between α_1 and α_2 is given by the expression

$$B_4 = (1-\tfrac{5}{3}\alpha_1-\tfrac{5}{7}\alpha_2)\eta = 0.30\pm 0.03. \tag{44}$$

In this equation η represents an efficiency of orientation; it is the fraction of the As^{76} atoms which act like isolated donors. Since B_4 has a maximum value of 1, it can be concluded from the experimental data that

$$0.3 \leqq \eta \leqq 1.$$

If we could find η, we should have a clue as to why the B_2 for the inner transitions varies as much as it does. In fig. 15 are plotted a series of straight lines which correspond to the B_4 data. The shaded area in fig. 15 gives the region

where the two sets of lines overlap. Thus we conclude that

$$0.1 \leqq \alpha_1 \leqq 0.35, \qquad 0 \leqq \alpha_2 \leqq 0.45.$$

To place further restrictions on the As^{76} β-decay matrix elements, we must take a closer look at the theory. There are in general six nuclear matrix elements which can contribute to a first forbidden transition. In the notation of Kotani [43, 44]), they are

$$\begin{aligned} \eta w &= C_A \int \boldsymbol{\sigma} \cdot \mathbf{r}, & \eta v &= C_A \int i\gamma_5, & & (\lambda = 0) \\ \eta u &= C_A \int i\boldsymbol{\sigma} \times \mathbf{r}, & \eta y &= -C_V \int i\boldsymbol{\alpha}, & \eta x &= -C_V \int \mathbf{r}, \quad (\lambda = 1) \\ & & \eta z &= C_A \int B_{ij} & & (\lambda = z). \end{aligned} \tag{45}$$

The parameter λ corresponds to the angular momentum carried off in the decay by the electron-neutrino system. Five of the matrix elements can be expressed in terms of the unique one, z, by choosing η so that $z = 1$. In the expression for the spectrum shape, angular corelation etc., there occur two particular combinations of matrix elements for which it is advantageous to define a special notation. These combinations are

$$V = v + \xi w, \qquad Y = y - \xi(u + x). \tag{46}$$

The parameter ξ is

$$\xi = \frac{\alpha Z}{2\rho},$$

where ρ is the nuclear radius in units of the electron Compton wavelength and Z is the charge on the nucleus. At present, the data for As^{76} are insufficient to determine all six matrix elements. In order to make an analysis possible, we assume that the modified B_{ij} approximation [43]) is valid; that is, we assume

$$z \neq 0, Y \neq 0, V \neq 0, \qquad \text{but} \qquad x = u = w = 0.$$

In terms of this approximation, the shape factor for the β-ray spectrum is given by

$$C(W) = [Y^2 + V^2 + \tfrac{1}{12}(q^2 + \lambda_1 p^2)], \tag{47}$$

where q is the neutrino momentum, p the electron momentum and λ_1 a relativistic parameter which has been tabulated by Kotani and Ross [45]). We make a non-relativistic approximation and put it equal to 1. In this case, the expressions for P_0, P_1 and P_2 become

$$P_0 = V^2 \int_1^{W_0} F(Z, W) pW (W_0 - W)^2 \, dW, \tag{48}$$

$$P_1 = Y^2 \int_1^{W_0} F(Z, W) pW (W_0 - W)^2 \, dW, \tag{49}$$

$$P_2 = \int_1^{W_0} \tfrac{1}{12}(p^2 + q^2) F(Z, W) pW (W_0 - W)^2 \, dW. \tag{50}$$

Numerical evaluation of these integrals gives

$$\alpha_0 = \frac{V^2}{V^2+Y^2+1.44}, \tag{51}$$

$$\alpha_1 = \frac{Y^2}{V^2+Y^2+1.44}, \tag{52}$$

$$\alpha_2 = \frac{1.44}{V^2+Y^2+1.44}. \tag{53}$$

The normalization relationship between these parameters can be expressed in the form

$$V^2+Y^2 = 1.44\left(\frac{1}{\alpha_2}-1\right). \tag{54}$$

This equation defines a domain in the V, Y plane of points which lie in the region which is compatible with the observed orientation, i.e. in the shaded area in fig. 15. This locus is shown in fig. 16.

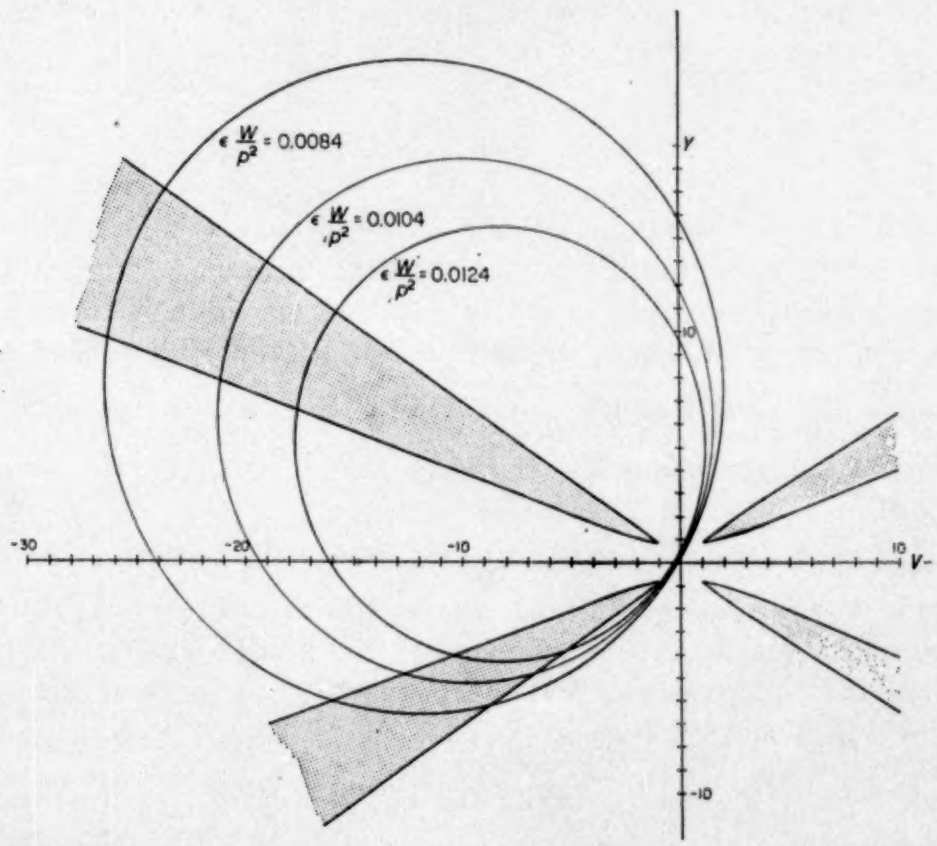

Fig. 16. A graphical representation of the relationship between V and Y imposed by the β-γ angular correlation and this orientation experiment. The circle represents the angular correlation and its experimental limits of error; the shaded area represents the orientation experiment.

In terms of the B_{ij} approximation, the β–γ angular correlation is given by the expression [43])

$$1+\varepsilon P_2(\cos\theta), \tag{55}$$

where

$$\varepsilon = \frac{p^2}{W}\,\frac{R_3k+eWk}{C(W)}, \tag{56}$$

$$R_3k = \lambda_2(\tfrac{1}{56})^{\frac{1}{2}}\{Y-(\tfrac{8}{3})^{\frac{1}{2}}V\}, \tag{57}$$

$$ek = -\frac{\lambda_1}{112}. \tag{58}$$

If this expression is valid, the quantity ε should be very nearly proportional p^2/w. That this is so is shown in table 3. The relationship between Y and V given by the angular correlation can be expressed in the form

$$\left(V+\frac{0.108}{\varepsilon\dfrac{W}{p^2}}\right)^2+\left(Y-\frac{0.067}{e\dfrac{W}{p^2}}\right)=\frac{0.0162}{\left(\varepsilon\dfrac{W}{p^2}\right)^2}-\frac{W}{112\varepsilon\dfrac{W}{p^2}}-\tfrac{1}{12}(p^2+q^2). \tag{59}$$

This is a circle in the V, Y plane. The three circles corresponding to the values

$$\varepsilon\frac{W}{p^2} = 0.0104\pm0.0050$$

are plotted in figs. 16 and 17. This gives the region compatible with the angular correlation.

In terms of the B_{ij} approximation, the circular polarization correlation is given by the expression [43])

$$1+\omega\left(\frac{v}{c}\right)\cos\theta, \tag{60}$$

where

$$\omega = \Big[-\frac{2}{\sqrt{6}}VY+\frac{Y^2}{6}+\frac{5W_0{}^2-3\lambda_1}{240}-\{\tfrac{1}{2}(\tfrac{7}{18})^{\frac{1}{2}}\lambda_4Y+\tfrac{1}{24}W_0\}W + \frac{5+3\lambda_1}{240}W^2-\frac{2\lambda_1}{35}p^2\{\tfrac{5}{2}\cos^2\theta-\tfrac{3}{2}\}\Big]/C(W)\{1+\varepsilon P_2(\cos\theta)\}. \tag{61}$$

If it is assumed that the reported measurement was made for an angle θ of 150° and for an electron total energy $W = 5$, then this equation can be written in the form

$$V^2\omega+0.8167\,VY+Y^2(\omega-0.1667)+1.450\,Y = 0.1978-2.117\,\omega. \tag{62}$$

This equation determines a set of hyperbolae in the V, Y plane. The hyperbolae

for the three values

$$\omega = +0.03, \qquad \omega = +0.17, \qquad \omega = -0.10,$$

are shown in fig. 17. The region between the two hyperbolae corresponding to the limits of error gives the locus of all points consistent with the reported polarization correlation.

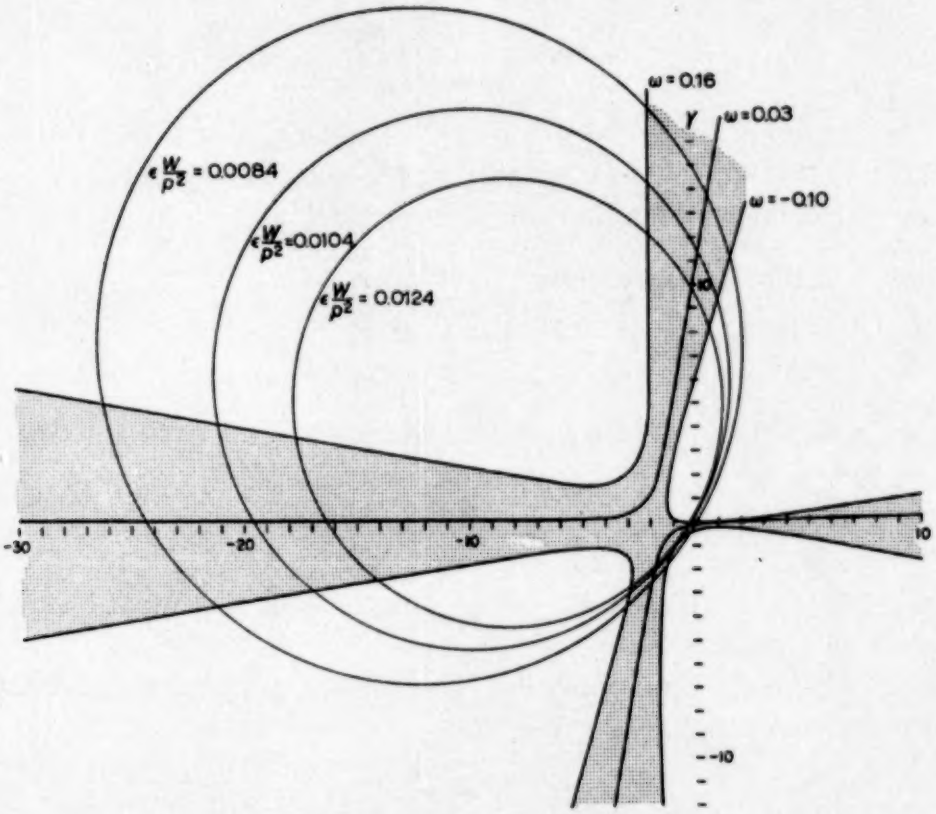

Fig. 17. A graphical representation of the relationship between V and Y imposed by the β-γ angular correlation and the circular polarization correlation experiment. The circles represent the angular correlations and their experimental limits of error; the shaded area between the hyperbolas represents the circular polarization correlation data.

The information from the observed shape of the spectrum is not precise enough to place any further limits on the values of Y and V. At present, there are no complete theoretical expressions for the correlation between the direction of the first forbidden β-ray and the resonance fluorescence of the subsequent γ ray.

If we superimpose all three curves, we find only one region of possible intersection. That is

$$V = -(0.9 \pm -0.2), \qquad Y = (0.9 \pm 0.2). \tag{63}$$

It is difficult, however, to rule out an intersection in the region

$$V = -(18 \pm 5), \qquad Y = 0 \pm 4. \tag{64}$$

Since B_2 and B_4 values are somewhat sensitive to the corrections made for the other gamma rays. The data should be taken with a multi-channel analyzer rather than as was done in this experiment. The first intersection point implies that the orientation efficiency is nearly 1; the second implies that the orientation efficiency is only 50 %.

7. Discussions

There is insufficient evidence at present to decide unambiguously between these two possibilities. Also, there are not enough data to indicate whether or not the B_{ij} approximation is valid for As^{76}. The situation does look very interesting, however, and additional work is worthwhile. We can suggest several experiments which would illuminate the situation. These are

(1) improved measurements of the β–γ angular correction to see if there is any violation of the modified B_{ij} approximations;

(2) better measurements of the polarization correlation: this would be especially useful since the error on the present measurement is quite large;

(3) a more precise measurement of the spectrum shape to see if the beta-ray has a component with a unique forbidden shape factor: this would be particularly useful in ruling out the region around the origin in the V, Y plane;

(4) a nuclear orientation experiment for As^{76} atoms dissolved in an iron matrix [45]). The arsenic could be oriented in an adiabatic demagnetization experiment. This would give an estimate of B_2. If, then, the nuclear resonance of stable As^{75} atoms in the iron matrix could be detected, the value for B_2 could be obtained. This would make it possible to determine the orientation efficiency in the silicon crystal and thus determine the actual value of B_4.

We are particularly indebted to Mr. Fong Chen for reducing the data, calculating the f_2 and f_4 parameters and making the runs on the analogue computer to correct for nuclear relaxation. We wish to thank the Raytheon Company for the gift of the sample.

References

1) E. J. Konopinski in Annual review of nuclear science, ed. by E. Segrè and L. I. Schiff (Annual Reviews, Palo Alto, California, 1959) p. 99
2) Ya. A. Smorodinskii Sov. Phys. Uspek. **2** (1959) 1, 557
3) H. Schopper, Fort. Phys. **8** (1960) 327
4) T. Kotani, Phys. Rev. **114** (1959) 795;
M. Morita and R. S. Morita, Phys. Rev. **109** (1958) 2048
5) F. M. Pipkin and J. W. Culvahouse, Phys. Rev. **109** (1958) 1423
6) C. D. Jeffries, Phys. Rev. **117** (1960) 1056

7) R. K. Girgis, R. A. Ricci and R. Van Lieshout, Nuclear Physics **13** (1959) 461
8) Nuclear data cards prepared by National Research Council, p. 59-5-35 59-5-45
9) R. L. Christensen, H. G. Bennewitz, D. R. Hamilton, J. B. Reynolds and H. H. Stroke, Phys. Rev. **107** (1957) 633
10) E. P. Tomlinson and S. L. Ridgway, Phys. Rev. **88** 170 (1952)
11) P. Hubert, Ann. Phys. **8** (1953) 662
12) J. D. Kurbatov, B. B. Murray and M. Sakai, Phys. Rev. **98** (1955) 674
13) A. V. Pohm, R. C. Waddell and E. N. Jensen, Phys. Rev. **101** (1956) 1315
14) D. R. Hamilton, A. Lemonick and F. M. Pipkin, Phys. Rev. **92** (1953) 1191
15) T. Wiedling, Thesis, University of Stockholm (1956)
16) J. J. Kraushaar and M. Goldhaber, Phys. Rev. **89** (1953) 1081
17) T. Lindqvist and I. Marklund, Nuclear Physics **4** (1957) 189
18) C. F. Coleman, Nuclear Physics **7** (1958) 488
19) E. G. Funk, Jr and M. L. Wiedenbeck, Phys. Rev. **109** (1958) 922
20) C. M. Temmer and N. P. Heydenburg, Phys. Rev. **104** (1956) 967
21) C. F. Coleman, Phil. Mag. **46** (1955) 1135
22) J. R. Pruett, Bull. Am. Phys. Soc. **4** (1959) 57
23) F. K. McGowan and P. H. Stelson, Bull. Am. Phys. Soc. **4** (1959) 232
24) P. H. Stelson and F. K. McGowan, Bull. Am. Phys. Soc. **4** (1959) 232
25) S. L. Ridgway and F. M. Pipkin, Phys. Rev. **87** (1952) 202
26) H. Rose, Phil. Mag. **44** (1953) 739
27) F. Boehm, Z. Phys. **152** (1950) 384
28) M. Spighel, Compt. Rend. **250** (1960) 3626
29) R. R. Lewis and R. B. Curtis, Phys. Rev. **110** (1958) 910
30) M. Morita, R. S. Morita and M. Yamada, Phys. Rev. **111** (1958) 237
31) M. Spighel, J. Phys. Radium **20** (1959) 488
32) S. R. De Groot and H. A. Tolhoek, in Beta- and gamma-ray spectroscopy, ed. by K. Siegbahn (North-Holland Publishing Co., Amsterdam, 1955) Chapt. 19, Part III, p. 613
33) E. Konopinski in Beta- and gamma-ray spectroscopy, ed. by K. Siegbahn (North Holland Publishing Co., Amsterdam 1955) Chap. 10, p. 292.
34) G. Feher, Phys. Rev. **114** (1959) 1219
35) J. W. Culvahouse and F. M. Pipkin, Phys. Rev. **109** (1958) 319
36) G. Feher and E. A. Gere, Phys. Rev. **114** (1959) 1245
37) A. Honig and E. Stupp, Phys. Rev. **117** (1960) 69
38) D. Pines, J. Bardeen and C. P. Slichter, Phys. Rev. **106** (1957) 489
39) R. V. Pound, Phys. Rev. **79** (1950) 685
40) F. M. Pipkin, Phys. Rev. **112** (1958) 935
41) C. O. Hartogh, H. S. Tolhoek and S. R. De Groot, Physica **20** (1954) 1310
42) P. R. Bell in Beta- and gamma-ray spectroscopy, ed. by K. Siegbahn (North Holland Publishing Co., Amsterdam, 1955) Chap. 5, p. 133
43) T. Kotani, Phys. Rev. **114** (1959) 795
44) T. Kotani and M. Ross, Phys. Rev. **113** (1959) 622
45) B. N. Samilov, V. V. Sklyarevskii and E. P. Stepnov, JETP (Soviet Physics) **11** (1960) 261
46) G. E. Bradley, F. M. Pipkin and R. E. Simpson, Bull. Am. Phys. Soc. **5** (1960) 425

8.B:9.A *Nuclear Physics* **27** (1961) 385—394; © *North-Holland Publishing Co., Amsterdam*
Not to be reproduced by photoprint or microfilm without written permission from the publisher

ON HIGH ENERGY NEUTRINO PHYSICS IN COSMIC RAYS

M. A. MARKOV and I. M. ZHELEZNYKH
P. N. Lebedev Physical Institute, Academy of Sciences, Moscow, USSR

Received 3 January 1961

Abstract: The paper is concerned with the problems of detecting high-energy cosmic neutrinos in underground experiments. Various kindred problems of high-energy neutrino physics are discussed, viz. (1) the magnitude of weak-interaction cut-off momentum, (2) muon and electron neutrinos and (3) intermediate boson. It is shown that a reasonable counting rate could be obtained with available equipment.

1. Introduction

Within a few years there will evidently appear a new branch of experimental physics — neutrino physics of medium and high energies — the results of which may prove fundamental in the elementary particle theory in general [1]).

An essential problem of high energy neutrino physics is how far the quadratic increase of the four-fermion interaction cross-section

$$\sigma \propto E_\nu^2, \tag{1}$$

where E_ν is the energy in the centre-of-mass system, continues to hold at very high energies.

From the viewpoint of the formalism of the theory of weak four-fermion interactions this cross-section is correct in principle up to the energy $k_{\text{llm}} \approx 300$ GeV in the centre-of-mass system. At these energies the effect of weak interactions is already comparable with electromagnetic effects [2]).

Unfortunately, such energies (i.e. colliding beams of 10^{11} eV) are unlikely to be accessible to experiment for some years and therefore an answer to this question should be sought in an indirect way.

One of these indirect ways involves the consideration of higher approximations of the perturbation theory of weak interactions permitting arbitrary large momenta in intermediary states. Several similar effects were analyzed theoretically by Pontecorvo [3]), Asanov and Valuev [4]), and Ioffe [5]) under the assumption that the momenta of the intermediate states are cut off at those $k_{\text{max}} (< k_{\text{llm}})$ which yield the maximum value for a given effect without yet contradicting experimental data.

These effects are of the type $\mu^+ + e^- \to e^+ + \mu^-$, $\mu^+ \to e^+ + e^- + e^+$, $\mu^+ \to e^+ + \gamma$, etc.

The immediate conclusion from the estimates obtained tends to show that the momenta in the intermediate states are cut off for some reason which comes into play when the momenta are smaller than those for which the applicability of the perturbation theory could be questioned.

The decay $\mu^+ \to e^+ + e^- + e^+$ proves to be the most critical by the estimates of ref. [4]) for, in accordance with the known experimental limit for this effect $W(3e)/W(e+\nu+\tilde{\nu}) \leqq 4\times 10^{-6}$, the critical momentum should be chosen as

$$k_{\max} < 60 \text{ GeV}.$$

According to Ioffe [5]) the critical momentum $k_{\max}$ for the effect $\mu \to e+\gamma$ is

$$k_{\max} < 50 \text{ GeV}.$$

One of the natural mechanisms capable of cutting off the weak interaction cross-sections at larger than critical lengths

$$l > \sqrt{\frac{G^2}{\hbar c}} \approx 0.6\times 10^{-16} \text{ cm}$$

could be a mechanism involving an intermediate vector boson. Another possibility is a difference in the nature of neutrinos ($\nu_\mu \not\equiv \nu_e$) which would prohibit a number of effects.

Against this background the problems emerging in high energy neutrino physics may be represented as follows:

1) intermediate boson,

2) ν_μ-neutrino and ν_e-neutrino,

3) the magnitude of the cut-off momentum of weak interactions for neutrino-baryon and neutrino-lepton interactions.

It is in this respect that the experimental possibilities of accelerators are considered [1, 6–11]).

In the present paper analysis is made of the corresponding possibilities in cosmic rays †.

We consider only that neutrino flux which originates as a result of the decay of π-mesons produced in the earth's atmosphere. Other sources of high-energy neutrinos, decay of μ-mesons ††, K-mesons etc. in flight, are ignored ††. Nor do we take into account the spectrum of "true"cosmic neutrinos, i.e. neutrinos reaching the earth from the depths of the universe, though here too there may be certain speculative considerations leading to some estimates.

Thus in the present paper we offer the lower estimates of the effects caused by "terrestrial" high-energy neutrinos.

† Different estimates of neutrino effects detectable in principle in cosmic rays were given preliminary consideration by the present authors in ref. [12]).

†† We have been kindly informed by Professor G. T. Zatsepin that the contribution of neutrinos originating in μ-decays may be essential for neutrino energies of the order of several GeV.

In the decay

$$\pi \to \mu + \nu \tag{2}$$

in the system of the π-meson at rest, the neutrino energy is

$$E_{\nu_\mu} \simeq 0.23 M_\pi c^2, \qquad \text{or} \qquad E_\mu \simeq 3.3\, E_{\nu_\mu}. \tag{3}$$

In the following it is assumed that on the average as well the energies of the corresponding neutrino and μ-meson in the laboratory system are connected through the same relation (3).

The energy neutrino spectrum was determined by the corresponding energy μ-meson spectrum. Ref. [13]), for example, offers an experimental energy spectrum of μ-mesons up to energies 10^{12} eV.

The analytical neutrino spectrum can be approximated in the following way:

$$f(E_\nu)\mathrm{d}E_\nu = \begin{cases} 5.5\times 10^{-3}\,\dfrac{\mathrm{d}E_\nu}{E_\nu^{2.5}} & (1\ \mathrm{GeV} < E_\nu < 30\ \mathrm{GeV}), \\ 6\times 10^{-2}\,\dfrac{\mathrm{d}E_\nu}{E_\nu^{3.2}} & (30\ \mathrm{GeV} < E_\nu < 300\ \mathrm{GeV}). \end{cases} \tag{4}$$

Here and in the following energy is expressed in GeV.

A small neutrino interaction cross-section makes it possible to perform experiments deep underground and thus isolate the reactions (with the production of μ-mesons and possibly of electrons) from the neutrinos coming from the lower hemisphere, i.e. passing through the earth. This experimental arrangement can in principle exclude the cosmic-ray background. All known particles with the exception of neutrinos are absorbed by scores of kilometres of the substance and thus are entirely screened by the planet, while the backward scattering of μ-mesons seems little probable (the detailed calculation is in progress).

In underground experiments the relatively small background makes it possible to use large detector "masses", which compensates to a certain degree for the weakness of high energy neutrino fluxes.

It is noteworthy that not only μ-mesons (from the reactions involving neutrino) produced in the detector itself, but also the μ-mesons from the adjoining layers of the ground † ("the cushion") are detected in the experiment. The effect is proportional to the μ-meson path and consequently to the first power of its energy, up to energies of order of 100 GeV. The path of μ-mesons in the "ground" ($Z = 10$, $A = 20$, $\rho = 2$) is taken equal to

$$R = 2.3 \cdot E_\mu \cdot 10^2\ \mathrm{cm}. \tag{5}$$

† Owing to a long path of μ-mesons in the substance, the set up may collect μ-mesons from a stratum equivalent to a 500 m layer of water (the path of a μ-meson of energy 10^{11} eV).

The "effective mass" of the detector can therefore increase essentially. For electrons this effect does not hold.

It will be noted that the background due to natural radioactivity in the ground can be avoided by using detectors with the corresponding energy release threshold.

2. Neutrino-Nucleon Interaction

In the framework of the available experimental data and theoretical concepts the following reactions for neutrino and anti-neutrino from the π-meson decay can be supposed:

$$\begin{aligned}
&\text{(a)} \quad && \nu_\mu + \mathrm{n} \to \mathrm{p} + \mu^-(\mathrm{e}^-), \\
&\text{(b)} \quad && \tilde{\nu}_\mu + \mathrm{p} \to \mathrm{n} + \mu^+(\mathrm{e}^+), \\
&\text{(c)} \quad && \tilde{\nu}_\mu + \mathrm{n} \to \Sigma^- + \mu^+(\mathrm{e}^+), \\
&\text{(d)} \quad && \tilde{\nu}_\mu + \mathrm{p} \to \Sigma^0 + \mu^+(\mathrm{e}^+), \\
&\text{(e)} \quad && \tilde{\nu}_\mu + \mathrm{p} \to \Lambda^0 + \mu^+(\mathrm{e}^+).
\end{aligned} \tag{6}$$

There are experimental grounds to believe that the effects (c), (d) and (e) are less probable than the reaction of the type (b).

Additional π-mesons may be produced in these reactions. Besides, the production of K-mesons is possible if the corresponding selection rules over the strangeness numbers are observed, as for example in

$$\tilde{\nu}_\mu + \mathrm{n} \to \Xi^- + \mu^+(\mathrm{e}^+) + \mathrm{K}^0,$$
$$\nu_\mu + \mathrm{n} \to \mathrm{p} + \mu^-(\mathrm{e}^-) + \mathrm{K}^0.$$

2.1. FORM-FACTORS

It seems worthwhile to investigate the behaviour of the cross-sections of the reactions (6) with increasing energy. The cross-section for type (a) is

$$\sigma_\nu \approx 1.5 \times 10^{-38} E_\nu, \tag{7}$$

and for the other reactions

$$\sigma_{\tilde{\nu}} \approx 0.5 \times 10^{-38} E_{\tilde{\nu}}, \tag{8}$$

if $E \gtrsim 1$ GeV.

The energy spectrum of μ-mesons in the neutrino-caused reactions is uniform and proportional to E_μ^2 in the reactions with the anti-neutrinos.

Therefore, the paths of the μ-mesons produced are estimated as

$$R_1 = 2.3 \left(\tfrac{1}{2} E_\nu - E_{\mathrm{thr}} + \frac{E_{\mathrm{thr}}^2}{2E_\nu} \right) \times 10^2 \text{ cm}, \tag{9}$$

$$R_2 = 2.3 \left(\tfrac{3}{4} E_{\tilde{\nu}} - E_{\mathrm{thr}} + \frac{E_{\mathrm{thr}}^4}{4E_{\tilde{\nu}}^3} \right) \times 10^2 \text{ cm}. \tag{10}$$

Here E_{thr} is the threshold energy for the detection of μ-mesons.

For the μ-meson flux through the surface S in the solid angle π (in the 120° cone) we have

$$N_\mu = \pi \int (\sigma_\nu R_1 + 4\sigma_{\tilde{\nu}} R_2) \frac{f(E_\nu)}{2} \mathrm{d}E_\nu \frac{\rho N_{\text{Avog}}}{2} S, \tag{11}$$

where σ_ν and $\sigma_{\tilde{\nu}}$ are determined from expressions (7) and (8), R_1 and R_2 from eqs. (9) and (10), $f(E_\nu)$ from eq. (4) and $\rho = 2$ is the density of the ground.

The factor $\frac{1}{4}$ appears since the quantities ν_μ and $\tilde{\nu}_\mu$ in the spectrum $f(E_\nu)$ are approximately equal, just as the numbers of neutrons and protons in the ground.

If the threshold for the detection of μ-mesons is equal to 0.5 GeV, one μ-meson will pass through 1000 m² within three days. If the threshold is equal to 5 GeV, one μ-meson will be detected within 5 days.

Now it seems likely that four-fermion interactions involving baryons are cut off (in the vector variant, "weak electrodynamics", for example) by the same Hofstadter form factor, i.e. at lengths

$$l \geqq \frac{\hbar}{M_{\text{n}} C} \approx 2 \times 10^{-14} \text{ cm}.$$

It is natural to assume that the total interaction V—A is cut off by the same form-factor, though this means a new hypothesis.

At neutrino energies of the order of some GeV the cross-sections of the effects of the type $\nu + \text{n} \to \text{p} + \mu(\text{e})$ become of the order of 10^{-38} cm² and for the antineutrino the cross-section decreases by a factor of 3 (see expressions (7) and (8)). At large energies the further growth of the cross-section with energy can only be said to be essentially modified by the form-factor [12]). The application of the extrapolation of the Hofstadter form-factor, not quite legitimate in the region of such large momenta, leads to a constant cross-section for large energy values.

If we take into account the possible role of the form-factor precisely of the type used in ref. [8]), μ-mesons in the centre-of-inertia system will be found to originate in a cone directed "forward" (with the direction of ν_μ and $\tilde{\nu}_\mu$) tapering with the growth of energy. In this case, energy of mesons in the laboratory system is close to the energy of a neutrino and antineutrino, and their paths can be evaluated as

$$R_1 = R_2 = 2.3(E_\nu - E_{\text{thr}}) \times 10^2 \text{ cm}. \tag{12}$$

Using a formula similar to formula (11), we find in the case of "cutting off" at the nucleon length, that one event can be detected within 30 days. In other words, as the cross-section continues to grow with energy, the μ-meson flux through the detector surface becomes roughly 10 times as large.

2.2. ELECTRON AND MUON NEUTRINOS

One of the fundamental problems awaiting experimental and theoretical substantiation is the establishment of the identity or difference of electron and muon neutrinos.

It is not impossible that neutrinos from π-meson decay (muon ν_μ) basically differ[14]) from electron neutrinos, ν_e, i.e. the neutrinos from the nucleon β-decay. In that case electron productions in the reactions (6) is impossible.

Yet in the atmosphere there occurs the decay

$$\mu \to e + \nu_\mu + \nu_e, \tag{13}$$

which yields electron neutrinos as well as muon neutrinos adding to the spectrum (4). If we assume that all μ-mesons are produced in the upper atmospheric strata, the differential energy spectrum of muon neutrinos from the μ-meson decay does not decrease at large neutrino energies ($E_\nu > 5$ GeV) more slowly than $1/E$ (in the directions close to the earth's radius) if compared with the differential energy spectrum (4). Therefore, the spectrum of the electron ν_e falls off more rapidly than the summary spectrum of the muon ν_μ at least by a factor of $(E+1)$. For E_ν of the order of one or several GeV, the ratio is actually less than $1/(E+1)$ because of the production of μ-mesons throughout the atmosphere and their energy losses before the decay.

In the case of different neutrinos there must originate, in any case, $\frac{1}{4}$ or $\frac{1}{5}$ of electrons than if ν_e and ν_μ were basically the same.

But the detection of electrons is a considerably more complex task than that of μ-mesons. Assuming the linear growth of the cross-section with energy and the identity of the neutrinos, one electron is produced in 1000 m^3 of water within 100 days, the neutrino spectrum being $f(E_\nu)$ given by eq. (4). But if the counters covering an area of 1000 m^2 can collect information from a layer of water of about 5 m thick, one event can be detected within 20 days.

3. Intermediate Boson

In the theory of weak interactions much attention has recently been paid to the possibility of the existence of a heavy meson [15]) which desintegrates within a very short time, according to

$$B^\pm \to \mu^\pm + \nu(\tilde{\nu}), \qquad \text{or} \qquad B_\pm \to e^\pm + \nu(\tilde{\nu}). \tag{14}$$

From this point of view, it seems worthwhile [8, 16]) to consider the reactions of the type

$$\begin{aligned} &\nu + X \to B^+ + \mu^-(e^-) + X' \to \mu^+ + \mu^-(e^-) + \nu' + X' \text{ or } e^+ + \mu^-(e^-) + \nu' + X', \\ &\tilde{\nu} + X \to B^- + \mu^+(e^+) + X' \to \mu^- + \mu^+(e^+) + \tilde{\nu}' + X' \text{ or } e^- + \mu^+(e^+) + \tilde{\nu}' + X', \end{aligned} \tag{15}$$

where X represents a nucleus with a charge Z.

These reactions are of the first order with respect to the weak interaction constant. A certain part of the effect, due to the Z^2-dependence of the cross-section, is given by [8])

$$\sigma = \frac{1}{6\pi\sqrt{2}} \frac{Z^2}{(137)^2} g_\nu \left(\ln \frac{2E_\nu q_0}{M^2}\right)^3, \qquad E_\nu \gg \frac{M^2}{2q_0} \approx 2\ \text{GeV}. \tag{16}$$

For $Z = 10$ we have

$$\sigma = 10^{-36} \times (\ln \tfrac{1}{2} E_\nu)^3. \tag{17}$$

The μ-meson flux from the "cushion" (from the neutrinos of $E > 10$ GeV) in the ground can be estimated by

$$N_\mu = 3\sigma_0 \pi \frac{N_{\text{Avog}}\rho}{A}\, 2.3 \times 10^2 \times S \int_{10}^{300} f(E_\nu) \tfrac{1}{3} \left(E_\nu - 2E_{\text{thr}} + \frac{E_{\text{thr}}^2}{E_\nu}\right) (\ln \tfrac{1}{2} E_\nu)^3 \mathrm{d}E_\nu. \tag{18}$$

When $S = 10^3$ m^2, there are 2 mesons per day detected, the threshold being 1 GeV.

It will be emphasized that in a detector of 1m thickness (without a "cushion"), the number of events is less by a factor of ≈ 30.

It is shown by the estimates that the μ-meson fluxes can be the same in the case of an intermediary meson or a linear growth of the νN cross-section with energy.

Two possibilities, the intermediate meson or the linear growth of the cross-section $\nu + \mathrm{N} \to \mathrm{N} + \mu$, can be discriminated if a thorough analysis is made of the dependence of the number of the events observed on the detection threshold, since the analytical dependences on the threshold of the μ-meson fluxes (11) and (18) are different in principle.

Yet it is more reliable to make measurements in ores with different Z. In the case of an intermediate meson the flux changes with the change of the factor Z^2/A.

4. Neutrino-Lepton Interactions

For the neutrino-lepton interactions of the type $\nu + \mathrm{e} \to \mu + \nu$, the expressions for the cross-section in the centre-of-mass system have the same form as relation (1). If there are fairly plausible considerations with respect to the restriction of the energy growth of the cross-sections of four-fermion lepton-baryon interactions, the restriction of lepton-lepton interactions by the characteristic nucleon or pion lengths can now be regarded as little probable from the viewpoint of generally accepted theoretical concepts.

A different situation arises in a non-linear conception like the Heisenberg theory.

The question is how do neutrino-lepton interactions actually behave as energy increases?

The cross-section (1) in the laboratory system of coordinates assumes the form

$$\sigma \propto mE_\nu.$$

Consequently the cross-sections for the (νe) interactions at the given neutrino energy are smaller by a factor of 10^3 than the corresponding neutrino-nucleon interactions, which makes any attempt to detect $(\nu e)-(\nu\mu)$ interactions meaningless for the time being.

There are effects of interaction of neutrinos on "bound" electrons which retain a higher energy dependence of the cross-section at higher energies in the laboratory system of coordinates as well.

We have pointed out one example of the effect of this type [12]), viz. the neutrino ν in the field of the nucleus X produces, in scattering, the pair, $e^-\mu^+$, e^-e^+, $\mu^+\mu^-$, μ^-e^+, i.e. the effect of the form

$$\nu+X \to X'+e^-+e^++\nu'.$$

Chou Kuang-chao (Dubna) evaluated this effect. He obtained the cross-section in the form

$$\sigma \propto G^2 \frac{Z^2}{(137)^2} E_\nu^2 \ln \frac{E_\nu}{m}. \tag{19}$$

As was pointed out by L. B. Okun and I. Ya. Pomeranchuk, the quadratic growth of the cross section is cut off by the form-factor of the nucleus, and the cross-section above the corresponding energies shows a linear and not a quadratic growth with the neutrino energy.

Despite the additional logarithmic factor, there being a small numerical coefficient does not make this effect superior to that of direct lepton-lepton [$(\nu e)-(\nu\mu)$, for example)] interaction. True, it is difficult to isolate the $(\nu e)-(\nu\mu)$ interaction against the background of the $(\nu N)-(\mu N)$ effects. Perhaps the Z^2-dependence of the effect indicated above will prove useful in the future. It is not impossible that the qualitative peculiarity of this effect manifest in lepton-pair production can also be used.

5. Neutrino From Cosmic Space

With the isotropy of sources and the isotropic distribution of cosmic rays in the galaxy, the neutrino flux in terrestrial conditions is bound to be determined entirely by the flux of neutrinos produced in the atmosphere.

Yet observations seemed to testify in favour of the theory of the production of cosmic particles in the shells of super new and new stars [17]). According to radio-astronomical data there are many relativistic electrons in the expanding shells of these stars. In the Crab nebula, the shell electron energy is set down at 10^{50} to 10^{53} GeV ($E > 0.25$ GeV), the electron spectrum falling to $1/E-1/E^{1,5}$.

If these electrons were produced in nuclear collisions, there must be three neutrinos for each electron of approximately the same energy. From the maximum data (and assuming that electrons have been accumulating for 900 y, $R = 5\times10^{21}$ cm, $E_{max} = 10^3$ GeV) we can find that a high-energy neutrino flux from the Crab nebula to the earth might have the spectrum $(3\times10^{-5}/E)$ cm$^{-2}\cdot$sec^{-1}. In any case the presence of high-energy photons beyond the atmosphere could be an argument in favour of the existence of, at least, the same fluxes of true cosmic high-energy neutrinos.

Thus, this paper points to the possibility of detecting neutrinos in cosmic rays.

Since neutrinos in modern accelerators usually have energies of the order of 1 GeV, the question of the behaviour of the neutrino-nuclear (νN) interaction cross-section in the energy region from 10 to 100 GeV can be solved experimentally with cosmic rays (see table 1).

TABLE 1

Comparison of cosmic rays with accelerators

Event		Cosmic rays (detector area = 1000 m^2 $E_p^{max} = 3\times10^{11}$ eV $E_{thr} = 0.5$ GeV)	Accelerators (detector area 1 m^3 of Pb, magnetic focussing 10^{11} protons/sec at $E_p = 10^{10}$eV)
Intermediate boson ($M \approx$ K-mass)		> two per day	
$\nu+N \rightarrow N'+\mu$	Linear growth of cross-section with energy	> one per three days	$\approx$ one per day
	Hofstadter form-factor	> one per month	$\approx$ one per day

Experiment with neutrinos in cosmic rays can furnish some information on the existence of the intermediary boson.

Finally, the upper limit can be established for high energy neutrino fluxes coming from the depths of cosmic space and certain cosmogonic hypotheses be verified thereby.

In conclusion it seems worthwhile to compare some estimates for the events induced by neutrinos in cosmic rays and accelerators.

Note added in proof: If the cross-section for neutrino absorption has a resonance behaviour due to the intermediate boson, as has been pointed out by Glashov (Phys. Rev. **118** (1960)316) and Kinoshita (Phys. Rev. Letters **4** (1960)378), then the counting rates in the underground experiment may be higher than those shown in table 1. On the other hand, we would like to emphasize the fact that the measurements of the total weak process cross-

sections could compete to some extent with electrodynamic experiments on the high-energy form-factor behaviour provided the nature of these form-factors is the same. Finally, it should be noted that the figures in table 1 will increase if one uses the neutrino spectra from the decay of π- and μ-mesons in the atmosphere, which have been recently calculated by Zatsepin and Kuzmin (JETP, in the press).

References

1) M. A. Markow, Hyperonen und K-mesonen (Verlag der Wissenschaften Berlin, 1960) p. 292
2) D. I. Blokhintsev, Nuovo Cim. **9** (1958) 925; Usp. Fiz. Nauk **62** (1957) 381
3) B. M. Pontecorvo, JETP **33** (1957) 549
4) P. A. Asanov and B. N. Valuev, Preprint of JINR D-577, Dubna (1960)
5) B. L. Ioffe, JETP **38** (1960) 1608; thesis
6) B. M. Pontecorvo, JETP **37** (1959) 1751; Proc. IX Int. Conf. High Energy Physics, Kiev 1959
7) M. Schwartz, Phys. Rev. Letters **4** (1960) 306
8) T. D. Lee and C. N. Yang, Phys. Rev. Letters **4** (1960) 307
9) N. Cabibbo and R. Gatto, Nuovo Cim. **15** (1960) 304
10) D. G. Fakirov, Diploma Moscow State University (1958)
11) I. Polubarinov, preprint JINR D-577, Dubna (1960);
V. S. Barashenkov and Hsien Ding-chang, preprint JINR D-577, Dubna (1960)
12) I. M. Zheleznykh, Diploma Moscow State University, Moscow (1958)
13) F. Ashton *et al.*, Nature **185** (1960) 364
14) M. A. Markov, Hyperons and K-mesons (Gosydarstvennoye Izdatelstvo Fiziko-Matematicheskoy Literatury Moscow, 1958) p. 295.
15) R. P. Feynman and M. G. Gell-Mann, Phys. Rev. **109** (1958) 193
16) B. Pontecorvo and R. Ryndin, IX Int. High Energy Physics Conf. Kiev 1959
17) V. L. Ginsburg, Usp. Fiz. Nauk **51** (1953) 343, **62** (1957) 37

1.B:8.B *Nuclear Physics* **27** (1961) 395—404; © *North-Holland Publishing Co., Amsterdam*
Not to be reproduced by photoprint or microfilm without written permission from the publisher

EFFECTS OF PARITY NON-CONSERVING INTERNUCLEON POTENTIALS ON THE PHOTOEFFECT IN H^2 AND H^3

R. J. BLIN-STOYLE
Clarendon Laboratory, Oxford University, Oxford, England
and
HERMAN FESHBACH
Department of Physics, Massachusetts Institute of Technology, Cambridge, Massachusets †

Received 4 April 1961

Abstract: Several effects of non-parity conserving potentials on the photodisintegration of the deuteron, on radiative neutron capture by hydrogen and deuterium have been estimated employing the non-parity conserving potential derived by one of us (R.B.S.). Observation of the correlation of the circular polarization with the direction of emission of the gamma rays emitted in radiative neutron capture by deuterium appears to be the most promising experiment.

1. Introduction

There is as yet no evidence for parity non-conservation in the strong nuclear interactions. Most of the experiments have been performed with light or medium weight nuclei [1, 2, 3]) and because of our rather limited knowledge of nuclear wave functions it is not possible to make a definitive interpretation of these negative results. Some idea of the complexity of the situation is indicated by the fact that there is no static single particle parity non-conserving potential [4]). So far it appears safe to say that the Lee-Yang [5]) parameter F has the upper bound [6])

$$F \leqq 10^{-4}-10^{-5}.$$

It is the object of the present paper to investigate the effects of parity non-conserving potentials on the neutron-proton system and to consider some of the possible experiments for the determination of their existence and, hopefully their strength. It is obvious that for such a simple system it will be relatively easy to relate the experimental results directly to the PNC potential. Moreover we would obtain direct evidence on the parity non-conserving potential between two nucleons.

Wilkinson [1]) has pointed out that the most sensitive experiments for our purpose here are those which involve electromagnetic transitions between

† This work is supported in part through AEC Contract AT (30-1)-2098, by funds provided by the U.S. Atomic Energy Commission, the Office of Naval Research and the Air Force Office of Scientific Research.

nuclear states since these give rise to effects which are linear in the strength of the PNC potential. In the case of the neutron-proton system the possible experiments include:

(A) Photodisintegration of the deuteron with polarized X-rays. The asymmetry of the emergent nucleons with respect to the plane of polarization is observed.

(B) Photodisintegration of the deuteron with unpolarized X-rays. The polarization of the emergent nucleons in the direction of the incident X-rays is observed

(C) Radiative capture of neutrons by hydrogen. The circular polarization of the emergent X-rays with respect to their direction of propogation is observed.

Process C is also considered for neutrons captured by deuterium to form H^3. This process is interesting because of a special circumstance; the very small magnetic dipole cross-section for this capture process.

For the theoretical evaluation of the cross-sections for the various processes A, B, and C it is convenient to use a specific PNC potential. We shall use the static potential which follows [4]) from the current-current interaction term in Feynman-Gell-Mann [7]) theory of weak interactions:

$$V_{\mathrm{PNC}} = \tfrac{1}{2} W(x)(\boldsymbol{\sigma}_1 \times \boldsymbol{\sigma}_2) \cdot \hat{\mathbf{x}}[\tau_{1z}\tau_{2z} - \boldsymbol{\tau}_1 \cdot \boldsymbol{\tau}_2], \tag{1}$$

where

$$W(x) = \frac{Gf^2\mu^3}{\pi\hbar c}\left[\frac{1}{x^3} + \frac{2}{x^4} + \frac{1}{x^5}\right] \mathrm{e}^{-2x}, \tag{2}$$

$$\mathbf{x} = \mu\mathbf{r}, \qquad \mathbf{r} = \mathbf{r}_1 - \mathbf{r}_2,$$

while $1/\mu$ is the meson Compton wavelength and G is the weak interaction coupling constant, $f^2 \approx 0.08$, the renormalized pseudovector meson-nucleon coupling constant. For the n–p system $\tau_{1z}\tau_{2z}$ equals -1. Thus for the deuteron ($T = 0$) $[\tau_{1z}\tau_{2z} - \boldsymbol{\tau}_1 \cdot \boldsymbol{\tau}_2]$ equals 2 while for the $T = 1$ state this bracket is -2. The effective coupling constant † is thus

$$W_0 = \frac{Gf^2\mu^3}{\pi\hbar c} = 0.57 \times 10^{-6}\ \mathrm{MeV}.$$

It should be noted that this potential is not a necessary consequence of the non-parity conservation in weak interactions but it is a possible consequence and it certainly can serve as a reasonable representation of such a potential whatever its source.

In this paper order of magnitude estimates of effects A, B and C will be

† If the schizon theory of weak interactions is adopted, in which the self interaction of neutral currents is allowed, the term $\tau_{1z}\tau_{2z}$ in the isobaric spin factor does not appear. In this case the effective coupling constant W_0 has to be multiplied by $\frac{3}{2}$ for the $T = 0$ state and $\frac{1}{2}$ for the $T = 1$ state.

obtained. To this end we shall consider only dipole induced transitions leading to the $^1S_0$, $^3P_{0,1,2}$ states in the continuum from the deuteron. We shall neglect tensor forces, so that the deuteron will be assumed to be in a pure $^3S_1$ state aside from the parity admixture induced by the PNC potential (1). We shall be completely qualitative in our discussion of the n-d radiative capture. More precise results for both the two-body and three-body cases are now being evaluated by F. Partovi.

2. Theory

The states of the two-nucleon system when the PNC potential is included are specified by the total angular momentum J, its z component, the total isobaric spin T, as well as T_z and of course the energy. The total spin S is no longer a constant of the motion. A state with a given value of J will now be a combination of all the orbital and spin states consistent with the values of J and T. The ground state of the deuteron, a $J = 1$ state, is a mixture of the $^3S_1$, $^3D_1$ and $^1P_1$ states. The $J = 0$ state is a mixture of the $^1S_0$ and $^3P_0$ states. There is no parity impurity in the $J = 1$, $T = 0$ state, the $^3P_1$. The $^3P_2$ state may be mixed with the $^1D_2$.

In our considerations below we shall neglect the effects of the $^3D_1$ and $^1D_2$ states. We therefore require appropriate representations for the $^1P_1$ and $^3P_0$ admixtures to the $^3S_1$ and $^3S_0$ states respectively.

(a) *The case* $J = 1, T = 0$

The wavefunction of the deuteron is

$$\psi_D = [R_S^{(1)}(r) + \tfrac{1}{2} i\sqrt{3}(\sigma_1 - \sigma_2) \cdot \hat{\mathbf{r}} R_P^{(1)}(r)]\chi_m^{(1)}, \tag{2}$$

where $R_S^{(1)}$ and $R_P^{(1)}$ are the radial wave functions for the $^3S_1$ and $^1P_1$ components, and $\chi_m^{(1)}$ the normalized triplet spin wave function. The numerical factors modifying $R_P^{(1)}$ have been chosen so that

$$\langle \psi_D | \psi_D \rangle = \int_0^\infty r^2 dr [(R_S^{(1)})^2 + (R_P^{(1)})^2] \tag{3}$$

and so that the equation satisfied by $R_P^{(1)}$ is

$$[E - T - V_c(^1P_1)] R_P^{(1)} = \tfrac{2}{3}\sqrt{3}\, W R_S^{(1)}, \tag{4}$$

where T is the radial kinetic energy, and $V_c(^1P_1)$ the central potential in the singlet P state. The function $R_P^{(1)}$ satisfies the usual finiteness condition at the origin and asymptotically must be proportional to $e^{-\alpha r}/r$, with $\alpha = \sqrt{(M\varepsilon/\hbar^2)}$, where ε is the deuteron binding energy.

(b) *The case* $J = 0, T = 1$

The wave function is

$$\psi = [R_S^{(0)} + \tfrac{1}{2} i(\sigma_1 - \sigma_2) \cdot \hat{\mathbf{r}} R_P^{(0)}]\chi^{(0)}, \tag{5}$$

$\chi^{(0)}$ is the normalized singlet spin wave function. The equation satisfied by $R_P^{(0)}$ is

$$[E - T - V_c(^3P_0)]R_P^{(0)} = 2WR_S^{(0)}. \tag{6}$$

For the case in which $R_S^{(0)}$ is the principal component of (5), $R_P^{(0)}$ is asymptotically proportional to $n_1(kr)$, where n_1 is the spherical Neumann function and $k^2 = ME/\hbar^2$. This P state parity impurity generated by the PNC potential acting on the $^1S_0$ state is of particular importance at low energies where the $^1S_0$ state is large and where the $^3P_0$ state would otherwise be very small. In the complementary situation when the dominant state is $^3P_0$ there is no energy region in which the effects of the parity impurity $^1S_0$ are not just a very small correction to those already obtained with the $J = 0$ state in which the $^1S_0$ state is the principal component. We shall therefore not include it in the discussion below.

It is now a relatively straightforward matter to determine the transition matrix T which, operating on the initial triplet spin wave function, yields the final amplitude for the photodisintegration of the deuteron. In the approximation in which we neglect the centre-of-mass momentum given to the system by the incident photon the only vectors occurring in the problem are the relative nucleon momentum $\mathbf{k}$ in the final state, a unit vector $\mathbf{e}$ in the direction of the electric field of the incident radiation, a unit vector $\mathbf{h}$ in the direction of the magnetic field and finally the spin operators $\boldsymbol{\sigma}_1$ and $\boldsymbol{\sigma}_2$. If the space dependence of the final state is chosen to consist asymptotically of a plane wave plus an incoming wave, we may define the transition matrix T by the equation

$$\langle \Psi_f, [\mathbf{e} \cdot \mathbf{r} + (\mu_1 - \mu_2)(\boldsymbol{\sigma}_1 - \boldsymbol{\sigma}_2) \cdot \mathbf{h}]\Psi_i \rangle = \langle \chi_f, T\chi_i \rangle, \tag{7}$$

where χ_f is the final spin wave function, which we take to be triplet or singlet in accordance with the spin dependence of the dominant state in Ψ_f. In terms of T the differential cross section for photodisintegration becomes

$$\frac{1}{4\pi}\frac{d\sigma}{d\Omega} = \frac{1}{12}\frac{e^2}{\hbar c}\left(\frac{Mc}{\hbar}\right)^2 \frac{kE_\gamma}{Mc^2}[\mathrm{Tr}(T^\dagger T) - \langle \chi^{(0)}, T^\dagger T \chi^{(0)} \rangle]. \tag{8}$$

The usual requirements of rotational invariance can be applied to determine the possible forms of T. Dividing T into the parity conserving and parity non-conserving parts T_{PC} and T_{PNC}, we find

$$iT_{PC} = A\mathbf{e} \cdot \hat{\mathbf{k}} + iB(\boldsymbol{\sigma}_1 + \boldsymbol{\sigma}_2) \cdot (\mathbf{e} \times \hat{\mathbf{k}}) + C[\boldsymbol{\sigma}_1 \cdot \mathbf{e}\, \boldsymbol{\sigma}_2 \cdot \hat{\mathbf{k}} + \boldsymbol{\sigma}_1 \cdot \hat{\mathbf{k}}\, \boldsymbol{\sigma}_2 \cdot \mathbf{e}] + iD(\boldsymbol{\sigma}_1 - \boldsymbol{\sigma}_2) \cdot \mathbf{h}, \tag{9}$$

$$iT_{\mathrm{NPC}} = iA'\mathbf{h}\cdot\hat{\mathbf{k}}+B'(\boldsymbol{\sigma}_1+\boldsymbol{\sigma}_2)\cdot(\mathbf{h}\times\hat{\mathbf{k}}) +iC'[\boldsymbol{\sigma}_1\cdot\mathbf{h}\,\boldsymbol{\sigma}_2\cdot\hat{\mathbf{k}}+\boldsymbol{\sigma}_1\cdot\hat{\mathbf{k}}\,\boldsymbol{\sigma}_2\cdot\mathbf{h}]+D'(\boldsymbol{\sigma}_1-\boldsymbol{\sigma}_2)\cdot\mathbf{e}. \quad (10)$$

The values of the coefficients in (9), keeping in mind the various approximations mentioned above are,

$$A = \tfrac{7}{12}e^{i\delta_2}M_2+\tfrac{1}{4}e^{i\delta_1}M_1+\tfrac{1}{6}e^{i\delta_0}M_0, \quad (11)$$

$$B = \tfrac{5}{24}e^{i\delta_2}M_2-\tfrac{1}{8}e^{i\delta_1}M_1-\tfrac{1}{12}e^{i\delta_0}M_0, \quad (12)$$

$$C = -\tfrac{1}{24}e^{i\delta_2}M_2+\tfrac{1}{8}e^{i\delta_1}M_1-\tfrac{1}{12}e^{i\delta_0}M_0, \quad (13)$$

$$D = (\mu_1-\mu_2)e^{i\delta_S}M_S. \quad (14)$$

Here δ_2, δ_1, δ_0 are the phase shifts for the $^3P_2$, $^3P_1$, $^3P_0$ states respectively; δ_S the phase shift for the $^1S_0$ state. The M_i are real radial integrals. If the radial functions for the three ^3P_i states are F_{Pi} and are normalized so as to approach $\sin(kr-\frac{1}{2}\pi+\delta_i)/kr$, we have

$$M_i = \int_0^\infty F_{Pi}\,r R_S^{(1)} r^2\,dr. \quad (15)$$

Similarly we have

$$M_S = \int_0^\infty R_S^{(0)} R_S^{(1)} r^2\,dr. \quad (16)$$

The values of the coefficients in (10) are

$$A' = \sqrt{3}(\mu_1-\mu_2)[\tfrac{7}{6}M'_2e^{i\delta_2}-\tfrac{1}{2}M'_1e^{i\delta_1}+\tfrac{1}{3}M'_0e^{i\delta_0}], \quad (17)$$

$$B' = \sqrt{3}(\mu_1-\mu_2)[-\tfrac{5}{12}M'_2e^{i\delta_2}-\tfrac{1}{4}M'_1e^{i\delta_1}+\tfrac{1}{6}M'_0e^{i\delta_0}], \quad (18)$$

$$C' = \sqrt{3}(\mu_1-\mu_2)[-\tfrac{1}{12}M'_2e^{i\delta_2}-\tfrac{1}{4}M'_1e^{i\delta_1}-\tfrac{1}{6}M'_0e^{i\delta_0}], \quad (19)$$

$$D' = [-\tfrac{1}{2}\sqrt{3}\,M'_S+\tfrac{1}{6}M''_S]e^{i\delta_S}, \quad (20)$$

where

$$M'_i = \int_0^\infty F_{Pi}R_P^{(1)}r^2\,dr, \quad (21)$$

$$M'_S = \int_0^\infty R_S^{(0)}rR_P^{(1)}r^2\,dr, \quad (22)$$

$$M''_S = \int_0^\infty R_P^{(0)}rR_S^{(1)}r^2\,dr. \quad (23)$$

3. Parity Non-conservation in Deuteron Photodisintegration

It is a comparatively simple matter to calculate the disintegration cross section for polarized X-rays. Employing eqs. (8), (9) and (10) we obtain

$$\mathrm{Tr}(T^\dagger T)-\langle\chi^0T^\dagger T\chi^0\rangle = 8|B|^2+8|C|^2+4|D|^2+(\mathbf{e}\cdot\hat{\mathbf{k}})^2[3|A|^2-8|B|^2+4|C|^2+2\mathrm{Re}(A^*C)] -2(\mathbf{e}\cdot\hat{\mathbf{k}})(\mathbf{h}\cdot\hat{\mathbf{k}})\mathrm{Im}[3A^*A'+8B^*B'+2(A^*C'+A'C^*)+4C^*C']. \quad (24)$$

The terms in unprimed quantities only come from T_{PC} and are the familar results given for example by Rarita and Schwinger [8]). The terms bilinear in the primed and unprimed quantities arise from the interference between T_{PC} and T_{PNC}. It is therefore linear in W_0. Note that it is multiplied by the only possible pseudo-scalar in the dipole approximation, namely $(\mathbf{e}\cdot\hat{\mathbf{k}})\,(\mathbf{h}\cdot\hat{\mathbf{k}})$. This term produces an asymmetry in the disintegration cross-section with respect to the plane of polarization.

The magnitude of the asymmetry with respect to the plane of polarization of the X-rays is given by

$$A(\vartheta,\varphi)=\frac{\frac{d\sigma}{d\Omega}(\vartheta,\varphi)-\frac{d\sigma}{d\Omega}(\vartheta,-\varphi)}{\frac{d\sigma}{d\Omega}(\vartheta,\varphi)+\frac{d\sigma}{d\Omega}(\vartheta,-\varphi)}, \tag{25}$$

where ϑ is the angle between $\hat{\mathbf{k}}$ and $\boldsymbol{\varkappa}=\mathbf{e}\times\mathbf{h}$ and φ is the angle between the $(\boldsymbol{\varkappa},\mathbf{h})$ plane and the $(\boldsymbol{\varkappa},\hat{\mathbf{k}})$ plane. Substituting the explicit expressions for A to C' given in eqs. (11)–(23) we obtain

$$A(\vartheta,\varphi)=\frac{\gamma\sin^2\vartheta\sin\varphi\cos\varphi}{\alpha+\beta\sin^2\vartheta\sin^2\varphi}, \tag{26}$$

where

$$\alpha=\tfrac{13}{36}(M_2)^2+\tfrac{1}{4}(M_1)^2+\tfrac{1}{9}(M_0)^2-\tfrac{1}{2}M_2M_1\cos(\delta_2-\delta_1)-\tfrac{2}{9}M_2M_0\cos(\delta_2-\delta_0)+4(\mu_1-\mu_2)^2M_S^2, \tag{27}$$

$$\beta=\tfrac{7}{12}(M_2)^2+\tfrac{1}{4}(M_1)^2+\tfrac{3}{2}M_2M_1\cos(\delta_2-\delta_1)+\tfrac{2}{3}M_2M_0\cos(\delta_2-\delta_0), \tag{28}$$

$$\gamma=-\sqrt{3}(\mu_1-\mu_2)[3\sin(\delta_2-\delta_1)(M'_2M_1+M'_1M_2)+\tfrac{4}{3}\sin(\delta_2-\delta_0)(M'_2M_0-M_2M'_0)]. \tag{29}$$

In the energy range for which these calculations are valid, $\alpha\ll\beta$, so that

$$A\approx\frac{\gamma}{\beta}\cot\varphi. \tag{30}$$

We see that the strength of the asymmetry with respect to the $(\boldsymbol{\varkappa},\mathbf{h})$ plane is measured by γ/β. By making the angle φ small we can enhance the relative strength of the parity non-conserving effects. This enhancement is limited however, by the finite value of α to $\frac{1}{2}(\beta/\alpha)^{\frac{1}{2}}$.

The factor γ/β has been evaluated approximately with the aid of a number of simplifying assumptions. First, we have assumed

$$M_i\approx\mathcal{M},\qquad M'_i\approx\mathcal{M}'. \tag{31}$$

This is equivalent to placing all the F_{Pi} in eq. (15) and eq. (21) equal to a

common function

$$F_{Pi} \approx F.$$

Under approximation (31), eqs. (28) and (29) become

$$\beta \approx \mathscr{M}^2[\tfrac{5}{6}+\tfrac{3}{2}\cos(\delta_2-\delta_1)+\tfrac{2}{3}\cos(\delta_2-\delta_0)],$$
$$\gamma \approx -3^{\frac{1}{2}}(\mu_1-\mu_2)\mathscr{M}\mathscr{M}'[6\sin(\delta_2-\delta_1)].$$

From the equation satisfied by $R_P^{(1)}$ we can approximate $\mathscr{M}'$ as follows:

$$\mathscr{M}' \approx -\frac{2}{3^{\frac{1}{2}}}\frac{1}{\hbar\omega}\int_0^\infty FWR_S^{(1)}r^2\,dr, \tag{32}$$

so that finally

$$\frac{\gamma}{\beta} \approx \frac{12(\gamma_1-\gamma_2)\sin(\delta_2-\delta_1)}{\frac{5}{6}+\frac{3}{2}\cos(\delta_2-\delta_1)+\frac{2}{3}\cos(\delta_2-\delta_1)}\,\frac{(\hbar/2Mc)\int_0^\infty FWR_S^{(1)}r^2\,dr}{\hbar\omega\int_0^\infty FrR_S^{(1)}r^2\,dr}, \tag{33}$$

where

$$\mu_i = \frac{\hbar}{2Mc}\gamma_i.$$

It is now a relatively easy matter to evaluate γ/β. For $R_S^{(1)}$ the Moravczik [9]) wave function (App. 3) was employed. The function F was taken to be the spherical Bessel function of order one (i.e. effects of interaction in the final state are omitted.) The phase shifts δ_i were taken from the recent analysis by Breit, Hull, Lassels and Pyatt, Jr. [10]). The results are shown in fig. 1). It is

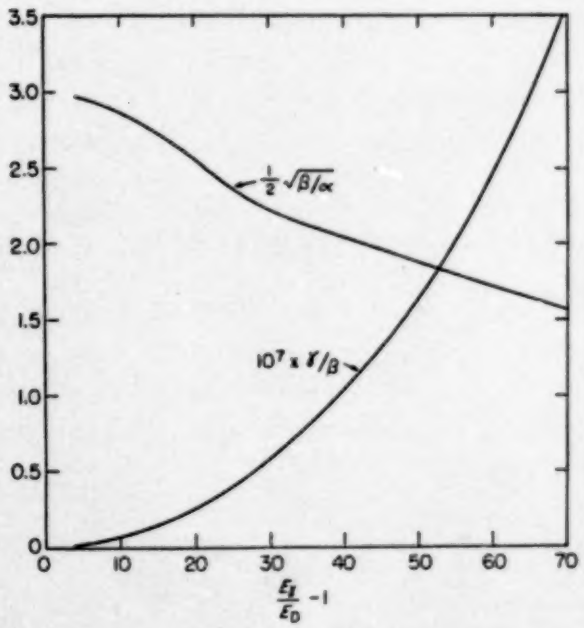

Fig. 1. The magnitude and enhancement factors are shown. Definitions of γ/β and $\frac{1}{2}\sqrt{\beta/\alpha}$ are given in eqs. (27)-(29). See also eq. (33). E_γ and E_D are the gamma ray energy and binding energy of the deuteron respectively.

clear that observation of this effect is very difficult since γ/β is small and the enhancement factor is never very large.

We turn next to the experiment in which the incident X-rays are unpolarised and observation is made of the polarization of the emergent nucleons with respect to the direction of incidence of the X-rays. The quantity of interest is therefore

$$P = \frac{\mathrm{Tr}(T^\dagger \boldsymbol{\sigma}_1 \cdot \boldsymbol{\varkappa} T) - \langle \chi^0, T^\dagger \boldsymbol{\sigma}_1 \cdot \boldsymbol{\varkappa} T \chi^0 \rangle}{\mathrm{Tr}(T^\dagger T) - \langle \chi_0, T^\dagger T \chi^0 \rangle}, \tag{34}$$

where an average over the polarization of the incident X-rays is understood in both numerator and denominator. Then

$$\begin{aligned} &\mathrm{Tr}(T^\dagger \boldsymbol{\sigma}_1 \cdot \boldsymbol{\varkappa} T) - \langle \chi^{(0)}, T \boldsymbol{\sigma}_1 \cdot \boldsymbol{\varkappa} T \chi^{(0)} \rangle \\ &\quad = 8\,\mathrm{Re}\,\{\tfrac{1}{2}\sin^2\vartheta (B^* A' - A^* B') - \cos^2\vartheta (B^* B' + B^* C' - C^* B') \\ &\qquad + (1+\sin^2\vartheta) C^* C' + \cos\vartheta [D^* (B' - C') - D'^* (C + B)]\}. \end{aligned} \tag{35}$$

Substituting from eqs. (11)—(20) and employing approximations (31) and (32), we obtain

$$\begin{aligned} P = -\frac{8}{3}\frac{\mu_1 - \mu_2}{\hbar\omega}\frac{\int_0^\infty FW R_S^{(1)} r^2\,\mathrm{d}r}{\int_0^\infty F r R_S^{(1)} r^2\,\mathrm{d}r}\,&\frac{\sin^2\vartheta + \frac{1}{6}(\mu_1 - \mu_2)(M_S/\mathscr{M})\cos\vartheta[\cos(\delta_0 - \delta_S) - \cos(\delta_2 - \delta_S)]}{\sin^2\vartheta + \frac{8}{3}(\mu_1 - \mu_2)^2 (M_S/\mathscr{M})^2} \\ &+ \frac{(4/3^{\frac{3}{2}})\cos\vartheta[(M'_S/\mathscr{M}) - (1/3^{\frac{3}{2}})(M''_S/\mathscr{M})][\cos(\delta_0 - \delta_S) - \cos(\delta_2 - \delta_S)]}{\sin^2\vartheta + \frac{8}{3}(\mu_1 - \mu_2)^2 (M_S/\mathscr{M})^2}. \end{aligned} \tag{36}$$

The first term in P is directly proportional to γ/β in eq. (33) and is thus of the same order of magnitude. We find from a rough evaluation of the second term that it is considerably smaller than the first. Since γ/β is so small, observation of this effect does not appear to be feasible.

4 Parity Non-Conservation in (n, p) Capture

We finally turn to experiment C in which we observe the polarization of the γ-ray emitted when neutrons are captured by protons. If the cross-section for the production of γ-rays right-circularly polarized in the direction of motion is $\sigma^{(+)}$, and for that of left-circularly polarized γ-rays $\sigma^{(-)}$, the quantity of interest is

$$A \equiv \frac{\sigma^{(+)} - \sigma^{(-)}}{\sigma^{(+)} + \sigma^{(-)}}. \tag{37}$$

For thermal neutrons we have

$$A = \frac{\mathrm{Re}\, D^* D'}{|D|^2 + |D'|^2}. \tag{38}$$

Inserting D and D' from eqs. (14) and (20) we find

$$A = \frac{1}{\mu_1 - \mu_2}\left[-\frac{3\sqrt{2}}{2}\frac{M'_S}{M_S} + \frac{1}{6}\frac{M''_S}{M_S}\right]. \tag{39}$$

A rough evaluation of the matrix elements gives

$$A \approx 5 \times 10^{-7}.$$

5. Parity Non-Conservation in (n, d) Capture

Another process in which parity non-conserving effects might readily appear is the radiative capture of slow neutrons by deuterons. It was first pointed out by Verde [11]) that the magnetic dipole matrix element for this process vanishes identically for a totally space-symmetric H^3 nucleus. Of course, H^3 does contain a non-symmetric part so that there is some contribution from the magnetic dipole transition. Thus, an analysis of the data on (n, d) capture by L. M. Delves [12]) indicates that just below 50 keV the E1 and M1 transitions are equally important, whereas at 1 keV the M1 transition is stronger by a factor 4. His analysis also shows that the amplitude of the non-symmetric part of the H^3 function is of the order 0.1.

Considering now parity non-conserving effects, two experimental possibilities suggest themselves, namely, (a) to measure the circular polarization of the emitted gamma radiation and (b) to use polarised neutrons and to look for a forward-backward asymmetry of this radiation relative to the direction of polarization. Both types of experiment are discussed by Blin-Stoyle [6]), who shows that the magnitude of both effects is of the order γ where, in our case, for sufficiently low energy neutrons, the M1 transition dominates

$$\gamma \approx \frac{\langle \mathrm{E1} \rangle}{\langle \mathrm{M1} \rangle}.$$

Here $\langle \mathrm{M1} \rangle$ and $\langle \mathrm{E1} \rangle$ are reduced matrix elements referring to the dominant parity conserving M1 transition and the spurious parity non-conserving E1 transition resulting from s-wave capture into parity impurities in the H^3 wave function. The latter contribution is not to be confused with the regular E1 transition resulting from p-wave capture which will not interfere and produce parity non-conserving effects.

Now the M1 transition is inhibited by a factor ≈ 100 (since the amplitude of the non-symmetric part of the H^3 wave function is ≈ 0.1) with respect to the single particle value. On the other hand, it is to be expected that the spurious E1 strength will be of the order $10F$ times the single particle M1 value, the factor 10 arising from the ratio of single particle E1 and M1 strengths. Thus the overall parity non-conserving effect could be of the order of magnitude $100F$

thus giving an amplification factor of the order 100. A further enhancement arises from the opposite parity admixture which will be present in the initial wave n-D system. This effect will be considerably greater here than in the n-p case where it was only 5 % of A because the p-state contributions to n-D scattering are significant at a much lower energy than in n-p scattering. Detailed calculations are clearly necessary in order to confirm these rough results. They are at present being performed by F. Partovi.

We are indebted to Professor F. Villars for some helpful suggestions.

References

1) D. H. Wilkinson, Phys. Rev. **109** (1958) 1603, 1610, 1614
2) R. Haas, L. B. Leipuner and R. K. Adair, Phys. Rev. **116** (1959) 1221
3) F. Boehm and U. Hauser, to be published
4) R. J. Blin-Stoyle, Phys. Rev. **118** (1960) 1605
5) T. D. Lee and C. N. Yang, Phys. Rev. **104** (1956) 254
6) R. J. Blin-Stoyle, Phys. Rev. **120** (1960) 181
7) R. P. Feynman and M. Gell-Mann, Phys. Rev. **109** (1958) 193
8) W. Rarita and J. Schwinger, Phys. Rev. **59** (1941) 556
9) M. J. Moravczik, Nuclear Physics **7** (1958) 113
10) G. Breit, M. H. Hull, Jr., K. E. Lassila and K. D. Pyatt, Jr., Phys. Rev. **120** (1960) 2227
11) M. Verde, Helv. Phys. Acta **23** (1950) 453
12) L. M. Delves, private communication

1.B:7.C. *Nuclear Physics* **27** (1961) 405—414; © *North-Holland Publishing Co., Amsterdam*
Not to be reproduced by photoprint or microfilm without written permission from the publisher

PROTON-PROTON SCATTERING AT RELATIVISTIC ENERGIES

H. S. GREEN
University of Adelaide, S. Australia

Received 4 April 1961

Abstract: It is shown in this paper that the cross-section for elastic p-p scattering at very high energies can be understood in terms of a hard sphere model for the nucleon, provided the Lorentz contraction of the sphere at relativistic velocities is taken into account. The relativistic mechanics of the collision of hard spheres is discussed on the basis of classical mechanics and wave-mechanics. Already in the classical theory there is some peaking of the angular distribution in the forward direction, which is further accentuated when wave-mechanical interference effects are considered. The behaviour of the total cross-section, and the angular distribution for p-p scattering, in the energy range 0.4—8.5 GeV, is reproduced satisfactorily by the model.

1. Introduction

The experimental study of the differential cross-section for nucleon-nucleon scattering beyond 100 MeV has revealed three rather remarkable features:

(i) The total cross-section, instead of decreasing rapidly with increasing energy, as at low energies, steadies and becomes almost constant up to the inelastic threshold. This first became apparent about 1949, when the experimental data of Chamberlain and Wiegand [1]), and of Kelly, Leith, Segrè and Wiegand [2]) first became available. Their results were soon interpreted by Jastrow [3]) as indicating the presence of a hard repulsive core at the centre of the nuclear force field, reflection from which is responsible for almost the entire elastic scattering.

(ii) There is still no marked change of the elastic cross-section beyond the inelastic threshold, though due to the inelastic contribution the total cross-section is much increased. Qualitatively this may be understood by assuming that meson production is not localized on the core, but distributed thinly through a much larger region within the range of the nuclear forces. Elastic scattering and meson production therefore interfere with one another only slightly, and for practical purposes may be treated as independent phenomena.

(iii) Below 500 MeV (laboratory energy) the p–p scattering is almost isotropic, and though the n–p scattering exhibits a p-wave, scattering through 90° (in the centre-of-mass frame) is still appreciable. But above 500 MeV the scattering becomes more and more restricted to the forward and backward directions, while scattering through intermediate angles almost disappears. This peaking

of the angular distribution around 0° and 180° is increasingly accentuated up to the highest energies. The phenomenon was deduced by Messel and Green [4]) in 1952, from a study of the lateral spread of cosmic ray showers in the atmosphere, and was confirmed later when the accelerator data of Nikitin, Selector, Bogomolov and Zombkovskij [5]) and the American school [6]) became available. The main object of this paper is to provide a simple theoretical explanation of the effect. A quantitative discussion of the elastic cross-section will be given, followed by some more qualitative remarks on the inelastic cross-section.

Jastrow's hypothesis of a hard repulsive core in the nuclear field of force has become an essential feature of all successful phenomenological potentials. It was also adopted, at first on a more or less *ad hoc* basis, by Lévy [7]) and his successors in developing the meson theories of the nucleon interaction. The hypothesis was put on a more fundamental basis following the work of Arnowitt and Gasiorowicz [8]), who treated the virtual creation of nucleon pairs accurately for the first time, and of Green and Biswas [9]), who also took account of nucleon recoil. This work showed that the hard core is a manifestation of the virtual pairs, which appears mathematically as a singularity (simple pole) in the effective nuclear potential, at a distance equal to the core radius from the force centre. The core radius depends on the isobaric spin state (singlet or triplet) but not on the spin. In this paper, the existence of the core, and its dominating role in elastic scattering at relativistic energies, will be taken for granted. It will, in fact, be shown that the scattering throughout the range can be accounted for quite well in this way.

The standard theoretical interpretation of the data was developed by Cork, Wenzel and Causey [10]), Rarita [11]) and Grishin, Saitov and Chuvilo [12]), on the basis of an optical model for the nucleon. By suitably varying the optical parameters, it is possible to fit the angular distribution at a particular energy, but there is no correlation of the data throughout the energy range. Actually it is quite wrong to attribute scattering at relativistic energies to diffraction by a sphere in this way, for in the centre-of-mass frame a sphere suffers contraction in the direction of motion and becomes spheroidal in shape. A similar criticism applies to the work of Brown [13]), who has used a hard-core-plus-external-absorption model of the nucleon, without taking account of the deviation of the potential from spherical symmetry at high energies. The importance of the Lorentz contraction in its effect on the scattering will be fully substantiated in the following sections.

The effect of the Lorentz contraction on the elastic scattering of hard spheres can be seen most easily in the context of classical mechanics. In the centre-of-mass frame, which is adopted for all subsequent calculations, the spheres appear as oblate spheroids, or, at extremely high energies, as circular discs. At the instant of collision, the shape and line of motion of these bodies

is reflected in the normal through their point of contact, and it is easy to see that as the spheroids grow more oblate, this normal approaches the line of incidence. Hence the direction of scattering also approaches the line of incidence, and the angular distribution will become more and more peaked in the forward and backward directions.

The explanation of the facts which this classical consideration suggests does not include any interference effects, and is certainly incomplete. In the context of wave mechanics, it is necessary to consider the scattering of a plane wave from a perfectly reflecting spheroid. The individual wavelets are scattered exactly as the classical theory suggests, but interfere with one another in such a way that the peaking in the forward and backward directions is increased, and scattering in other directions is much reduced. There is, therefore, a wave-mechanical effect superposed on the purely classical effect, and these together can account for the observational data. It is of interest to disentangle the relative contributions of the two effects, and for this reason the classical description will be examined briefly in the next section; a rigorous wave-mechanical treatment will follow in section 3.

2. Relativistic Mechanics of Colliding Spheres

Consider two impenetrable bodies, of spherical shape in their respective rest-frames, of equal mass M and radius b, and approaching one another with velocity $\pm v$ along the asymptotes $y = \pm y_0, z = 0$, parallel to the x-axis. Owing to the Lorentz contraction, they are foreshortened in the x-direction by the factor $(1-v^2)^{\frac{1}{2}}$ (in units with the velocity of light $c = 1$). The deformed spheres are then ellipsoids (spheroids, in fact), with semi-axes $a = (1-v^2)^{\frac{1}{2}}b$, b and b parallel to the x, y and z-axes respectively. If the line joi ing their centres passes through the origin, these will be located at the points $(\mp x_0, \pm y_0, 0)$ at the instant of initial contact, where

$$(x_0/a)^2+(y_0/b)^2 = 1. \tag{1}$$

It is required to find the angle of scattering θ, which is determined by the following considereations:

(1) Although the apparent shape of the two bodies changes, together with their direction of motion, during contact, there is no change of momentum parallel to the common tangent plane. This tangent plane, which passes through the origin, is therefore not displaced.

(2) The total energy and angular momentum remain unaltered as a result of the collision. From this it follows that the separation of the final asymptotes is the same as the separation of the initial asymptotes, *i.e.*, $2y_0$.

These conditions, together, imply that, in the instant of contact, the shape of each body, and its line of motion, are reflected in the plane which is normal to both the plane of motion and the common tangent plane.

The equations of the spheroids at initial contact are

$$\frac{(x\pm x_0)^2}{a^2}+\frac{(y\mp y_0)^2}{b^2}+\left(\frac{z}{b}\right)^2=1, \tag{2}$$

and the plane in which the line of motion is reflected is therefore determined by

$$\frac{x_0x}{a^2}+\frac{y_0y}{b^2}=1. \tag{3}$$

Hence the angle of scattering is given by

$$\mathrm{tg}(\tfrac{1}{2}\theta)=\frac{a^2y_0}{b^2x_0}. \tag{4}$$

The differential cross-section can be written

$$\mathrm{d}\sigma=2\pi y_0\mathrm{d}y_0=\pi\mathrm{d}\,\frac{b^2(1-\cos\theta)}{2-v^2(1+\cos\theta)} \tag{5}$$

with the help of eqs. (1), (4), and the relation $a^2=b^2(1-v^2)$, so that, if $\mathrm{d}\Omega=-2\pi\mathrm{d}(\cos\theta)$ is the differential solid angle,

$$\frac{\mathrm{d}\sigma}{\mathrm{d}\Omega}=\frac{b^2(1-v^2)}{[2-v^2(1+\cos\theta)]^2}. \tag{6}$$

As v^2 increases from zero to 1, the angular distribution changes from one which is isotropic to one which is strongly peaked around $\theta=0$. A comparison with the p–p scattering data shows that this classical prediction is quite good quantitatively below 750 MeV. At higher energies the experimental peaking in the forward direction is stronger, and the scattering around 90° weaker, than eq. (6) would suggest. This is, of course, an indication that interference effects become important as soon as the departure from isotropy is pronounced.

3. The Wave-Mechanical Formulation

To adapt the model suggested in the previous section to the requirements of wave mechanics, one has to consider the scattering of a plane wave by a perfectly reflecting spheroid. It should be noted that there is no advantage in the use of the laboratory frame of reference, as although one of the particles is spherical in this frame, the other remains spheroidal and the symmetry of the barycentric frame is lost.

Let $\mathbf{x}=(x, y, z)$ be the displacement of one of the nucleons from the mass-centre, in the barycentric frame of reference. If E is the energy (including the rest-energy M), the wave function ψ of the free nucleon satisfies the Klein-Gordon equation

$$(E^2-M^2+\Delta)\psi=0, \tag{7}$$

where Δ is Laplace's operator, natural units having been chosen so that Planck's constant $\hbar$, as well as c, is equal to 1. The effect of the nucleon's core is to exclude it from the interior of the spheroid

$$\frac{x^2}{a^2}+\frac{y^2+z^2}{b^2}=1. \tag{8}$$

within which it would penetrate the core of the other nucleon. The wave function ψ must therefore vanish inside and on the surface of this spheroid.

The boundary condition thus imposed on the solutions of eq. (7) is most conveniently applied by transformation to the spheroidal coordinates α, β and ϕ defined by

$$\begin{aligned} x &= u\sinh\alpha\cos\beta, & y &= u\cosh\alpha\sin\beta\cos\phi, \\ z &= u\cosh\alpha\sin\beta\sin\phi, & u &= (b^2-a^2)^{\frac{1}{2}} = bv, \end{aligned} \tag{9}$$

were the velocity v is given by

$$v = k/E, \qquad k = (E^2-M^2)^{\frac{1}{2}}. \tag{10}$$

The separable solutions of eq. (7) which are continuous and finite for $\cos\beta = \pm 1$ then have the form

$$\begin{aligned} \psi_l^{(m)} &= R_l^{(m)}(\xi)sS_l^{(m)}(\eta)\exp(im\phi), \\ \xi &= \sinh\alpha, \qquad \eta = \cos\beta, \end{aligned} \tag{11}$$

where $R_l^{(m)}(\xi)$ and $S_l^{(m)}(\eta)$ are the radial and angular spheroidal harmonics described in the Bateman manuscript [14]) and a monograph, with tables, by Flammer [15]). [In Flammer's notation, $R_l^{(m)}(\xi) = R_{ml}(-iuk, i\xi)$ and $S_l^{(m)}(\eta)$ is the same as $S_{ml}(-iuk, \eta)$, apart from the normalization.] They satisfy

$$\begin{aligned} &\left\{\frac{\mathrm{d}}{\mathrm{d}\xi}(1+\xi^2)\frac{\mathrm{d}}{\mathrm{d}\xi}+q^2\xi^2+\frac{m^2}{1+\xi^2}-\lambda_l^{(m)}\right\}R_l^{(m)}=0, \\ &\left\{\frac{\mathrm{d}}{\mathrm{d}\eta}(1-\eta^2)\frac{\mathrm{d}}{\mathrm{d}\eta}+q^2\eta^2-\frac{m^2}{1-\eta^2}+\lambda_l^{(m)}\right\}S^{(m)}=0, \\ &q = uk = bMv^2/(1-v^2)^{\frac{1}{2}}, \end{aligned} \tag{12}$$

where $\lambda_l^{(m)}$ are the eigenvalues corresponding to the finite continuous functions $S_l^{(m)}$; l and m are both integers.

The scattering problem requires only the solutions of eq. (7) with cylindrical symmetry, corresponding to $m = 0$, and R_l, S_l and λ_l will be used to denote $R_l^{(0)}$, $S_l^{(0)}$ and $\lambda_l^{(0)}$. The angular functions will be normalized by the relation

$$\int_{-1}^{1} S_l(\eta)S_m(\eta)\mathrm{d}\eta = \delta_{lm}, \tag{13}$$

so that, when $q = 0$, $S_l(\eta)$ coincides with $(1+\frac{1}{2})^{\frac{1}{2}}P_l(\eta)$, where $P_l(\eta)$ is the Legendre polynomial. There are two independent radial functions, which will

be denoted by $R_{li}(\xi)$ and $R_{l0}(\xi)$, and both can be expressed as definite integrals involving $S_l(\eta)$:

$$\begin{aligned} R_{l1}(\xi) &= \int_{-1}^{1} \exp(iq\zeta\eta) S_l(\eta) \mathrm{d}\eta, \\ R_{l0}(\xi) &= \int_{-1}^{1} \frac{\exp[-q(\eta - i\xi)] S_l(\eta) \mathrm{d}\eta}{q(\eta - i\xi)}. \end{aligned} \tag{14}$$

The solution which satisfies the boundary condition, i.e., which vanishes on the spheroid $\sinh \alpha = a/u$, i.e., $\xi = M/k$, must be a linear combination of these:

$$R_l(\xi) = R_{l1}(\xi) + C_l R_{l0}(\xi), \tag{15}$$

with the constant C_l determined by

$$C_l = -R_{l1}(2\mathrm{M}/k)/R_{l0}(M/k). \tag{16}$$

The incident wave $\exp(ikx)$, in spheroidal coordinates $\exp(iq\xi\eta)$, can be developed as a series of separable solutions, in the form

$$\exp(iq\xi\eta) = \sum_{l=0}^{\infty} R_{l1}(\xi) S_l(\eta), \tag{17}$$

as one sees from the definition of R_{l1}, and the normalization (13). Of course, it will be necessary to omit from the summation terms corresponding to odd or even values of l, if the parity of the scattering state is even or odd, respectively. For large values of ξ, the function $R_{l0}(\xi)$ has the asymptotic form

$$\begin{aligned} & R_{l0}(\xi) (f_l/u\zeta) \exp(iq\xi), \\ & f_l = (i/k) \int_{-1}^{1} \exp(-q\eta) S_l(\eta) \mathrm{d}\eta, \end{aligned} \tag{18}$$

and is therefore appropriate for the representation of outgoing waves. The solution of the original wave equation which represents incident plus outgoing waves, and satisfies the boundary condition, is therefore

$$\psi = \sum_{l=0}^{\infty} R_l(\xi) S_l(\eta). \tag{19}$$

Asymptotically, this has the form

$$\begin{aligned} \psi &\sim \exp(ikx) + f(\eta) \exp(iq\xi)/(u\xi), \\ f(\eta) &= \sum_{l=0}^{\infty} c_l f_l S_l(\eta). \end{aligned} \tag{20}$$

For large values of ξ, the variable η is the cosine of the scattering angle θ, and the differential cross-section is therefore

$$\mathrm{d}\sigma = |f(\cos\theta)|^2 \, \mathrm{d}\Omega. \tag{21}$$

Also, by using eqs. (20) and (13), one finds for the total cross-section

$$\sigma = 2\pi \sum_{l=0}^{\infty} |c_l f_l|^2. \tag{22}$$

To determine the differential and the total cross-section one has therefore: (i) to obtain the solutions $S_l = S_l^{(0)}$ of eq. (12), subject to the normalization (13); (ii) to compute $R_{ll}\,(M/k)$ and $R_{lo}(M/k)$ from eq. (14), and hence the coefficients c_l from eq. (16); (iii) to determine the constants f_l from eq. (18); and finally (iv) to substitute the values of $S_l(\eta)$, c_l and f_l obtained in this way into eqs. (20) and (22).

The method just described depends, of course, for its efficacy on the rapid convergence of the series (20) and (22), and it may be shown that the expansion in spheroidal harmonics has the special merit that its first few terms suffice for both low and high energies. At low energies, q is very small and the spheroidal wave functions degenerate to Legendre polynomials. The expansion is therefore equivalent to the usual expansion in spherical harmonics, the rapid convergence of which is well known. At high energies, on the other hand, q is very large, and both $S_0(\eta)$ and $S_1(\eta)$ are closely approximated by $\exp(-q\eta)$ (times the normalizing constant) near $\eta = -1$. Taking account of the orthogonality of the $S_l(\eta)$, one sees from eq. (18) that f_l must then be very small except for $l = 0$ or $l = 1$, and the series (20) and (22) are therefore well represented by their first two terms. Incidentally, one sees also that at very high energies $f(\eta)$ is proportional to $\exp(-q\eta)$ near $\eta = -1$ and $\exp(q\eta)$ near $\eta = 1$, i.e., that the angular distribution is very strongly peaked around the forward and backward directions.

4. Computational Procedure

It is quite feasible to perform the calculations indicated accurately, with the help of the tables for $S_l(\eta)$ given by Flammer [15]). However, the simple nature of the model and the rather poor statistics of the experimental data hardly justify a very accurate calculation, and the following approximate procedure has been adopted.

For large values of q, the function $S_l(\eta)$ assumes the form

$$\begin{gathered} S_l(\eta) \sim L_\nu^-(\eta)e^{q\eta} + (-1)L_\nu^+(\eta)e^{-q\eta}, \\ L_\nu^-(\eta) = L_\nu[2q(1-\eta)], \qquad L_\nu^+(\eta) = L_\nu[2q(1+\eta)]. \\ \nu = 2l-1+(-1)^l, \end{gathered} \tag{23}$$

where L_ν is a Laguerre polynomial of order ν. One can interpolate between this limiting form and the Legendre polynomials appropriate to low energies, with an approximation of the type

$$\begin{aligned} S_{2l}(\eta) &= A_{2l}(\eta)\cosh(q\eta) + A_{2l+1}(\eta)\sinh(q\eta), \\ S_{2l+1}(\eta) &= A_{2l+1}(\eta)\cosh(q\eta) + A_{2l}(\eta)\sinh(q\eta), \end{aligned} \tag{24}$$

where A_l is an even or odd polynomial of the l-th degree in η, with coefficient so chosen that the approximate $S_l(\eta)$ satisfy the ortho-normality conditions (13) For small q values $A_l(\eta)$ will be proportional to $P_l(\eta)$, and, for large q values, $A_l(\eta)$ will be proportional to $L_\nu^-(\eta)+(-1)^l L_\nu^+(\eta)$. Only $S_0(\eta)$ and $S_1(\eta)$ will actually be needed, and for these the coefficients are given by

$$\begin{gathered} A_0(\eta) = A, \qquad A_1(\eta) = \sqrt{3}A\eta, \\ [(8/q-2\sqrt{3}/q^2+3/q^3)\sinh(2q;+(4\sqrt{3}/q-6/q^2)\cosh(2q)]A^2 = 4. \end{gathered} \tag{25}$$

Comparison with the exact developments of $S_0(\eta)$ and $S_1(\eta)$ shows that the above approximations are satisfactory above 500 MeV. At lower energies the error is also not large, but the rapidly convergent expansion in Legendre polynomials given by Flammer gives more accurate results.

A similar interpolation to simplify the computation of $c_l f_l$ is motivated by the fact that $\frac{1}{2}ikf_l r_{l1}(\xi)/S_l(1)$ is rigorously equal to the real or imaginary part of $R_{l0}(\xi)$ according as l is even or odd, as one can see from the asymptotic values of these functions. Since $R_{l0}(\xi)$ is $(1-i\xi)$ exp $(iq\xi)$ times a real function of ξ for both large and small values of q, the approximation

$$\frac{R_{l0}(\xi)}{R_{l1}(\xi)} = \begin{cases} \dfrac{ikf_l e^{iq\xi}(1-i\xi)}{2S_l(1)[\cos(q\xi)+\xi\sin(q\xi)]}, & l \text{ even}, \\ \dfrac{kf_l e^{iq\xi}(1-i\xi)}{2S_l(1)[\sin(q\xi)-\xi\ \mathrm{cls}(q\xi)]}, & l \text{ odd}, \end{cases} \tag{26}$$

has similar validity. Hence

$$\begin{gathered} c_l f_l = 2g_l S_l(1)\exp(-qM/k)/(k-iM), \\ g_l = \begin{cases} i[\cos(qM/k)+(M/k)\sin(qM/k)], & l \text{ even}, \\ -[\sin(qM/k)-(M/k)\cos(qM/k)], & l \text{ odd}. \end{cases} \end{gathered} \tag{27}$$

This result requires a correction near the zeros of g_l, which are obviously spurious; a numerical integration is needed there to determine R_{l0}. But for the most part, the calculations are relatively simple.

The core radius b has been given the value $2\hbar/(Mc)$, i.e. 0.42 fm, which is the wave-length corresponding to the reduced mass of the nucleon-anti-nucleon pairs, and is near to the values required to fit the data at the relativistic threshold. Only contributions from $l = 0$ and $l = 1$ have been calcuated; but contributions from $l = 2$ and $l = 3$ have been estimated, and they do not appear to change the results much except in the neighbourhood of 1.5 GeV where they may account for as much as 30 % of the elastic cross-section. The calculated elastic cross-section is compared with the nearest experimental value in table 1.

The agreement is satisfactory, and would be more so if estimated contributions from $l = 3$ and $l = 4$ were included. The calculated angular distributions, normalised to 1 at $\cos\theta = 0.8$, are set out in table 2.

TABLE 1

Total elastic cross-sections

E_{lab}(GeV)	0.375	0.563	0.75	1.50	2.25	3.00	4.50	6.00	7.50
$\sigma_1+\sigma_1$(mb)	18.6	16.8	15.5	12.8	11.3	10.6	10.0	9.2	8.5
σ_{exp}(mb)	23	22	21	20	15	9	9.5	7.5	8.5

E_{lab} is the laboratory energy; $\sigma_0+\sigma_1$ is the contribution from the $l = 0$ and $l = 1$ states to the elastic cross-section and σ_{exp} the nearest experimental value.

TABLE 2

Angular distribution

E_{lab} \ $\cos\theta$	0.0	0.5	0.8	0.9	1.0
0.563	0.19	0.47	1.00	1.27	1.61
1.50	0.05	0.31	1.00	1.43	2.03
3.00	0.00	0.18	1.00	1.71	2.89
6.00	0.00	0.09	1.00	2.15	4.57

θ is the scattering angle in the barycentric frame.

The statistics of the experiments are too poor to justify a quantitative comparison, but qualitatively the agreement is again very satisfactory.

One concludes that the present hard sphere model is a suitable representation of the proton at very high energies, provided relativistic effects are taken into account. One thing which might affect this conclusion is the neglect of absorption due to inelastic scattering, in the region round the core. But consideration shows that this effect is likely to be small. For, whereas the elastic scattering takes place almost entirely at the surface of the core, meson production is distributed through a region whose radius is four times greater, and whose volume is sixty times greater than the core. Taking account of the fact that the inelastic cross-section is of the same order of magnitude as the elastic cross-section, the protons which fail to be elastically scattered by the core due to inelastic processes must be relatively few. It is, of course, desirable that calculations should be made in which the absorption is taken into account; it is hoped to present in the future results based on an extended model of the nucleon.

References

1) O. Chamberlain and C. Wiegand, Phys. Rev. **79** (1950) 81
2) E. Kelly, C. Leith, E. Segrè and C. Wiegand, Phys. Rev. **79** (1950) 96
3) R. Jastrow, Phys. Rev. **81** (1951) 165
4) H. Messel and H. S. Green, Phys. Rev.. **87** (1952) 738
5) S. J. Nikitin, J. M. Selector, E. G. Bogomolov and S. M. Zombkovshij, Nuovo Cim. **10** (1954) 1269

6) F. F. Chen, C. P. Leavitt and A. M. Shapiro, Phys. Rev. **103** (1956) 211;
T. W. Morris, E. C. Fowler and J. D. Garrison, Phys. Rev. **103** (1956) 1472;
W. B. Fowler, R. P. Shutt, A. M. Thorndike and W. L. Wittemore, Phys. Rev.**103** (1956) 1479
M. M. Block, E. M. Harth, V. T. Cocconi, E. Hart *et al.*, Phys. Rev. **103** (1956) 1484;
R. Cester, T. F. Hoang and A. Kernan, Phys. Rev. **103** (1956) 1443
7) M. M. Lévy. Phys. Rev. **86** (1952) 806, **88** (1952) 725
8) R. Arnowitt and S. Gasiorowicz, Phys. Rev. **94** (1954) 1057
9) H. S. Green and S. N. Biswas, Prog. Theor. Phys. **18** (1957) 121;
S. N. Biswas, Prog. Theor. Phys. **19** (1958) 725
10) B. Cork, W. A. Wenzel and C. W. Causey, Phys. Rev. **107** (1957) 859
11) W. Rarita, Phys. Rev. **104** (1956) 221
12) V. G. Grishin, I. S. Saitov and I. V. Chuvilo, JETP **34** (1958) 1221
13) G. E. Brown, Phys Rev. **111** (1948) 1178
14) C. Flammer, Spheroidal wave functions (Stanford Univ. Press, 1957)
15) A. Erdélyi *et al.*, Higher transcendental functions (Bateman Manuscript Project) (McGraw-Hill, New York, 1955) Vol. **3**

1.E.1:
3.A

Nuclear Physics **27** (1961) 415—417; © *North-Holland Publishing Co., Amsterdam*
Not to be reproduced by photoprint or microfilm without written permission from the publisher

AN ISOMERIC STATE OF Y^{90}

C. CARTER-WASCHEK and B. LINDER

Department of Chemistry, The Florida State University, Tallahassee, Florida †

Received 20 May 1961

Abstract: An isomeric state of Y^{90} decaying with a half-life of 3.2 ± 0.1 h was obtained in the bombardment of Rb and Y, respectively, with 12 MeV alphas and deuterons of the Florida State University Tandem Van der Graaff accelerator. The observed gamma peaks can be fitted into an energy diagram with levels at 0.202 ± 0.005 and 0.690 ± 0.003 MeV. Consideration of the shell model and existing decay schemes for Y^{90} leads to the assignment of 7^+ for the isomeric state at 0.690 MeV.

1. Introduction

During recent investigations on the activation of rubidium by alpha particles, we found an yttrium activity which could not be reconciled with the published decay schemes of any of the known yttrium isotopes. This activity, which decays with a half-life of 2.3 ± 0.1 h and has three characteristic gamma peaks at 0.202 ± 0.005, 0.483 ± 0.003 and 0.690 ± 0.003 MeV, proved to be an isomer of Y^{90}. We base our conclusions on the following evidence: a) this activity was produced by alpha bombardment on natural Rb and Rb^{87} (enriched to 71.5 %); b) it was produced also in (d, p) reactions from Y^{89} (100 % abundance); c) it was not obtained when Rb^{85} (enriched to 99.5 %) was bombarded with alpha particles. Details of the experimental procedure and level assignments are discussed below ††.

2. Experimental

Targets made of rubidium chloride and of yttrium oxide were pressed into pellets and bombarded for 1 h with 12 MeV alphas and 12 MeV deuterons, respectively, of the Florida State University Tandem Van der Graaff accelerator. The pellets weighed 200 to 300 mg and were 1 cm^2 in diameter. In making targets of enriched RbCl, a soft pellet of sulphur was first prepared; then, about 35 mg of RbCl were sprinkled on one face of the sulphur pellet and the whole mass pressed into a firm pellet. The RbCl was thus concentrated on the face of the pellet exposed to the beam.

† Work supported by the U.S. Atomic Energy Commission.

†† After completion of this work we learned that the same isomer had been prepared by Haskins and Vandenbosch [1]) in (α, n) and (d, n) reactions. The stripping reaction Y^{89} (d, p) Y^{90} had also been previously studied [2, 3]) but the occurrence of an isomeric level in this reaction was apparently not noted before.

6) F. F. Chen, C. P. Leavitt and A. M. Shapiro, Phys. Rev. **103** (1956) 211;
T. W. Morris, E. C. Fowler and J. D. Garrison, Phys. Rev. **103** (1956) 1472;
W. B. Fowler, R. P. Shutt, A. M. Thorndike and W. L. Wittemore, Phys. Rev.**103** (1956) 1479
M. M. Block, E. M. Harth, V. T. Cocconi, E. Hart *et al.*, Phys. Rev. **103** (1956) 1484;
R. Cester, T. F. Hoang and A. Kernan, Phys. Rev. **103** (1956) 1443
7) M. M. Lévy. Phys. Rev. **86** (1952) 806, **88** (1952) 725
8) R. Arnowitt and S. Gasiorowicz, Phys. Rev. **94** (1954) 1057
9) H. S. Green and S. N. Biswas, Prog. Theor. Phys. **18** (1957) 121;
S. N. Biswas, Prog. Theor. Phys. **19** (1958) 725
10) B. Cork, W. A. Wenzel and C. W. Causey, Phys. Rev. **107** (1957) 859
11) W. Rarita, Phys. Rev. **104** (1956) 221
12) V. G. Grishin, I. S. Saitov and I. V. Chuvilo, JETP **34** (1958) 1221
13) G. E. Brown, Phys Rev. **111** (1948) 1178
14) C. Flammer, Spheroidal wave functions (Stanford Univ. Press, 1957)
15) A. Erdélyi *et al.*, Higher transcendental functions (Bateman Manuscript Project) (McGraw-Hill, New York, 1955) Vol. 3

1.E.1:
3.A

Nuclear Physics **27** (1961) 415—417; © *North-Holland Publishing Co., Amsterdam*
Not to be reproduced by photoprint or microfilm without written permission from the publisher

AN ISOMERIC STATE OF Y^{90}

C. CARTER-WASCHEK and B. LINDER

Department of Chemistry, The Florida State University, Tallahassee, Florida †

Received 20 May 1961

Abstract: An isomeric state of Y^{90} decaying with a half-life of 3.2 ± 0.1 h was obtained in the bombardment of Rb and Y, respectively, with 12 MeV alphas and deuterons of the Florida State University Tandem Van der Graaff accelerator. The observed gamma peaks can be fitted into an energy diagram with levels at 0.202 ± 0.005 and 0.690 ± 0.003 MeV. Consideration of the shell model and existing decay schemes for Y^{90} leads to the assignment of 7^+ for the isomeric state at 0.690 MeV.

1. Introduction

During recent investigations on the activation of rubidium by alpha particles, we found an yttrium activity which could not be reconciled with the published decay schemes of any of the known yttrium isotopes. This activity, which decays with a half-life of 2.3 ± 0.1 h and has three characteristic gamma peaks at 0.202 ± 0.005, 0.483 ± 0.003 and 0.690 ± 0.003 MeV, proved to be an isomer of Y^{90}. We base our conclusions on the following evidence: a) this activity was produced by alpha bombardment on natural Rb and Rb^{87} (enriched to 71.5 %); b) it was produced also in (d, p) reactions from Y^{89} (100 % abundance); c) it was not obtained when Rb^{85} (enriched to 99.5 %) was bombarded with alpha particles. Details of the experimental procedure and level assignments are discussed below ††.

2. Experimental

Targets made of rubidium chloride and of yttrium oxide were pressed into pellets and bombarded for 1 h with 12 MeV alphas and 12 MeV deuterons, respectively, of the Florida State University Tandem Van der Graaff accelerator. The pellets weighed 200 to 300 mg and were 1 cm^2 in diameter. In making targets of enriched RbCl, a soft pellet of sulphur was first prepared; then, about 35 mg of RbCl were sprinkled on one face of the sulphur pellet and the whole mass pressed into a firm pellet. The RbCl was thus concentrated on the face of the pellet exposed to the beam.

† Work supported by the U.S. Atomic Energy Commission.

†† After completion of this work we learned that the same isomer had been prepared by Haskins and Vandenbosch [1]) in (α, n) and (d, n) reactions. The stripping reaction Y^{89} (d, p) Y^{90} had also been previously studied [2, 3]) but the occurrence of an isomeric level in this reaction was apparently not noted before.

After irradiation, all targets were subjected to chemical separation.

The rubidium chloride was first dissolved in water (the sulphur, in the case of the enriched isotopes, remained undissolved) and yttrium, barium and strontium carriers were added. Yttrium was precipitated as $Y(OH)_3$ with concentrated NH_4OH and taken up in 15 *N* HNO_3. Barium and strontium carriers were again added, and subsequently removed with fuming HNO_3. The remaining solution was evaporated to dryness, and yttrium was next extracted with 0.6*M* DBPA solution from a mixture of sulphuric acid, ammonium sulphate, oxalic acid and hydrogen peroxide according to the specifications of Scadden and Ballou [4]). The yttrium was then back-extracted into aqueous solution with 4*N* HCl, and precipitated with oxalic acid. The oxalate was dried, weighed and mounted in a standard way.

The chemical separation for the activated yttrium oxide was similar to the procedure discussed above except for the initial steps. The target was dissolved in 12*N* HCl and zirconium carrier was added. Yttrium was precipitated out with 5*N* HF and dissolved in a mixture of nitric and boric acids. Barium and strontium carriers were added and yttrium was precipitated as the hydroxide with concentrated NH^4OH. The subsequent steps in the procedure were the same as in the separation used in the bombardment of RbCl.

3. Results and Discussion

The decay characteristics of the purified yttrium samples were determined with the aid of a 256-channel pulse-height analyzer, using a 7.6 cm × 7.6 cm NaI (Tl-activated) crystal. Two prominent peaks at 0.202 ± 0.005 and 0.483 ± 0.003 MeV and one of much lower intensity at 0.690 ± 0.003 MeV were observed in all samples except those obtained from activation of Rb^{85}. The 0.690 MeV peak is clearly a sum peak as shown by the fact that small changes in geometry produced large relative changes in intensity. The intensities of the other two peaks at 0.202 and 0.483 MeV showed a constant ratio of 1.12 : 1. A typical example of a spectrum, obtained in the bombardment of Y^{89} by deuterons, is shown in fig. 1.

A search was made for β-active components by running an absorption curve on Al with a Geiger counter, but no activity other than the 2.26 MeV β^-, belonging to the 64 h ground state [5]) of Y^{90}, could be detected.

The results can be interpreted on the basis of the shell model. The level assignment so obtained fits in with the partial decay scheme of Bartholomew and co-workers [6]). According to the shell theory [7]), the $p_{\frac{1}{2}}$ proton and $g_{\frac{9}{2}}$ neutron shells are filled with Zr^{90}. In Y^{90} there is an additional neutron in the $d_{\frac{5}{2}}$ shell (outside the $g_{\frac{9}{2}}$ shell) and one proton less in the $p_{\frac{1}{2}}$ shell. If, in the process of excitation, a proton is moved to a higher orbit, it will occupy the $g_{\frac{9}{2}}$ shell. Each of the configurations $(p_{\frac{1}{2}} d_{\frac{5}{2}})$ can split into two levels, thus giving rise to doublets

having spins and parities (2−, 3−) and (2+, 7+), respectively. Three of the four levels are known; the 2−, 3− and 2+ spins and parities belong to the levels, 0, 0.2024 and 0.7767 MeV, respectively [6]). Consideration of the requirement that the isomeric state have a large spin value and a level close to the 0.7767 MeV level leads to the assignment 7+ for the 0.690 MeV level. Accordingly, the isomeric level has the same configuration ($g_{\frac{9}{2}}d_{\frac{5}{2}}$) as the 0.7767 MeV level.

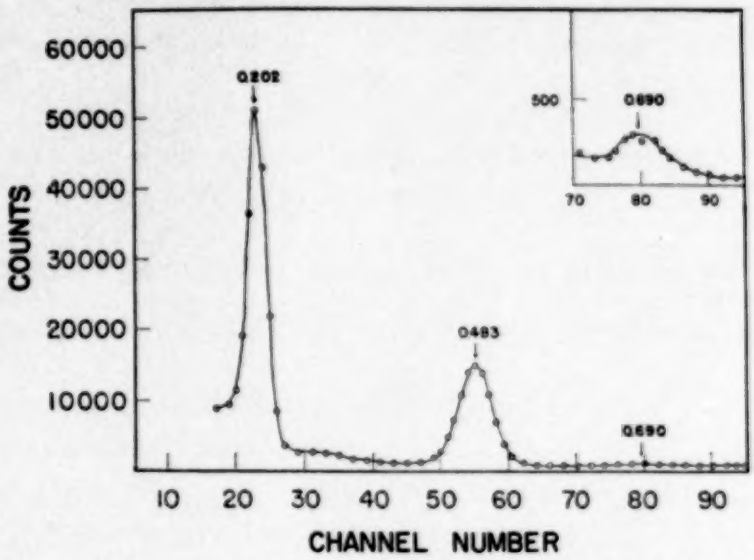

Fig. 1. Gamma-ray spectrum from the bombardment of Y^{89} with 12 MeV deuterons.

The assignment of 7+ to the isomeric state predicts that de-excitation of the 0.690 MeV level takes place through M4 radiation followed by E1 radiation through the intermediate state at 0.202 MeV. A rough estimate of the coefficients of internal conversion associated with these radiations gives the values 0.09 and 0.02, respectively. These values are consistent with the observed relative intensities for the 0.483 and 0.202 MeV gamma radiations.

We wish to express our appreciation to Dr. R. H. Davis and Dr. R. K. Sheline for their cooperation in the use of the accelerator and to Andrew Wasilewski for his assistance in compiling and analyzing the data. We also wish to thank the U.S. Atomic Energy Commission for providing financial support.

References

1) L. Haskin and R. Vandenbosch, Phys. Rev. **123** (1961) 184
2) N. S. Wall, Phys. Rev. **96** (1954) 664, 670
3) D. W. Stewart, J. L. Lawson and J. M. Cork, Phys. Rev. **52** (1937) 901
4) E. M. Scadden and N. E. Ballou, Anal. Chem. **11** (1953) 1602
5) D. Strominger, J. M. Hollander and G. T. Seaborg, Rev. Mod. Phys. **30** (1958) 585
6) G. A. Bartholomew, P. J. Campton, J. W. Knowles and G. Manning, Nuclear Physics **10** (1959) 590
7) P. F. A. Klinkenberg, Rev. Mod. Phys. **24** (1959) 63

7.C

Nuclear Physics **27** (1961) 418—420; © *North-Holland Publishing Co., Amsterdam*

Not to be reproduced by photoprint or microfilm without written permission from the publisher

AN ESTIMATION OF THE SPECTRUM OF TRUE MULTIPLICITIES IN ANTINUCLEON ANNIHILATIONS

E. M. FRIEDLÄNDER

Cosmic-Ray Laboratory, Institute of Atomic Physics, Bucharest, Rumania

and

M. E. MAYER

Physico-Mathematical Faculty, Parhon University, Bucharest, Rumania

Received 17 April 1961

Abstract: A method is devised for estimating "true" multiplicities of pions in $\bar{p}$-p and $\bar{p}$-n annihilations from observed frequencies of charged prongs, on the basis of isospin and charge conservation. The procedure is illustrated by applying it to available data.

All analyses of pion multiplicities in antinucleon annihilations to date (e.g. ref. [1])) have been based on the computation of overall multiplicities, starting from a theory (statistical or other); from these total multiplicities the expected multiplicities of charged pions are deduced by using charge symmetry arguments and then compared with experiment.

Obviously, an explicit knowledge of the distribution of "true" multiplicities, obtained from experimental data without reference to any theory of the annihilation process would be highly desirable. We show in this note how such information can be obtained, solely on the assumption of isospin conservation.

An "observed" multiplicity k of charged prongs can result from any annihilation into $n \geqq k$ pions (charged and neutral). Let P_n denote the probability of annihilation into n pions and f_{nk} the probability that out of the n produced pions, k come out charged. The probability Q_k of observing k charged pions will then be given by

$$Q_k = \sum_n f_{nk} P_n. \tag{1}$$

The coefficients f_{nk} can be determined on the basis of isospin and charge conservation alone. Replacing the probabilities Q_k by the observed frequencies q_k of charged multiplicities, eq. (1) becomes a linear system which allows to obtain estimates P_n for the probabilities P_n (the expectation value of p_n is P_n).

We are thus led to a typical problem of estimating the "prior probability distribution" from given observed frequencies [2]).

Although the available experimental information on antiproton-nucleon annihilation is still very scarce, we thought it of interest to illustrate the procedure by processing all data that were at our disposal.

For the frequencies q_k we have used all data contained in Segrè's report [1]), referring to $\bar{p}$-p and $\bar{p}$-n annihilations in bubble chambers. The coefficients f_{nk} have been computed simply from the very convenient tables of statistical weights published by Cerulus [3]). The resulting system is triangular and can be easily solved; nor does the computation of the statistical error matrix present any difficulties.

As no multiplicities k larger than 7 have been observed, we have assumed that all P_n for $n > 7$ vanish. Events with even and odd multiplicities, corresponding to $\bar{p}$-p and $\bar{p}$-n annihilations were treated separately, yielding separate systems of equations for even and odd indices. In order to avoid underdeterminateness of the equations we had to assume that $P_{2j+1} = 0$ for annihilations with protons and $P_{2j} = 0$ for annihilations with neutrons. This assumptions would be rigorously true for annihilations from an S° state (G-parity conservation; cf. e.g. ref. [4])). This had been justified theoretically in a recent paper [5]), and can be justified, a posteriori, by the self-consistency of the results obtained in this note. The remarks below regarding S-state annihilation should be considered in the light of these remarks.

The resulting estimates p_n (normalized to 100 %), together with the corresponding standard errors, are given in table 1.

TABLE 1

Estimates for the probabilities of pion multiplicities

n	0	1	2	3	4	5	6	7
p_n	2±2	0	−6±7	12±6	42±8	31±13	12±4	7±7

In spite of the large statistical errors, obviously due to the scarceness of experimental data, it is visible that the most likely number of pions produced in the annihilation is 4. The average multiplicity is 4.83±0.03, in good agreement with the value given by Segrè. The average energy of pions turns out to be 388 MeV, again in good agreement with the experimental data (385±10 for $\bar{p}$-p and 371±17 for $\bar{p}$-n).

The values of p_n seem to favour annihilation from an S°-state since final states with $n = 2$ seem to be strongly suppressed (cf. the remarks above), in agreement with theoretical predictions on annihilation via protonium [5]). It would be desirable to apply such an analysis to larger samples, in order to obtain more detailed information.

We should like to mention that the same method applies, mutatis mutandis, to multiple pion production in high-energy collisions. An analysis of data from 9 GeV proton collisions is now in progress.

In conclusion, we would like to express our gratitude to Prof. J. Ausländer and Prof. S. Titeica for helpful discussions.

References

1) E. Segrè, Report at the 9th Int. Conf. on High-Energy Physics, Kiev, July 1959 (to be published)
2) M. Annis, W. Cheston and H. Primakoff, Rev. Mod. Phys. **25** (1953) 818
3) F. Cerulus, Nuovo Cim. Suppl. **15** (1960) 402
4) T. D. Lee and C. N. Yang, Nuovo Cim. **3** (1956) 749
5) B. R. Desai, Phys. Rev. **119** (1960) 1385

1.B:2.B *Nuclear Physics* **27** (1961) 421—430; © *North-Holland Publishing Co., Amsterdam*
Not to be reproduced by photoprint or microfilm without written permission from the publisher

DIFFERENTIAL CROSS SECTIONS FOR THE T(p, n)He^3 REACTION

W. E. WILSON †, R. L. WALTER and D. B. FOSSAN ††
University of Wisconsin, Madison, Wisconsin †††

Received 29 May 1961

Abstract: The zero-degree differential cross section of the T(p, n) He^3 reaction was measured with a recoil-proton counter telescope at about 0.5-MeV intervals from 5 to 13.5 MeV. Relative angular distributions of the neutrons from the reaction were also obtained at 0.5-MeV intervals from 5 to 13 MeV proton energy. Cross sections were obtained by normalization to the zero-degree telescope measurements. The distributions, when transformed to the centre-of-mass system, are strongly peaked in the backward hemisphere. The centre-of-mass distributions were fitted with a Legendre series expansion and the total reaction cross section obtained from the coefficients.

Introduction

The T(p, n)He^3 reaction [1]) has been used extensively as a source of monoenergetic fast neutrons of a few MeV. A relatively large yield near threshold, absence of excited states in the residual nucleus which give rise to competing groups of neutrons and a yield which varies slowly with energy make this reaction particularly useful as a neutron source. Threshold for the reaction is 1.019 MeV (ref. [2])) and above 1.148 MeV it is free of the kinematic effect associated with the centre-of-mass motion which gives rise to neutrons of two energies near threshold. From 1.148 MeV to a proton energy of 8.34 MeV, the threshold for the tertiary process T(p, np)D, the p+T source produces strictly monoenergetic neutrons.

Extensive measurements [3–8]) of the angular distributions of neutrons from p+T have been made from threshold to approximately 5 MeV. Many of these investigations have employed the supposedly flat-response long-counter as the neutron detector. Only in the work of the Los Alamos group [8]) was the detailed energy variation in sensitivity of the long-counter taken into account. This group has measured p+T neutron angular distributions from 1.5 to 5.5 MeV and the zero-degree differential cross section up to a proton energy of 7.5 MeV. To measure the latter a recoil-proton counter telescope [9]) was employed as the neutron detector.

† Now at the University of Basle, Switzerland
†† Now at the University of Copenhagen, Denmark
††† Work supported in part by the U.S. Atomic Energy Commission and by the Graduate School from funds supplied by the Wisconsin Alumni Research Foundation.

Measurements above 7.5 MeV have been much less extensive. Stewart, Frye and Rosen [10]) reported some early emulsion work on the T(p, n) reaction. Bogdanov *et al.*[11]) have reported zero-degree differential cross section measurements in the proton energy range 7 to 12 MeV and angular distributions of neutrons at 6.8, 8.9 and 12 MeV. A telescope of four proportional counters and also a time-of-flight spectrometer were used to determine the neutron flux. The source of protons was a 12-MeV fixed energy cyclotron and lead foils were used to slow the beam for lower-energy measurements.

Concurrently with the present investigation Goldberg *et al.*[12]) obtained angular distributions of neutrons from T(p, n) at 9 energies from 3.4 to 12.4 MeV. A time-of-flight spectrometer was used to separate the monoenergetic neutrons from background. The Livermore variable energy cyclotron was the source of protons.

This paper reports the measurement of the zero-degree differential cross section and angular distributions of neutrons from the T(p, n) reaction for bombarding energies between 5 and 13 MeV. Distributions were obtained at about 500-keV intervals and in each distribution measurements were made every 10° up to a maximum angle between incident proton and emerging neutron of 150° in the laboratory frame of reference. A recoil-proton counter telescope was used to measure the differential cross section at zero degrees and a single stilbene crystal with pulse shape discriminator was employed to obtain the relative angular distributions of neutrons.

2. Experimental Method

Gas targets were bombarded by protons from a tandem electrostatic accelerator. The tritium gas was contained in a thin-walled steel cylinder 2 cm long and 0.6 cm in diameter. Target pressures were such that the tritium gas caused 5 and 13 MeV protons to lose 40 and 30 keV of energy, respectively. A nickel foil 1.3 μm in thickness through which the protons passed separated the gas from the vacuum of the beam tube. Protons which did not interact with target nuclei were stopped in a gold beam stop.

The target assembly was electrically insulated from the beam tube and integration of the beam current provided the measurement of the number of incident particles. A negative bias applied to an insulated section of the beam tube prevented secondary electrons from leaving the target assembly. A tantalum diaphragm preceding the target entrance foil collimated the beam. Since this diaphragm was a potential source of neutron background, the diaphragm was electrically insulated and the current striking it minimized with beam focusing lenses. The beam current hitting the diaphragm could be reduced to less than 0.5 % of the target current. The relative accuracy of the current integrator was better than 0.5 %.

Above a proton bombarding energy of about 6 MeV, gold produces large numbers of neutrons [13]). The low-energy thick-target neutrons arising from the gold beam stop severely handicapped the angular distribution measurements at high energies particularly at back angles where the monoenergetic T(p, n) neutrons are lowest in energy. To reduce this low-energy neutron background for angular distribution measurements at angles greater than 100° and at energies above 10 MeV, 0.5 mm of graphite was used to slow the protons before they entered the beam stop. The reduction of the low energy neutron background more than offset the relatively higher-energy neutron background arising from the 1.1 % carbon-13 contained in natural carbon.

The differential cross section at zero degrees was measured using a recoil-proton counter telescope [9]) as the neutron detector. With this type of counter one can measure fluxes of 2 to 30 MeV neutrons. The general principle of operation is to expose a known number of hydrogen nuclei to the flux to be measured and count the number of protons recoiling into a fixed solid angle. Precisely defined geometry and an absence of multiple scattering corrections make it possible to calculate the efficiency of the counter. The telescope used in the present measurements follows the design of counter telescopes described by Bame *et al.*[14]) and by Goldberg and LeBlanc [15]).

Because the efficiency of the counter telescope is several orders of magnitude less than that of an organic scintillator, it was decided to measure relative angular distributions of neutrons with a stilbene detector and obtain cross sections by normalizing to the telescope measurement of the zero-degree differential cross section. The stilbene crystal was 0.6 cm thick and subtended an angle of about 4° at the target. The efficiency of the detector was calculated from the size of the crystal and the n—p scattering cross section [16]). These calculations were done ignoring the presence of carbon in the scintillator and corrections were included for double scattering of the neutrons from hydrogen and for loss of recoil protons from the end of the crystal.

The monoenergetic T(p, n) neutrons were used to calibrate the pulse height of the detector system in terms of neutron energy. The bias level of the detector was then obtained from this calibration. Stability of the gain of the amplifier was checked with a Cs γ-source.

3. Results

Fig. 1 presents the zero-degree differential cross section measured with the counter telescope. The line below 7.5 MeV is taken from the data obtained by Perry *et al.*[8]). Because the composition of the target gas was unknown in the present case, the present work is a relative measurement of the differential cross section and is normalized to the data of Perry *et al.* in the region of 5 to 6 MeV. Above 7.5 MeV in fig. 1 the line is continued through the present data.

The error bars shown are ± 7 % which is the estimated error of the data of Perry *et al.* Statistical probable errors are less than 2 % at each point. The cross section at zero degrees to which the relative angular distributions were normalized is indicated by the line in fig. 1.

The laboratory angular distributions of neutrons are shown in figs. 2 and 3. The smooth lines only connect the data and have no theoretical significance. To avoid confusion each distribution is offset by 20 mb/sr from the one below it and therefore the amount indicated at the right must be subtracted from the ordinate to obtain the correct magnitude for the cross section. For example, to

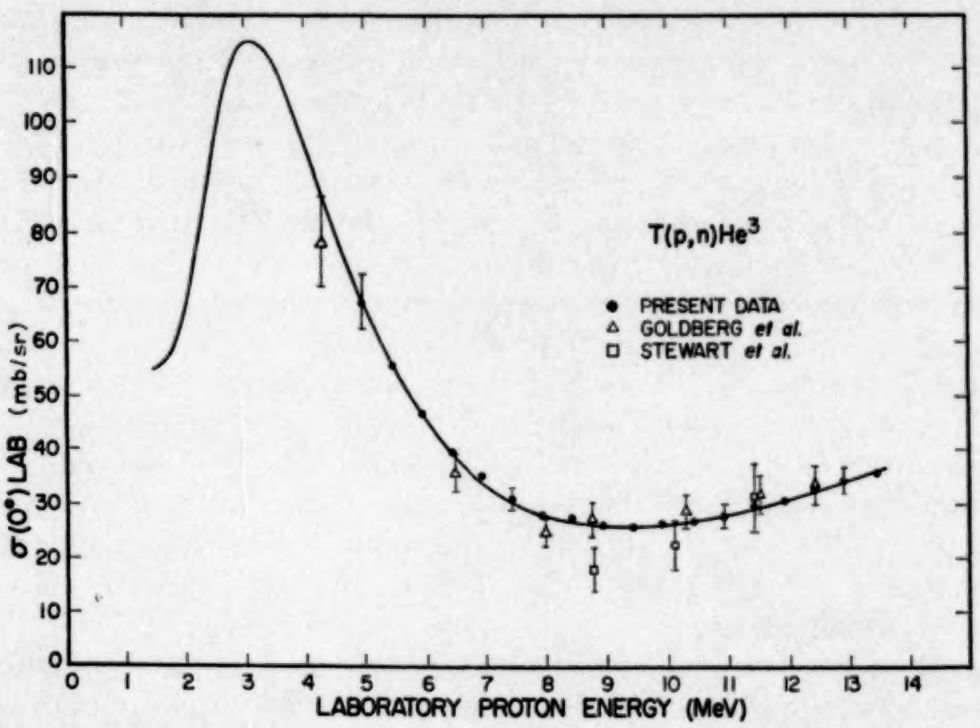

Fig. 1. The T(p, n) He^3 differential cross section at zero degrees as a function of laboratory proton energy. The line below 7.5 MeV indicates data of Perry *et al.* [8]). The open triangles are data of Goldberg *et al.* [12]) and the open squares are from Stewart *et al.* [10]).

obtain the cross section at 6.44 MeV, 80 mb/sr should be subtracted from the ordinate.

For the distributions up to 10 MeV enough counts were recorded at each angle so that the statistical errors are less than 1.5 %. At higher energies the background of neutrons from the gold beam stop became very large, in some instances as much as 75 % of the total count. This resulted in a larger statistical uncertainty for the angular distributions above 10 MeV. For the 12.9-MeV distribution for which the background was highest, the statistical errors for angles less than 100° were not greater than 5 %. At angles larger than 100° the statistical uncertainty may approach 15 %.

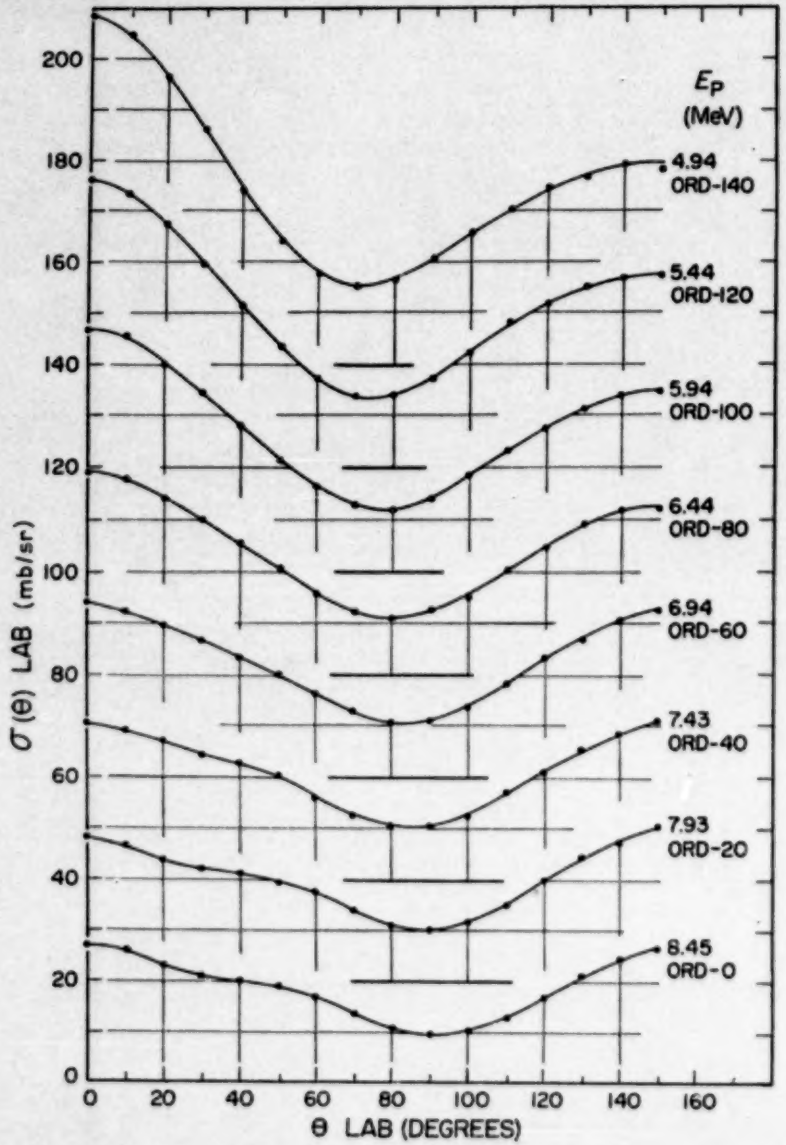

Fig. 2. Laboratory differential cross sections for the T(p, n)He³ reaction, 4.94 to 8.45 MeV. Each distribution is offset by 20 mb/sr, so the amount indicated at the right must be subtracted from the ordinate to obtain the correct magnitude. For example, to obtain the cross section for $E_p = 6.44$ MeV, 80 mb/sr must be subtracted from the ordinate scale.

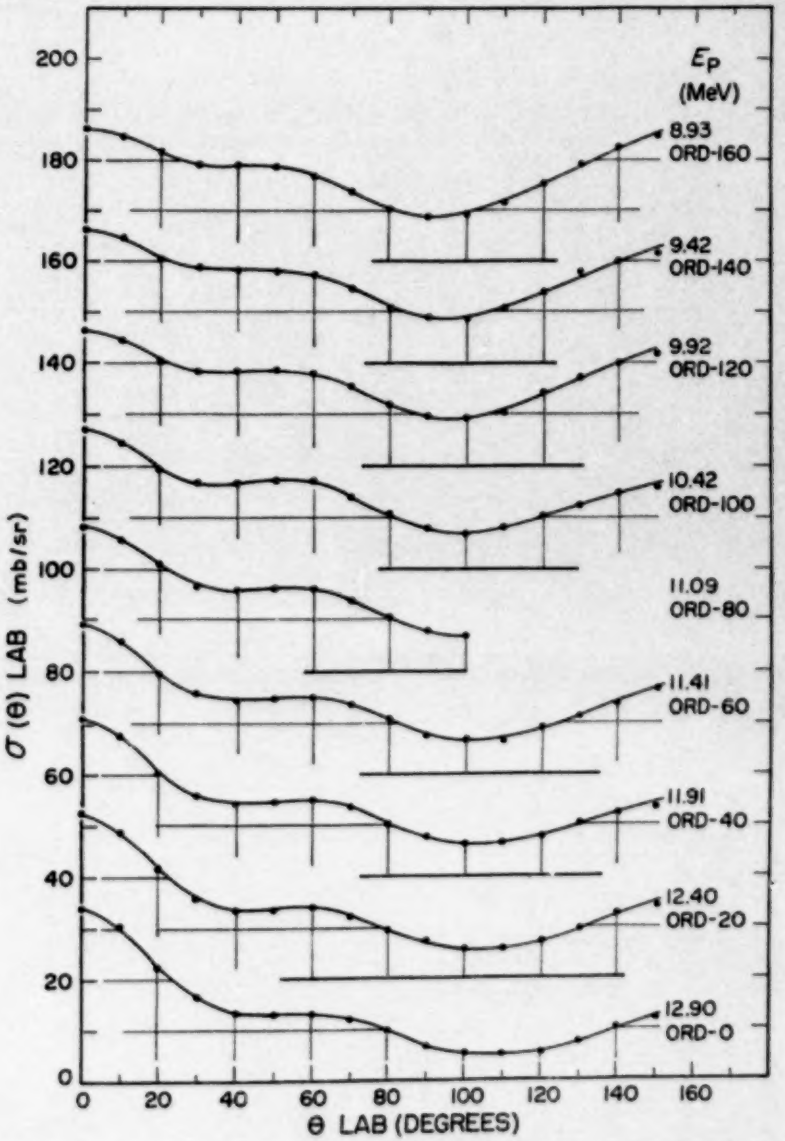

Fig. 3. Laboratory differential cross sections for the T(p, n)He³ reaction, 8.93 to 12.90 MeV. Each distribution is offset by 20 mb/sr.

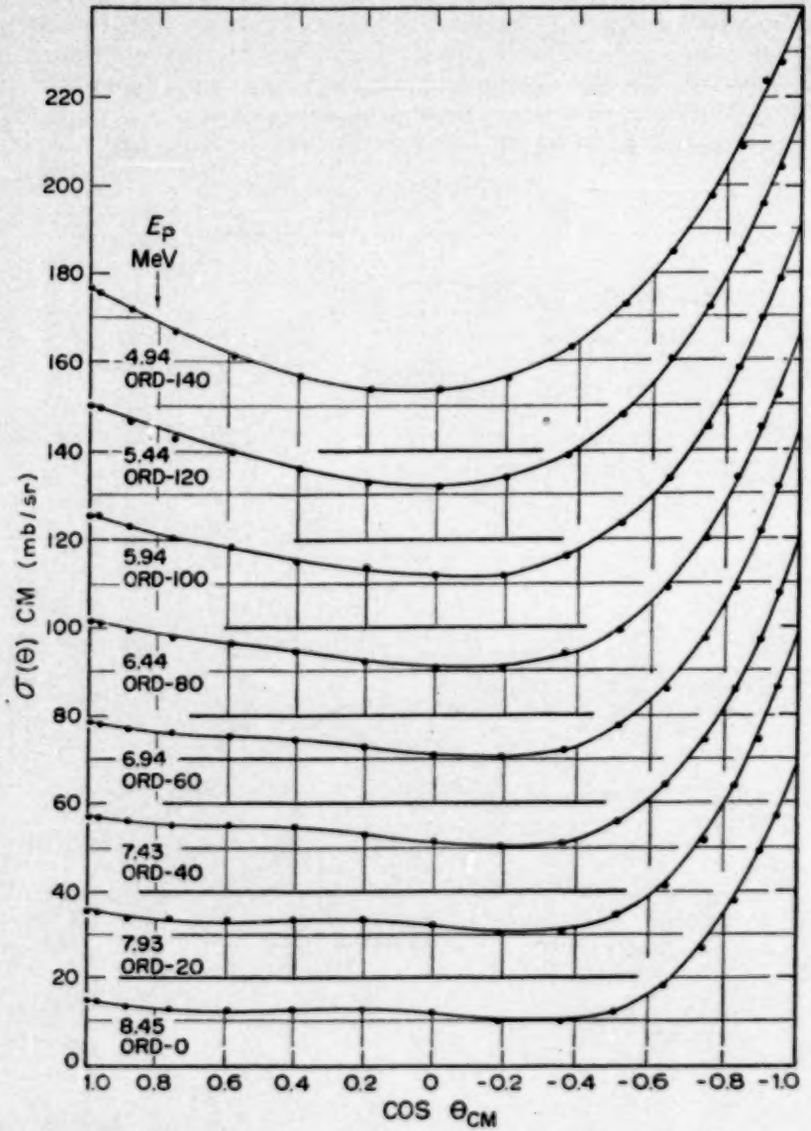

Fig. 4. Centre-of-mass differential cross sections for the T(p, n)He^3 reaction, 4.94 to 8.45 MeV. Each distribution is offset by 20 mb/sr. The curves are least square fits of the data to a series of the form of eq. (1).

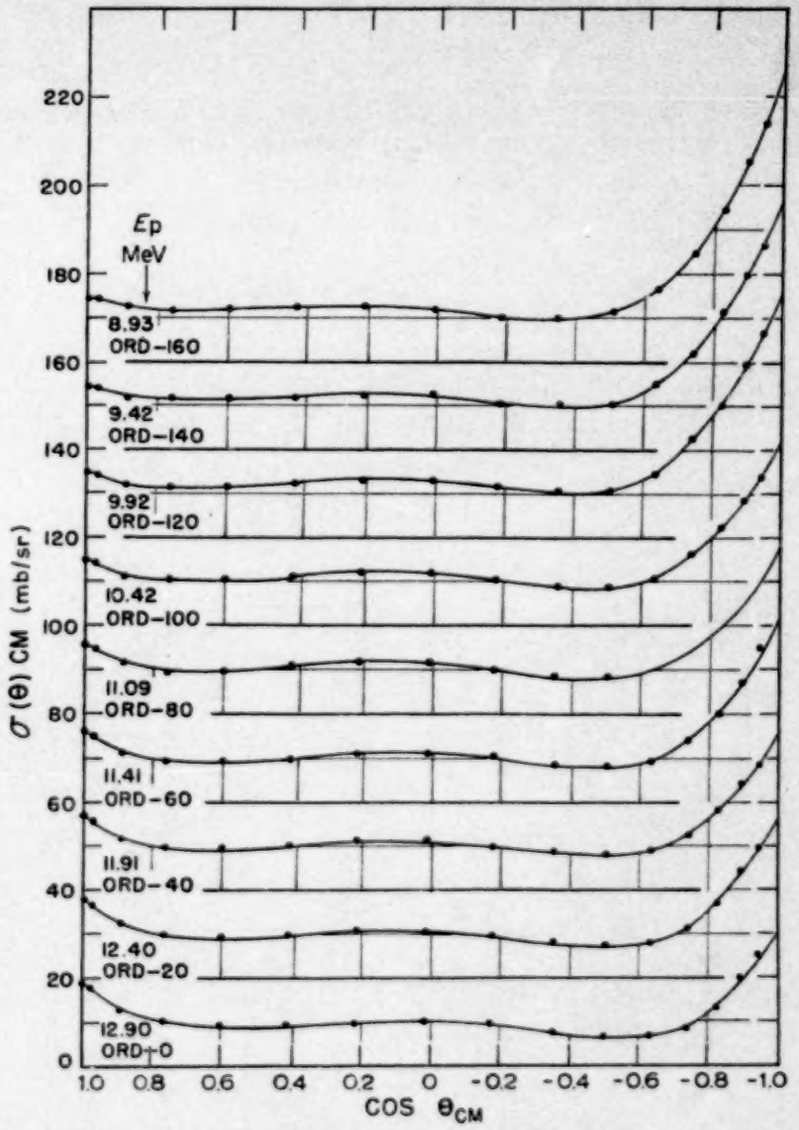

Fig. 5. Centre-of-mass differential cross sections for the T(p, n)He^3 reaction, 8.93 to 12.90 MeV. Each distribution is offset by 20 mb/sr. The curves are least square fits of the data to a series of the form of eq. (1).

Since double scattering of the neutrons from hydrogen in the crystal is most important at low energies, the corrections to the data for this effect were largest at the back angles and in the lower-energy distributions. The largest correction at 150° was 17 % and was typically about 10 % at this angle in distributions up to 10 MeV. Above 10 MeV the average correction was about 5 % at 150°. The correction for double scattering did not exceed 2 % at 90° in any of the distributions.

Loss of recoil protons from the end of the crystal is important for high neutron energies. The maximum correction for this effect was 2 % at 12.9 MeV. The absolute accuracy of the differential cross sections is estimated to be about 15 %.

The angular distributions of neutrons in the centre-of-mass system are presented in figs. 4 and 5. Again the distributions are each offset by 20 mb/sr. Strong backward peaking of the neutrons is quite apparent. This feature persists through the highest energy measured, though the backward peaking is not as pronounced at the higher energies.

At about 7 MeV proton energy a broad maximum begins to appear in the distributions near 65° in the centre-of-mass system. This broad maximum becomes more prominent and shifts to a larger angle, approaching 90° at 13 MeV.

The centre-of-mass angular distributions were fitted with a series of Legendre polynomials using a least squares program and an electronic computer. The dependence of the cross section on the wave number k was made explicit by using a series of the form

$$\sigma(\mu) = k^{-2} \sum_n B_n P_n(\mu). \tag{1}$$

Polynomials up to and including P_4, *i.e.*, $\cos^4 \theta$, were sufficient to fit the angular distributions. The smooth lines through the data in figs. 4 and 5 are the least squares fits to the distributions using the first five terms in the series.

Fig. 6 presents the Legendre coefficients obtained from fitting the angular distributions. This plot provides a means of calculating the differential cross section at intermediate energies and angles. The angular distributions measured by Perry *et al.*[8]) were taken at about 250-keV intervals and the coefficients required to fit these distributions are indicated by the dotted lines in fig. 6. The open symbols represent the Legendre coefficients from the data of Goldberg *et al.*[12]). This group used a power series in $\cos \theta_{\text{c.m.}}$ to fit the angular distributions. Linear combinations of the cosine coefficients were taken to obtain the Legendre coefficients indicated here. The solid lines above 6 MeV are weighted averages of the respective coefficients.

The increase of B_4 with energy corresponds to the appearance and increase of the broad maximum in the angular distributions; the broad maximum re-

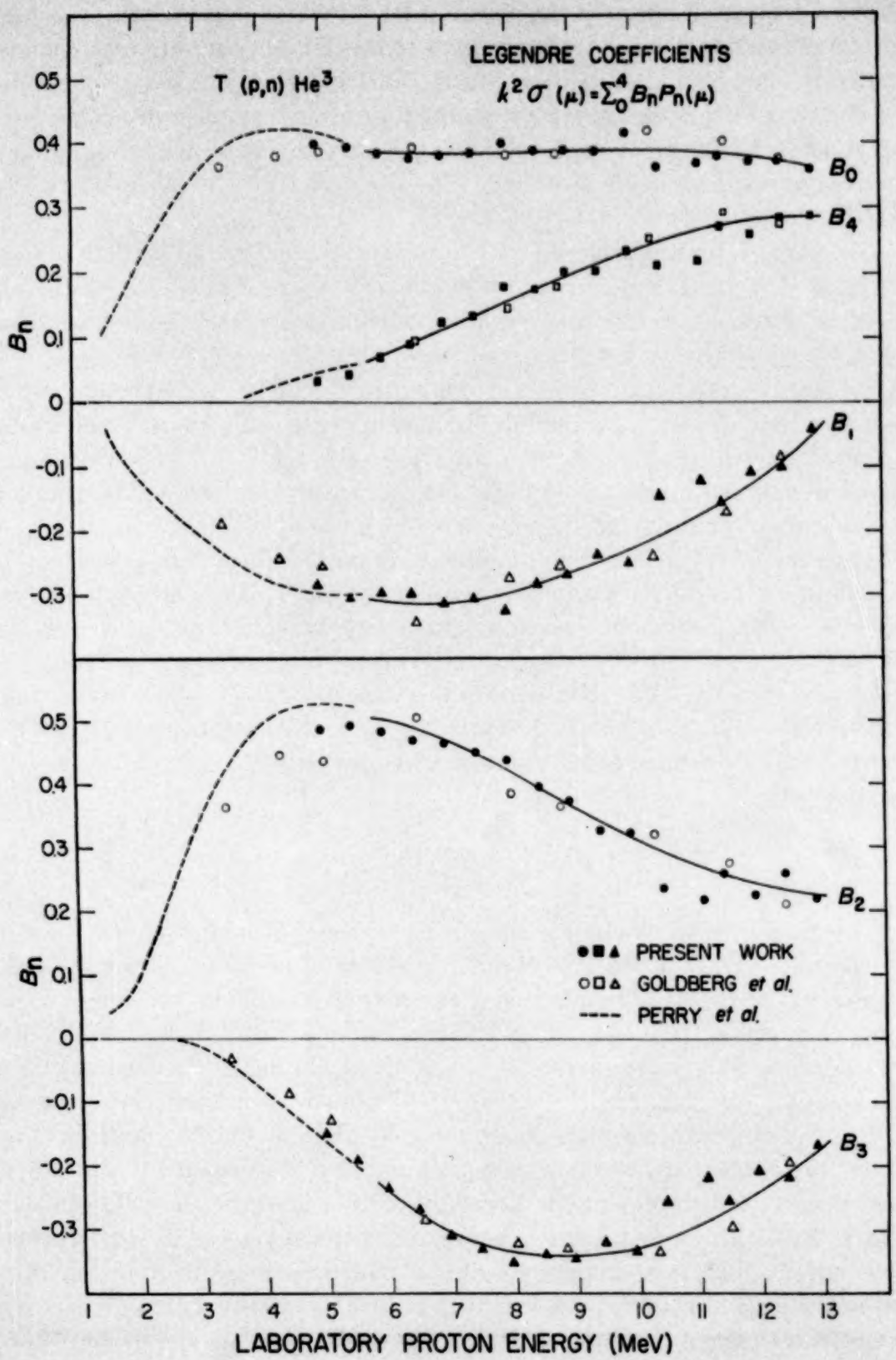

Fig. 6. Legendre coefficients for the centre-of-mass angular distributions. The open symbols are data of Goldberg *et al.* [12]) and the dotted lines from Perry *et al.* [8]).

quires a term in $\cos^4\theta$ in the series in order to obtain a satisfactory fit. One notable feature of the coefficients is the fact that B_0 is essentially independent of energy above about 4 MeV.

The coefficient B_0 is closely related to the total reaction cross section. By integrating the Legendre series (1) over solid angle one obtains for the total reaction cross section

$$\sigma_R = \frac{4\pi}{k^2} B_0. \tag{2}$$

The total reaction cross section thus obtained by integrating the angular distributions is shown in fig. 7 along with other measurements. Gibbons and

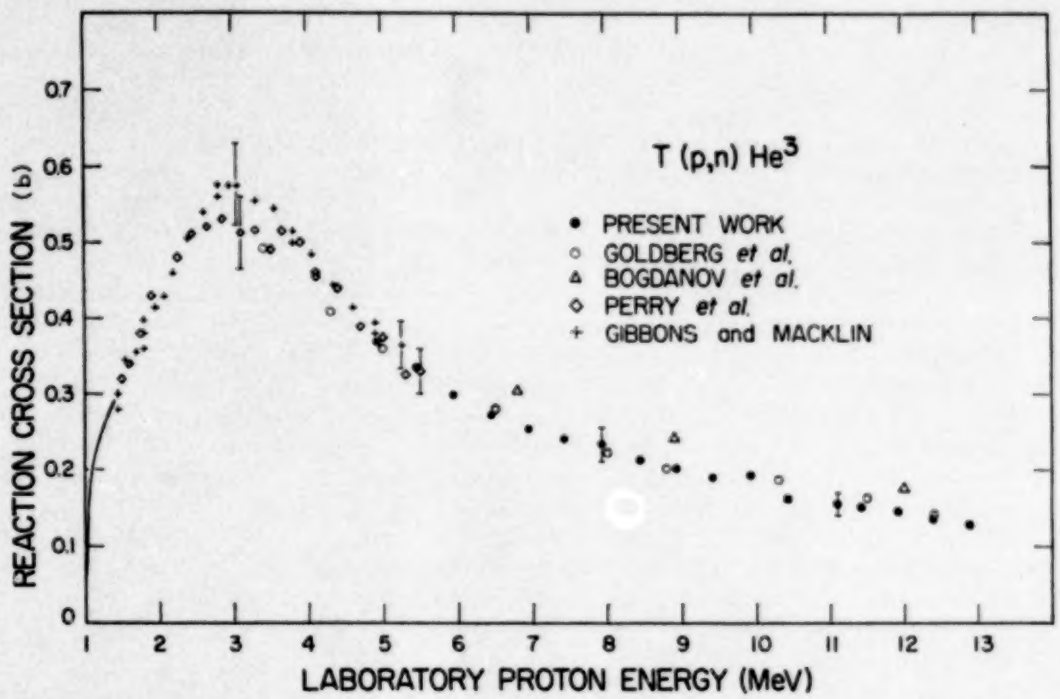

Fig. 7. Total T(p, n)He³ reaction cross section. The data of Gibbons and Macklin [17]) were obtained by thermalization of neutrons in a large graphite sphere. All other data were obtained by integrating angular distributions of neutrons. The comparisons are from the experiments of Goldberg *et al.* [12]), Bogdanov *et al.* [11]) and Perry *et al.* [8]).

Macklin [17]) obtained total cross sections by thermalizing the T(p, n) neutrons in a large graphite sphere and hence experimentally integrating over solid angle. All other data presented in fig. 7 were obtained by numerical integration of experimental angular distributions of neutrons. The measurements of Bogdanov *et al.*[11]) are approximately 10 % higher than the measurements of Goldberg *et al.* and those reported here.

Using the spectrometer properties of the counter telescope, an attempt was made to observe the continuum of neutrons from the reaction T(p, np)D. At a bombarding energy of 11.9 MeV no neutrons were observed that could definitely

be attributed to the reaction and the upper limit placed on the differential cross section at zero degrees is 10 mb/sr.

The authors wish to thank Prof. H. H. Barschall for suggesting the experiment and for his continued interest in this work. Also, we wish to thank Dr. M. D. Goldberg for communicating his data prior to publication.

References

1) R. F. Taschek, G. A. Jarvis, A. Hemmendinger, G. G. Everhart and H. T. Gittings, Phys. Rev. **75** (1949) 1361
2) R. F. Taschek, H. V. Argo, A. Hemmendinger and G. A. Jarvis, Phys. Rev. **76** (1949) 325
3) G. A. Jarvis, A. Hemmendinger, H. V. Argo and R. F. Taschek, Phys. Rev. **79** (1950) 929
4) H. B. Willard, J. K. Bair and J. D. Kington, Phys. Rev. **90** (1953) 865
5) N. A. Vlasov, S. P. Kalinin, A. A. Ogloblin, L. N. Samoilov, V. A. Sidorov and V. I. Chuev, JETP (USSR) **28** (1955) 639; [translation: JETP (Soviet Physics)**1** (1955) 500)
6) G. V. Gorlov, B. M. Gokhberg, V. M. Morozov and V. A. Shigin, Zh. Teck. Fiz. (USSR) **26** (1956) 985 [translation: Soviet Phys. Tech. Phys. **1** (1956) 964]
7) R. L. Macklin and J. H. Gibbons, Phys. Rev. **109** (1958) 105
8) J. E. Perry, Jr., E. Haddad, R. L. Henkel, G. A. Jarvis and R. J. Smith (unpublished), reported by J. D. Seagrave, at the Conf. on Nuclear Forces and the Few-Nuclei on Problem, London, 1959 (Pergamon Press, New York, 1960)
9) C. H. Johnson, in Fast neutron physics, Part I, ed. by J. B. Marion and J. L. Fowler (Interscience Publishers, New York, 1960) chapt II. C
10) L. Stewart, G. M. Frye and L. Rosen, Bull. Am. Phys. Soc. **2** (1956) 93
11) G. F. Bagdanov, N. A. Vlasov, S. P. Kalinin, B. V. Rybakov, L. N. Samoilov and V. A. Sidorov, JETP (USSR) **36** (1959) 633; [translation: JETP (Soviet Physiscs **9** (1959) 440]
12) M. D. Goldberg, J. D. Anderson, J. P. Stoering and C. Wong, Phys. Rev. **122** (1961) 1510
13) D. A. Bromley, A. J. Ferguson, H. E. Gove, J. A. Kuehner, A. E. Litherland, E. Almqvist and R. Batchelor, Can. J. Phys. **37** (1959) 1514
14) S. J. Bame, Jr., E. Haddad, J. E. Perry, Jr. and R. K. Smith, Rev. Sci. Instr. **28** (1957) 997
15) M. D. Goldberg and J. M. LeBlanc, Phys. Rev. **119** (1960) 1992
16) C. D. Swartz and G. E. Owens, in Fast neutron physics, Part I ed. by J. B. Marion and J. L. Fowler (Interscience Publishers, New York, 1960) chapt. II.B
17) J. H. Gibbons and R. L. Macklin, Phys. Rev. **114** (1959) 571

2.F:2.L

Nuclear Physics **27** (1961) 431—447; © *North-Holland Publishing Co., Amsterdam*

Not to be reproduced by photoprint or microfilm without written permission from the publisher

GAMMA-RAYS FROM INELASTIC SCATTERING OF HIGH ENERGY NUCLEONS

A. B. CLEGG

Clarendon Laboratory, Oxford

and

G. R. SATCHLER

Oak Ridge National Laboratory, Oak Ridge, Tennessee

Received 17 April 1961

Abstract: It is shown that the angular distribution of de-excitation gamma-rays following the inelastic scattering of high energy nucleons by nuclei can give additional information on both nuclear structure and the effective interaction. Formulae are derived using the impulse approximation; distortion effects due to elastic scattering of incident and outgoing nucleons are included. A simple case is first discussed in terms of individual scattering amplitudes, then the general formalism is introduced. The effect on the angular distribution of using polarized incident nucleons is also described and shown to give further information about the scattering interaction.

1. Introduction

The inelastic scattering of protons of energy 100 MeV and over is a very fruitful source of information about nuclear structure. Detailed measurements have been made of the proton angular distribution, the polarization of the outgoing protons and the asymmetry in scattering polarized protons in a number of cases and it has been shown that they can be understood as examples of a simple direct interaction process (see, for example, Kerman, McManus and Thaler [1]), to be referred to as KMT, where many other references are given). Because of this comparative simplicity it is of value to study these inelastic scattering reactions in detail and thus to use them as a tool for studying nuclear structure. (Conversely, in studying the reaction mechanism one is also determining the interaction of the incident proton with the nucleons inside the nucleus). To add to the experimental information it is also useful to measure the polarization of the residual nuclear excited state: this is conveniently done by observing the angular distribution of any further radiation and, as gamma-rays are the easiest to observe, one usually chooses to study states which decay by gamma-radiation. In practice, usually one wishes to know the polarization of the nuclear state produced when the proton is scattered through a definite angle, and one therefore measures the angular correlation between outgoing proton and gamma-ray: the variation in proton-

gamma-ray coincidence rate as the gamma-ray angle is varied while the proton angle is held fixed. The simple theory of this correlation has been described [2]) (in particular it predicts that the gamma-rays are symmetric about the nuclear recoil direction) while more detailed calculations including distorted wave effects have been presented by Banerjee and Levinson [3]). However, these authors have largely neglected the complicated spin and spin-orbit dependence of the nucleon-nucleon scattering interaction which is necessary to understand the proton polarization results [1]). In this paper we present formulae for the proton-gamma correlation in this general case: they are basically an extension of the results of KMT. We conform to the notation of KMT where possible, and for completeness we repeat a number of their definitions and results. The general methods of Fano, and Biedenharn and Rose [4]) are used, but because of the complicated spin dependence we think it useful to present also the older methods, in which the sums over magnetic substates are carried out explicitly. Such methods are, in general, more tedious for calculating specific cases but have the merit of showing more clearly what is going on: here they display explicitly the coherent feeding of the nuclear magnetic substates whose interference produces the complicated ϕ-dependent terms in the angular correlation, and also the effects of distorted waves when these are included.

It is straightforward to take into account distorted waves (deviations from plane wave motion due to elastic scattering of incident and outgoing nucleon); methods and some results are presented. Further, since the isospin formalism is used, charge exchange scattering, namely (p, n) and (n, p) reactions, are automatically included.

2. Impulse Approximation

When plane waves are used to describe the relative motion of target and projectile, the inelastic transition amplitude for scattering from $\mathbf{k}$ to $\mathbf{k}'$ is given by KMT as proportional to

$$A(\mathbf{k}', \mathbf{k}) = \langle n|M(q)\exp(-i\mathbf{q}\cdot\mathbf{r})|0\rangle, \tag{1}$$

where $\mathbf{q} = \mathbf{k}'-\mathbf{k}$ is the recoil momentum and $M(q)$ is the two-nucleon scattering amplitude. The differential cross-section is then

$$\frac{\mathrm{d}\sigma}{\mathrm{d}\omega} = \left(\frac{2N^2}{N+1}\right)^2 \frac{k'}{k} |A(\mathbf{k}', \mathbf{k})|^2,$$

where N is the number of target nucleons. In the two-nucleon centre-of-mass system we have

$$M = A+B\boldsymbol{\sigma}_1\cdot\hat{\mathbf{n}}\boldsymbol{\sigma}_2\cdot\hat{\mathbf{n}}+C(\boldsymbol{\sigma}_1\cdot\hat{\mathbf{n}}+\boldsymbol{\sigma}_2\cdot\hat{\mathbf{n}})+E\boldsymbol{\sigma}_1\cdot\hat{\mathbf{q}}\boldsymbol{\sigma}_2\cdot\hat{\mathbf{q}}+F\boldsymbol{\sigma}_1\cdot\hat{\mathbf{p}}\boldsymbol{\sigma}_2\cdot\hat{\mathbf{p}}, \tag{2}$$

where $(\hat{\mathbf{q}}, \hat{\mathbf{n}}, \hat{\mathbf{p}})$ form a right-handed coordinate system defined by

$$\begin{aligned} \hat{\mathbf{q}} &= \mathbf{q}/q, \qquad \mathbf{q} = \mathbf{k'}_0 - \mathbf{k}_0 = \mathbf{k'} - \mathbf{k}, \\ \hat{\mathbf{n}} &= \mathbf{n}/n, \qquad \mathbf{n} = \mathbf{k}_0 \times \mathbf{k'}_0 = \mathbf{k} \times \mathbf{k'}, \qquad \hat{\mathbf{p}} = \hat{\mathbf{q}} \times \hat{\mathbf{n}}, \end{aligned} \tag{3}$$

and $\mathbf{k'}_0$, $\mathbf{k}_0$ are the ingoing and outgoing nucleon momenta in the two-nucleon centre-of-mass system. The isobaric spin dependence of the coefficients in (1) is, for example,

$$A = A_\alpha + A_\beta \boldsymbol{\tau}_1 \cdot \boldsymbol{\tau}_2 = \tfrac{1}{4}(3A_1 + A_0) + \tfrac{1}{4}(A_1 - A_0)\boldsymbol{\tau}_1 \cdot \boldsymbol{\tau}_2, \tag{4}$$

where A_1, A_0 are the coefficients for the triplet and singlet isobaric spin states, respectively. They are tabulated by KMT for energies of 40, 90, 156 and 310 MeV.

A more correct treatment replaces the plane waves by distorted waves, the distortion taking account of the elastic scattering before and after the inelastic collision and usually assumed to arise from an optical potential. This introduces other momenta $\mathbf{p}$ and $\mathbf{p'}$ differing both in magnitude and direction from $\mathbf{k}$ and $\mathbf{k'}$,

$$\exp i\,\mathbf{k} \cdot \mathbf{r} \to \phi^{(+)}(\mathbf{k}, \mathbf{r}) = \int \mathrm{d}\mathbf{p} a(\mathbf{p}, \mathbf{k}) \exp i\,\mathbf{p} \cdot \mathbf{r}, \qquad \text{etc.}$$

Then q in $M(q)$ should be replaced by the $\mathbf{q'} = \mathbf{p'} - \mathbf{p}$ corresponding to these local momenta, and $M(q')$ then averaged over the distorted waves; we get

$$\begin{aligned} M(q) \exp(-i\mathbf{q} \cdot \mathbf{r}) \to \int \mathrm{d}\mathbf{p'} \int \mathrm{d}\mathbf{q'} \exp(-i\mathbf{q'} \cdot \mathbf{r}) M(q') a'(\mathbf{p'}, -\mathbf{k'}) a(\mathbf{p}, \mathbf{k}), \\ = \overline{M(q')} \phi^{(-)}(\mathbf{k'}, \mathbf{r})^* \phi^{(+)}(\mathbf{k}, \mathbf{r}). \end{aligned}$$

However, if the elastic scattering is mostly forward, we may ignore the variation of M over the range of q' indiced by it and approximate $\overline{M(q')}$ by $M(q)$. (This is commensurate with the other approximations already implied [1]) by the use of expression (1) for the amplitude.) Then the only effect is to replace $\exp(-i\mathbf{q} \cdot \mathbf{r})$ in the amplitude (1) by the product of the distorted waves. This may be expanded in partial waves:

$$\phi^{(-)}(\mathbf{k'}, \mathbf{r})^* \phi^{(+)}(\mathbf{k}, \mathbf{r}) \equiv \rho(\mathbf{k'}, \mathbf{k}, \mathbf{r}) = \sum_{lm} \rho_l{}^m(\mathbf{k'}, \mathbf{k}, r) Y_l{}^m(\theta, \phi). \tag{5}$$

The $\rho_l{}^m$ are complex and $\rho_l{}^{-m} = \rho_l{}^m$ if we use coordinates with z-axis along $\mathbf{q}$ and x-axis along $\mathbf{n}$. Plane waves would allow $m = 0$ only, and give $\rho_l{}^0 = \rho_l = [4\pi(2l+1)]^{\frac{1}{2}}(-i)^l j_l(qr)$. The distortion allows transfer of orbital angular momentum with $m \neq 0$. However, in the adiabatic limit, in which the energy lost in the collision may be neglected, the similarity of the initial and final distorted waves may be shown [5]) to impose a further symmetry which forbids odd m values.

An estimate of the distortion effects may be obtained at these energies

by the WKB approximation, which modulates the plane waves by a damping and phase factor $\exp iS(\mathbf{r})$. The expansion (5) for $l = 0$ and 2 is given by Hooton and Allcock [6]) for example (who write $\rho_l{}^m = (4\pi)^{\frac{1}{2}}\, a_l{}^m$, but referred to $-\mathbf{q}$ as z-axis and $\mathbf{n}$ as y-axis). However, the WKB approximation neglects reflection effects [7]) which may still be important at 100 MeV.

The discussion so far has neglected any spin-orbit coupling which may be present in the distorted waves. If it is important, the distorted waves become matrices in spin space $\phi_{\mu\sigma}(\mathbf{k}, \mathbf{r})$ where μ, σ are values of the z-component of the spin of the projectile. Terms with $\mu \neq \sigma$ allow the possibility of spin-flip during the *elastic* scattering, in addition to that induced by M during the inelastic collision. However, we shall not consider this effect in the present paper.

3. Angular Correlation by the Amplitude Method

We now calculate the matrix element (1) and then the proton-gamma-ray angular correlation for a simple case: the excitation of a state of spin J, parity $(-1)^J$ and isobaric spin T in an even nucleus by inelastic scattering off the ground state with spin and isobaric spin zero and positive parity. This case illustrates the methods quite adequately but is sufficiently simple to prevent the principles of the calculation from being obscured by the length of the formulae involved. The isobaric spin can be ignored in the calculation; all we have to remember is to put $A = \frac{1}{4}\ (3A_1+A_0)$, etc., if $T = 0$ and $A = \frac{1}{4}\ (A_1-A_0)$, etc., if $T = 1$. In (1) we now write $\langle n| = \langle J, M|$ and $|0\rangle = |0, 0\rangle$, denoting thus the spin of the state and its component along the z-axis. The outgoing wave-function is given by

$$|\mathrm{f}\rangle = \sum_M |J, M\rangle\langle J, M|M(q)\rho_l(qr)Y_l{}^0(\theta, \phi)|0, 0\rangle|\alpha_1\rangle, \tag{6}$$

where we use plane waves and only $l = J$ contributes. By writing the matrix element in this form we have set the z-axis along the recoil direction $\mathbf{q}$. The spin state of the ingoing nucleon is denoted by $|\alpha_1\rangle$. The coefficients of $|J, M\rangle$ in this expression are then the probability amplitudes for forming the excited state with z-components M; these then describe the polarization of the residual nucleus, which is measured by observing the angular distribution of the γ-rays it emits. Explicitly, we have

$$\begin{aligned}|\mathrm{f}\rangle = {} & |J, 0\rangle\langle J, 0|\rho_J Y_J{}^0|0, 0\rangle(A+C\boldsymbol{\sigma}_1\cdot\hat{\mathbf{n}})|\alpha_1\rangle \\ & + \sum_M |J, M\rangle\langle J, M|\rho_J Y_J{}^0\boldsymbol{\sigma}_2\cdot\hat{\mathbf{n}}|0, 0\rangle(C+B\boldsymbol{\sigma}_1\cdot\hat{\mathbf{n}})|\alpha_1\rangle \\ & + \sum_M |J, M\rangle\langle J, M|\rho_J Y_J{}^0\boldsymbol{\sigma}_2\cdot\hat{\mathbf{q}}|0, 0\rangle E\boldsymbol{\sigma}_1\cdot\hat{\mathbf{q}}|\alpha_1\rangle \\ & + \sum_M |J, M\rangle\langle J, M|\rho_J Y_J{}^0\boldsymbol{\sigma}_2\cdot\hat{\mathbf{p}}|0, 0\rangle F\boldsymbol{\sigma}_1\cdot\hat{\mathbf{p}}|\alpha_1\rangle.\end{aligned} \tag{7}$$

If there were no spin-flip ($B = C = E = F = 0$), only the $M = 0$ substates would be populated; spin-flip allows $M = \pm 1$ to be reached also. Following KMT we write the $Y_l^m(\theta, \phi)\ \boldsymbol{\sigma}_2 \cdot \mathbf{a}$ in terms of irreducible tensors † of rank k

$$T_k^q(l1) = \sum_\mu (1\ l\ \mu\ q-\mu|kq) Y_l^{q-\mu}(\theta, \phi)\sigma_\mu, \tag{8}$$

corresponding to a total angular momentum transfer $\mathbf{k} = \mathbf{1}+\mathbf{l}$. The extra unit of angular momentum arises from spin-flip by the σ_μ, which are tensor operators of rank one in the spin of the target nucleon, $\sigma_0 = \boldsymbol{\sigma}_2 \cdot \hat{\mathbf{q}}$ and $\sigma_{\pm 1} = \mp\, \boldsymbol{\sigma}_2 \cdot (\hat{\mathbf{n}} \pm i\hat{\mathbf{p}})/\sqrt{2}$. In making these definitions we set the x-axis along $\mathbf{n}$. We write for the reduced nuclear matrix elements

$$\begin{aligned} N_J &= \langle J||\rho_J Y_J||0\rangle, \\ Q_J &= \langle J||\rho_J T_J(J1)||0\rangle = (2\lambda)^{\frac{1}{2}} N_J e^{i\delta}, \end{aligned} \tag{9}$$

where

$$\langle JM|T_k^q|J_0 M_0\rangle (2J+1)^{\frac{1}{2}} = (kJ_0 qM_0|JM)\langle J||T_k||J_0\rangle.$$

The time reversal properties of the operators ensure that N and Q are both real [4]), so that their relative phase δ can only be 0 or π. Further, the ratio λ may depend upon the scattering angle [8]); only if the *nuclear* radial dependence is the same for spin-flip and spin independent transitions will λ be a constant.

We have from eq. (7)

$$\begin{aligned} (2J+1)^{\frac{1}{2}}|\mathrm{f}\rangle = N_J\{&|J, 0\rangle(A + C\boldsymbol{\sigma}_1 \cdot \hat{\mathbf{n}}) \\ &- (\tfrac{1}{2}\lambda)^{\frac{1}{2}} e^{i\delta}(|J, 1\rangle + |J, -1\rangle)(C + B\boldsymbol{\sigma}_1 \cdot \hat{\mathbf{n}}) \\ &+ i(\tfrac{1}{2}\lambda)^{\frac{1}{2}} e^{i\delta}(|J, 1\rangle - |J, -1\rangle) F\boldsymbol{\sigma}_1 \cdot \hat{\mathbf{p}}\}|\alpha_1\rangle. \end{aligned} \tag{10}$$

We now have to multiply the amplitudes for forming the state $|J, M\rangle$ by the photon amplitude (vector potential) $\mathbf{A}_{JM}(\theta, \phi)$ from 2^J-pole radiative decay to the spin zero ground state [9]). Explicit expressions for dipole and quadrupole transitions are given by Condon and Shortley [10]) and for octupole by French [11]). We then find the angular correlation of the decay gamma-ray with respect to $\mathbf{q}$ by summing (coherently) over the intermediate orientations M, squaring and averaging over the projectile spin states. For an unpolarized incident beam we get

$$\begin{aligned} W(\theta, \phi) = {} & (|A|^2+|C|^2)|\mathbf{A}_{J0}|^2 + \tfrac{1}{2}\lambda(|C|^2+|B|^2)|\mathbf{A}_{J1}+\mathbf{A}_{J-1}|^2 \\ & + \tfrac{1}{2}\lambda|F|^2|\mathbf{A}_{J1}-\mathbf{A}_{J-1}|^2 - (2\lambda)^{\frac{1}{2}} \mathrm{Re}\,[(A^*C+C^*B)\mathbf{A}_{J0}^*(\mathbf{A}_{J1}+\mathbf{A}_{J-1})]e^{i\delta}. \end{aligned} \tag{11}$$

For example, for $J = 2$ (discussed further in appendix I) this becomes

$$\begin{aligned} W(\theta, \phi) = {} & (|A|^2+|C|^2)\sin^2 2\theta + \tfrac{4}{3}\lambda(|C|^2+|B|^2)(\cos^2 2\theta \sin^2\phi + \cos^2\theta\cos^2\phi) \\ & + \tfrac{4}{3}\lambda|F|^2(\cos^2 2\theta\cos^2\phi + \cos^2\theta\sin^2\phi) + (\tfrac{4}{3}\lambda)^{\frac{1}{2}} e^{i\delta}\,\mathrm{Im}(A^*C+C^*B)\sin 4\theta \sin\phi. \end{aligned} \tag{12}$$

† There is a phase difference $(-)^{k-l-1}$ between the tensors defined by KMT in their eq. III.4 and the following equation. We use the former; then our Q_J is the same as the Q_{JJ} of their eq. III.5.

(These distributions are the same for electric and magnetic radiation, although their polarizations will differ.) Integrating W over the gamma-ray directions gives the proton differential cross section, proportional to

$$(2J+1)I_0 = |N_J|^2[|A|^2+|C|^2+\lambda(|B|^2+|C|^2+|F|^2)]. \tag{13}$$

If measurements are confined to the scattering plane (calling θ positive for $\phi = \frac{1}{2}\pi$ and negative for $\phi = \frac{3}{2}\pi$, the correlation (12) reduces to

$$w(\theta) = (|A|^2+|C|^2)\sin^2 2\theta+\tfrac{4}{3}\lambda(|C|^2+|B|^2)\cos^2 2\theta$$
$$+\tfrac{4}{3}\lambda|F|^2\cos^2\theta+(\tfrac{4}{3}\lambda)^{\frac{1}{2}}e^{i\delta}\,\mathrm{Im}(A^*C+C^*B)\sin 4\theta. \tag{14}$$

However, the finite solid angles subtended by actual counters usually make it necessary to use the full formula (12).

In previous calculations the only spin dependence considered was due to exchange, and corresponds to

$$M = A+B\boldsymbol{\sigma}_1\cdot\boldsymbol{\sigma}_2, \tag{15}$$

with A, B constants (antisymmetrization alone gives $A = \frac{3}{4}$, $B = \frac{1}{4}$). In this case the correlation (12) reduces to

$$W(\theta,\phi) = |A|^2\sin^2 2\theta+\tfrac{4}{3}\lambda|B|^2(\cos^2 2\theta+\cos^2\theta), \tag{16}$$

and the terms depending on ϕ, which are due to the coherence between magnetic substates, disappear. With no spin-flip ($\lambda = 0$ or $B = 0$), eq. (16) becomes the familiar $\sin^2 2\theta$.

Using the expansion (5) it is easy to generalize these results to include distorted wave effects. We now have angular momentum transfers l with z-components along $\mathbf{q}$ of $m \neq 0$. For $J = 1, 2, 3$ the final state (6) becomes (when the small $m = 1$ terms are neglected)

$$|\mathrm{f}\rangle = \sum_M |J, M\rangle\langle J, M|\bar{M}[\rho_l{}^0Y_l{}^0+\rho_l{}^2(Y_l{}^2+Y_l{}^{-2})]|0, 0\rangle|\alpha_1\rangle. \tag{17}$$

The calculation follows the same principles as before, the only change being an increase in the labour involved. We give as an example the results for $J = 2$, for an unpolarized incident beam:

$$\begin{aligned}W(\theta,\phi) = {} & (|A|^2+|C|^2)[|N_2{}^0|^2-2(\tfrac{2}{3})^{\frac{1}{2}}\mathrm{Re}(N_2{}^0N_2{}^{2*})\cos 2\phi]\sin^2 2\theta \\ & +\tfrac{2}{3}(|C|^2+|B|^2)|Q_2{}^0+(\tfrac{2}{3})^{\frac{1}{2}}Q_2{}^2|^2(\cos^2 2\theta\sin^2\phi+\cos^2\theta\cos^2\phi) \\ & +\tfrac{2}{3}|F|^2|Q_2{}^0-(\tfrac{2}{3})^{\frac{1}{2}}Q_2{}^2|^2(\cos^2 2\theta\cos^2\phi+\cos^2\theta\sin^2\phi) \\ & +(\tfrac{2}{3})^{\frac{1}{2}}\mathrm{Im}\{(A^*C+C^*B)(Q_2{}^0+(\tfrac{2}{3})^{\frac{1}{2}}Q_2{}^2)[N_2{}^{0*}\sin 4\theta\sin\phi \\ & \qquad -(\tfrac{2}{3})^{\frac{1}{2}}N_2{}^{2*}(\sin 4\theta\sin\phi\cos 2\phi-2\sin 2\theta\cos\phi\sin 2\phi)]\} \\ & +\tfrac{2}{3}(|A|^2+|C|^2)|N_2{}^2|^2(\sin^2 2\theta\cos^2 2\phi+4\sin^2\theta\sin^2 2\phi) \\ & +\tfrac{4}{9}|E|^2|Q_2{}^2|^2(\sin^2 2\theta\sin^2 2\phi+4\sin^2\theta\cos^2 2\phi),\end{aligned} \tag{18}$$

where we have put for the reduced matrix elements

$$N_2^m = \langle 2||\rho_2{}^m Y_2||0\rangle, \qquad Q_2^m = \langle 2||\rho_2{}^m T_2||0\rangle. \tag{19}$$

Because the distorted wave $\rho_l{}^m$ is complex, the $N_l{}^m$ and $Q_l{}^m$ are no longer real, and their relative phase is no longer restricted to 0 or π. Again, in general all the reduced matrix elements will vary with scattering angle in different ways [8]). Only if the *nuclear* radial dependence is the same for spin-flip and spin-independent transitions will the ratios $Q_2{}^m/N_2{}^m$ be independent of scattering angle. Confining our attention to the scattering plane, using the same convention for θ as in (14), we find

$$\begin{aligned} w(\theta) = {} & (|A|^2+|C|^2)|N_2{}^0+(\tfrac{2}{3})^{\frac{1}{2}}N_2{}^2|^2 \sin^2 2\theta \\ & +\tfrac{2}{3}(|B|^2+|C|^2)|Q_2{}^0+(\tfrac{2}{3})^{\frac{1}{2}}Q_2{}^2|^2 \cos^2 2\theta \\ & +\tfrac{2}{3}|F|^2|Q_2{}^0-(\tfrac{2}{3})^{\frac{1}{2}}Q_2{}^2|^2 \cos^2\theta \\ & +(\tfrac{2}{3})^{\frac{1}{2}}\,\mathrm{Im}[(A^*C+C^*B)(N_2{}^0+(\tfrac{2}{3})^{\frac{1}{2}}N_2{}^2)^*(Q_2{}^0+(\tfrac{2}{3})^{\frac{1}{2}}Q_2{}^2)]\sin 4\theta \\ & +\tfrac{16}{9}|E|^2|Q_2{}^2|^2]\sin^2\theta. \end{aligned} \tag{20}$$

We see that this angular correlation is of the same form as the plane wave case, the only change being in the coefficients and the introduction of a small $\sin^2\theta$ term. Further, as $N_2{}^2/N_2{}^0$ and $Q_2{}^2/Q_2{}^0$ are small over the main peak of the proton angular distribution ($\lesssim 10\,\%$ at 150 MeV) [6, 7]) we see that the change in the angular correlation in going from plane waves to distorted waves may be small. The chief effect is on the ratio $Q_2{}^0/N_2{}^0$, which was denoted $(2\lambda)^{\frac{1}{2}}$ in the is a tendency for any variation of λ with scattering angle to be enhanced by the distortion [7]). The $m = 2$ terms become comparable to the $m = 0$ for small plane wave case; in particular there scattering angles ($<20°$ at 150 MeV) for the cases $J = 2$ and 3, so measurement at these angles would be necessary to detect these effects. The $m = 1$ terms (neglected above) are smaller still, and only play a role at even smaller angles ($<10°$ at 150 MeV).

These conclusions are similar to those of Squires [12]) who showed in WKB approximation that the polarization of the outgoing proton is scarcely altered in going from plane-waves to distorted waves. The main effect of the distorting potential at these energies is to absorb the protons, which results in a uniform decrease of the feeding of the magnetic substates of the state of spin J so that the gamma-ray angular correlation or the polarization of the outgoing proton are not changed, although the cross-section is considerably reduced.

4. Correlation with Incident Beam Polarized

Using the amplitude method it is easy to see, from eq. (10) for plane waves or eq. (17) for distorted waves, the effect on the angular correlation of using polarized protons, by putting for $|\alpha_1\rangle$ the Pauli spinor describing the incident beam polarization.

For example, protons completely polarized along a direction with polar angles (β, α) are represented by

$$|\alpha_1\rangle = \cos(\tfrac{1}{2}\beta)|+\rangle + e^{i\alpha}\sin(\tfrac{1}{2}\beta)|-\rangle,$$

where $\pm$ denotes the $\pm\frac{1}{2}$ components of the spin along $\mathbf{q}$. We quote some results of using plane-waves for the example we have given in sect. 2; the excitation of a state of spin J and parity $(-1)^J$ by inelastic scattering off the ground state of spin zero of an even nucleus. If the polarization is perpendicular to the scattering plane, the angular correlation is

$$W(\theta, \phi) = K|\mathbf{A}_{J0}(\theta, \phi)|^2 + \tfrac{1}{2}\lambda L|\mathbf{A}_{J1}(\theta, \phi) + \mathbf{A}_{J-1}(\theta, \phi)|^2 + \tfrac{1}{2}\lambda M|\mathbf{A}_{J1}(\theta, \phi) - \mathbf{A}_{J-1}(\theta, \phi)|^2 - (2\lambda)^{\frac{1}{2}} e^{i\delta}\,\mathrm{Re}\,[N\mathbf{A}^*_{J0}(\mathbf{A}_{J1} + \mathbf{A}_{J-1})], \quad (21)$$

where $K\ L, M, N$ are given in the following table:

	Incident unpolarized	Polarized along $\mathbf{n}$	Polarized along $-\mathbf{n}$
K	$\lvert A\rvert^2+\lvert C\rvert^2$	$\lvert A+C\rvert^2$	$\lvert A-C\rvert^2$
L	$\lvert C\rvert^2+\lvert B\rvert^2$	$\lvert C+B\rvert^2$	$\lvert C-B\rvert^2$
M	$\lvert F\rvert^2$	$\lvert F\rvert^2$	$\lvert F\rvert^2$
N	(A^*C+C^*B)	$(A+C)^*(C+B)$	$(A-C)^*(C-B)$

This correlation has the same form as the unpolarized, but with changed coefficients. Any component of polarization in the scattering plane, however, will introduce additional terms (see appendix 2); for example, terms proportional to $\sin 2\phi$ and $\cos\phi$ occur when $J = 2$. Thus one can, by the use of an incident polarized beam, obtain further details of the inelastic scattering interaction, in particular further information about the parameters of the proton-nucleon scattering interaction. This is supplementary to the information obtained from the polarization of the scattered proton, or the asymmetry of inelastically scattering polarized protons (these two being equal with the present model [12]), an equality which agrees with experiment).

For $J = 2$ the polarization (or asymmetry coefficient) P is obtained, by using distorted waves, from

$$5I_0 P = 2\,\mathrm{Re}(A^*C)(|N_2{}^0|^2 + 2|N_2{}^2|^2) + \mathrm{Re}(B^*C)|Q_2{}^0 + (\tfrac{2}{3})^{\frac{1}{2}}Q_2{}^2|^2, \quad (22)$$

where

$$5I_0 = (|A|^2+|C|^2)(|N_2{}^0|^2+2|N_2{}^2|^2) + \tfrac{1}{2}(|C|^2+|B|^2)|Q_2{}^0+(\tfrac{2}{3})^{\frac{1}{2}}Q_2{}^2|^2 + \tfrac{1}{2}|F|^2|Q_2{}^0-(\tfrac{2}{3})^{\frac{1}{2}}Q_2{}^2|^2 + \tfrac{4}{3}|E|^2|Q_2{}^2|^2 \quad (23)$$

is the unpolarized proton angular distribution. The latter expression for I_0 also indicates the terms additional to those in eq. (13) which the distorted waves have introduced (we have again neglected $m = 1$ contributions).

5. General Formalism

We now present the general formalism, using the tensor algebra of Racah and including distorted wave effects in the way discussed in sect. 2. It is thus a development of some of the results given by KMT. It may also be used at lower bombarding energies where distortion effects are important and the effective two-body interaction $\overline{M(q')}$ has to be treated phenomenologically rather than taken as the free nucleon-nucleon scattering amplitude.

Following KMT † we write $M(q)$ as

$$M = M_0 + \mathbf{M}_1 \cdot \boldsymbol{\sigma}(2) = M_0 + \sum_{\mu} (-)^{\mu} M_{1-\mu} \sigma_{\mu}(2),$$

where $\boldsymbol{\sigma}(2)$ refers to the target nucleon, and

$$\begin{aligned} M_0 &= A + C\boldsymbol{\sigma}(1) \cdot \hat{\mathbf{n}}, \qquad M_{10} = E\boldsymbol{\sigma}(1) \cdot \hat{\mathbf{q}}, \\ M_{1\pm1} &= \mp(\tfrac{1}{2})^{\frac{1}{2}}(C + B\boldsymbol{\sigma}(1) \cdot \hat{\mathbf{n}} \pm iF\boldsymbol{\sigma}(1) \cdot \hat{\mathbf{p}}). \end{aligned} \tag{24}$$

Now $\boldsymbol{\sigma}(1)$ refers to the projectile. Each coefficient is isospin dependent so that $M_s = M_s(\alpha) + M_s(\beta)\boldsymbol{\tau}(1) \cdot \boldsymbol{\tau}(2)$, etc. Only the β-terms can give "charge exchange" reactions (p, n) or (n, p). Using the partial wave expansion (5) and the spin-angle tensors (8), the amplitude (1) for scattering from nuclear state $|J_A M_A, T_A T_{A3}\rangle$ to state $|J_B M_B, T_B T_{B3}\rangle$ becomes

$$\begin{aligned} A(\mathbf{k}', \mathbf{k}) \equiv \langle J_B M_B, T_B T_{B3}; \tfrac{1}{2} m_b | \bar{M} \rho(\mathbf{k}', \mathbf{k}, \mathbf{r}) | J_A M_A, T_A T_{A3}; \tfrac{1}{2} m_a \rangle \\ = \sum_{klsm\mu} (J_A J_B M_A - M_B | k, -q)(sl\mu m | kq)(-)^{k+J_B-M_B} \\ \times (2k+1)^{-\frac{1}{2}} (-)^m \mathbf{b}_m(kls) \cdot (\mathbf{M}_{s-\mu})_{m_b m_a}. \end{aligned} \tag{25}$$

The initial and final spin states of the projectile are denoted m_a and m_b, respectively. We have put $T_k{}^q(l0) = \delta_{kl} Y_l{}^q(\theta, \phi)$, and written

$$\mathbf{b} \cdot \mathbf{M} = b(\alpha) M(\alpha) + b(\beta) M(\beta), \tag{26}$$

where the (complex) nuclear reduced matrix elements are

$$\begin{aligned} b_m(\alpha; kls) &= \langle J_B T_B || \rho_l{}^m T_k(ls) || J_A T_A \rangle \delta_{T_A T_B}, \\ b_m(\beta; kls) &= f(T_B T_A) \langle J_B T_B || \rho_l{}^m T_k(ls) \boldsymbol{\tau} || J_A T_A \rangle, \end{aligned} \tag{27}$$

and the isospin factor is

$$f(T_B T_A) = \sqrt{3}(2T_B+1)^{-\frac{1}{2}} (-)^{\eta} (1\tfrac{1}{2}, -\eta t_{a3} | \tfrac{1}{2} t_{b3}) (1 T_A \eta T_{A3} | T_B T_{B3}),$$

where t_{a3} and t_{b3} denote the initial and final isospin states of the projectile. If axes are chosen as in KMT with z-axis along $\mathbf{q}$ and x-axis along $\mathbf{n}$, we have the symmetry $\mathbf{b}_{-m} = \mathbf{b}_m$. In the adiabatic approximation [5]) (zero energy loss) only even values of m are allowed. With plane waves we have $m = 0$ only, and

$$\rho_l{}^m(r) \to \delta_{m0} \rho_l = [4\pi(2l+1)]^{\frac{1}{2}} (-i)^l j_l(qr). \tag{28}$$

† The $M^1_{\pm1}$ given by KMT have the wrong sign.

The b_0 then become the reduced matrix elements of KMT, $b_0\,(ll0) = N_l$ and $b_0(kl1) = Q_{kl}$, which are real.

Each term in the amplitude (25) corresponds to a transfer to the target of angular momentum $\mathbf{k}$ made up of an orbital part $\mathbf{l}$ and spin part $\mathbf{s}$, $\mathbf{k} = \mathbf{s}+\mathbf{l}$. The spin transfer can only have the values $s = 0$ or 1, and we refer to these as spin-independent and spin-flip transition, respectively. In the absence of spin-orbit and tensor coupling in the two-body interaction ($C = 0$ and $B = E = F$), a spin transfer $s \neq 0$ arises only from a coupling to the projectile spin; we then have

$$M = A + B\boldsymbol{\sigma}(1)\cdot\boldsymbol{\sigma}(2),$$

$$(M_{s,-\mu})_{m_b m_a} = (\tfrac{1}{2}s m_a,\ -\mu|\tfrac{1}{2}m_b)\,a_s(2s+1)^{\frac{1}{2}}, \tag{29}$$

where $a_0 = A$ and $a_1 = B$. If $B = 0$, only $s = 0$ is allowed.

The differential cross-section is given by

$$\frac{\mathrm{d}\sigma}{\mathrm{d}\omega} = \left(\frac{2N^2}{N+1}\right)^2 \frac{k'}{k}\,\frac{I_0}{2J_A+1},$$

where

$$\begin{aligned} I_0 &= \tfrac{1}{2}\sum_{M_B M_A m_b m_a} |A(\mathbf{k}',\mathbf{k})|^2 \\ &= \tfrac{1}{2}\sum (2k+1)^{-1}(sl\mu q-\mu|kq)(s'l'\mu' q-\mu')kq)(-)^{\mu-\mu'} \\ &\quad\times[\mathbf{b}_{q-\mu}(kls)\cdot(\mathbf{M}_{s-\mu})_{m_b m_a}][\mathbf{b}_{q-\mu'}(kl's')\cdot(\mathbf{M}_{s'-\mu'})_{m_b m_a}]^*. \end{aligned} \tag{30}$$

The summation takes place over k, l, l', s, s', μ, μ', m_b and m_a. With plane waves, $q = \mu-\mu'$, interference between $s = 0$ and $s = 1$ vanishes, and I_0 is given explicitly by eq. (8.2) of KMT. In the adiabatic approximation (when only even m are allowed) the interference between $s = 0$ and $s = 1$ vanishes even with distorted waves. The special case for a $T = 0$ target and $k = l = l' = 2$ only, is given in eq. (23), where $b_m(ll0) = N_l{}^m$ and $b_m(ll1) = Q_l{}^m$.

The polarization P induced by scattering an unpolarized beam is the expectation value of $\boldsymbol{\sigma}(1)\cdot\hat{\mathbf{n}}$; within this model it is equal to the asymmetry from scattering a completely polarized beam [12]). With the direction of $\mathbf{n}$ as positive we have

$$\begin{aligned} I_0 P = \tfrac{1}{2}\sum (2k+1)^{-\frac{1}{2}}&(sl\mu q-\mu|kq)(s'l'\mu' q-\mu'|kq)(-)^{\mu-\mu'} \\ &\times[\mathbf{b}_{q-\mu}(kls)\cdot(\mathbf{M}_{s-\mu})_{m_b m_a}][\mathbf{b}_{q-\mu'}(kl's')\cdot(\mathbf{M}_{s'-\mu'})_{-m_b m_a}]^*, \end{aligned} \tag{31}$$

where I_0 is given by eq. (30). Again, with plane waves $q = \mu - \mu'$ and $I_0 P$ is given explicitly by eq. (8.3) of KMT.

The orientation of the residual nucleus following the scattering from $\mathbf{k}$ to $\mathbf{k}'$ is described by statistical tensors [4]):

$$\begin{aligned} \rho_{KQ}(J_B J_B) = \sum_{M_A M_B \tilde{m}_a m_b} &(J_B J_B M_B Q - M_B|KQ)(-)^{J_B+Q-M_B} \\ &\times\langle J_B M_B,\tfrac{1}{2}m_b|M\rho|J_A M_A,\tfrac{1}{2}m_a\rangle\langle J_B M_B - Q,\tfrac{1}{2}m_b|M\rho|J_A M_A,\tfrac{1}{2}m_a\rangle, \end{aligned} \tag{32}$$

when the incident beam is unpolarized. These tensors then give the angular distribution of any further radiation; since its detection must be in coincidence with the outgoing nucleon in order to define $\mathbf{k}'$, the measurement is really of an angular correlation. For gamma-rays emitted in a direction (θ, ϕ) this angular correlation is

$$W(\theta, \phi) = \sum_{KQ} \rho_{KQ}(J_B J_B) F_K C_{KQ}(\theta, \phi), \tag{33}$$

where $C_{KQ}(\theta, \phi) = (4\pi)^{\frac{1}{2}}(2K+1)^{-\frac{1}{2}} Y_K^Q(\theta, \phi)$ is the spherical harmonic normalized so that $C_{00} = 1$ and $C_{K0}(\theta, \phi) = P_K(\cos\theta)$. The coefficients F_k depend on the initial and final nuclear spins J_B and J_C in the gamma transition:

$$F_K = \sum_{LL'} C_L C_{L'} F_K(LL' J_C J_B),$$

where C_L is the reduced matrix element for a 2^L-pole gamma transition; the F_k have been extensively tabulated [4]). Only even values of K enter the sum for W, but the tensors of odd rank K are needed to predict the degree of circular polarization of the gamma-rays, which is given by

$$C(\theta, \phi) = \frac{\sum_{K \text{ odd}, Q} \rho_{KQ} F_K C_{KQ}(\theta, \phi)}{\sum_{K \text{ even}, Q} \rho_{KQ} F_K C_{KQ}(\theta, \phi)}.$$

A more detailed discussion of the circular polarization has been given elsewhere [13]).

Since W and C are real, the tensors must have the symmetry $\rho_{KQ} = (-)^Q \rho^*_{K-Q}$. The distribution W has symmetry of reflection through the scattering plane, while C changes sign, so with our choice of axes we also have $\rho_{KQ} = (-)^{K-Q} \rho^*_{KQ}$.

Using the amplitude (25) the tensor (32) can be written

$$\rho_{KQ}(J_B J_B) = \sum_{kk'} (-)^{J_A - J_B - 1} W(J_B J_B kk'; K J_A) \rho_{KQ}(kk'), \tag{34}$$

where

$$\begin{aligned}\rho_{KQ}(kk') &= \sum (kk'qQ-q|KQ)(sl\mu q-\mu|kq)(s'l'\mu' q-Q-\mu'|kq-Q) \\ &\times (-)^{K-Q-q+\mu-\mu'-1} [\mathbf{b}_{q-\mu}(kls) \cdot (\mathbf{M}_{s-\mu})_{m_b m_a}][\mathbf{b}_{q-Q-\mu'}(k'l's') \cdot (\mathbf{M}_{s'-\mu'})_{m_b m_a}]^* \\ &= (-)^Q \rho_{K-Q}(k'k)^*,\end{aligned} \tag{35}$$

summed over l, l', s, s', μ, μ', q, m_a and m_b. With plane waves, $q = \mu$ and $Q = \mu - \mu'$, so that Q can take the values $0, \pm 1, \pm 2$ only. When $K = Q = 0$, the scalar ρ_{00} is proportional to the differential cross-section (30)

$$(2J_B+1)^{\frac{1}{2}} \rho_{00}(J_B J_B) = 2I_0. \tag{36}$$

Explicit expressions for the ρ_{KQ} when plane waves are used are given in appendix 2.

In the absence of spin-orbit or tensor coupling in the two-body interaction ($C = 0$, $B = E = F$) we have no interference between $s = 0$ and $s = 1$, and we may use eq. (29) to further reduce [13]) eq. (34),

$$\rho_{KQ}(J_B J_B) = 2 \sum_{kk'll's} [(2k+1)(2k'+1)]^{\frac{1}{2}}(-)^{J_A - J_B - s - l'} W(kk' J_B J_B; K J_A) \times W(ll' kk'; Ks)\rho_{KQ}(kls, k'l's), \quad (37)$$

where now

$$\rho_{KQ}(kls, k'l's) = \sum_m (ll' mQ - m|KQ)(-)^{l'+Q-m}[\mathbf{b}_m(kls) \cdot \mathbf{a}_s][\mathbf{b}_{m-Q}(k'l's) \cdot \mathbf{a}_s]^*. \quad (38)$$

In this case plane waves will allow only $Q = 0$ (since $m = 0$), and we regain the well-known symmetry [2]) about the recoil $\mathbf{q}$.

If the incident beam is polarized, the amplitudes in the definition (32) of the statistical tensors must be weighted with the corresponding spin density matrix

$$2\boldsymbol{\rho}(\text{spin}) = \mathbf{1} + \boldsymbol{\sigma} \cdot \mathbf{P}', \quad (39)$$

where $\mathbf{P}'$ is the polarization vector of the incident beam: $\mathbf{P}' = \langle \boldsymbol{\sigma} \rangle_{\text{in}}$. Eq. (34) is still valid, but now we have

$$\boldsymbol{\rho}_{KQ}(kk') = \rho^{(1)}_{KQ}(kk') + \boldsymbol{\rho}^{(2)}_{KQ}(kk') \cdot \mathbf{P}', \quad (40)$$

where $\rho^{(1)}$ is given by eq. (35), and $\boldsymbol{\rho}^{(2)}$ is similar, but now with the spin trace over $\boldsymbol{\sigma}$ ($\text{tr} = \sum_{m_b m_a}$):

$$\boldsymbol{\rho}^{(2)}_{KQ}(kk') = \sum (kk' qQ - q|KQ)(sl\mu q - \mu|kq)(s'l'\mu' q - Q - \mu'|k'q - Q)(-)^{K+Q-q+\mu-\mu'-1} \times \text{tr}[\mathbf{b}_{q-\mu}(kls) \cdot \mathbf{M}_{s-\mu}]\boldsymbol{\sigma}[\mathbf{b}_{q-Q-\mu'}(k'l's') \cdot \mathbf{M}_{s'-\mu'}]^\dagger. \quad (41)$$

The spherical components $\rho_\lambda{}^{(2)}$ of the vector $\boldsymbol{\rho}^{(2)}$ now have the symmetry

$$\rho^{(2)}_{KQ,\lambda}(kk') = (-)^{Q-\lambda}\rho^{(2)}_{K-Q,-\lambda}(k'k)^*.$$

The scalar ρ_{00} now gives the differential cross-section for polarized particles

$$(2J_B+1)^{\frac{1}{2}}\rho_{00}(J_B J_B) = 2I_0(1 + \mathbf{P} \cdot \mathbf{P}'), \quad (42)$$

where $\mathbf{P}$ is parallel to $\mathbf{n}$ and is given by eq. (31). Eq. (42) thus exhibits the polarization-asymmetry equality of this model [12]). Again, explicit expressions for the $\boldsymbol{\rho}^{(2)}$, when plane waves are used, are given in appendix 2.

The authors wish to thank D. M. Brink, G. L. Salmon and D. J. Rowe for helpful discussions.

Appendix 1

An often-studied case of inelastic scattering is the excitation of the $J = 2^+$ first excited state of even nuclei [3, 14, 15]), especially the 4.43 MeV level in C^{12}. It may be helpful to remark on a number of ways in which the correlation function can be written in this case. When distortion can be neglected, the correlation for E2 decay of this state is given by eq. (12), which is of the form

$$W(\theta, \phi) = P \sin^2 2\theta + Q(\cos^2 2\theta \sin^2 \phi + \cos^2 \theta \cos^2 \phi) + R(\cos^2 2\theta \cos^2 \phi + \cos^2 \theta \sin^2 \phi) + S \sin 4\theta \sin \phi.$$

It can be written as

$$W = P \sin^2 2\theta + \tfrac{1}{2}(R+Q)(\cos^2 2\theta + \cos^2 \theta) + \tfrac{1}{2}(R-Q)(\cos^2 2\theta - \cos^2 \theta)\cos 2\phi + S \sin 4\theta \sin \phi, \quad (43)$$

and also as

$$W = \alpha + (\beta_1 + \beta_2 \cos 2\phi)\cos 2\theta + (\gamma_1 + \gamma_2 \cos 2\phi)\cos 4\theta + S \sin 4\theta \sin \phi,$$

where

$$\alpha = \tfrac{1}{2}(P+Q+R), \quad \beta_1+\beta_2 = \tfrac{1}{2}Q, \quad \beta_1-\beta_2 = \tfrac{1}{2}R, \quad \gamma_1 = 3\beta_1-\alpha, \quad \gamma_2 = -\beta_2.$$

In the scattering plane, calling θ positive for $\phi = \frac{1}{2}\pi$ and negative for $\phi = \frac{3}{2}\pi$, we have

$$\begin{aligned} w(\theta) &= P \sin^2 2\theta + Q \cos^2 2\theta + R \cos^2 \theta + S \sin 4\theta \\ &= \tfrac{1}{2}(P+Q+R) + \tfrac{1}{2}R \cos 2\theta + \tfrac{1}{2}(Q-P)\cos 4\theta + S \sin 4\theta. \end{aligned}$$

Slight rearrangement gives the familiar form [2, 3])

$$w(\theta) = V - R \sin^2 \theta + W \sin^2 2(\theta - \theta'), \quad (44)$$

where

$$V = \tfrac{1}{2}(P+Q-W)+R, \qquad W = [(Q-P)^2+4S^2]^{\frac{1}{2}}, \qquad \tan 4\theta' = 2S/(Q-P).$$

The shift θ' away from the recoil direction $\mathbf{q}$ here arises entirely from the spin-orbit coupling term C in the two-body interaction. The distorted wave theory gives exactly the same form (44) in the adiabatic limit, but the distortion modifies the coefficients and contributes to the shift θ'. In the non-adiabatic case, the distortion also introduces a shift θ'' into the $R \sin^2 \theta$ term, but this is very small at high energy.

For the ^{12}C(p, p′) reaction mentioned above, λ is found to be small [14]) so that R is small, and over the range of observation $10° < |\theta| < 60°$ the angular correlation is apparently of the form $V + W \sin^2 2\theta$, where θ is here measured from an axis displaced an angle θ' from the recoil direction defined by $\mathbf{q}$. θ' is a small angle, typically less than 5°, and as, to measure S, one has

effectively to measure this angle, it is evident that a measurement of S will require great care in the measurement of angles. Alternatively, if one restricts attention to the plane defined by $\phi = 0$ and π, that is one makes measurements moving the gamma-ray counter in a plane through the recoil direction and perpendicular to the scattering plane, the angular correlation is simpler, being of the form

$$w'(\theta) = P \sin^2 2\theta + R \cos^2 2\theta + Q \cos^2 \theta.$$

In the plane prependicular to the recoil direction where $\theta = \frac{1}{2}\pi$, the correlation (43) has the azimuthal dependence

$$f(\phi) = \tfrac{1}{2}(Q+R) + \tfrac{1}{2}(R-Q)\cos 2\phi.$$

Along **n**, the perpendicular to the scattering plane, $\phi = 0$ and

$$f(0) = R = \tfrac{4}{3}\lambda|F|^2,$$

which in principle can thus be measured as a function of proton scattering angle.

Thus one sees that a suitable selection of angular correlation measurements will enable the separate coefficients, P, Q, R and S to be determined. Combined with information from measurements of the polarization of the outgoing proton and the asymmetry in scattering polarized protons, one reaches a considerable knowledge of the inelastic scattering interaction and is able to use it as a tool to study nuclear structure.

Appendix 2

When plane waves are used we may follow KMT and write for the reduced matrix elements $b_0(ll0) = N_l$ and $b_0\ (kl1) = Q_{kl}$, both real. Expressions for the $\rho_{KQ}\ (kk')$ are given in eqs. (35) and (41). The properties of the spin trace and the Clebsch-Gordan coefficients lead to the symmetries

$$\rho_{KQ}(kk') = (-)^{K-P}\rho_{K-Q}(kk') = (-)^{K-Q-P}\rho_{KQ}(k'k)^*,$$

where $P = 0$ for $\rho^{(1)}$ and $\rho_x^{(2)}$, but $P = 1$ for $\rho_y^{(2)}$ and $\rho_z^{(2)}$ (The x-component behaves differently from the y- and z-components because **n** is an axial vector while **p** and **q** are polar). The coefficients in eq. (34) are symmetrical in k and k', so that only the symmetrical parts of $\rho(kk')$ contribute. These are real (imaginary) as $(K-Q-P)$ is even(odd), using the symmetries just mentioned. We may then write explicitly, taking a (b) as K is even (odd):

$$\rho_{K0}^{(1)}(kk') = 0$$

if K is odd, and

$$\rho^{(1)}_{K0}(kk') = 2(kk'1, -1|K0)\sum_{ll'}(1l10|k1)(1l'10|k'1)$$
$$\times \mathrm{Re}[(\mathbf{Q}_{kl}\cdot\mathbf{B})^*(\mathbf{Q}_{k'l'}\cdot\mathbf{B})+(\mathbf{Q}_{kl}\cdot\mathbf{C})^*(\mathbf{Q}_{k'l'}\cdot\mathbf{C})+(\mathbf{Q}_{kl}\cdot\mathbf{F})^*(\mathbf{Q}_{k'l'}\cdot F)]$$
$$-2(kk'00|K0)\sum_{ll'}\mathrm{Re}\{[\mathbf{N}_l\cdot\mathbf{A})^*(\mathbf{N}_{l'}\cdot\mathbf{A})+(\mathbf{N}_l\cdot\mathbf{C})^*(\mathbf{N}_{l'}\cdot\mathbf{C})]\delta_{kl}\delta_{k'l'}$$
$$+(1l00|k0)(1l'00|k'0)(\mathbf{Q}_{kl}\cdot\mathbf{E})^*(\mathbf{Q}_{k'l'}\cdot E)\},$$

if K is even. The last term vanishes if $k = l$ or $k' = l'$.
Further we have

$$\rho^{(1)}_{K1}(kk') = -(8)^{\frac{1}{2}}(kk'10|K1)\sum_{ll'}(1l10|k1)\delta_{k'l'}$$
$$\times(i\,\mathrm{Im}/\mathrm{Re})[(\mathbf{Q}_{kl}\cdot\mathbf{C})^*(\mathbf{N}_{l'}\cdot\mathbf{A})+(\mathbf{Q}_{kl}\cdot\mathbf{B})^*(\mathbf{N}_{l'}\cdot\mathbf{C})],$$

$$\rho^{(1)}_{K2}(kk') = (kk'11|K2)\sum_{ll'}(1l10|k1)(1l'10|k'1)(-)^{k'+l'}$$
$$\times(\mathrm{Re}/i\,\mathrm{Im})[(\mathbf{Q}_{kl}\cdot\mathbf{C})^*(\mathbf{Q}_{k'l'}\cdot\mathbf{C})+(\mathbf{Q}_{kl}\cdot\mathbf{B})^*(\mathbf{Q}_{k'l'}\cdot\mathbf{B})-(\mathbf{Q}_{kl}\cdot\mathbf{F})^*(\mathbf{Q}_{k'l'}\cdot\mathbf{F})].$$

The polarization terms $\boldsymbol{\rho}^{(2)}$ are most conveniently given by their Cartesian components. We have

$$\rho^{(2)}_{K0,x}(kk') = 0$$

if K is odd, but if K is even

$$\rho^{(2)}_{K0,x}(kk') = 4(kk'1, -1|K0)\sum_{ll'}(1l10|k1)(1l'10|k'1)\mathrm{Re}(\mathbf{Q}_{kl}\cdot\mathbf{C})^*(\mathbf{Q}_{k'l'}\cdot\mathbf{B})$$
$$-4(kk'00|K0)\sum_{ll'}\mathrm{Re}(\mathbf{N}_l\cdot\mathbf{A})^*(\mathbf{N}_{l'}\cdot\mathbf{C})\delta_{kl}\delta_{k'l'}.$$

The other terms are

$$\rho^{(2)}_{K1,x}(kk') = -(8)^{\frac{1}{2}}(kk'10|K1)\sum_{ll'}(1l10|k1)(i\,\mathrm{Im}/\mathrm{Re})$$
$$\times\{[(\mathbf{Q}_{kl}\cdot\mathbf{B})^*(\mathbf{N}_{l'}\cdot\mathbf{A})+(\mathbf{Q}_{kl}\cdot\mathbf{C})^*(\mathbf{N}_{l'}\cdot\mathbf{C})]\delta_{k'l'}$$
$$-(1l'00|k'0)(\mathbf{Q}_{kl}\cdot\mathbf{F})^*(\mathbf{Q}_{k'l'}\cdot\mathbf{E})\},$$

$$\rho^{(2)}_{K2,x}(kk') = 2(kk'11|K2)\sum_{ll'}(1l10|k1)(1l'10|k'1)(-)^{k'+l'}$$
$$\times(\mathrm{Re}/i\,\mathrm{Im})(\mathbf{Q}_{kl}\cdot\mathbf{C})^*(\mathbf{Q}_{k'l'}\cdot\mathbf{B}),$$

$$\rho^{(2)}_{K0,y}(kk') = 0, \qquad (K \text{ even}),$$

$$\rho^{(2)}_{K0,y}(kk') = 4(kk'00|K0)\sum_{ll'}(1l'00|k'0)\mathrm{Im}(\mathbf{N}_l\cdot\mathbf{C})^*(\mathbf{Q}_{k'l'}\cdot\mathbf{E})\delta_{kl}$$
$$-4(kk'1, -1|K0)\sum_{ll'}(1l10|k1)(1l'10|k'1)\mathrm{Im}(\mathbf{Q}_{kl}\cdot\mathbf{C})^*(\mathbf{Q}_{k'l'}\cdot\mathbf{F}), \qquad (K \text{ odd}),$$

$$\rho^{(2)}_{K1,y}(kk') = (8)^{\frac{1}{2}}(kk'10|K1)\sum_{ll'}(1l10|k1)(-)^{K+1}(\mathrm{Im}/i\,\mathrm{Re})$$
$$\times[(\mathbf{Q}_{kl}\cdot\mathbf{F})^*(\mathbf{N}_{l'}\cdot\mathbf{A})\delta_{k'l'}-(1l'00|k'0)(\mathbf{Q}_{kl}\cdot\mathbf{B})^*(\mathbf{Q}_{k'l'}\cdot\mathbf{E})],$$

$$\rho^{(2)}_{K2,y}(kk') = 2(kk'11|K2)\sum_{ll'}(1l10|k1)(1l'10|k'1)(-)^{k'+l'+K+1} \times (i\,\mathrm{Re/Im})(\mathbf{Q}_{kl}\cdot\mathbf{C})^*(\mathbf{Q}_{k'l'}\cdot\mathbf{F}),$$

$$\rho^{(2)}_{K0,x}(kk') = 0, \qquad (K \text{ even}),$$

$$= 4(kk'00|K0)\sum_{ll'}(1l'00|k'0)\mathrm{Re}(\mathbf{N}_l\cdot\mathbf{A})^*(\mathbf{Q}_{k'l'}\cdot\mathbf{E})\delta_{kl}$$

$$-4(kk'1,-1|K0)\sum_{ll'}(1l10|k1)(1l'10|k'1)\mathrm{Re}(\mathbf{Q}_{kl}\cdot\mathbf{B})^*(\mathbf{Q}_{k'l'}\cdot\mathbf{F}), \quad (K \text{ odd}),$$

$$\rho^{(2)}_{K1,x}(kk') = (8)^{\frac{1}{2}}(kk'10|K1)\sum_{ll'}(1l10|k1)(\mathrm{Re}/i\,\mathrm{Im}) \times[(\mathbf{Q}_{kl}\cdot\mathbf{F})^*(\mathbf{N}_{l'}\cdot\mathbf{C})+(1l'00|k'0)(\mathbf{Q}_{kl}\cdot\mathbf{C})^*(\mathbf{Q}_{k'l'}\cdot\mathbf{E})],$$

$$\rho^{(2)}_{K2,x}(kk') = 2(kk'11|K2)\sum_{ll'}(1l10|k1)(1l'10|k'1)(-)^{k'+l'} \times (i\,\mathrm{Im/Re})(\mathbf{Q}_{kl}\cdot\mathbf{B})^*(\mathbf{Q}_{k'l'}\cdot\mathbf{F}).$$

As an example of the reduction to a special case we consider one in which $k = k' = l = l' = 2$ only; for example excitation of the first 2^+ state of an even nucleus. We then have relations between the components $\rho_{KQ}(kk')$:

$$\rho_{41} = -(6)^{\frac{1}{2}}\rho_{21}, \qquad \rho_{42} = -(\tfrac{4}{3})^{\frac{1}{2}}\rho_{22},$$
$$\rho_{40}+(14)^{\frac{1}{2}}\rho_{00}+(20)^{\frac{1}{2}}\rho_{20} = 0.$$

The remaining tensors become, for even K,

$$\rho^{(1)}_{00} = -(\tfrac{1}{5})^{\frac{1}{2}}[|\mathbf{Q}\cdot\mathbf{B}|^2+|\mathbf{Q}\cdot\mathbf{C}|^2+|\mathbf{Q}\cdot\mathbf{F}|^2+2(|\mathbf{N}\cdot\mathbf{A}|^2+|\mathbf{N}\cdot\mathbf{C}|^2)],$$
$$\rho^{(1)}_{20} = (\tfrac{1}{14})^{\frac{1}{2}}[|\mathbf{Q}\cdot\mathbf{B}|^2+|\mathbf{Q}\cdot\mathbf{C}|^2+|\mathbf{Q}\cdot\mathbf{F}|^2+4(|\mathbf{N}\cdot\mathbf{A}|^2+|\mathbf{N}\cdot\mathbf{C}|^2)],$$
$$\rho^{(1)}_{21} = (\tfrac{2}{7})^{\frac{1}{2}}i\,\mathrm{Im}[(\mathbf{Q}\cdot\mathbf{C})^*(\mathbf{N}\cdot\mathbf{A})+(\mathbf{Q}\cdot\mathbf{B})^*(\mathbf{N}\cdot\mathbf{C})],$$
$$\rho^{(1)}_{22} = -(\tfrac{3}{28})^{\frac{1}{2}}(|\mathbf{Q}\cdot\mathbf{B}|^2+|\mathbf{Q}\cdot\mathbf{C}|^2-|\mathbf{Q}\cdot\mathbf{F}|^2),$$
$$\rho^{(2)}_{00,x} = -(\tfrac{4}{5})^{\frac{1}{2}}\,\mathrm{Re}[(\mathbf{Q}\cdot\mathbf{C})^*(\mathbf{Q}\cdot\mathbf{B})+2(\mathbf{N}\cdot\mathbf{A})^*(\mathbf{N}\cdot\mathbf{C})],$$
$$\rho^{(2)}_{20,x} = (\tfrac{2}{7})^{\frac{1}{2}}\,\mathrm{Re}[(\mathbf{Q}\cdot\mathbf{C})^*(\mathbf{Q}\cdot\mathbf{B})+4(\mathbf{N}\cdot\mathbf{A})^*(\mathbf{N}\cdot\mathbf{C})],$$
$$\rho^{(2)}_{21,x} = (\tfrac{2}{7})^{\frac{1}{2}}\,i\,\mathrm{Im}[(\mathbf{Q}\cdot\mathbf{B})^*(\mathbf{N}\cdot\mathbf{A})+(\mathbf{Q}\cdot\mathbf{C})^*(\mathbf{N}\cdot\mathbf{C})],$$
$$\rho^{(2)}_{22,x} = -(\tfrac{3}{7})^{\frac{1}{2}}\,\mathrm{Re}(\mathbf{Q}\cdot\mathbf{C})^*(\mathbf{Q}\cdot\mathbf{B}),$$
$$\rho^{(2)}_{21,y} = (\tfrac{2}{7})^{\frac{1}{2}}\,\mathrm{Im}(\mathbf{Q}\cdot\mathbf{F})^*(\mathbf{N}\cdot\mathbf{A}),$$
$$\rho^{(2)}_{22,y} = (\tfrac{3}{7})^{\frac{1}{2}}\,i\,\mathrm{Re}(\mathbf{Q}\cdot\mathbf{C})^*(\mathbf{Q}\cdot\mathbf{F}),$$
$$\rho^{(2)}_{21,z} = -(\tfrac{2}{7})^{\frac{1}{2}}\,\mathrm{Re}(\mathbf{Q}\cdot\mathbf{F})^*(\mathbf{N}\cdot\mathbf{C}),$$
$$\rho^{(2)}_{22,z} = (\tfrac{3}{7})^{\frac{1}{2}}\,i\,\mathrm{Im}(\mathbf{Q}\cdot\mathbf{F})^*(\mathbf{Q}\cdot\mathbf{B}).$$

Here we have abbreviated $N_2 = N$, $Q_{22} = Q$. For a zero-spin target $J_A = 0$, we have from eq. (34) that

$$\rho_{KQ}(J_B J_B) = (-)^{J_B+K+1}(2k+1)^{-1}\rho_{KQ}(kk),$$

with, of course, $J_B = k$. In the present example $k = 2$, and if we assume quadrupole de-excitation back to the ground state so that $F_0 = 1$, $F_2 = -(\frac{5}{14})^{\frac{1}{2}}$ and $F_4 = -(\frac{8}{7})^{\frac{1}{2}}$, the correlation (33) can be written as in appendix 1 (neglecting irrelevant factors),

$$W(\theta, \phi) = \alpha + (\beta_1 + \beta_2 \cos 2\phi + \beta_3 \sin 2\phi) \cos 2\theta + (\gamma_1 + \gamma_2 \cos 2\phi + \gamma_3 \sin 2\phi) \cos 4\theta + (\delta_1 \sin \phi + \delta_2 \cos \phi) \sin 4\theta.$$

Since we neglected distorted-wave effects, terms in 3ϕ and 4ϕ do not appear. The terms β_3, γ_3 and δ_2 only arise if the incident beam is polarized with components in the scattering plane. The coefficients are

$$\alpha = 3(|\mathbf{N}\cdot\mathbf{A}|^2 + |\mathbf{N}\cdot\mathbf{C}|^2) + 2(|\mathbf{Q}\cdot\mathbf{B}|^2 + |\mathbf{Q}\cdot\mathbf{C}|^2 + |\mathbf{Q}\cdot\mathbf{F}|^2) + 2P_x[3\,\mathrm{Re}(\mathbf{N}\cdot\mathbf{A})^*(\mathbf{N}\cdot\mathbf{C}) + 2\,\mathrm{Re}(\mathbf{Q}\cdot\mathbf{B})^*(\mathbf{Q}\cdot\mathbf{C})],$$

$$\beta_1 + \beta_2 = 2(|\mathbf{Q}\cdot\mathbf{B}|^2 + |\mathbf{Q}\cdot\mathbf{C}|^2) + 4P_x\,\mathrm{Re}(\mathbf{Q}\cdot\mathbf{B})^*(\mathbf{Q}\cdot\mathbf{C}),$$

$$\beta_1 - \beta_2 = 2|\mathbf{Q}\cdot\mathbf{F}|^2,$$

$$\beta_3 = 2[P_z\,\mathrm{Im}(\mathbf{Q}\cdot\mathbf{F})^*(\mathbf{Q}\cdot\mathbf{B}) + P_y\,\mathrm{Re}(\mathbf{Q}\cdot\mathbf{C})^*(\mathbf{Q}\cdot\mathbf{F})],$$

$$\gamma_1 = 3\beta_1 - \alpha, \qquad \gamma_2 = -\beta_2, \qquad \gamma_3 = -\beta_3,$$

$$\delta_1 = -(24)^{\frac{1}{2}}\,\mathrm{Im}\{(\mathbf{Q}\cdot\mathbf{C})^*(\mathbf{N}\cdot\mathbf{A}) + (\mathbf{Q}\cdot\mathbf{B})^*(\mathbf{N}\cdot\mathbf{C}) + P_x[(\mathbf{Q}\cdot\mathbf{B})^*(\mathbf{N}\cdot\mathbf{A}) + (\mathbf{Q}\cdot\mathbf{C})^*(\mathbf{N}\cdot\mathbf{C})]\}$$

$$\delta_2 = (24)^{\frac{1}{2}}[P_y\,\mathrm{Im}(\mathbf{Q}\cdot\mathbf{F})^*(\mathbf{N}\cdot\mathbf{A}) - P_z\,\mathrm{Re}(\mathbf{Q}\cdot\mathbf{F})^*(\mathbf{N}\cdot\mathbf{C})].$$

The results of sect. 4 follow upon putting $P_y = P_z = 0$ and $P_x = \pm 1$. Other special cases follow readily from the general formulae given above.

References

1) Kerman, McManus and Thaler, Ann. Phys. **8** (1959) 551;
H. McManus in Nuclear forces and the few-nucleon problem I, ed. by T. C. Griffith and E. A. Power (Pergamon Press, London, 1960)
2) G. R. Satchler, Proc. Phys. Soc. **68** (1955) 1037
3) M. K. Banerjee and C. A. Levinson, Ann. Phys. **2** (1957) 499
4) L. C. Biedenharn and M. E. Rose, Rev. Mod. Phys. **25** (1953) 729
5) G. R. Satchler, Nuclear Physics **18** (1960) 289;
J. S. Blair and L. Wilets, Phys. Rev. **121** (1961) 1493
6) D. J. Hooton and G. R. Allcock, Proc. Phys. Soc. **73** (1959) 881
7) Drisko, Bassel and Satchler, Bull. Am. Phys. Soc. **6** (1961) 56
8) W. T. Pinkston and G. R. Satchler, in Proc. Conf. on Nuclear Structure at Kingston, ed. by D. A. Bromley and E. Vogt (North-Holland Publishing Co., Amsterdam, 1960) p. 394
9) D. S. Ling and D. L. Falkoff, Phys. Rev. **76** (1949) 1639
10) E. U. Condon and G. H. Shortley, Theory of atomic spectra (Cambridge University Press, Cambridge, 1951) chapt. 4;
J. M. Daniels, Can. J. Phys. **35** (1957) 1133
11) A. P. French, Phil. Mag. **42** (1951) 263
12) E. J. Squires, Nuclear Physics **6** (1958) 504
13) G. R. Satchler, Nuclear Physics **16** (1960) 674
14) Salmon, Clegg, Foley, Fisher and Rowe, to be published
15) H. S. Adams and N. M. Hintz in Nuclear forces and the few nucleon problem II, ed. by T. C. Griffith and E. A. Power (Pergamon Press, London, 1960)

2.A.1

Nuclear Physics **27** (1961) 448—466; © *North-Holland Publishing Co., Amsterdam*

Not to be reproduced by photoprint or microfilm without written permission from the publisher

THE DISINTEGRATION OF B^{10} AND F^{19} BY FAST NEUTRONS

E. A. DAVIS, F. GABBARD †, T. W. BONNER and R. BASS ††

Rice University, Houston, Texas †††

Received 17 April 1961

Abstract: The disintegration of B^{10} and F^{19} by fast neutrons has been studied using a grid-type ionization chamber filled with argon and boron trifluoride enriched in B^{10}. Monoenergetic neutrons for studying the reactions from 0.2 to 8.2 MeV were produced with the Li^7(p, n)Be^7, T(p, n)He^3 and D(d, n)He^3 reactions. Alpha groups from the B^{10}(n, α)Li^7 reaction leaving Li^7 in its ground and first excited state at 478 keV were studied over the entire energy range. The cross section for the (n, α) reaction decreased rapidly from 1048 mb at 0.2 MeV to 180 mb at 1.2 MeV and then increased to 451 ± 60 mb at the 1.84 MeV resonance. For higher energies broad resonance structure was observed with the cross section generally decreasing and reaching a value of 31 mb at 8.2 MeV. The B^{10}(n, t2α) reaction was observed for neutron energies above 1.3 MeV. The cross section for this reaction increased to 80 mb at 4.5 MeV and was comparable to that for the B^{10}(n, α)Li^7 reaction above 5 MeV. The B^{10} (n, t2α) reaction was found to proceed mainly by three-body breakup or through the 4.63 MeV excited state of Li^7. Some reactions may have proceeded through the 2.9 MeV level of Be^8 but few, if any, proceeded through the ground state of Be^8. The total excitation function for the F^{19}(n, α)N^{16} reaction leaving N^{16} in the ground and first three excited states was studied for neutron energies above 2.9 MeV. Ten resonances were observed. The cross section increases to 135 ± 50 mb at 5.80 MeV and then decreases at higher energies.

1. Introduction

Early experiments [2–5]) in 1935 on neutron reactions in boron created considerable interest because of the large absorption cross section for slow neutrons and because the disintegrations are almost entirely by charged particle emission. Since that time there have been many investigations of the neutron reactions in boron for slow [1]) and fast neutrons [6–16]). The purpose of the present work is to extend the measurements of fast neutron reactions in boron-10 leading to charged particle emission. The reactions that are energetically possible below a neutron energy of 9 MeV are the following [1]):

$$\begin{aligned} B^{10}+n &\rightarrow Li^7+\alpha+2.793\ \text{MeV},\\ &\rightarrow H^3+He^4+He^4+0.328\ \text{MeV},\\ &\rightarrow Be^{10}+p+0.227\ \text{MeV},\\ &\rightarrow Be^9+d-4.358\ \text{MeV}. \end{aligned}$$

† Present address: University of Kentucky, Lexington, Kentucky

†† Present address: Institut für Kernphysik der Universität Frankfurt

††† Work supported in part by the U.S. Atomic Energy Commission

All these reactions have been reported in the literature for neutron energies below 9 MeV except for the (n, d) reaction. Ribe and Seagrave [10]) have observed the (n, d) reaction with 14 MeV neutrons and report for the integrated cross section (0° to 90°) a value of 21 mb for the ground state transition and 16 mb for the transition to the 2.4 MeV state of Be^9. Frye and Gammel [6]) have studied the B^{10}(n, dn'2α) reaction for six neutron energies above 12 MeV. Petree, Johnson and Miller [11]) have measured the cross section for the (n, α) reaction from a neutron energy of 0.35 to 2.6 MeV using a proportional counter filled with boron trifluoride and argon. Groups of alpha particles to the ground state and the 478 keV level of Li^7 were observed and their ratio determined. Bichsel *et al.* [12, 13]) have also measured this ratio at six neutron energies from thermal to 3.9 MeV. One unusual feature of the (n, α) reaction is the strength of the transition to the 478 keV level of Li^7 which is 94 % for thermal neutrons[17]) and remains important at higher neutron energies. At this laboratory Bichsel and Bonner [14]) have used a boron trifluoride proportional counter to measure the total (n, α) cross section in the neutron energy range from 20 keV to 4.8 MeV.

There have been several studies of the (n, t2α) reaction using boron-loaded nuclear emulsions [5–8]). In one of these, Frye and Gammel [6]) have measured the cross section at eight neutron energies between 5 and 20 MeV. They have also made a study of the various intermediate stages in the reaction process. Wymann, Fryer and Thorpe[15]) have used absolute beta counting of the tritium activity to measure the cross section at four neutron energies between 4 and 14 MeV. The (n, t2α) reaction has also been observed in connection with other experiments [9, 10]).

The (n, p) reaction has not been observed with fast mono-energetic neutrons. Using pile neutrons to activate B^{10} samples Eggler *et al.* [16]) have estimated the cross section to be $\approx$ 3 mb. Observation of this reaction with an ionization chamber is difficult since the Q value is very close to that for the (n, t2α) reaction. In the present work these two reactions cannot be resolved by measurement of energy, but an attempt was made to detect the (n, p) reaction by making use of the different ranges of the disintegration products in the two reactions.

The only inverse reaction of the ones studied in this experiment that can be observed is Li^7 (α, n)B^{10}. A second group of neutrons with threshold at an alpha energy of 5.51 MeV limits the energy region in which this reaction can be compared by detailed balance to the B^{10}(n, α)Li^7 reaction. The cross section for the Li^7(α, n)B^{10} reaction has been measured in this region by Bichsel and Bonner [14]) and by Gibbons and Macklin [18]). The latter have calculated the cross section for the B^{10}(n, α)Li^7 reaction by detailed balance for neutron energies from 100 to 800 keV.

Since boron trifluoride was used in the present experiment, neutron reactions

in fluorine leading to charged particle emission were also observed. The reactions that are energetically possible below a neutron energy of 9 MeV are as follows [1]):

$$\begin{aligned} F^{19}+n &\rightarrow N^{16}+\alpha-1.500 \text{ MeV}, \\ &\rightarrow O^{19}+p-4.006 \text{ MeV}, \\ &\rightarrow O^{18}+d-5.737 \text{ MeV}, \\ &\rightarrow O^{17}+t-7.548 \text{ MeV}. \end{aligned}$$

Only the (n, α) and (n, p) reactions have been reported in the literature for neutron energies below 9 MeV. Marion and Brugger [19]) have studied the cross section for the (n, α) reaction by observing the N^{16} radioactivity induced in a CaF_2 crystal as a function of neutron energy from 3.1 to 8.0 MeV. They have simultaneously obtained the cross section for the (n, p) reaction by measuring the induced O^{19} radioactivity. Using a similar technique Bostrom *et al.* [20]) made a preliminary report on the excitation function for the (n, α) reaction. Smith, Bostrom and Hudspeth [21]) have used the radioactivity induced in a BaF_2 crystal to study the cross section for the (n, α) reaction for neutron energies from 3.2 to 6.0 MeV. The (n, α) reaction has been observed by several other investigators using various techniques [1]).

2. Experimental Method

A grid-type ionization chamber using electron collection has been used in the present investigation to detect the charged particles emitted in the fast neutron disintegrations of B^{10} and F^{19}. The construction and operation of the chamber has been described by Gabbard, Bichsel and Bonner [22]).

Monoenergetic neutron sources used in the experiments were the Li^7(p, n)Be^7 T(p, n)He^3 and D(d, n)He^3 reactions. The lithium target, made by evaporating natural lithium metal on a 0.5 mm tantalum backing, was 20 keV thick to 1.9 MeV protons. This target was used to obtain neutrons in the energy range $200 < E_n < 700$ keV. A tritium gas target was used in the range $0.35 < E_n < 4.50$ MeV and a deuterium gas target in the range $4.0 < E_n < 8.2$ MeV. The tritium gas target consisted of a thin-walled platinum chamber 1.6 cm long and 0.9 cm in diameter separated from the vacuum of the Van de Graaff accelerator by a 2.30 mg/cm^2 aluminium foil. The target was filled to about 0.8 atm by heating a uranium tritide oven reservoir [23]) in which 50 Cur of tritium were stored. The deuterium gas target was a thin-walled platinum chamber 4.2 cm long and 1.28 cm in diameter separated from the vacuum system by a 0.77 mg/cm^2 nickel foil. The target was filled with deuterium to either $\frac{1}{4}$ or $\frac{1}{2}$ atm. A series of two tantalum diaphragms placed before the nickel entrance foil and kept at the proper voltage insured correct beam current integration (similar

to the arrangement † described by Fowler and Brolley [24]). The targets were cooled by an air jet.

The neutron energy resolution in the experiments was limited by the target thickness and the energy spread across the ionization chamber due to the variation of the energy of the neutrons with angle of emission. Secondary effects which influence the energy resolution and their maximum contributions were (1) multiple scattering in the entrance foil (< 30 keV based on theory of Moliere [25])), (2) non-uniformity of entrance foil thickness (≈ 10 keV if assume 10 % non-uniformity) and (3) scattering of neutrons in the stainless steel pressure vessel of the ionization chamber (negligible since scattering into the sensitive volume is quite small). The combined effect of these factors on the energy resolution was always less than 10 keV. The neutron energy resolution for neutrons from the lithium target was 25 keV. For the tritium target the resolution varied from 75 keV at a neutron energy of 350 keV to 50 keV at 1.9 MeV and then to 80 keV at 4.2 MeV. For the deuterium target filled to $\frac{1}{4}$ atm it varied from 100 keV at 4.2 MeV to 85 keV at 6 MeV and then to 120 keV at 8.2 MeV, while with $\frac{1}{2}$ atm of deuterium the resolution was 190, 145 and 195 keV at the same respective energies.

The ionization chamber was filled with a mixture of boron trifluoride and argon and positioned so that the centre of the chamber was 20 cm from the neutron source and at 0° to the accelerator beam. The neutrons were not collimated. Directly behind the ionization chamber at one meter from the neutron source a long counter was placed to monitor the neutron flux. The long counter was constructed according to the recipe of Hanson and McKibben [26]) with some differences noted by Gabbard *et al.* [22]) The scattering and absorption of neutrons by the ionization chamber at a neutron energy of 1.9 MeV caused the neutron flux at the long counter to be 16 % higher when the chamber was removed. It was asssumed that the ion chamber wall nearest the neutron source caused one-half of the attenuation so that the neutron flux inside the chamber would be 8 % greater than that recorded by the long counter. This effect has been estimated and verified experimentally to be constant to within 4 % over the energy range of this experiment. The resolving time of the long counter system was experimentally determined to be 60 ± 4 μsec by observing the counting rate with various accelerator beam intensities and also with 2 calibrated Pu-Be neutron sources of nearly equal strength. Losses in the neutron flux measurement due to this effect were generally less than or about 1 % although a few measurements had to be corrected by as much as 10 %.

The pulses produced in the ionization chamber by the disintegrations in the gas were amplified first by a cascade-type preamplifier with cathode follower output [27]) and then by a linear amplifier so that the overall gain for the system

† See fig. 11 of ref. [24]).

was about 40 000. The amplified pulses were recorded with a 256-channel pulse-height analyzer. Loss of counts due to the resolving time of the analyzer was estimated to be $< 2\,\%$ throughout the experiments.

The pulse height spectrum for a neutron energy of 3.52 MeV is shown in fig. 1. The chamber was filled to 0.21 atm with boron trifluoride enriched to 96 % in B^{10} and then argon was added to a total pressure of 2.4 atm in order to stop the products of the disintegrations in the chamber. The group of pulses observed at channel 166 is due to aplha particles from the disintegration of B^{10} by 3.52 MeV neutrons leaving Li^7 in its ground state, while the group at

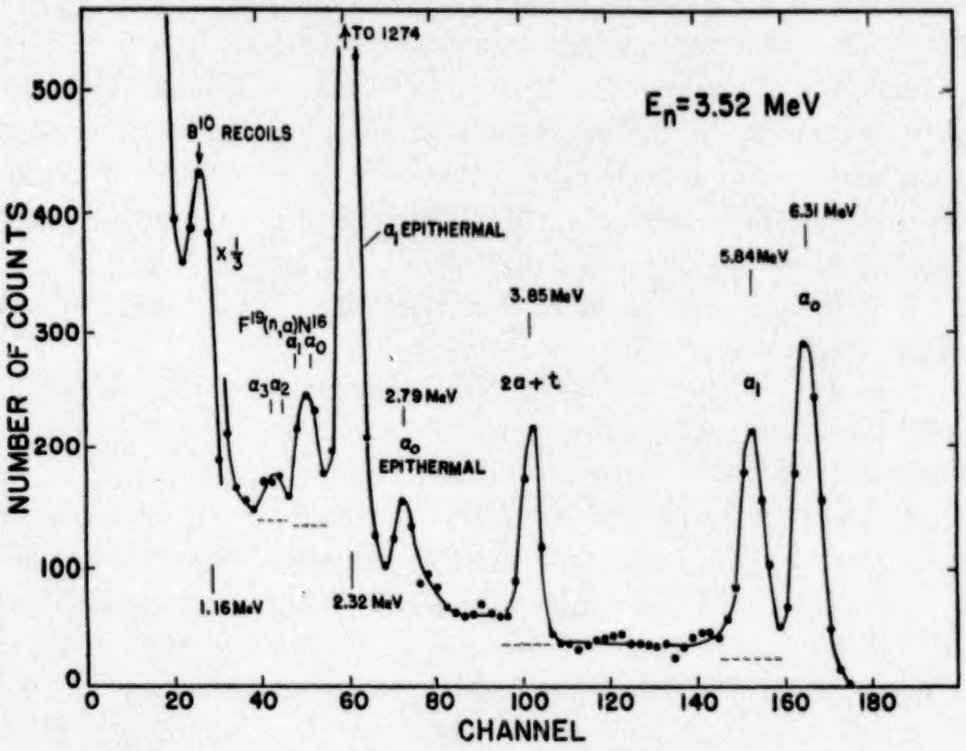

Fig. 1. Pulse-height distribution from the disintegration of enriched boron trifluoride by 3.52 MeV neutrons. Dotted lines under groups indicate backgrounds to be subtracted.

channel 154 is due to alpha particles form the same reaction leaving Li^7 in its first excited state at 478 keV. Due to the large cross section for these reactions with slow neutrons, two groups are seen at channels 74 and 61 corresponding to the (n, α_0) and (n, α_1) reactions, respectively. The intensity of the α_0-group is observed to be about 6 % of the α_1-group as expected. These groups of pulses remain in the same channel positions throughout the experiment and are useful in the energy calibration of the pulse-height scale. However, for some regions of neutron energy they interfere with groups from the B^{10}(n, t2α) and F^{19}(n, α)N^{16} reactions. The ion chamber was completely covered with a 0.08 cm cadmium shield to reduce the effect of the slow neutrons. Neutron reactions in B^{10} leading to a triton and two alpha particles as well as those involving emission of a proton leaving Be^{10} in its ground state are observed as the group

in channel 103. The groups in channels 43 to 53 correspond to the (n, α_0), (n, α_1), (n, α_2) and (n, α_3) reactions in fluorine leaving N^{16} in its ground and first three excited states, respectively. All these groups are not resolved. The rapidly rising tail below the fluorine groups is due largely to recoils of B^{10} nuclei from elastically scattered neutrons. The B^{10} recoils show a peak in channel 28 and have a maximum pulse-height corresponding to back-scattered neutrons at channel 30 ($E = 1.16$ MeV). The pulse-height resolution for the data shown in fig. 1 is 4 % for the alpha particle groups and 5 % for the $2\alpha+t$ group. The tails seen below the groups are mainly due to disintegrations that occur between the grid and the collection plate of the ion chamber, which give a continuous pulse size distribution, and to the wall effect discussed below. Other contributions to the background are (n, p) reactions in the material of the walls and plates of the ion chamber, neutron reactions in argon and reactions with neutrons other than those in the primary beam.

The wall effect is caused by disintegrations within the sensitive volume producing particles whose tracks cross the boundary of this volume or strike the high voltage electrode. Pulses produced by these shortened tracks are not full size and hence do not fall into their appropriate energy group. These pulses as well as those from tracks entering the sensitive volume contribute to the tail under the groups. In order to determine the actual number of disintegrations occurring in the sensitive volume, it is necessary to correct the number of pulses in the group for the wall loss. The fraction lost can be easily computed for track lengths very short compared to the dimensions of the sensitive volume. The result is given by Gabbard *et al* [22]). For particle tracks longer than 1 cm, the wall loss correction was measured experimentally by observing the alpha particles from the B^{10}(n, α)Li^7 reaction at a neutron energy of 7.67 MeV for different chamber pressures. The results were in good agreement with those of Gabbard *et al* [22]), who observed the protons from the N^{14} (n, p)C^{14} reaction over a wide range of pressures. For the (n, t2α) reactions a particle track length cannot be easily calculated. To correct the number of pulses in this group the wall loss correction was determined as a function of neutron energy. The experiment was performed at energies of 3.40, 5.25, 6.21, 7.58 and 7.67 MeV. The number of counts in the group was observed as argon was added in successive steps of about 1 atm until the number of counts became constant indicating that the wall effect had become small. This occurred for chamber pressures of 4 to 6 atm depending on the neutron energy. The saturated count divided by the count at any other pressure gave the wall loss correction for that pressure.

Fig. 2 shows the pulse-height distribution for a neutron energy of 7.67 MeV and a chamber filling of 2.1 atm containing 0.22 atm of enriched BF_3. The reactions in B^{10} are the same as in fig. 1. The (n, α_0) reaction with slow neutrons is not clearly seen because of the pulse distribution of B^{10} recoils. The (n, α_0),

(n, α_1), (n, α_2) and (n, α_3) reactions in F^{19} are no longer partially resolved but have become much more intense than at 3.52 MeV. In addition two more groups have appeared (marked A and B). In a preliminary report [28]), these groups were identified as alpha transitions leaving N^{16} in excited states at 1.2 and 1.7 MeV. A later investigation indicated that these groups are due to disintegrations in the ion chamber produced by background neutrons together with neutron reactions in argon induced by the primary neutron flux. The neutron background effects were observed by removing the deuterium from the target. The neutron reactions in argon were measured by filling the ion chamber with a

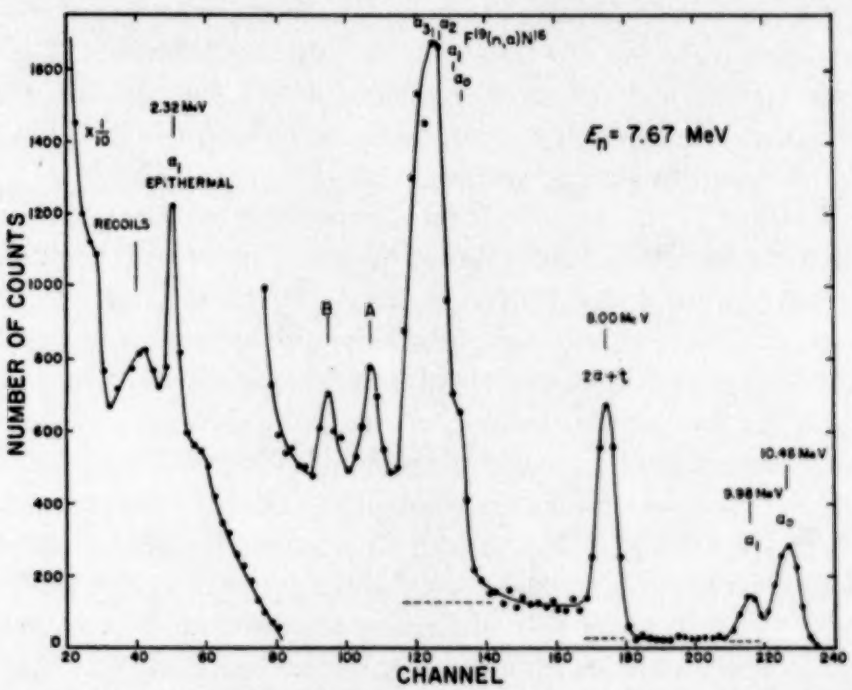

Fig. 2. Pulse-height distribution from the disintegration of enriched boron trifluoride by 7.67 MeV neutrons. Dotted lines under groups indicate backgrounds to be subtracted. Groups A and B are discussed in text.

pure argon filling. The results of the latter experiment are reported separately[29]) The pulse-height resolution in fig. 2 is 4 % for all the groups except the one corresponding to the four (n, α) reactions in fluorine. The line width for this group is spread to the low energy side, an effect observed for all neutron energies above 5 MeV. The same phenomenon has been observed at this laboratory for the α_1-group in the N^{14}(n, α)B^{11} reaction at 7.2 MeV studied by Gabbard *et al* [22]) and for the α_0-group in the O^{16}(n, α)C^{13} reaction currently being studied in the same energy region. The effect is atributed to the alpha particles being emitted strongly at or near 90°. The tracks of such particles parallel the collecting field and hence would tend to have more recombination giving smaller pulses than those perpendicular to the field. This explanation is also supported by the fact that the effect increases markedly with increasing chamber pressure.

For a neutron energy of 7.67 MeV it is energetically possible to observe the (n, d) reaction in B^{10} and the (n, d) and (n, p) reactions in F^{19}. The expected positions in fig. 2 of groups corresponding to these reactions are channels 72, 42 and 80, respectively. However, with a chamber pressure of 2.1 atm the wall losses for these reactions are large being 80, 50 and 100 %. Pulses from these reactions would merge with those from B^{10} recoils and other background effects. The peak in the pulse distribution for B^{10} recoils is in channel 42 in fig. 2. When the chamber pressure is increased to 6 atm, a group is observed in channel 80 corresponding to the (n, p) reaction in F^{19}. In addition to these reactions the $B^{11}(n, \alpha)Li^8$ reaction is energetically possible ($Q = -6.636$ MeV) but the cross section is expected to be small. Pulses from this reaction would merge with those from the recoils.

Factors which cause fluctuations in pulse size and hence influence the pulse-height resolution include electron attachment, columnar recombination, electronic noise and incomplete shielding of the collection plate by the grid. The first three factors have been discussed by Gabbard, Bichsel and Bonner [22]). From the theoretical analysis of Buneman [30]) the grid is estimated to have a shielding efficiency of 97 %. Recombination was not important for the pressures used in the present experiment. Only when the pressure was increased to 5 or 6 atm were strong recombination effects observed.

Electron attachment was the most troublesome factor. This is not unexpected since BF_3 is electronegative and tends to capture electrons. In addition common impurities in BF_3 such as SiF_4, SF_6 and SO_2 have strong affinity for electrons and are known to cause poor performance in gas counters [31]). The pulse-height resolution depended to a large extent on the purity attained in preparing the BF_3 and on the amount used independent of the total pressure in the chamber indicating that electron attachment was occurring. For example, the resolution in one case was 4 % with 0.22 atm BF_3 while in another 12 % with 0.39 atm BF_3 when the total chamber pressure was 2.4 atm in each case. When less care was used in preparing the BF_3 a filling of 1.3 atm containing 0.08 atm BF_3 gave 7 % resolution. In addition to using small amounts of BF_3, it was found necessary to make the electric field in the ion chamber about 1000 V/cm in order to achieve the best pulse-height resolution. For fields one-half this value the line width for the alpha groups increased by 50 %. For fields one-fourth as large the line width tripled. When the BF_3 concentration was reduced to < 1 %, the line width was not appreciably affected by the field used. No deterioration of counting rate or pulse-height resolution was observed over a period of 3d, the longest duration that any one filling was used. After one month the pulse-height resolution in one case deteriorated from 7 % to 10 %.

Since the chamber performance depended on the purity of the boron trifluoride, great care was exercised in its preparation. Four separate fillings of BF_3 enriched to 96 % in B^{10} were prepared by degassing and then decomposing

the complex $CaF_2 \cdot BF_3$ in a flask [32]). The gas evolved was passed through a glass trap cooled with a dry ice-alcohol mixture, and then the BF_3 was trapped as a solid in a second glass trap cooled with liquid air. The trapping process was then repeated with a third and fourth trap. The system was pumped on at all times through a liquid air trap. The solid BF_3 was pumped on for 30 min before allowing the trap to warm and the gas to flow into the ion chamber through a third dry ice-alcohol trap. One filling of natural BF_3 was prepared by passing commercial grade BF_3 through a similar series of cold traps. For each filling argon was added to the chamber by allowing it to evaporate from a trap where it had been liquified.

3. Data Analysis and Results for Boron-10

Excitation functions for the various reactions were obtained by analyzing pulse-height distributions similar to those in figs. 1 and 2. The number of disintegrations associated with each particle group was determined by adding the counts in that group, subtracting the background tail caused by higher energy groups and correcting for wall loss. The wall loss for alpha particles varied from 3 % to 35 % while that for the $2\alpha + t$ group varied from 1 % to 35 %.

The relative number of neutrons at each neutron energy was determined by correcting the number of counts recorded by the long counter for any deadtime losses and for the efficiency of the counter relative to a Pu-Be source using the data of Haddad *et al.* [33]). The absolute neutron flux was then obtained by comparison with a calibrated Pu-Be source placed 1 m from the long counter. To obtain the average flux incident on the ion chamber sensitive volume an increase of 8 % was made to account for attenuation by the chamber pressure vessel and a decrease of 7 % to account for the variation of the source intensity with angle. These two corrections are constant to within 2 % and tend to cancel. For neutron energies above 4.5 MeV the relative neutron flux was computed at each energy from the integrated beam current and the known cross section for the D(d, n)He^3 reaction [24]) taking into account the variation of the neutron yield with angle of emission from the source. The relative flux was normalized to absolute values obtained with the long counter below 4.5 MeV. The neutron background with the T(p, n)He^3 source was measured by removing the tritium from the target and was always found to be negligible.

Fig. 3 shows the cross sections for the reactions in B^{10} as a function of the average neutron energy incident on the ion chamber. The data below 400 keV are the result of one experiment, while that above 400 keV represents the average of two separate experiments. Above 4.5 MeV, the α_0- and α_1-groups were resolved in only one of the experiments.

Three separate chamber fillings of BF_3 were used to determine the absolute

cross section for the total (n, α) reaction in B^{10} at 1.84 MeV. Two determinations using BF_3 enriched to 96 % in B^{10} gave cross sections of 419 ± 67 mb and 452 ± 64 mb. The enrichment was taken as that quoted by the Stable Isotopes Division, Oak Ridge National Laboratory. One determination using natural BF_3 gas gave 459 ± 64 mb. The natural abundance [34]) of B^{10} was taken as 19 ± 1 %. The precision of these three measurements is ±3 % (% standard deviation of the mean). The average of these values weighted according to the estimated experimental errors for each is 451 ± 60 mb. This is to be compared

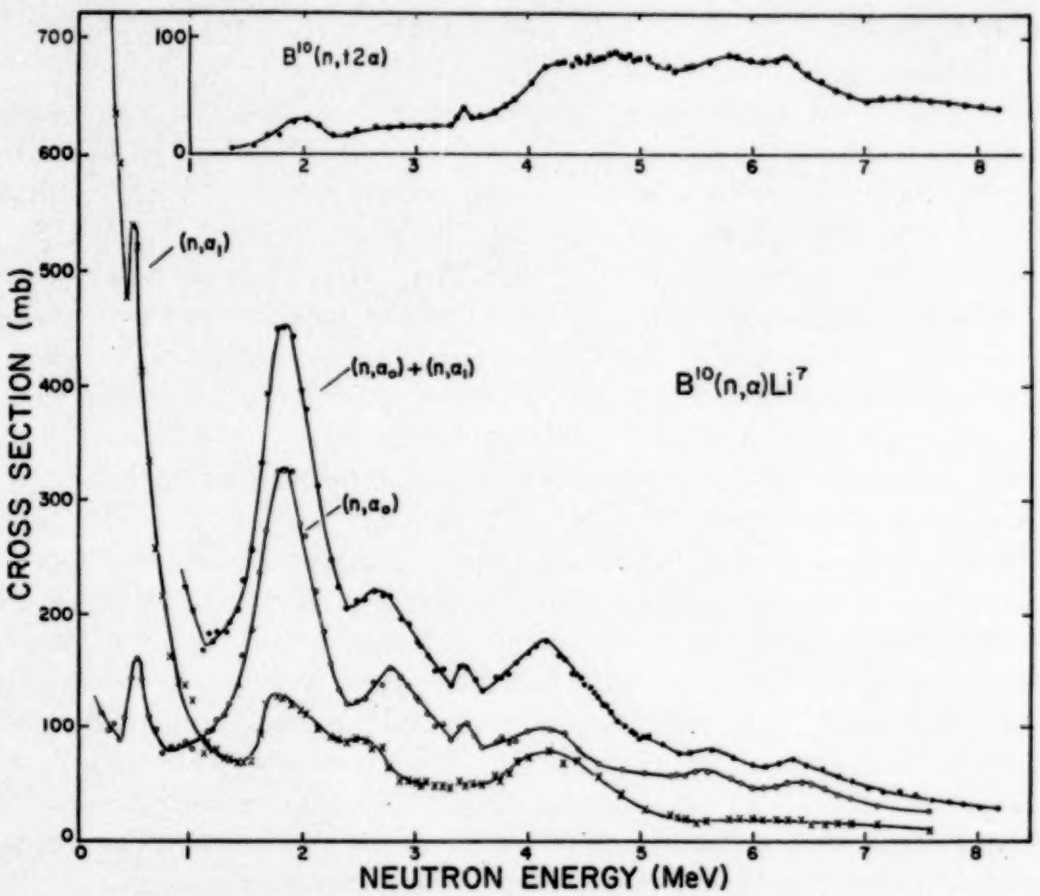

Fig. 3. Cross section for (n, α) and (n, t2α) disintegrations of B^{10}

with 520 ± 130 mb obtained by Petree *et al.* [11]) and 410 ± 100 mb obtained by Bichsel and Bonner [14]) at the peak of the 1.86 MeV resonance. The three measurements agree within the quoted experimental errors. Also Gibbons and Macklin [18]) have computed the (n, α_0) cross section by reciprocity from the $Li^7(\alpha, n)B^{10}$ reaction. Their value of 215 mb at the 0.53 MeV resonance is 35 % greater than our value of 161 mb.

The errors quoted for each cross section measurement in the present work include the experimental errors as well as those arising in the operations on the data. The former include errors resulting from (1) counting statistics and adding

the counts in each group of the pulse-height distribution, (2) background corrections, (3) measurement of distance and angle to the ion chamber and long counter and (4) measurement of the amount of BF_3 in the ion chamber. The combined effect of these errors for the cross section determinations was ± 9 %, ± 3 % and ± 5 %, respectively, and were used to weight the average. Measuring the amount of BF_3 was responsible for the larger error in the first and last determinations. Background corrections for the α_0-group are negligible and for the α_1-group amount to about 20 % at 1.84 MeV becoming 10 % at higher energies. The resulting error in the (n, α_1) cross section is about ± 3 %. Counting statistics are about ± 1 % for the neutron monitor and about ± 2 % for the alpha particles throughout the experiment.

The inaccuracy in the cross section arising from operations on the data includes errors resulting from (1) determination of the absolute neutron flux from the long counter measurements, (2) correction of the particle groups for the wall effect and (3) calculation of the sensitive volume of the ion chamber. Item (3) is believed to cause about $\pm$ 1 % error. Item (1) is the major source of error in the experiment. The calibration of the long counter with a Pu-Be source and correction for the relative efficiency, chamber wall attenuation and angular distribution effects should be accurate to $\pm$ 15 %. The wall loss correction is estimated to have an absolute error of about $\pm$ 6 % at 1.84 MeV and a relative error about ± 5 % for the range of particle track lengths encountered in this experiment.

Based on the above considerations, the excitation functions for the (n, α) reactions are estimated to be in error by $\pm$ 20 % for neutron energies below 4.5 MeV, the (n, α_0) cross section being more accurate than the (n, α_1) cross section by a few per cent. Above 4.5 MeV the error increases to about ± 30 % at 8.2 MeV. Due to larger background corrections and poorer statistics the (n, t2α) cross section is less accurate than the (n, α) data below 4 MeV, but it becomes comparable to or exceeds the accuracy of the (n, α) cross section at higher neutron energies. The relative errors in the cross sections are expected to be somewhat less than the estimates of the absolute errors.

From 1.7 to 2.6 MeV the groups corresponding to slow neutron reactions in boron interfere with the 2α+t group. In this region the cross section for the (n, t2α) reaction was determined at each energy by subtracting out the counts due to the slow neutron groups. Since the magnitude of these groups was observed to be a smooth function of energy above and below this energy region, the amount to be subtracted was obtained by interpolation. The slow neutron groups were from 6 to 20 times more intense than the 2α+t group resulting in errors in the (n, t2α) cross section ranging from ± 30 % to ± 60 %. The cross section obtained in this manner fit smoothly with that measured above and below this energy region.

The excitation functions show resonances for the neutron energies listed in

table 1. The resonances at 0.53, 1.86, 2.79 and 4.1 MeV have been observed by Bichsel and Bonner [14]) in the total (n, α) cross section. Petree *et al.* [11]) have studied the 1.86 MeV resonance in both the (n, α_0) and (n, α_1) reactions. The total neutron cross section does not show sharp resonance structure but has maxima at 1.8, 2.8 and 4.1 MeV and some indication [35, 36]) of structure near 0.5 MeV. Above 4.5 MeV the total cross section does not show any definite structure [37]). The fairly narrow resonance at 3.43 MeV has not been previously

TABLE 1

Resonances in the reaction B^{10}(n, α)Li^7

Neutron energy (MeV)	Level in B^{11} (MeV)	Level width (MeV)
0.53	11.95	0.14
1.86	13.15	0.57
2.79	14.00	0.53
3.43	14.58	<0.12
4.1	15.2	0.8
5.7	16.7	
6.4	17.3	

observed. In the present experiment the region around 3.43 MeV was studied three times in two separate experiments and each time the anomaly was observed. Although the (n, α_0) and (n, t2α) cross sections show this resonance, the (n, α_1) cross section does not. There is also some indication of broad, resonance structure in the (n, α_0) cross section at 5.7 and 6.4 MeV. This structure is also evident in the (n, t2α) excitation function. The 1.86 and 2.79 MeV resonances exhibit an unusual structure in the (n, α_1) reaction which may be attributed to interference between the levels involved.

In previous investigations, considerable interest has been shown in the branching ratio of the α_0- and α_1-transitions. Petree *et al.* [11]) report a maximum in the α_0/α_1 ratio at 1.9 MeV, whereas Bichsel *et al.* [12, 13]) report a maximum at 2.9 MeV. Examination of fig. 3 shows that the intensity of the α_0-transition exceeds that of the α_1-transition above 1.2 MeV, and that the ratio α_0/α_1 has a maximum of about 2.6 at both 1.9 and 2.9 MeV. In addition there are maxima in the ratio of about 3.2 at 5.6 and 6.6 MeV.

Table 1 also gives the levels in the B^{11*} compound nucleus corresponding to the resonances observed in this experiment. The level widths, where given, were computed from the observed widths and the neutron energy resolution and then reduced to centre-of-mass energy. Except for the 0.53 and 3.43 MeV resonances the observed structure is very broad. It is likely that some of these resonances are due to more than one level in B^{11}. The broad structure in the (n, t2α) cross section between 4.0 and 5.3 MeV indicates more than one level. The two levels reported [1]) in B^{11} at 16.77 and 16.93 MeV correspond to the

5.7 MeV resonance in the present experiment. We report 7 levels in the range of excitation energy from 11.6 to 18.9 MeV, while in the 7 MeV range immediately below there have been 16 levels reported [1]). Many of the levels in the lower region of excitation are very narrow levels decaying by gamma emission only. In the higher range of excitation energies the widths are expected to be larger due to decay by particle emission. This fact together with closer level spacing would make levels more difficult to resolve in this region.

The spins and parities for the 11.95 and 13.15 MeV levels in B^{11} can be estimated if the single-level Breit-Wigner formula is assumed to be a valdi description of each level. Then the observed change in cross section due to the resonance is given by

$$\sigma(\mathrm{n},\alpha) = \pi\lambda\!\!\!^{-2}\,\frac{2J+1}{2(2I+1)}\,\frac{\Gamma_\alpha\Gamma_\mathrm{n}}{(\frac{1}{2}\Gamma)^2},$$

where $\lambda\!\!\!^{-}$ is the reduced wavelength of the incident neutron, J is the spin of the B^{11} state, I is the ground-state spin of B^{10}(equals 3^+), Γ is the observed level width and Γ_α and Γ_n are partial widths for alpha particles and neutrons, respectively.

The 11.95 MeV level corresponds to the resonance at a neutron energy of 0.53 MeV .The observed change in the total (n, α) cross section is about 240 mb. By comparing this with the change of 400 ± 200 mb observed in the total neutron cross section [35]) an estimate of Γ_α and Γ_n can be obtained. The limiting cases are $\Gamma_\alpha \approx \Gamma_\mathrm{n} = \frac{1}{2}\Gamma$ and $\Gamma_\alpha \gg \Gamma_\mathrm{n}$. Table 2 shows the J^π values resulting

TABLE 2

Possible spin and parity assignments for two levels in B^{11*}

E_n (MeV)	B^{11*} (MeV)	J^π	Γ_α/Γ	Γ_n/Γ
0.53	11.95	$\frac{1}{2}^+$	0.5	0.5
		$\frac{3}{2}^-$ [a])	0.8	0.2
		$\frac{5}{2}^+$ [a])	0.88	0.12
1.86	13.15	$\frac{11}{2}^+$	0.5	0.5
		$\frac{17}{2}^-$	0.4	0.5

[a]) The parity assignments are arbitrary and the opposite assignments are also possible.

from various choices of Γ_α and Γ_n. The single particle reduced withs for each case were computed from the relation $\gamma^2 = \Gamma/2\ P_l$ where the penetrabilities $P_l = \rho/A_l^2$ were obtained from published tabulations. The angular momenta were restricted to $l_\mathrm{n} \leqq 2$ for neutrons and to $l_\alpha \leqq 3$ for alpha particles. For the spin and parity assignments of $\frac{1}{2}^+$, $\frac{3}{2}^-$ and $\frac{5}{2}^+$ the reduced width for the α_1-transition exceeds that for the α_0-transition by factors of three, five and eleven, respectively. The opposite parity assignments $J = \frac{3}{2}^+$ and $J = \frac{5}{2}^-$ are also possible, and the reduced width for the α_1-transition exceeds that for the α_0-

transition by a factor of three for each choice of spin. In every case the single particle reduced width is from 1 to 10 % of the Wigner limit, $\gamma_W^2 = \frac{3}{2}\hbar^2/MR^2$, where M is the reduced mass of the channel and R is the radius of interaction taken to be 5.0 fm for alphas. The Wigner limit is 975 keV for the alpha channels. With two exceptions the neutron reduced widths are 1 to 2 % of the 3380 keV Wigner limit for the neutron channel when the interaction radius is taken as 4.5 fm. The exceptions occur when the $J^\pi = \frac{1}{2}^+$ and $\frac{3}{2}^+$ assignments require neutron angular momenta with $l_n = 2$. In these cases the reduced width is 30 % of the Wigner limit.

A similar analysis was made of the 13.15 MeV level corresponding to the resonance at a neutron energy of 1.86 MeV. It was assumed that the broad 2.8 MeV resonance does not interfere with this resonance. Using the experimental width obtained in the (n, α) experiment, the observed change in the total neutron cross section [35]) was estimated to be 1000 ± 300 mb. The observed change in the (n, α) cross section is 360 mb. Other reactions contribute to the total cross section at this neutron energy. The (n, t2α) reaction was observed to be $\approx$ 30 mb.

The inelastic scattering of neutrons was estimated to contribute less than 100 mb using the elastic scattering data of Willard *et al.* [38]) at 1.5 MeV. Using these data it was estimated that $\Gamma_\alpha \approx 0.4\Gamma$ and $\Gamma_n \approx 0.5\Gamma$. These partial widths and the observed change in the (n, α) cross section yield an unreasonable spin of $J = \frac{17}{2}$ which requires neutrons with $l_n = 5$. The minimum spin assignment consistent with the observed cross section is $J^\pi = \frac{11}{2}^+$ when $\Gamma_\alpha = \Gamma_n = \frac{1}{2}\Gamma$. These results agree with those of Petree *et al.* [11]), who suggest that this resonance may be due to two unresolved levels of lower spin. However, in the present experiment this resonance, which has an experimental width of 630 keV, was examined four different times with a neutron energy resolution of about 50 keV, and each time the resonance showed a smooth Breit-Wigner shape with no sign of multi-level structure. For the spin assignment of $J = \frac{11}{2}^+$ the reduced widths for the α_0- and α_1-transitions are 60 % and 20 % of the Wigner limit while that for the neutron channel is 20 %.

Fig. 3 shows that the cross section for the (n, t2α) reaction becomes comparable to that for the (n, α) reactions above a neutron energy of 5 MeV. The observed cross section of 60 ± 18 mb at a neutron energy of 4.0 MeV is somewhat lower than the value of 95 ± 10 mb reported by Wyman, Fryer and Thorpe [15]) using absolute counting of the tritium beta activity. However, at 5.6 MeV the cross section of 230 ± 25 mb reported by these investigators and that of 239 ± 40 mb reported by Frye and Gammel [6]) are a factor of three greater than our measurement of 80 ± 24 mb. The same is true of the measurement by Frye and Gammel [6]) at 7.7 MeV. In the present experiment the ratio between the (n, α) and (n, tα2) reactions should be accurate to about $\pm$ 10 %; then the fair agreement among the reported values for the cross section of

the $B^{10}(n, \alpha)Li^7$ reaction tends to substantiate the (n, t2α) cross section data. In the following section of this paper the cross section for the $F^{19}(n, \alpha)N^{16}$ reaction which was measured simultaneously with that of the (n, t2α) reaction is found to be smaller than the values reported by others [19–21]) although it agrees within the quoted experimental errors. The data in the present investigation should not be in error by as much as a factor of three. The maximum error given by the arithmetic sum of all estimated errors is about ± 50 %.

The (n, t2α) reaction can occur as a three-body breakup of B^{11*} into two alphas and a triton, or it can take place as a succession of two-body reactions involving Li^7 or Be^8 as the intermediate nucleus. The following mechanisms are possible [1]):

$$B^{10}+n \rightarrow \alpha_1+\alpha_2+t+0.328 \text{ MeV}, \quad (1)$$

$$B^{10}+n \rightarrow Li^{7*}+\alpha-1.84 \text{ MeV},$$
$$Li^{7*} \rightarrow \alpha+t+2.17 \text{ MeV}, \quad (2)$$

$$B^{10}+n \rightarrow Be^8+t+0.234 \text{ MeV},$$
$$Be^8 \rightarrow \alpha+\alpha+0.094 \text{ MeV}, \quad (3)$$

$$B^{10}+n \rightarrow Be^{8*}+t-2.67 \text{ MeV},$$
$$Be^{8*} \rightarrow \alpha+\alpha+3.00 \text{ MeV}. \quad (4)$$

Mechanism (2) proceeds through the 4.63 MeV level of Li^7 although for sufficiently high neutron energies the levels at 6.54 and 7.47 MeV could be involved in a similar manner. Mechanism (3) proceeds through the ground state of Be^8, while mechanism (4) proceeds through the 2.9 MeV level. The end result in each of the four cases is two alpha particles and a triton with 328 keV plus the incident neutron energy shared between them. The distribution of this energy among the three particles is different in each case giving a means of studying these mechanisms in the ionization chamber through the different wall losses. The change in the number of counts in the 2α+t group can be calculated for each mechanism and compared with the change observed when the ion chamber pressure is increased in successive steps. In general, only the maximum possible contribution of each mechanism can be uniquely determined. As described in sect. 2, the number of counts in the 2α+t group as a function of chamber pressure was measured at neutron energies of 3.40, 5.25, 6.21, 7.58 and 7.67 MeV. In every case the observed data can be fully explained by either (a) three-body breakup, (b) the mechanism involving Li^{7*} or (c) any combination of these two mechanisms. The maximum possible contribution of mechanism (4) involving the 2.9 MeV level of Be^8 is estimated to be near zero at 3.40 MeV, as large as 100 % at 5.25 and 6.21 MeV and about 50 % at 7.58 and 7.67 MeV. These results are not very accurate because the wall losses for the three mechanisms do not differ greatly. However, the wall loss for mechanism (3) involving

the ground state of Be^8 is much greater than that of the other three mechanisms due to the long range triton. The data clearly show that the contribution of this mechanism is very small at each neutron energy investigated. The maximum possible contribution is estimated to be near zero at 3.40 and 5.25 MeV, less than 5 % at 6.21 MeV and less than 15 % at 7.58 and 7.67 MeV. Summarizing, it appears that the (n, t2α) reaction proceeds mainly by three-body breakup or through the 4.63 MeV level of Li^7. Some reactions may proceed through the 2.9 MeV level of Be^8, but few if any proceed through the ground state. These results agree with those of Frye and Gammel [6]), who have used nuclear emulsions to observe these mechanisms more directly at 5.6 MeV, 7.7 MeV and higher neutron energies.

The cross section for the (n, tα2) reaction below 3 MeV is comparable to that at 3.4 MeV. However, the mechanisms involving Li^{7*} and Be^{8*} are not energetically possible below 2.0 and 2.9 MeV, respectively, and are not expected to be important for somewhat higher energies. The data at 3.4 MeV indicate that triton emission to the ground state of Be^8 is very small. The major contribution to the (n, t2α) reaction below 3 MeV appears to be three-body breakup although it should decrease due to Coulomb barrier effects. As mentioned earlier the disintegrations from the B^{10}(n, p)Be^{10} reaction also are counted in the 2α+t group. Above 3 MeV the wall loss for protons from this reaction exceeds 90 % for the chamber pressure used. The situation is more favourable at lower energies with the wall loss becoming 40 % at 1.6 MeV. Unfortunately the contribution of protons to the 2α+t group could not be studied in this experiment below 3 MeV because the intense alpha groups due to slow neutron disintegrations in B^{10} interfere with the 2α+t group. An attempt was made to observe the (n, p) reaction at 3.40 MeV by increasing the chamber pressure to 5 atm. The results were negative. It is estimated that some effect would have been observed if the cross section for the (n, p) reaction were 25 mb or larger.

4. Data Analysis and Results for F^{19}

The excitation function for the (n, α) reactions in F^{19} was obtained in the same manner as those for the reactions in B^{10}. The results are shown in fig. 4. The excitation function for the (n, α) reactions leaving N^{16} in its ground and first three excited states was measured three times and the results averaged. The cross section at 5.90 MeV was determined to be 135 ± 50 mb by comparison with the B^{10}(n, α)Li^7 reaction which was observed simultaneously. A value of 138 mb was obtained directly by using the neutron flux measured by the long counter. Marion and Brugger [19]) have reported a cross section of 265 ± 110 mb for the total (n, α) reaction at this neutron energy, while Smith *et al.* [21]) reported 220 ± 40 mb. Although our value of the cross section is lower than

these results obtained from induced radioactivity measurements, the three values do agree within the quoted experimental errors. The $F^{19}(n, p)O^{19}$ reaction leaving O^{19} in its ground and first excited state at 0.096 MeV was observed at 7.67 MeV by using a chamber pressure of 6 atm to reduce the wall loss. The cross section was found to be 24 ± 10 mb as compared to 60 ± 24 mb for the total (n, p) cross section reported by Marion and Brugger [19]).

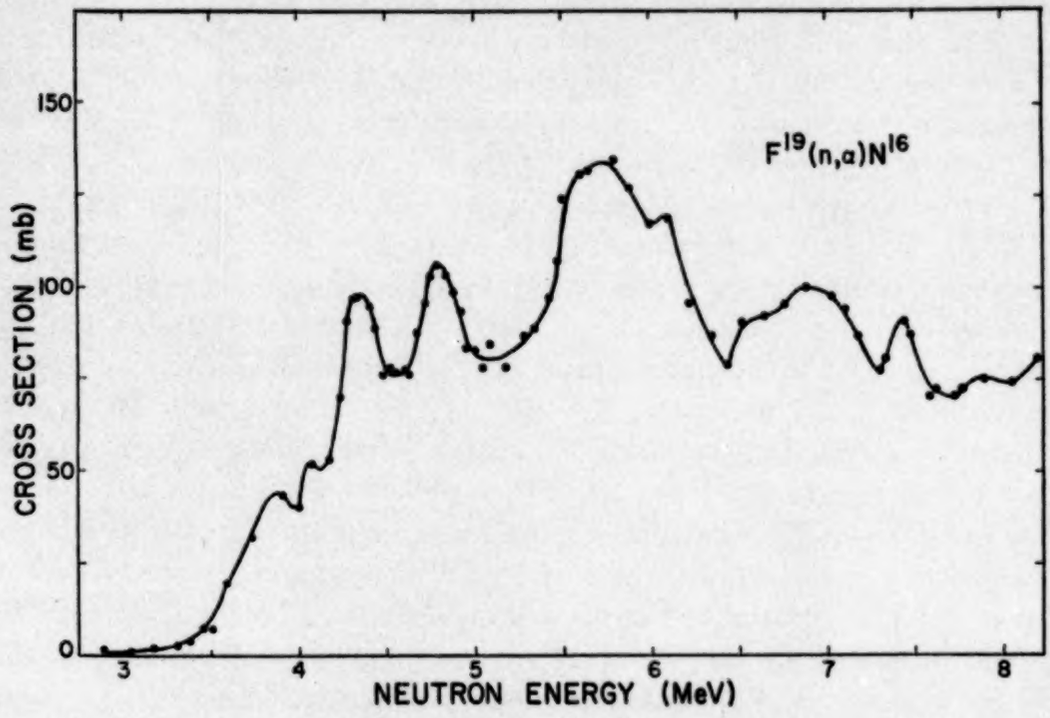

Fig. 4. Cross section for (n, α) disintegrations of F^{19} leading to ground and first three excited states of N^{16}.

The errors involved in the cross section measurements of the unresolved α_0, α_1, α_2 and α_3 groups are comparable to those discussed earlier for the B^{10} (n, α) Li^7 reaction. The cross section is estimated to be in error by ± 35 % for neutron energies above 5.2 MeV. From 3.8 to 5.2 MeV the alpha groups from slow neutron reactions in B^{10} interfere with the (n, α) reactions in F^{19}. A correction of 25 % to 50 % was made for this effect in the same manner as for the (n, t2α) reaction in B^{10}. The accuracy of the cross section below 5.2 MeV is estimated to be ± 40 %.

For neutron energies between 3.38 and 3.58 MeV the alpha groups to the ground and first three states of N^{16} were partially resolved as shown in fig. 1 for example. From the four measurements in this energy region it appears that the transitions to the ground and first excited state of N^{16} are from 1.5 to 2.5 times as intense as those to the second and third excited states. For higher neutron energies the groups were not resolved.

Resonances are observed in the excitation function at the neutron energies

listed in table 3. The excitation energy in F^{20*} is given in the preceding column of table 3, while the third and fourth columns give the resonance energies observed by Marion and Brugger [19]) and Smith *et al.* [21]), respectively. Marion

TABLE 3

Resonances observed in the $F^{19}(n, \alpha)N^{16}$ reaction

Excitation in F^{20} (MeV)	Neutron energy (MeV)		
	Present experiment	Marion and Brugger [19])	Smith *et al* [21])
		3.4	
		3.61	
10.27	3.85	3.69	3.75
		3.77	
10.5	4.1	4.11	4.08
10.74	4.35	4.42	4.36
			4.52
11.17	4.80	4.86	4.79
			5.15
			5.40
12.0	5.7		
		5.9	5.9
12.40	6.10		(6.1)
12.83	6.55		
13.2	6.9		
13.67	7.44		
14.0	7.8		

and Brugger have observed three resonances in the region of the 3.85 MeV resonance reported in the present experiment. In the energy range between 4.0 and 6.1 MeV Smith *et al.* have observed three resonances in addition to those reported here. The resonances in the energy region above 6.1 MeV have not been previously reported although those at 7.44 and 7.8 MeV correspond to levels in F^{20*} that have been studied by Bostrom, Hudspeth and Morgan [39]) in the $O^{18}(d, \alpha)N^{16}$ reaction.

References

1) F. Ajzenberg-Selove and T. Lauritsen, Nuclear Physics **11** (1959) 100
2) Amaldi, D'Agostino, Fermi, Pontecorvo, Rasetti and Segré, Proc. Roy. Soc. **149** (1935) 522
3) J. Chadwick and M. Goldhaber, Nature **135** (1935) 65
4) H. J. Taylor and M. Goldhaber, Nature **135** (1935) 341
5) H. J. Taylor, Proc. Phys. Soc. **47** (1935) 873
6) G. M. Frye, Jr. and J. H. Gammel, Phys. Rev. **103** (1956) 328
7) J. L. Perkin, Phys. Rev. **81** (1951) 892
8) E. W. Titterton and T. A. Brinkley, Nature **179** (1957) 369
9) James, Kubelka, Heiberg and Warren, Can. J. Phys. **33** (1955) 219
10) F. L. Ribe and J. D. Seagrave, Phys. Rev. **94** (1954) 934
11) Petree, Johnson and Miller, Phys. Rev. **83** (1951) 1148

12) Bichsel, Hälg, Huber, and Stebler, Helv. Phys. Acta **25** (1952) 119,
13) Bichsel, Hälg, Huber and Stebler, Phys. Rev. **81** (1951) 456,
14) H. Bichsel and T. W. Bonner, Phys. Rev. **108** (1957) 1025
15) Wymann, Fryer and Thorpe, Phys. Rev. **112** (1958) 1264
16) Eggler, Hughes and Huddleston, Phys. Rev. **74** (1948) 1239
17) G. C. Hanna, Phys. Rev. **80** (1950) 530
18) J. H. Gibbons and R. L. Macklin, Phys. Rev. **114** (1959) 571
19) J. B. Marion and R. M. Brugger, Phys. Rev. **100** (1955) 69
20) Bostrom, Hudspeth and Morgan, Phys. Rev. **99** (1955) 643
21) Smith, Bostrom and Hudspeth, Phys. Rev. **117** (1960) 514
22) Gabbard, Bichsel and Bonner, Nuclear Physics **14** (1959) 277
23) A. B. Lillie and J. P. Conner, Rev. Sci. Instr. **22** (1951) 210
24) J. L. Fowler and J. E. Brolley, Jr., Rev. Mod. Phys. **28** (1956) 110
25) E. Segre Experimental nuclear physics, vol. 1 (John Wiley & Sons, Inc., New York, 1952) p. 287
26) A. O. Hanson and J. L. McKibben, Phys. Rev. **72** (1947) 673
27) Harvey, Jackson, Eastwood and Hanna, Can, J. Phys. **35** (1957) 258
28) Bonner, Davis, Din and Kuan in Proc. Int. Conf. Nuclear Structure, Kingston (1960) ed. by D. A. Bromley and E. W. Vogt (North Holland Publ. Co., Amsterdam, 1960) chapt. 5
29) Davis, Bonner, Worley and Bass, to be published
30) Buneman, Cranshaw and Harvey, Can. J. Res. **27** (1949) 191
31) J. D. Aponte and S. A. Korff, Rev. Sci. Instr. **31** (1960) 532
32) Miscellaneous physical and chemical techniques of the Los Alamos project, national nuclear energy series div. V, vol. 3, ed. by A. C. Graves and D. K. Froman (McGraw-Hill Book Co., Inc., New York, 1952) p. 156
33) Haddad, Henkel, Perry and Smith in fast neutron physics, part. I, ed. by J. B. Marion and J. L. Fowler (Interscience Publishers, Inc., New York, 1960) p. 373
34) Strominger, Hollander and Seaborg Rev. Mod. Phys. **30** (1958) 585
35) Bockelman, Miller, Adair and Barschall, Phys. Rev. **84** (1951) 69
36) Los Alamos (unpublished) given in Hughes and Schwartz, Neutron Cross Sections BNL-325, 2nd ed. (1958)
37) R. L. Becker and H. H. Barschall, Phys. Rev. **102** (1956) 1384
38) Willard, Bair and Kingston, Phys. Rev. **98** (1955) 669
39) Bostrom, Hudspeth and Morgan, Phys. Rev. 1545 **105** (1957)

1.E.4:
3.A

Nuclear Physics **27** (1961) 467—489; © *North-Holland Publishing Co., Amsterdam*
Not to be reproduced by photoprint or microfilm without written permission from the publisher

THE (p, p′ γ) REACTION IN EVEN ISOTOPES OF Zn, Ge and Se

D. M. VAN PATTER, R. RIKMENSPOEL † and P. N. TREHAN ††

Bartol Research Foundation of the Franklin Institute, Swarthmore, Pennsylvania †††

Received 7 April 1961

Abstract: It has been found possible to study the systematic properties of the second 2+ level in medium-weight even nuclei by investigation of gamma-radiation from the (p, p′ γ) reaction. For the mass region A = 60-80, the present method of observing (p, p′γ) spectra has been successful for nuclei whose (p, n) threshold exceeds about 4 MeV. Measurements of the branching ratio of the second 2+ level have been made for Zn^{64}, Zn^{66}, Zn^{68}, Ge^{72}, Se^{76}, and Se^{78}, which are in reasonable agreement with available results from radioactivity. New levels have been found in Ge^{70} at 1.71±0.01 and 2.16±0.01 MeV. The 1.71 MeV level is considered to be the second 2+ level with a branching (cross-over/cascade) of 0.9±0.1. Information concerning the excitation curves for various (p, p′γ) radiations of Zn^{66} and Ge^{70} have been obtained for proton energies in the range of 3.0 to 5.2 MeV.

1. Introduction

Most experimental determinations of the branching ratio of the second 2+ level of medium-weight even nuclei have been obtained from radioactivity experiments. A rather systematic behaviour of this branching ratio is predicted by the various collective models now available, especially the asymmetric rotor model of Davydov and Filippov [1]). Analysis of the available data has shown this to be generally true [2]). However, some anomalies do seem to be present. For example, the level schemes of Zn^{64}, Zn^{66} and Zn^{68} are very similar; however, the branching ratios from radioactivity measurements turn out to vary widely [3]).

It would then seem to be worthwhile to have measurements of the branching ratio of the second 2+ level of these nuclei made independently of the radioactive decay experiments. Inelastic proton scattering on isotopically enriched targets of even isotopes of Zn, Ge and Se was investigated as a means of exciting the second 2+ level of these nuclei. This approach proved to be successful, and the results of these experiments are reported in this paper. In the process, some γ-rays from (p, γ) and (p, nγ) reactions of these nuclei were also observed. Preliminary reports of these measurements have been presented [4]).

† Now with the Biopysics Laboratory, Stanford University, Porto Alto, Calif.

†† On leave from the Panjab University, Chandigarh, Panjab, India.

††† This research was supported by the United States Air Force through the Air Force Office of Scientific Research of the Air Research and Development Command under Contract AF 49(638)-512.

2. Experimental Method

For these experiments, a proton beam of energy $\leqq 5.2$ MeV was provided by the Bartol-ONR Van de Graaff accelerator. After magnetic analysis, the definition of the proton beam was better than 5 keV.

Gamma-radiation was detected with a 5.1×5.1 cm NaI (Tl) crystal coupled to a Dumont 6292 photomultiplier. Gamma-ray spectra were displayed on a 100-channel RIDL pulse-height analyser. The spectral shapes were obtained for $E_\gamma = 0.28$ to 1.84 MeV using sources of Hg^{203}, Cs^{137}, Na^{22} and Y^{88} for calibration. The photopeak efficiency of the crystal was first found by comparison with a 12.7×12.7 cm NaI(Tl) crystal, the total efficiency for which was taken from the tables of Wolicki *et al* [5]).

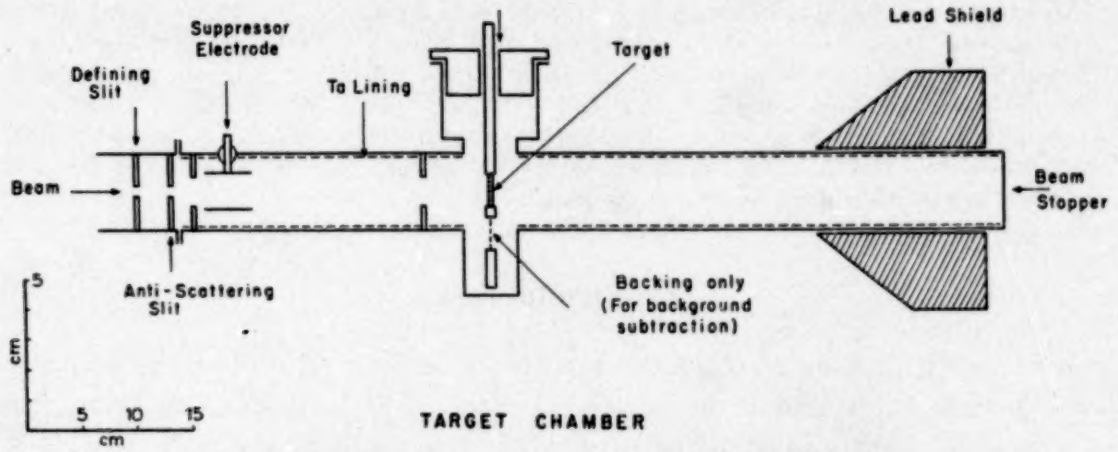

Fig. 1. Scheme of the target chamber and experimental arrangement.

Later comparison with the theoretical total efficiency for a 5.1×5.1 cm NaI(Tl) crystal given by Heath[6]) revealed an error in the original efficiency calibration using Cs^{137}. As a result, the branching ratios given in preliminary reports [4]) must be corrected. The revised calibration for photopeak efficiency is believed to be accurate to better than 10 %, with a relative error of about 5 %. Using the revised efficiency calibration, corrections for summing have been applied.

In order to establish the most favourable experimental circumstances, some preliminary bombardments at $E_p = 4.8$ MeV were performed on thin targets of natural Zn on Ta and W backings. In these experiments gamma ray were observed with energies of 1.0 MeV (a composite peak of the decay of the first level of $Zn^{64, 66, 68}$) and of 1.80 MeV (assigned to the cross-over of the second level of Zn^{64} on the basis of earlier work by Van Patter *et al* [7]) for inelastic proton scattering of Zn.) It also turned out, however, that for doing accurate intensity measurements a reduction of background radiation was necessary.

Background was observed as a continuum, from bremsstrahlung produced by the beam in the beam stopper, and from (p, γ) and (p, nγ) reactions. Discrete

γ-rays were also present in the background, particularly from the Si^{28} (p, p'γ) reaction (1.78 MeV) and the Fe^{56} (p, p'γ) reaction (0.845 MeV). In order to reduce all background not originating in the target, a final arrangement was adopted as illustrated in fig. 1. With appropriate lead shielding around the crystal (not shown), the γ-ray background was substantially reduced. A small amount of 1.78 MeV radiation due to the Si^{28} (p, p'γ) reaction still remained, especially at the resonance [8]) at $E_p \simeq 5.0$ MeV. Background radiation at $E_\gamma \simeq 1.37$ MeV, tentatively assigned to the Al^{27} (p, αγ) reaction, also proved to be troublesome for some of the observations.

The NaI(Tl) detector was mounted on a horizontal table so that γ-radiation from the target could be detected at various angles with respect to the proton beam. For the target chamber shown in fig. 1, an angular range of about 20° to 160° was available.

3. Target Preparation

Samples of 20—50 mg of enriched isotopes of $Zn^{64, 66, 68}$, $Ge^{70, 72, 74}$ and $Se^{74, 76, 78}$ were obtained from ORNL, Stable Isotope Division. The percentage of enrichment available for the different isotopes varied from 98 % to 11 %. Targets were produced by vacuum evaporation of 3 to 5 mg of material on thin formvar backings. The backings were mounted in a Ta frame of 12×12 mm².

3.1. ZINC

The condensation of a Zn vapour beam on a surface is known to be difficult. It was found, according to Holland [9]) that reliable condensation can be assured by sensitizing the surface with a very thin freshly deposited layer of silver or gold. This layer then acts as a set of condensation nuclei for the zinc vapour. The amount of gold used for sensitizing turned out to be critical. The optimum was found when the surface was pre-exposed to a gold source of approximately 2×2 mm² at 1300° C, for 5 sec at a distance of about 7.5 cm.

Evaporation of the Zn was performed from a small stainless steel crucible with an aperture to limit the solid angle of the vapour beam. This is important in view of the small amount of enriched material available. A graphite inner wall in the crucible is essential as melted zinc tends to amalgamate with most metals. Heating of the crucible was done by a surrounding r.f. coil.

3.2. GERMANIUM

The available material was in the form of a very fine powder. It turned out to be necessary first to melt 3 to 5 mg of the powder in a closed crucible similar to that used for the zinc evaporation. After cooling, the germanium solidifies into a small globule of ≈ 1 mm diameter. Vacuum evaporation of the germanium was performed without difficulties by placing the Ge globule in a small well in a graphite AC-heated filament.

3.3. SELENIUM

Se was easily evaporated from crucibles similar to those used for the evaporation of zinc.

4. Results

4.1. GENERAL

From isotopes which have (p, n) thresholds $\gtrsim 5$ MeV ($Zn^{64, 66}$, $Ge^{70, 72}$, Se^{76}) gamma rays from the decay of the first and second excited 2+ states were observed during bombardment for proton energies near 5.0 MeV. The spectra obtained are discussed for each case in sect. 4.2. The case of Ge^{70}, where the second 2+ level had not been previously observed, is discussed in some detail.

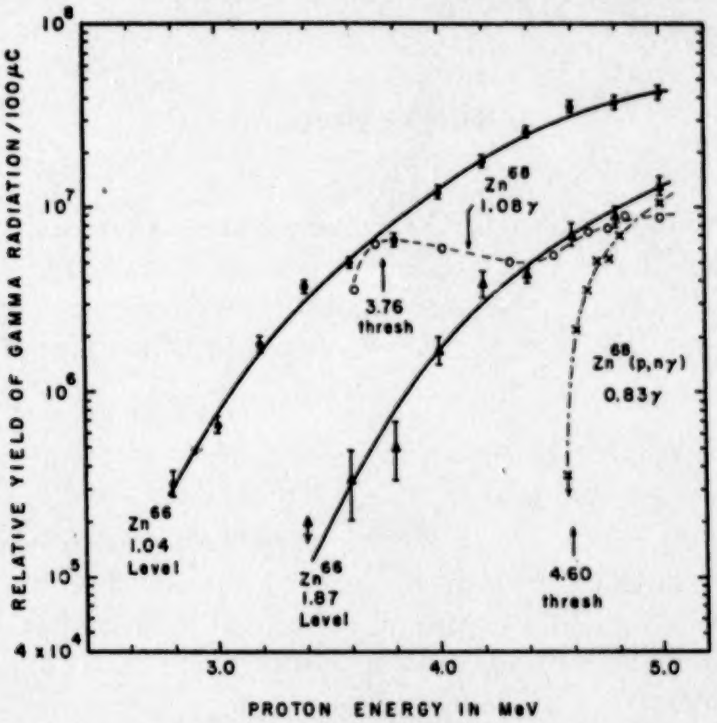

Fig. 2. Relative yield of γ-radiation from proton bombardment of Zn^{66}, $\theta = 55°$, $d = 10$ cm; and Zn^{68}, $\theta = 90°$, $d = 3$ cm ($E_p = 3.6-4.6$ MeV) and $\theta = 55°$, $d = 10$ cm ($E_p = 4.5-5.0$ MeV). The yields corrected for crystal efficiency) for Zn^{66} represent relative (p, p') cross sections for the first 2+ levels at 1.04 and 1.87 MeV. The yields of the 0.83 and 1.08 MeV γ-rays from Zn^{68} are normalised to the Zn^{66} excitation curves (see text). Thresholds for the Zn^{68} (p, n) Ga^{68} reaction corresponding to the ground state and 0.83 MeV level of Ga^{68} are indicated by arrows at 3.76 and 4.60 MeV.

In this type of experiment, the (p, p'γ) yield as a function of proton energy, and the relative importance of competing reactions like (p, nγ) and (p, γ) reactions, are the most important considerations.

Excitation curves for Zn^{66} (p, p'γ) radiations, observed at an angle of 55° with respect to the incoming beam, were measured for $E_p = 2.8-5.0$ MeV. The total yield of the γ-rays was found by taking account of the crystal effi-

ciency for a distance of 10 cm, and the yield of the 1.04 MeV γ-ray was corrected for 1.87 → 1.04 MeV cascades. Therefore, the Zn^{66} (p, p'γ) excitation curves shown in fig. 2 are proportional to the (p, p') cross sections for the 1.04 and 1.87-MeV 2+ levels. The Zn^{66} target thickness was not determined, but the absence of pronounced resonance structure indicates a target thickness in excess of $\approx$ 50 keV. For $E_p \leqq 3.4$ MeV, the yield of the 0.83-MeV γ-ray from the second 2+ level could not be measured reliably, because of the presence of γ-rays at 0.83±0.02 and 0.91±0.02 MeV. These γ-rays are assigned to the Zn^{66} (p, γ) Ga^{67} reaction, since prominent γ-rays of 0.84 and 0.92 MeV have been recently observed in the Ge^{67} → Ga^{67} decay [10]). Examination of the excitation curves for Zn^{66} reveals the steady increase of the (p, p') cross sections for the first two 2+ levels with increasing proton energy. For $E_p = 3.4-5.0$ MeV, the ratio of cross sections, $\sigma_2(2+)/\sigma_1(2+)$ increases from 0.07 to 0.30.

A considerably different situation is found for the case of Zn^{68}, whose (p, n) threshold occurs at 3.76 MeV. A Zn^{68} target of comparable thickness was bombarded at proton energies ranging from 3.6 to 5.0 MeV. Excitation curves were measured for the 1.08-MeV γ-ray from the first 2+ level of Zn^{68}, as well as for a 0.83-MeV γ-ray assigned to the Zn^{68}(p, n'γ)Ga^{68} reaction (see sect. 4.2.3). These curves are normalized at $E_p = 4.66$ MeV to the Zn^{66} excitation curves by using the relative intensities of inelastic proton groups observed from natural Zn at 90° by Van Patter *et al* [7]). This normalization indicated that the Zn^{68} target thickness was about 30 % less than the Zn^{66} target thickness. A considerable correction had to be applied to the yield of the Zn^{68} 1.08-MeV γ-ray for induced Ga^{68} activity. Also for $E_p \lesssim 3.7$ MeV, the presence of several Zn^{68} (p, γ) radiations was observed. These facts indicated that the excitation curve for the 1.08-MeV γ-ray of Zn^{68} was not as well determined as the Zn^{66} excitation curves. The second 2+ level of Zn^{68} was only weakly excited, so that no attempt was made to measure its excitation curve.

The excitation curves for the first 2+ levels of Zn^{66} and Zn^{68} are strikingly different. It can be concluded that as the proton bombarding energy is increased above the Zn^{68} (p, n) threshold, the cross section for the Zn^{68} (p, p'γ) reaction is reduced by a factor of the order 5, compared to the Zn^{66} (p, p'γ) reaction cross section.

4.2. REMARKS ON INDIVIDUAL CASES

4.2.1. The Zn^{64} Isotope

A γ-ray spectrum from a 89.3 % enriched Zn^{64} target (6.7 % Zn^{66}, 3.0 % Zn^{68}) at a bombarding energy of 5.0 MeV is shown in fig.3. In addition to annihilation radiation attributed mainly to induced Ga^{68} activity, γ-rays of energies 0.809±0.004, 0.995±0.003, 1.33±0.01, 1.62±0.01 and 1.803±0.005 MeV were observed. Energy determinations were based on calibrations using annihilation radiation, and the 1.332-MeV γ-ray from Co^{60}. The three most prominent

γ-rays (see table 1) can be definitely assigned to the Zn^{64} (p, p'γ) reaction, and correspond to transitions from the first two 2+ levels at 0.99 and 1.80 MeV. Their energies are in excellent agreement with the best previous determinations of the level energies at 0.991 ± 0.005 and 1.799 ± 0.005 MeV from observations of inelastic proton groups [7]). Excitation curves for the first two 2+ levels of Zn^{64} measured for $E_p = 2.6-5.0$ MeV were very similar to those shown in fig. 1 for Zn^{66}.

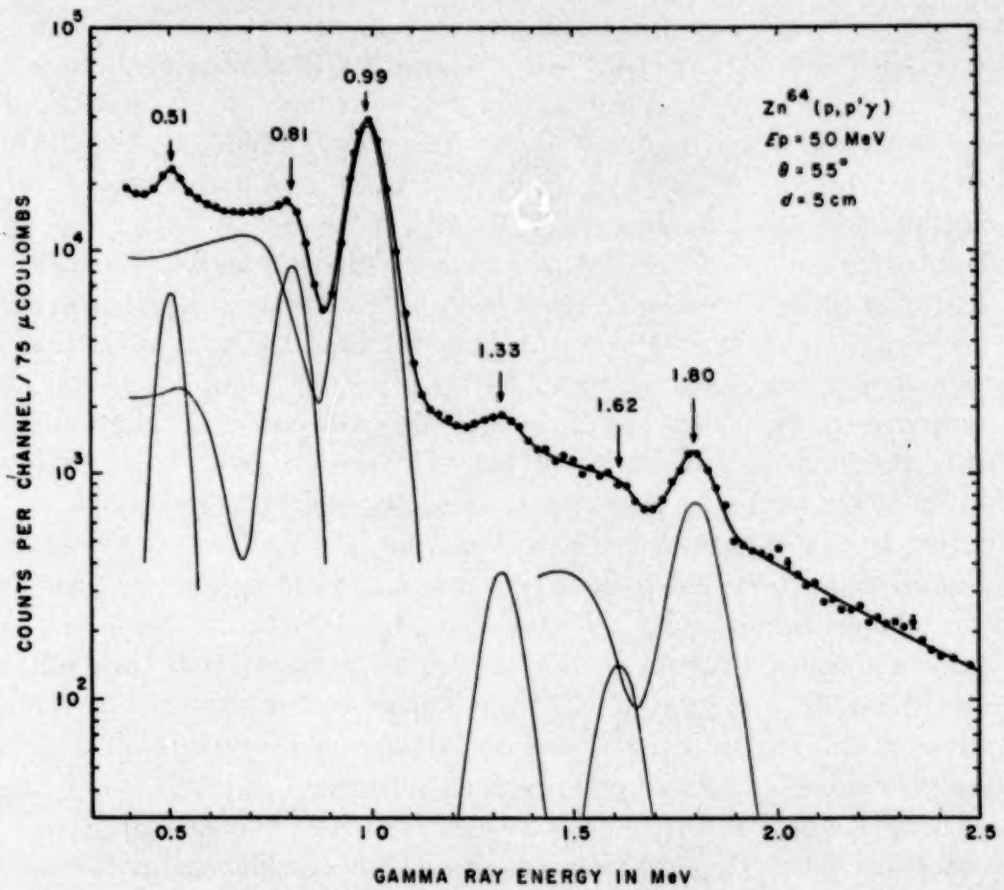

Fig. 3. Gamma-ray spectrum from Zn^{64} bombarded by 5.0-MeV protons, obtained using a 5.1 × 5.1 cm NaI (Tl) crystal, source to crystal face distance $d = 5$ cm.

After correction of the γ-ray intensities for absorption in the wall of the target chamber and for summing effects, a branching ratio (cross-over/cascade) of 0.25 ± 0.02 was obtained for the decay of the 1.80-MeV level of Zn^{64}. Since the measurement was done at an angle of 55° to the proton beam, corresponding to $P_2(\cos\theta) = 0$, angular distribution effects can be expected to nearly cancel out. The angular distributions of the three prominent γ-rays were measured at $E_p = 5.0$ MeV, $d = 10$ cm, at intervals of 30°. Corrections for background contributions were found to be important at $\theta = 150°$ and 30°, at which angles the effects of radiation from the defining slits and beam stopper

TABLE 1

Gamma-rays observed from proton bombardment of even nuclei at $\theta = 55°$

Target nucleus	(p, n) thresh (MeV)	E_p (MeV)	γ-ray energy (MeV)	Relative yield	Reaction assignment
Zn^{64}	8.0	5.0	0.809±0.004	29.5± 1.4	p, p′γ
			0.995±0.003	[100]	p, p′γ
			1.33 ±0.01 [a])	1.8± 0.4	p, p′γ
			1.62 ±0.01 [a])	0.9± 0.5	p, p′γ
			1.803±0.005	4.9± 0.4	p, p′γ
Zn^{66}	6.05	5.0	0.829±0.003	23 ± 3	p, p′γ
			1.037±0.004	[100]	p, p′γ
			1.33 ±0.01 [a])	2.2± 0.5	p, p′γ
			1.43 ±0.01 [a])	1.2± 0.4	p, p′γ
Zn^{68}	3.76	4.7	0.574±0.004	380 ±60	p, nγ
			0.82 ±0.003		p, p′γ
			0.829±0.013	70 ±15	p, nγ
			1.078±0.004	[100]	p, p′γ
			1.893±0.008	5 ± 3	p, p′γ
Ge^{70}	7.4	5.0	0.075±0.010		p, γ
			0.145±0.010		p, γ
			0.175±0.005		p, p′γ
			0.500±0.009	0.8± 0.2	p, p′γ
			0.672±0.004	12.9± 1.4	p, p′γ
			1.040±0.003	[100]	p, p′γ
			1.124±0.013	2.2± 0.3	p, p′γ
			1.709±0.008	11.7± 1.4	p, p′γ
			2.161±0.010	1.6± 0.3	p, p′γ
Ge^{72}	5.22	5.0	(0.60 ±0.01)	≈5	p, p′γ [b])
			0.63 ±0.01	22 ± 4	p, p′γ
			0.832±0.004	[100]	p, p′γ
			1.20 ±0.01	2.1± 0.4	
			1.47 ±0.01	2.4± 0.3	p, p′γ
			1.73 ±0.02	1.7± 0.3	
Ge^{74}	3.36	4.3	0.354±0.005	31 ± 6	p, nγ
			0.441±0.005	46 ± 9	p, nγ
			[0.596]	[100]	p, p′γ
			0.72 ±0.01	8 ± 3	p, nγ
			0.83 ±0.01	<7	p, nγ [b])
Se^{74}	(6.3)	4.2	0.53 broad		
		4.6	0.64 broad [a])		p, p′γ
			0.85 ±0.01 [a])		p, γ [b])
			1.37 ±0.02 [a])		p, γ [b])
Se^{76}	5.5	5.0	0.56 ±0.01	[100]	p, p′γ
			0.66 ±0.01	17 ± 2	p, p′γ
			1.21 ±0.01	8.5± 0.8	p, p′γ
Se^{78}	4.40	4.1	0.390±0.004	15 ± 6	p, γ
			0.523±0.005	16 ± 3	p, γ
			0.614±0.005	[100]	p, p′γ
			0.70 ±0.01	6.5± 2	p, p′γ
			0.84 ±0.01 [a])	1.6± 0.6	
			1.11 ±0.01 [a])	2.7± 1	
			1.31 ±0.01	3.3± 0.5	p, p′γ

[a]) It is not certain that this γ-ray can be assigned to the target nucleus.

[b]) This reaction assignment is subject to uncertainty.

respectively became appreciable After correcting for wall absorption and integrating over θ, a branching of 0.26 ± 0.02 is obtained, in agreement with the measurement at 55°. The value of 0.34 previously reported by Jacobi [11]) from the decay of Ga^{64} is not considered to be in disagreement with our data. A branching value of 0.27 ± 0.04 has also been listed in table 1, which was obtained from measurements of Zn (n, n'γ) spectra [12]). (See discussion for Zn^{68}.)

The present limited knowledge of the level scheme of Zn^{64} does not permit an unambiguous assignment of the 1.33 and 1.62-MeV γ-rays. Measurement of the background using only a formvar backing as target indicated that these γ-rays did originate from the target material. However, the possibility that some target contamination could be the source of these γ-rays is difficult to eliminate completely. The 1.33-MeV γ-ray is observed for $E_p \geqq 4.4$ MeV (below 4.4 MeV the 1.37 MeV background line predominates), while the 1.62 MeV γ-ray is observed for $E_p \gtrapprox 5.0$ MeV. These observations, combined with the observed intensities relative to the 0.99-MeV γ-ray (see table 1), are consistent with the tentative assignment of the 1.33 and 1.62 MeV γ-rays to cascade transitions from possible levels in Zn^{64} at 2.32 and 2.61 MeV. Further investigations are needed to verify these tentative assignments. There is evidence for a level in Zn^{64} at 2.30 MeV, both from the $Ga^{64} \rightarrow Zn^{64}$ decay[11]) and the Zn (n, n'γ) reaction [12]), however, these studies indicate a cascade γ-ray of $1\,30 \pm 0.02$ MeV, whose energy seems to be slightly lower than 1.33 MeV.

4.2.2. The Zn^{66} Isotope

In fig. 4 is shown a spectrum observed at $E_p = 4.8$ MeV, $\theta = 55°$, from a 97.8 % enriched Zn^{66} target. The proton energy was chosen to be lower than the 5.0-MeV resonance for the Si^{28} (p, p'γ) reaction, on order to reduce the amount of 1.78-MeV radiation in the background. No cross-over decay from the second 2+ level of Zn^{66} at 1.87 MeV was observed, in accordance with the results of a recent study of the Ga^{66} decay [13]). Taking an upper limit for the intensity of this possible cross-over corresponding at peak height to twice the standard deviation of the background radiation, a branching ratio of $\leqq 0.02$ is obtained for the second level of Zn^{66}.

At $E_p = 5.0$ MeV, γ-rays with energies 0.829 ± 0.003, 1.037 ± 0.004, 1.33 ± 0.01 and 1.43 ± 0.01 MeV were observed. These energy measurements (and most of those following in sect. 4.2) are based on calibrations using Y^{88} γ-ray energies given by Peele and Lowe [14]). The energies of the first three γ-rays are in excellent agreement with the more precise measurements of Schwarzschild and Grodzins [13]) for γ-ray transitions from the first three levels of Zn^{66} at 1.037, 1.865 and 2.370 MeV. The 1.33 and 1.43 MeV γ-rays are observed for $E_p \geqq 4.6$ MeV, and their yields (see table 1) are consistent with a tentative assignment to cascade transitions from Zn^{66} levels at 2.37 and (2.47) MeV. Further investigations are required before these assignments can be made

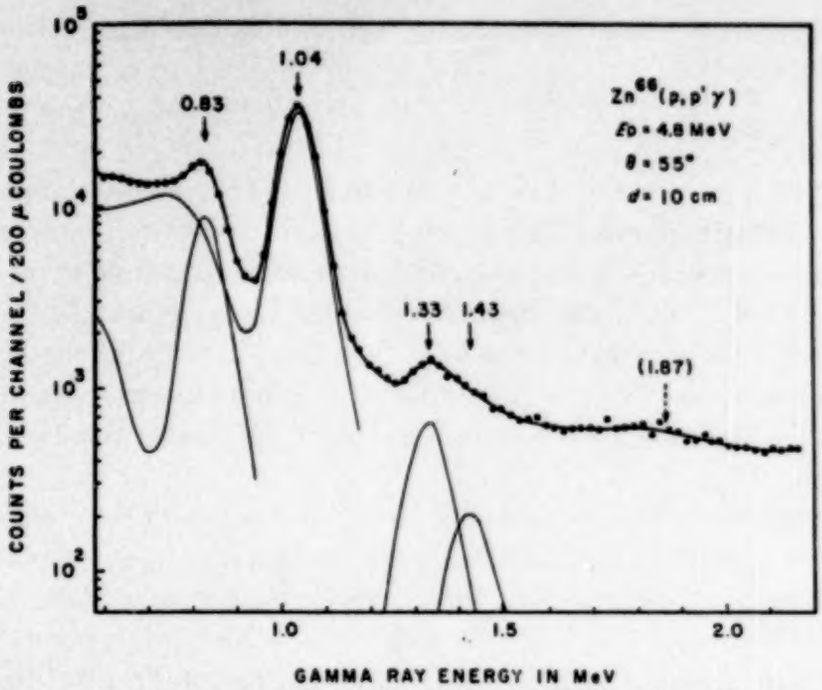

Fig. 4. Gamma-ray spectrum from Zn^{66} bombarded by 4.8-MeV protons. The expected position for a cross-over transition from the 1.87-MeV second 2+ level of Zn^{66} is indicated.

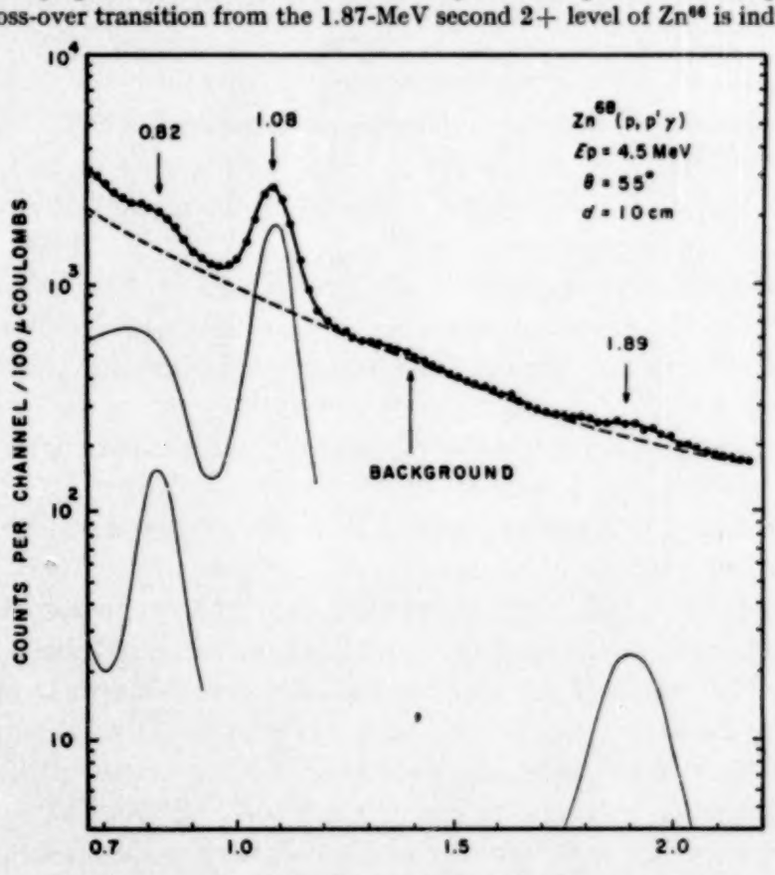

Fig. 5. Gamma-ray spectrum from Zn^{68} bombarded by 4.5 MeV protons. The continuous background assumed for spectral analysis is shown. The contribution of Ga^{68} activity produced during the run has not been subtracted.

definitely, such as measurements of γ-γ coincidences or inelastic proton groups.

4.2.3. The Zn^{68} *Isotope*

As the Zn^{68} (p, n) threshold occurs at 3.76 MeV, the yield of the Zn^{68} (p, p'γ) reaction is greatly reduced for $E_p = 3.76$, compared to the Zn^{66} (p, p'γ) reaction, as shown in fig. 2. In an attempt to observe excitation of the 1.89-MeV second 2+ level of Zn^{68}, long runs were taken at $E_p \geqq 4.5$ MeV, just below the threshold for excitation of the 0.83-MeV level in Ga^{68} by the Zn^{68} (p, nγ) reaction. Ground-state decay of this level makes observation of the cascade γ-ray (0.82 MeV) from the second level of Zn^{68} impossible for $E_p = 4.6$ MeV (see fig. 2).

A spectrum observed at $E_p = 4.5$, $\theta = 55°$ from a 96.8 % enriched Zn^{68} target on formvar is shown in fig. 5. A weak excitation of the 1.89-MeV second level is visible. Analysis revealed that a substantial fraction (about one-half) of the yield of the 1.89 MeV γ-ray in this run originated from Ga^{68} activity produced during bombardment. A large γ-ray background is present, primarily due to the Zn^{68} (p, γ) reaction, with some contribution from bremsstrahlung of positons from Ga^{68} activity. Two such measurements of the relative intensities of the 1.89 and 0.82-MeV γ-rays yielded a ratio of $0.7\pm \approx 0.4$. If this value is taken for the branching of the 1.89-MeV level, it is subject to considerable uncertainty, because of the possible presence of 0.87-MeV radiation from the Zn^{68} (p, γ) Ga^{69} reaction, which was clearly indicated at $E_p = 3.7$ MeV.

The γ-ray spectrum of the Ga^{68} source formed during the bombardment was measured. The source was surrounded by 1.3 cm of graphite, in order to annihilate the positrons with a minimum of background due to bremsstrahlung. A weak excitation of the second 2+ level at 1.89-MeV was seen, in accord with Horen [3]). However, the 1.89 MeV γ-ray was much more clearly defined above background than in fig. 5 since the contribution due to (p, γ) radiation had been removed. This observation gave a branching ratio of 1.1 ± 0.4, which is in agreement with the approximate value of 1.4 reported by Horen [3]). This value of 1.1 ± 0.4 is considered to be more reliable than that resulting from the Zn^{68} (p, p'γ) measurements, and therefore has been listed in table 2.

An unreported value of 1.9 ± 0.5 for the Zn^{68} branching ratio has been obtained independently at this laboratory from studies of (n, n'γ) spectra from natural zinc [12]). Measurements were made of (a) the average branching ratio for even isotopes and (b) the intensity ratio for 1.89 (Zn^{68}) and 1.80 (Zn^{64}) γ-rays. Since it is known [13]) that the Zn^{66} branching is < 0.008, and the contribution of Zn^{70} (0.62 % abundance) is negligible, measurements (a) and (b) provide separate values for the branching of Zn^{64} and Zn^{68}. Since no correction has been applied to this (n, n'γ) value for γ-ray angular distributions,

possibly the best value for the Zn^{68} branching can be obtained using a combination of measurement (b) and the present value of 0.26 ± 0.02 for the branching of Zn^{64}. This yields a value of 1.6 ± 0.2 for the branching of the 1.89-MeV level of Zn^{68}, which has been used for calculation of the ratio of B(E2) values given in column 8, table 2.

TABLE 2

Experimental data concerning the properties of the second 2+ level for the even isotopes of Zn, Ge and Se

Nucleus	$E_1(2+)$ (keV)	$E_2(2+)$ (keV)	$\frac{E_2(2+)}{E_1(2+)}$	Branching r		δ	$\frac{B(E2;\,2'\to 2)}{B(E2;\,2'\to 0)}$
				Present	Previous		
Zn^{64}	993 3	1801 4	1.81	0.26 ± 0.02	0.27 ± 0.04 [a] 0.34 [b]		210 ± 15 [f, m]
Zn^{66}	1037 2	1865 3	1.80	<0.02	<0.008 [c] <0.04 [d]	$1.5<\delta<3$ [e]	>5000
Zn^{68}	1078 3	1893 7	1.76	1.1 ± 0.4	1.9 ± 0.5 [a] ≈ 1.4 [e]		42 ± 6 [m]
Ge^{70}	1040 3	1710 5	1.64	0.9 ± 0.1			121 ± 12 [m]
Ge^{72}	834.5 <1.0	1465 <1	1.75	0.11 ± 0.02	0.13 [f] 0.19 [g]	$\lvert\delta\rvert \geqq 4.4$ [d]	550 ± 90
Ge^{74}	596 1	1200 6	2.01		0.59 ± 0.16 [h]	$-(1.0^{+\infty}_{-0.4})$ [h]	52 ± 14 [m]
Se^{76}	559.3 0.1	1216.6 0.2	2.18	0.50 ± 0.07	0.55 ± 0.04 [i] 0.52 ± 0.10 [k] 0.62 [d]	-6.5 ± 0.5 [j]	41 ± 3
Se^{78}	614 3	1309 5	2.13	0.5 ± 0.2	0.78 [l]		37 ± 12 [m]

The nucleus Se^{80} has not been included in this table, because a preliminary report by C. F. Carter, Jr., [27]) has indicated the presence of a doublet (1.444, 1.470 MeV) at the position of second level. The interpretation of the (n, n′γ) data used for estimating the branching [2]) of the second 2+ level of Se^{80} is now open to question.

[a]) See ref. [12]). [b]) See ref. [11]). [c]) See ref. [13]). [d]) Listed in ref. [2]). [e]) See ref. [3]). [f]) See ref. [20]). [g]) See ref. [21]). [h]) See ref. [22]). Other branching values for Ge^{74} listed in ref. [3]) have not been included, since there is evidence from various sources that these earlier values are incorrect [19]). [i]) See ref. [25]). [j]) See ref. [30]). [k]) See ref. [24]). [l]) See ref. [19]). [m]) For lack of sufficient information, this value has been calculated assuming 100 % E2 for the $(2'\to 2)$ cascade transition; however, the quoted error does not include this uncertainty.

$E_1(2+)$ and $E_2(2+)$ are the present best values with associated errors for the energies of the first two 2+ levels, obtained by taking a weighted average of the available determinations. The γ-ray branching of the second 2+ level is given by r (cross-over/cascade). δ is the ratio of E2 and M1 matrix elements for the $(2'\to 2)$ cascade transition. The $B(E2)$ ratios (column 8) are calculated using the best value of the branching r from the presently available data.

The Zn^{68} (p, p′γ) radiations from the first two 2+ levels had energies of 1.078 ± 0.004, 0.82 ± 0.02 and 1.893 ± 0.008 MeV (see table 1), which compare favourably with Horen's results [3]). For $E_\gamma > 0.5$ MeV, two Zn^{68} (p, nγ) radiations were identified, with energies 574 ± 4 and 829 ± 3 keV. These evidently correspond to ground-state transitions from levels in Ga^{68} measured at 574 ± 13

and 848±11 keV by Chapman and Slattery [15]), by observation of (p, n) thresholds. The relative intensities of these γ-rays are listed in table 1 for $E_p = 4.7$ MeV, since at $E_p = 5.0$ MeV analysis of the observed γ-ray spectrum was complicated by the presence of additional (p, nγ) radiations in the energy region of 0.9—1.05 MeV. The yields of both the 1.08 and 1.89 MeV γ-rays have been corrected for the contribution of Ga^{68} activity present during the run. Observations have also been made of (p, nγ) radiations with $E_\gamma < 0.5$ MeV, and (p, γ) spectra at lower proton energies; however, these are not be described in this paper.

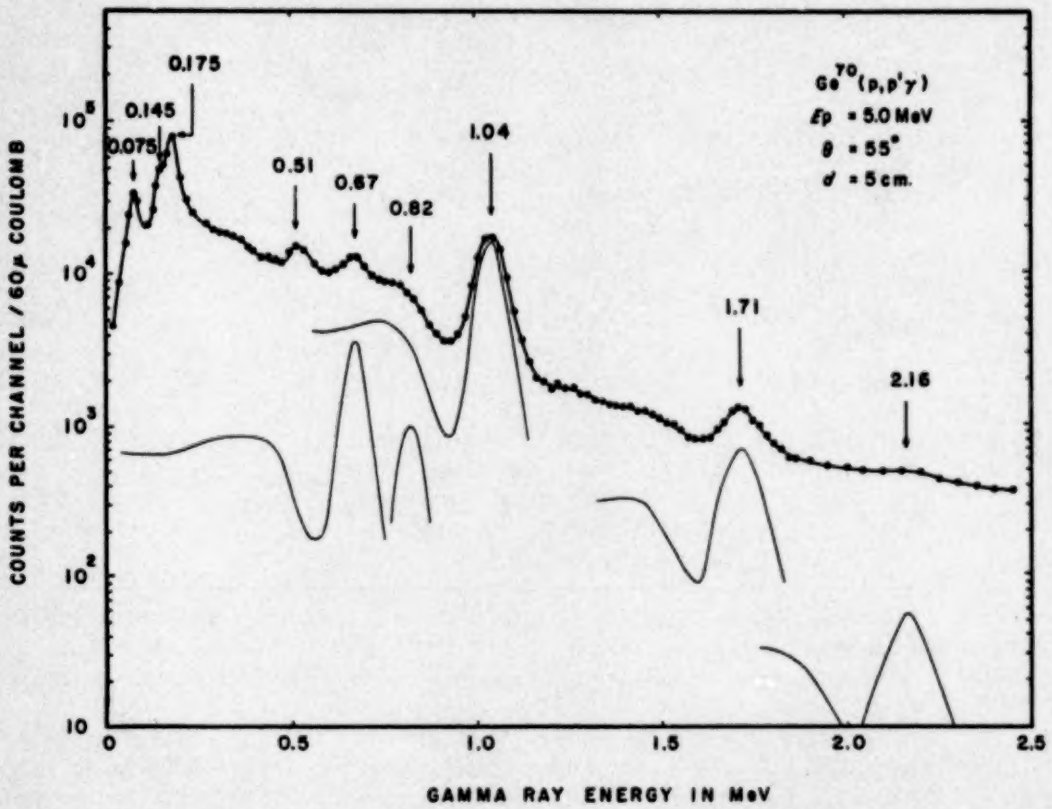

Fig. 6. Gamma-ray spectrum from Ge^{70} bombarded by 5.0 MeV protons. The 0.82-MeV γ-ray is attributed to the 2.7 % of Ge^{72} present in the target.

4.2.4. The Ge^{70} *Isotope*

The γ-ray spectrum observed at $\theta = 55°$ from a 92.6 % enriched Ge^{70} target (2.7 % Ge^{72}, 2.9 % Ge^{74}) bombarded by 5.0-MeV protons is shown in fig. 6. Gamma-rays of 0.175, 0.67, 1.04, 1.71 and 2.16 MeV are indicated which are attributed to the Ge^{70} (p, p'γ) reaction. Their energies and relative intensities observed at $E_p = 5.0$ MeV are listed in table 1. Energy determinations are based on a calibration run using annihilation radiation, and the latest value [16]) for the Na^{22} γ-ray of 1273.6±1.6 keV. Most of the intensity of a weak γ-ray at 0.82±0.01 MeV is contributed by the 2.7 % of Ge^{72} present in this target, due

to excitation of the 0.835 MeV state in Ge^{72}. Two low energy γ-rays of 0.07 and 0.15 MeV are also seen which could be attributed to the de-excitation of low-lying state in As^{71}, excited by the Ge^{70} (p, γ) As^{71} reaction. After prolonged bombardment, the 175-keV γ-ray from the decay of As^{71} is seen in the activity from the target. The γ-ray peak at 0.51 MeV is largely annihilation radiation.

A coincidence circuit with a resolving time of $2\tau = 0.6$ μsec was used for (γ–γ) coincidence measurements made at $E_p = 4.8$, 5.0 and 5.2 MeV. Two 5.1 × 5.1 cm NaI(Tl) crystals were placed at a distance of 3 cm from the target, each at 90° to the beam direction, and 180° to each other. A single channel was

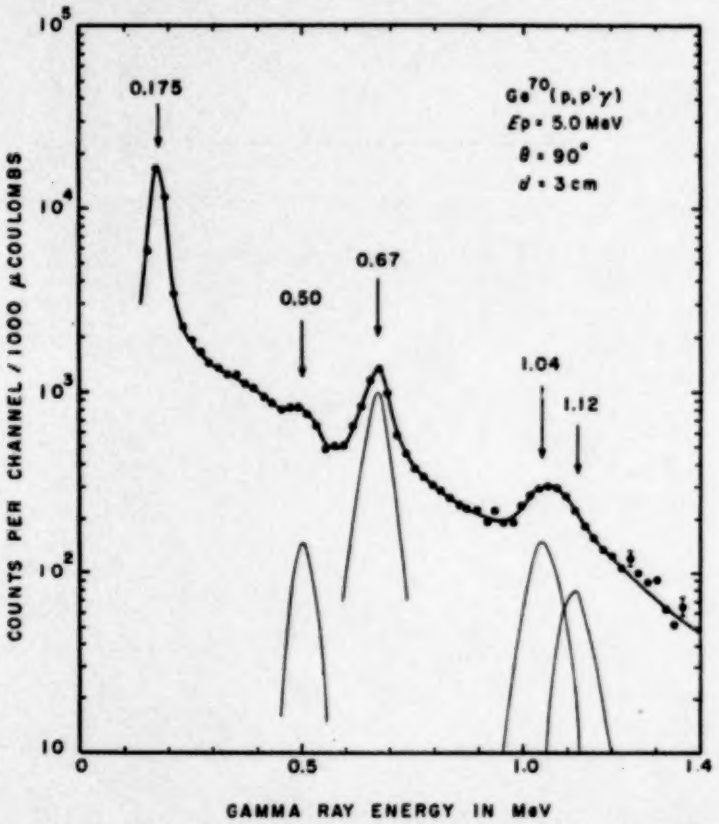

Fig. 7. Gamma-ray spectrum from Ge^{70} in coincidence with 1.04-MeV radiation, observed using two 5.1 × 5.1 cm NaI(Tl) crystals separated by 6 cm, at $E_p = 5.0$ MeV. The NaI(Tl) crystals were placed at 90° to the beam direction, and at 180° to each other.

set on the 1.04 MeV photopeak and the coincident γ-ray spectrum recorded on the 100-channel analyser. The coincidence spectrum observed at $E_p = 5.0$ MeV is shown in fig. 7, which includes appreciable contributions from chance coincidences. When correction is made for chance coincidences, then it is found that γ-rays of 0.18, 0.50, 0.67, and 1.12 MeV are in coincidence with 1.04 MeV radiation.

In fig. 8 is presented a level scheme for Ge^{70} consistent with these observations. The 1.04 and 0.175-MeV γ-rays arise from de-excitation of known levels at 1.04 MeV (2+) and 1.21 MeV (0+). New levels at 1.71 ± 0.01 and 2.16 ± 0.01

MeV in Ge^{70} are proposed. Observation of spectra coincident with 0.17 and 0.67-MeV radiation verified this scheme, but added no new information.

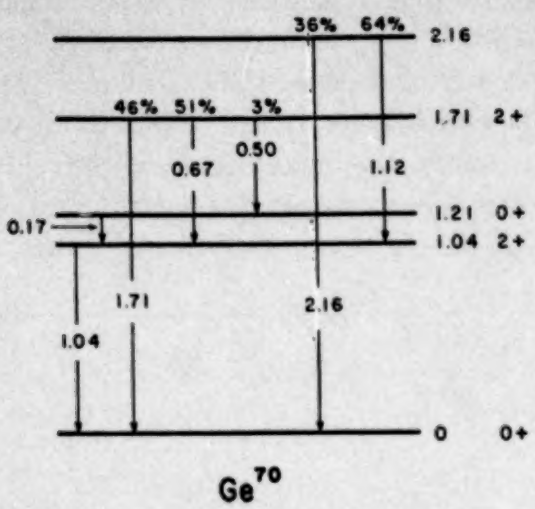

Fig. 8. Energy level scheme for Ge^{70}.

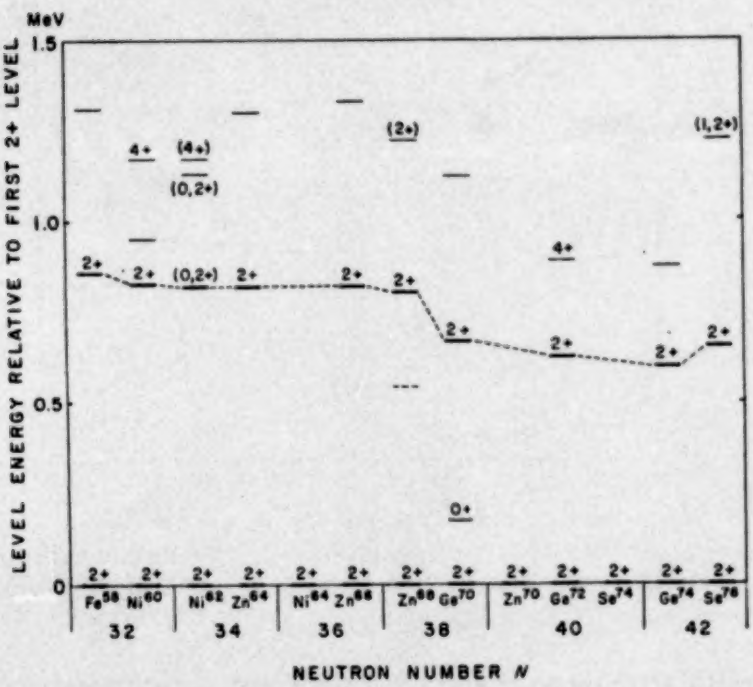

Fig. 9. Systematics of low-lying energy levels for even nuclei with $N = 32$—42, plotted relative to the position of the first 2+ level.

The prominent γ-rays of 0.67 and 1.71 MeV are assigned to the new level at 1.71 MeV, which is considered to be the second 2+ level, for several reasons. First, the position of this level agrees within 0.1 MeV with the expected position for the previously missing second 2+ level predicted from a study [17]) of the systematic properties of the energy levels of neighbouring even nuclei as shown in fig. 9. Second, the prominence of the 0.67 and 1.71 MeV γ-rays in the

spectrum of fig. 6 is similar to γ-rays seen from the excitation of known 2+ levels, such as in Zn^{64} and Zn^{66}. Finally, the excitation curve for 1.71-MeV radiation as shown in fig. 10 is very similar to that for the second 2+ level in Zn^{66} (see fig. 2).

After correction for the absorption in the wall of the reaction chamber, a branching ratio of 0.92 ± 0.15 was obtained for this 1.71-MeV level from the analysis of singles spectra such as shown in fig. 6. At $E_p = 5.0$ MeV, angular distributions of the 0.67 and 1.71-MeV γ-rays were measured from 30° to 150° in steps of 30°. After correcting for wall absorption as a function of angle, and

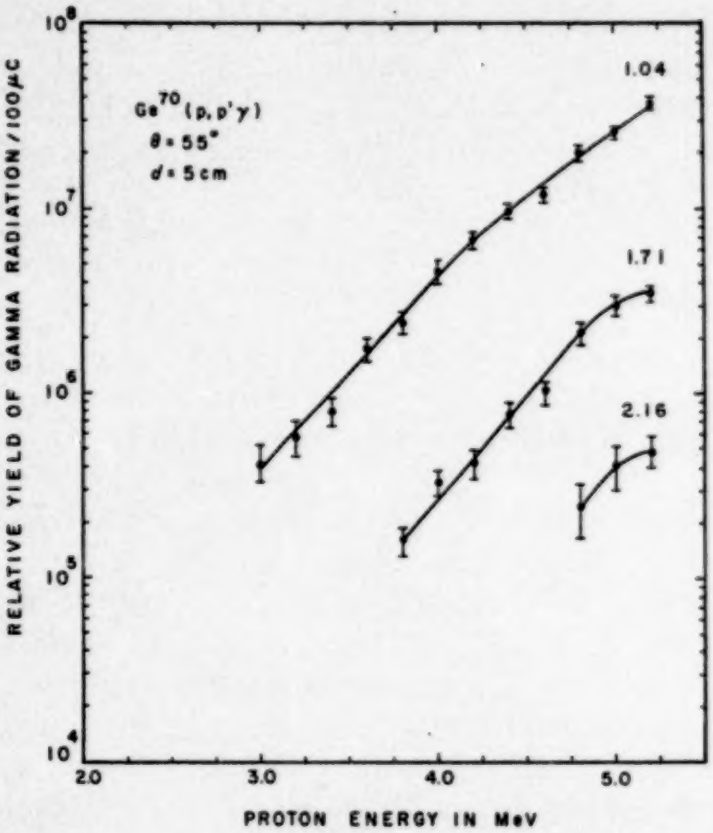

Fig. 10. Relative yield of 1.04, 1.71 and 2.16 MeV γ-rays from the proton bombardment of Ge^{70}, corrected for the efficiency of the 5.1×5.1 cm NaI(Tl) crystal at $d = 5$ cm.

integrating over θ, a branching ratio of 0.90 ± 0.08 was found. The excellent agreement between the two measurements confirm that a reliable branching ratio can be measured at $\theta = 55°$ where $P_2(\cos\theta) = 0$.

An attempt was made to measure the percentage decay of the 1.71 MeV level via the 1.21-MeV 0+ state, by looking for 0.50-MeV γ-radiation in coincidence with the 1.04 MeV γ-ray. A substantial amount ($\approx 30\,\%$) of the 0.50-MeV peak shown in fig. 7. can be attributed to chance coincidences involving annihilation radiation. After subtraction of this contribution, the percentage branching of the 1.71-MeV state via the 1.21-MeV state is estimated as $3 \pm 1\,\%$.

Evidence for a new state in Ge^{70} at 2.16 $\pm$0.01 MeV is obtained from the 2.16 MeV γ-ray seen in the singles spectra, and the 1.12 MeV γ-ray seen in coincidence with 1.04 MeV radiation (see fig. 7). By using comparisons with the yields of other γ-rays seen in these two spectra, a branching ratio was measured as 0.6$\pm$0.2. No evidence was found in the coincidence data of fig. 7 for 0.95-MeV γ-ray corresponding to a 2.16 $\rightarrow$ 1.21 MeV cascade transition, the upper limit being about 10 % of the decays of the 2.16-MeV level.

The discovery of these new states in Ge^{70} indicate that a re-investigation of the decay scheme of As^{70} would be worthwhile, since some of the γ-rays already reported [18]) might involve these states.

The relative yield of 1.04, 1.71, and 2.16 MeV γ-rays as a function of proton energy was studied and is shown in fig. 10. Since the yield of the 0.17-MeV cascade γ-ray from the 1.21-MeV 0+ state is not well determined, relative (p, p') cross sections for the 1.04, 1.71 and 2.16 MeV states of Ge^{70} have not been calculated from these measurements.

4.2.5. The Ge^{72} *Isotope.*

A γ-ray spectrum from a 89.2 % enriched Ge^{72} target at $E_p = 5.0$ MeV, $\theta = 55°$, is shown in fig. 11. A small amount of annihilation radiation is observed, which is attributed to the decay of As^{74} and As^{76} formed during bombardment from Ge^{74} (4.3 %) and Ge^{76} (1.6 %) present in the target. The time background taken immediately after the run revealed no γ-rays of appreciable intensity except annihilation radiation.

Gamma-rays from the decay of the first 2+ level (0.83 MeV) and second 2+ state (1.47 MeV cross-over, 0.63 MeV cascade) are identified. The 0.63-MeV group appears to be double, with some 0.60-MeV radiation present. Subtracting the contribution of 0.60-MeV reduces the intensity of the 0.63-MeV γ-ray by 15 %. About $\frac{1}{4}$ of the intensity of the 0.60-MeV γ-ray can be accounted for by the expected 0.596-MeV radiation from Ge^{74} (4.3 %) in the target. Some of the remainder could arise from (p, p') excitation of the third known 2+ state [19]) in Ge^{72} at 2.06 MeV. Both the energy and intensity of the 1.04-MeV γ-ray agree with its assignment to the Ge^{70} (2.7 %) present in the target. At the present time, no assignment can be given for the 1.20$\pm$0.01 and 1.73$\pm$0.02 MeV γ-rays shown in fig. 11.

About 20 % of the intensity of the 1.47 MeV γ-ray shown in fig. 11 can be attributed to summing at $d = 3$ cm. This summing correction was reduced to 5 % for a shorter run taken at $d = 10$ cm. These two measurements yielded a branching ratio of 0.11 $\pm$0.02 for the 1.47-MeV 2+ level of Ge^{72}. This result is in reasonable agreement with the value of 0.13 given by Kraushaar *et al.* [20]), who first subtracted 23 % from the intensity of the 0.63-MeV group for a contribution of a 0.60-MeV cascade γ-ray in the decay of Ga^{72}. On the other hand,

both values are considerably lower than the branching of 0.19 given by Johns *et al.* [21]) who resolved the 0.601 and 0.630-MeV γ-rays †.

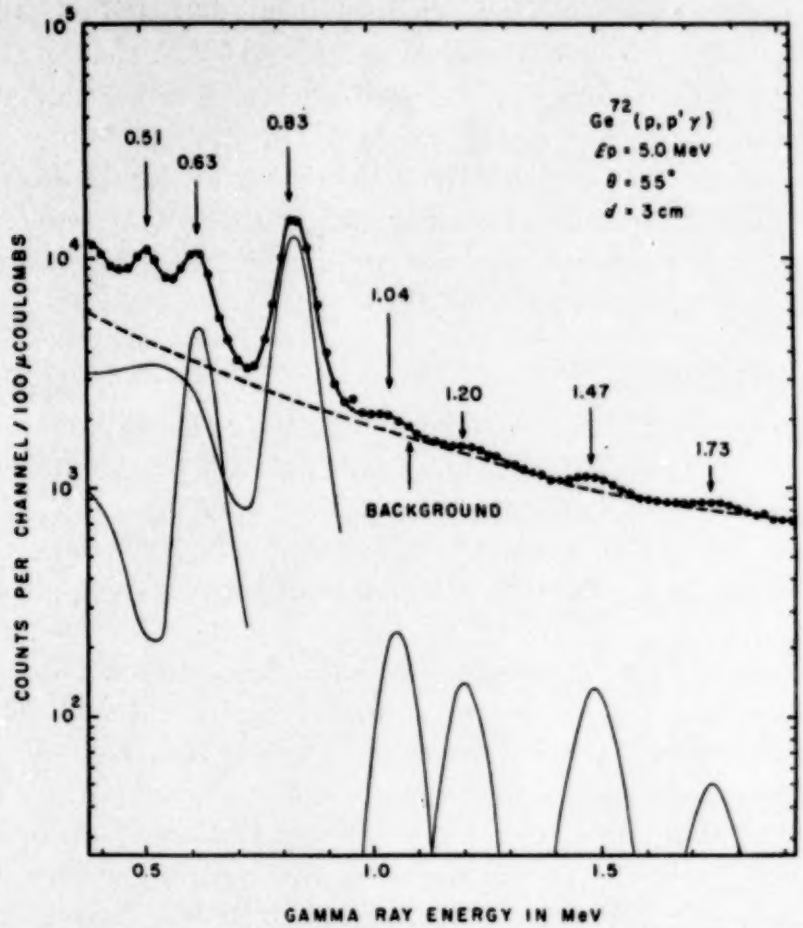

Fig. 11. Gamma-ray spectrum from Ge^{72} bombarded by 5.0-MeV protons. The continuous background assumed for spectral analysis is shown. The 1.04-MeV γ-ray is attributed to the 2.7 % of Ge^{70} present in the target.

4.2.6. *The* Ge^{74} *Isotope*

The (p, n) threshold for Ge^{74} occurs at 3.36 MeV. As the energy of the first 2+ level (596 keV) is nearly equal to the cascade γ-ray (604 keV) from the second 2+ level, a γ–γ coincidence measurement would be required to determine the branching of the 1.20-MeV second 2+ level. The excitation curves for Zn^{66} and Zn^{68} (fig. 2) indicate that a detectable excitation of the 1.20-MeV level cannot be expected below the Ge^{74} (p, n) threshold.

Bombardment of a 97.7 % enriched Ge^{74} target at $E_p = 4.1$ and 4.3 MeV did not reveal a measurable amount of the 1.20-MeV cross-over γ-ray from the second 2+ state. As the branching of this state has been recently found to be about 0.6 ± 0.2 from measurements of the As^{74} decay [22]), it is concluded that excitation of the 1.20-MeV level of Ge^{74} was not sufficient to be observed in this experiment.

† The revised intensities for ref. [21]) are quoted in ref. [30]).

At $E_p = 4.3$ MeV, $\theta = 55°$, $d = 3$ cm, in addition to the 0.60-MeV Ge^{74} (p, p'γ) radiation, prominent γ-rays of energies 354 ± 5 and 441 ± 5 keV were observed, together with weaker γ-rays of 0.72 ± 0.01 and 0.83 ± 0.01 MeV. (The region of $E_\gamma \leqq 0.32$ MeV was not examined.) The yield of the 0.72-MeV γ-ray could not be detected at $E_p = 4.1$ MeV, indicating that it should be assigned to the Ge^{74} (p, nγ) As^{74} reaction, corresponding to a ground-state transition from a 0.72-MeV level. While the thresholds for the 354 and 441 keV γ-rays were not determined, a similar assignment is reasonable. These four γ-rays would then be transitions from previously undetermined levels in As^{74}. In addition, there was evidence for Ge^{74} (p, γ) As^{75} radiations of higher energies.

4.2.7. The Se^{74} *Isotope.*

The isotopically enriched material obtained for this experiment contained only 12 % of Se^{74} (normal abundance 0.9 %), with considerable amounts of Se^{76} (11 %), Se^{77} (7 %), Se^{78} (20 %) and Se^{80} (42 %). Since the last three isotopes have (p, n) thresholds of 2.18, 4.40 and 2.70 MeV, respectively, γ-ray spectra observed from proton bombardment of such a target can be expected to have contributions from the (p, nγ) reactions of these isotopes, and from the Br^{77}, Br^{78} and Br^{80} activities produced during bombardment.

Proton bombardments were performed at $E_p = 4.2$, 4.6 and 5.0 MeV. At time zero, no activity in the target was present. Immediately following a bombardment, the induced activity was subtracted for a period of time chosen by calculation to compensate for the activity produced during the run. At $E_p = 4.2$ MeV, only the 18-min decay of Br^{80} was taken into account; at $E_p = 4.6$ and 5.0 MeV, only the 6.5-min decay of Br^{78} was accounted for in the subtraction.

The subtracted spectra measured at $\theta = 55°$ showed composite γ-ray groups at 0.53 and 0.64 MeV. The 0.64-MeV γ-ray can be mainly attributed [19]) to (p, p') excitation of the known first level of Se^{74} at 0.635 MeV. The intensity and shape of the 0.53-MeV group was subject to uncertainty caused by small gain shifts when the more intense annihilation peak in the time background was subtracted. However, even after correction for this effect, the intensity of the 0.53-MeV group appeared to be too large to be explained by (p, p') excitation of a second 2+ level in Se^{74} at 1.17 MeV, since the cross-section ratio $\sigma_2(2+)/\sigma_1(2+)$ is expected to be ≈ 0.3 at $E_p = 5.0$ MeV, on the basis of our results for neighbouring nuclei. There were also indications of weaker γ-rays of energies 0.85 ± 0.01 and 1.37 ± 0.82 MeV, which, if attributed to Se^{74} (rather than some target contamination), should be Se^{74} (p, γ) Br^{75} radiations.

4.2.8. The Se^{76} *Isotope.*

A (p, p'γ) spectrum obtained from a 57.4 % enriched Se^{76} target (4.1 % Se^{77}, 11.2 % Se^{78}, 22.7 % Se^{80}) at $E_p = 5.0$ MeV, $\theta = 55°$, is shown in fig. 12. The

three prominent γ-rays of 0.56, 0.66 and 1.21 MeV are assigned to decay of the first two 2+ levels of Se^{76}. Due to the presence of 22.7 % of Se^{80} in the target, a time background subtraction was performed immediately after the run, for a time calculated to compensate for the induced Br^{80} activity. The Br^{78} activity produced by the Se^{78} (p, n) reaction was neglected; this is justified in first order in view of the data for activation of natural Se by proton bombardment [23]).

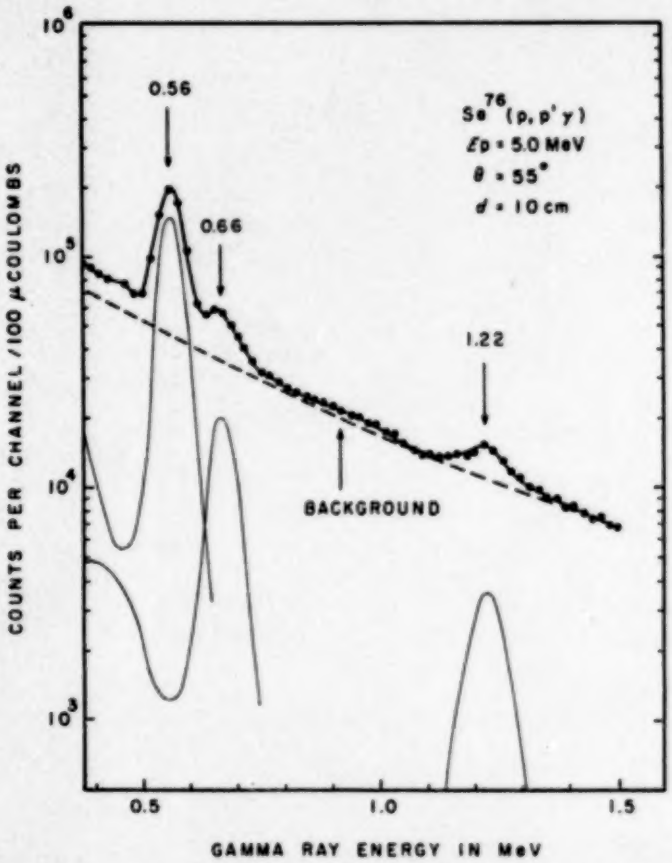

Fig. 12. Gamma-ray spectrum from Se^{76} bombarded by 5.0-MeV protons, after subtraction of time background. The continuous background assumed for spectral analysis is shown.

From two measurements an average branching of 0.50 ± 0.07 was found for the 1.216-MeV level of Se^{76}. There was some indication that the 1.22-MeV γ-ray group was complex, with a possible weak component (intensity ≤ 10 %) at a lower energy of about 1.15 MeV. The measured branching ratio is in agreement with the most recent values [24, 25]) of 0.52 ± 0.10 and 0.55 ± 0.04 from studies of the As^{76} decay. The chief uncertainty in these measurements is the fact that the 1.22 MeV group is complex, with three components whose intensities are found from γ–γ coincidences. In the present Se^{76} (p, p'γ) experiment, γ-ray contributions from the third Se^{76} level at 1.79 MeV (1,2+) are not expected to be important. From the results obtained for other nuclei (table 1), $\sigma_{1.73}/\sigma_{0.56} \lesssim 0.05$ is expected, which means that the 1.229-MeV γ-ray

from the 1.79 MeV level would have an intensity $\lesssim 9$ % of the intensity of the 1.216 MeV γ-ray, which is within the error quoted for the branching.

4.2.9. The Se^{78} *Isotope*

Gamma-radiation from a 96.6 % enriched Se^{78} target (2.5 % Se^{80}) observed at $E_p = 4.1$ MeV, $\theta = 55°$, is shown in fig. 13. A background run using a blank formvar target has been subtracted from these data. At the time this investigation was made, the location of the Se^{78} (p, n) threshold to the ground-

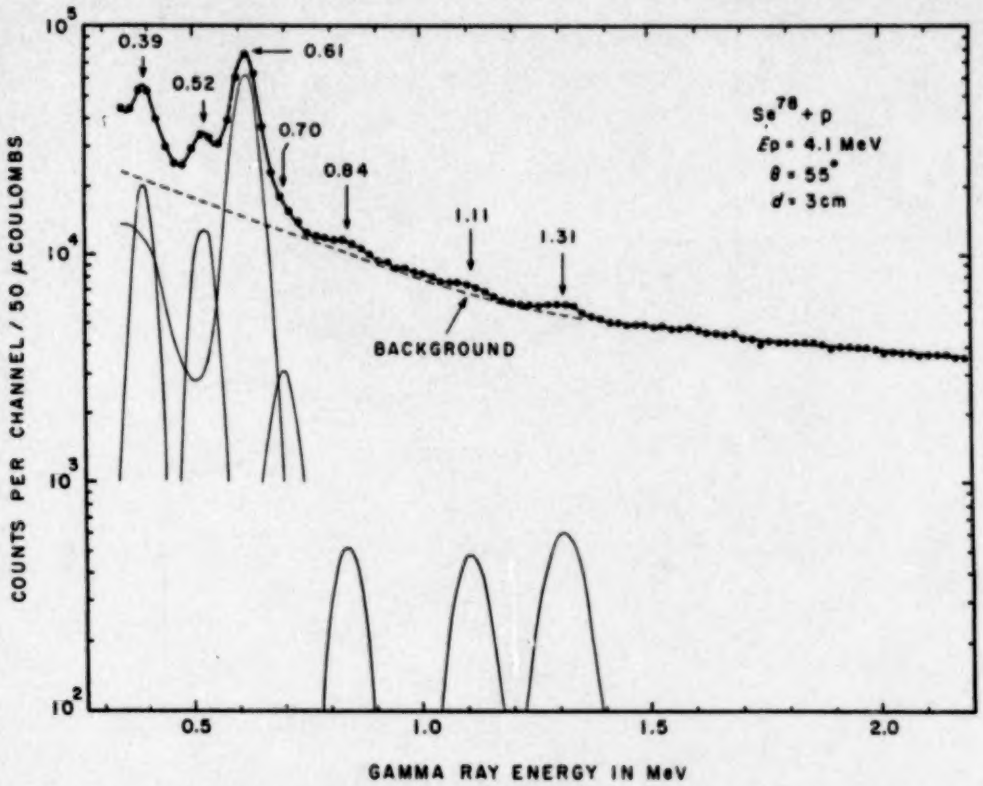

Fig. 13. Gamma-ray spectrum from Se^{78} bombarded by 4.1 MeV protons, after subtraction of from background. The continuous background assumed for spectral analysis is shown.

state of Br^{78} was subject to an uncertainty of about 0.2 MeV. Since then, the Se^{78} (p,n) threshold has been measured [26]) at 4.40 ± 0.01 MeV, so that a bombarding energy of 4.3—4.4 MeV would have been a more suitable choice for investigation of the Se^{78} (p, p'γ) radiations. It was found that at $E_p = 5.0$ MeV, the Br^{78} activity produced during bombardment prevented observation of the Se^{78} (p, p'γ) radiations.

The energies and intensities of the γ-rays observed from (Se^{78}+p) at $E_p = 4.1$ MeV are listed in table 1. It seems reasonable to assign the prominent γ-rays of 0.39 and 0.52 MeV to the Se^{78} (p, γ) Br^{79} capture process, although it is not exactly clear how these fit into the present decay scheme [19]) of $Kr^{79} \rightarrow Br^{79}$. Further information is needed before the weaker γ-rays of 0.84 and 1.11

MeV can be positively assigned to either the Se^{78} (p, γ) or Se^{78} (p, p'γ) reaction. Recent work on the $As^{78} \rightarrow Se^{78}$ decay indicated the possibility [19]) that γ-rays of these energies may be produced by the decay of possible states in Se^{78} at 1.44 and 1.71 MeV.

The γ-rays of 0.61 ,0.70 and 1.31 MeV are assigned to (p, p') excitation of the first two 2+ levels of Se^{78}. The yield of the γ-rays assigned to decay of the 1.31-MeV second 2+ level appears to be reasonable for $E_p = 4.1$ MeV giving $\sigma_2(2+)/\sigma_1(2+) = 0.1$. The cascade 0.70-MeV γ-ray is located at the high energy tail of the intense 0.61-MeV γ-ray, and therefore there is considerable uncertainty for the intensity of this γ-ray. Two observations at $d = 3$ and 5 cm yielded a branching ratio of 0.5 ± 0.2, which is somewhat lower than the preliminary value of 0.78 found from the $As^{78} \rightarrow Se^{78}$ decay †. However, this latter value is subject to some uncertainty, because both the 0.695 and 1.31-MeV γ-rays observed in this decay have been assumed to be multiple[19]). The systematics for energy levels of neighbouring even nuclei (fig. 9), and the present Se^{78} (p, p'γ) results seem to rule out the possible levels at 0.27 and 0.69 MeV in Se^{78} suggested by Nemilov *et al.* [28]). This same conclusion has been reached by the Nuclear Data Group [19]).

5. Discussion

The experiments reported here have shown that excitation of the second 2+ level of a medium-weight even nucleus ($A \approx 60$—80) can be studied by detecting (p, p'γ) radiations, provided that the (p, n) threshold exceeds ≈ 4 MeV, and if material enriched to a high enough percentage is available. For those nuclei with (p, n) thresholds $\lesssim 4$ MeV, it appears that p'–γ coincidence measurements are necessary, if (p, p'γ) radiations from the second 2+ level are to be studied.

For those nuclei with high (p, n) thresholds, the yield curves for (p, p') excitation of the first 2+ level are similar, rising about a factor of 100 as E_p increases from 3.0 to 5.0 MeV. This is true for the average cross section, since no attempt was made to observe detailed resonance structure using a thin target. At $E_p = 5.0$ MeV, the (p, p') cross section for the second 2+ level has risen to $\approx 30\,\%$ of the cross section of the first 2+ level, while cross sections for higher levels generally remain $\lesssim 5\,\%$. This indicates that the second 2+ levels can be readily identified from studies of the (p, p') reaction, such as the 1.71 -MeV level of Ge^{70} which has been discovered.

In table 2 are listed our measurements for the branching ratios of the second 2+ levels of Zn^{64}, Zn^{66}, Zn^{68}, Ge^{70}, Ge^{72}, Se^{76} and Se^{78}. The agreement with previous results from radioactivity studies is reasonable. It is noted that the γ-ray spectra obtained from proton bombardment are generally easier to

† R. van Lieshout (1958), quoted by ref. [19])

interpret than the γ-ray spectra found in the corresponding radioactive decays. Taking a weighted average (or best value) from all the branching determinations, together with the latest available information for δ, the ratio of E2 and M1 matrix elements for the $(2' \rightarrow 2)$ cascade, a value for the ratio of reduced E2 transition probabilities $B(\mathrm{E2};\ 2' \rightarrow 2)/B(\mathrm{E2};\ 2' \rightarrow 0)$ is then calculated. For those nuclei listed in table 2, the large fluctuations in this ratio of $B(\mathrm{E2})$ values cannot be accounted for by present theories [1, 29]). The nuclei with $E_2(2+)/E_1(2+) < 2$ are particularly interesting cases, such as Zn^{64}, Zn^{66} and Zn^{68}, for which this ratio of $B(\mathrm{E2})$ values varies by a factor of at least 100.

In addition to (p, p'γ) radiations, some information concerning (p, nγ) and (p, γ) radiations was obtained. It is clear that further studies (e.g. of the (p, nγ) and (p, γ) radiations of Zn^{68} and Ge^{74} will reveal considerable new information concerning the level schemes of the residual nuclei formed.

The authors are indebted to Dr. C. P. Swann and Dr. S. M. Shafroth for their participation and interest in these experiments. Steady operation of the Van de Graaff accelerator was provided by the help of Mr. T. Howard. The assistance of Mrs. H. R. Kryka and Mrs. M. E. Brandt in the preparation of the manuscript and figures is acknowledged.

References

1) A. S. Davydov and G. F. Filippov, Nuclear Physics **8** (1958) 237
2) D. M. Van Patter, Nuclear Physics **14** (1959) 42
3) D. J. Horen, Phys. Rev. **113** (1959) 572
4) R. Rikmenspoel and D. M. Van Patter, Bull. Am. Phys. Soc. **5** (1960) 66;
P. N. Trehan, R. Rikmenspoel and D. M. Van Patter, Bull. Am. Phys. Soc. **6** (1961) 48
5) E. A. Wolicki, R. Jastrow and F. Brooks, NRL report 4833 (1956)
6) R. L. Heath, Phillips Petroleum report IDO-16408 (July 1, 1957)
7) D. M. Van Patter, M. A. Rothman, W. C. Porter and C. E. Mandeville, Phys. Rev. **107** (1957) 171;
W. C. Porter, D. M. Van Patter, M. A. Rothman and C. E. Mandeville, Phys. Rev. **112** (1958) 468
8) E. Okada, T. Miura, T. Wakatsuki and Y. Hirao, .J Phys. Soc. Japan **13** (1958) 541
9) L. Holland, Vacuum deposition of thin films (John Wiley & Sons, New York, 1956) p. 180
10) R. A. Ricci and R. van Lieshout, Nuclear Physics **10** (1959) 360
11) T. H. Jacobi, H. A. Howe and J. R. Richardson, Phys. Rev. **117** (1960) 1086
12) N. Nath, S. S. Malik, M. A. Rothman and D. M. Van Patter, Bull. Am. Phys. Soc. **4** (1959) 258;
D. M. Van Patter, N. Nath and M. A. Rothman, Bull. Am. Phys. Soc. **5** (1960) 266 and private communication
13) A. Schwarzschild and L. Grodzins, Phys. Rev. **119** (1960) 276
14) R. W. Peele and T. A. Love, ORNL-2790 (Nov. 6, 1959)
15) R. A. Chapman and J. C. Slattery, Phys. Rev. **105** (1957) 633
16) P. P. Singh, H. W. Dosso and G. M. Griffiths, Can, J. Phys. **37** (1959) 1055
17) D. M. Van Patter, Bull. Am. Phys. Soc. **3** (1958) 212
18) F. D. S. Butemont and E. G. Prout, Phil. Mag. **46** (1955) 357;
A. E. Souch, Proc. Phys. Soc. **68** (1955) 760
19) K. Way, F. Everling, G. H. Fuller, N. B. Gove, C. L. McGinnis and R. Nakasima, Nuclear Data Sheets (National Research Council Washington, D. C.)

20) J. J. Kraushaar, E. Brun and W. E. Meyerhof, Phys. Rev. **101** (1956) 139
21) M. W. Johns, B. Chidley and I. R. Williams, Phys. Rev. **99** (1955) 1645
22) T. Yamazaki, H. Ikegami and M. Sakai, J. Phys. Soc. Japan **15** (1960) 957
23) G. E. Valley and R. L. McGreary, Phys. Rev. **56** (1939) 863
24) R. K. Girgis, R. A. Ricci and R. van Lieshout, Nuclear Physics **13** (1959) 461
25) G. Bäckström and I. Marklund, Ark. f. Fys. **17** (1960) 393
26) R. Rikmenspoel and D. M. Van Patter, Nuclear Physics **24** (1961) 494
27) C. F. Carter, Jr., M.I.T.-LNS report (May 1960) p. 90.
28) Yu. A. Nemilov, A. N. Pisarevskii and L. D. Soshin, Zh. Eksp. Teor. Fiz. **35** (1958) 801, Soviet Physics JETP **35** (1959) 555
29) N. MacDonald, Nuclear Physics **14** (1959) 70;
M. Jean, Nuclear Physics **21** (1960) 142
30) Z. Grabowski, S. Gustafsson and I. Marklund, Ark. f. Fys. **17** (1960) 411

2.G

Nuclear Physics **27** (1961) 490—506; © *North-Holland Publishing Co., Amsterdam*

Not to be reproduced by photoprint or microfilm without written permission from the publisher

THE APPLICATION OF DISTORTED WAVE BORN APPROXIMATION CALCULATIONS TO THE ANALYSIS OF SOME (d, p) ANGULAR DISTRIBUTIONS

H. D. SCOTT

Department of Physics, University of Liverpool

Received 19 April 1961

Abstract: Using distorted wave Born approximation calculations, some proton angular distributions obtained by bombarding the nuclei Na^{23}, Ni^{58} and Ni^{60} with 9 MeV deuterons have been analysed. It has been possible to fit the distributions with unique l-value distorted wave curves in cases where l-value ambiguities have previously existed in the Butler analysis. The reduced widths extracted in both Butler and distorted wave calculations for a particular l-value have been compared. The relative values obtained by both methods have been found to be generally in good agreement.

1. Introduction

Several investigations have been carried out to improve on the simple stripping theories [1]) by using distorted waves for the incident and emergent particles [2]). Tobocman [3]) has shown that by distorting the incident deuteron wave and outgoing proton wave with a combination of the Coulomb force and the appropriate optical model potential, it is possible to obtain much better agreement with stripping data than is possible with the simple Butler theory. However, the time taken to calculate a single case using an IBM 650 computer was between 10 and 30 h so that extensive application was prohibited.

Recently a much faster computer programme has been written by Buck and Hodgson [4]) and some theoretical results obtained have already been reported [5]). This calculation uses conventional type Saxon-Woods optical model potentials for the deuterons and protons and calculates the neutron wave functions for a purely real potential, also of Saxon-Woods form. The time taken by the programme to calculate cases where the neutron is captured with orbital angular momentum $l = 0$, 1 or 2 is approximately $11(l+1)$ min. Using the programme it has been possible to make an investigation into how far this theory can remove existing discrepancies which occur when the Butler theory is used to analyse stripping angular distributions.

One of the main features of the distorted wave Born approximation (DWBA) theory is that it is possible to eliminate the "cut-off" radius R which occurs

in the Butler theory. This parameter has often proved most troublesome especially when analysing angular distributions from medium heavy nuclei bombarded with 9 MeV deuterons [6]). It has been usual to use the Gamow-Critchfield [7]) value for this radius parameter when dealing with fairly low mass nuclei, but as the target mass is increased it is found that the theoretical Butler peak does not necessarily coincide with that of the experimental distribution. It is often possible to adjust the theoretical peak position to give a reasonable fit, for a particular l-value, by allowing the cut-off radius to vary over a range in the vicinity of the Gamow-Critchfield value. However, this method of analysis leads to ambiguity in the l-value assignments as the Q-value for the proton groups progressively decreases. This occurs when the experimental points lie on a curve somewhere between the theoretical Butler curves for adjacent l-values obtained using the Gamow-Critchfield radius. Equally good fits to the data can then be obtained by decreasing the radius parameter for the lower l-value or by increasing the radius parameter for the higher l-value. Frequently this leads to a choice between unacceptable R values of about 4 fm and 9 fm, compared to the Gamow-Critchfield value of about 6.5 fm. It was primarily to overcome this difficulty in the l-value assignments that the following DWBA calculations were carried out.

The reduced widths extracted by using Butler theory are dependent upon the value chosen for the cut-off radius. Strictly, therefore, only reduced widths which have been calculated for the same cut-off radius should be compared. Since the cut-off radius is often a variable parameter in the analysis, the relative values of the extracted reduced widths are influenced accordingly. This difficulty is also removed by using the DWBA theory, which yields a "reduced width" θ_{jl}^2 of the form defined by Huby, Refai and Satchler [8]). Here j and l are the total and orbital angular momenta with which the neutron enters the nucleus, and θ_{jl} is a measure of the amount of the initial configuration contained in the wave function of the final nucleus.

The calculations reported here are for selected proton groups from the reactions Na^{23}(d, p) Na^{24}, Ni^{58}(d, p) Ni^{59} and Ni^{60}(d, p) Ni^{61} investigated in this laboratory using approximately 9 MeV deuterons [9]). The angular distributions for the proton groups from sodium were all satisfactorily fitted with Butler curves using the Gamow-Critchfield radius of 5.2 fm. This reaction therefore provided a good test for examining the validity of the conclusions usually obtained from Butler theory. Unfortunately no absolute cross sections were available for this reaction. The results of the Butler analysis are tabulated in the review article by Macfarlane and French [10]). This table contains some errors. The doublet group corresponding to the states at 1.844 and 1.884 MeV was observed to be an $l = 0$ transition, not $l = 1$ plus 2, and an additional doublet at 2.464 and 2.561 MeV was observed and fitted with an $l = 1$ plus 2 combination.

The data from the two nickel isotopes typically illustrated the difficulties experienced in the analysis of proton groups from medium heavy nuclei. Absolute cross sections for these two reactions were known so that absolute values of $(2J+1)\ \theta_{jl}^2$ were obtainable.

The $l = 3$ transitions occurring in the nickel results necessitated a programme being written for this l-value. This was done using the Buck and Hodgson programme as a basis, and satisfactorily produced Butler curves when the Coulomb and nuclear distortions were made zero and a cut-off radius was introduced. The programme also correctly predicted zero polarisation of the emitted protons when the nuclear distortions of the deuteron and proton waves were made identical [11]).

2. Computational Procedure

In order to carry out DWBA calculations it is necessary to know the relevant optical model parameters. These are usually taken from the optical model analyses [12]) of the elastic scattering experiments of the deuteron on the target nucleus and the proton on the final nucleus, at the appropriate energies.

The deuteron and proton optical model potentials used in the calculation were of the form

$$V(r) = Uf(r)+iWf(r),$$

where $f(r)$ is the Saxon-Woods form factor given by

$$f(r) = \left[1 + \exp\left(\frac{r-R_0}{a}\right)\right]^{-1}$$

and $R_0 = r_0 A^{\frac{1}{3}}$ is the nuclear radius and a the diffuseness of the nuclear surface. There was also a facility in the programme to use a Gaussian form factor for W given by

$$g(r) = \exp\left[-\left(\frac{r-R_0}{a}\right)^2\right].$$

The refracting potential U elastically scattered the incident particles and the absorbing potential W took account of all the inelastic processes including absorption. Thus it was necessary to know four parameters, U, W, r_0 and a for each of the deuteron and proton potentials. The radius $R_n = r_n A^{\frac{1}{3}}$ and the diffuseness a_n of the neutron potential well had also to be specified. The depth of this well was calculated in the programme by an iteration procedure which found the depth necessary to give a smooth neutron wave function across the nuclear surface and also the known binding energy of the final state.

The Coulomb potential was taken to be that due to a charged sphere of

radius $R_c = r_c A^{\frac{1}{3}}$ giving

$$V_c = \begin{cases} \dfrac{Z_I Z_T e^2}{2R_c}\left(3 - \dfrac{r^2}{R_c^2}\right) & \text{for } r < R_c, \\ \dfrac{Z_I Z_T e^2}{r} & \text{for } r > R_c, \end{cases}$$

where Z_I and Z_T are the charges of the incident deuteron and the target nucleus.

Because of the lack of elastic scattering data it was necessary to choose the parameters independently in the light of data already available on nuclei of about the same mass and at energies similar to those in the experiment under consideration. No scattering parameters were available for the initial and final sodium nuclei. However, deuteron parameters obtained for an energy of 15 MeV [13]) and proton parameters obtained for a proton energy of 17 MeV [14]) were available for the nucleus Al^{27}. These parameters are shown in table 1 together with similar data known for natural nickel [13, 14]) and these parameters were therefore taken as a preliminary basis for the computations.

TABLE 1

Available optical model data for aluminium and natural nickel

	Target	Energy (MeV)	U (MeV)	W (MeV)	r_0 (fm)	a (fm)
Protons	Al^{27}	17	40	9	1.30	0.73
	Natural Ni	17	46	9	1.33	0.48
Deuterons	Al^{27}	15	55	25	1.50	0.60
	Natural Ni	13.5	59	19	1.43	0.63

Since the investigation was primarily concerned with the general features of DWBA calculations, it was considered justifiable to vary the parameters within reasonable limits in order to fit the stripping angular distributions as well as possible. Unfortunately, the experimental stripping angular distributions did not extend beyond 60° but nevertheless, this region of investigation was sufficient to provide interesting information. Theoretical distributions were first calculated with the trial parameters shown in table 1 for the ground state transitions only. A few of these parameters were then varied until satisfactory fits were obtained for the ground state proton groups. In the Ni^{60}(d, p) Ni^{61} reaction the second excited state at 0.284 MeV was used for the parameter determinations as the ground state and first excited state at 68 keV were not resolved. The parameters were then used to calculate curves for particular angular distributions corresponding to certain excited states. For states at

high excitation the values of the proton well depth parameters U_p and W_p were adjusted slightly to take account of the reduced energies of the outgoing protons. Curves presented by Bjørklund [15]) have shown that U increases slowly and W decreases slowly as the proton energy is decreased. The parameters used for the ground state and low excited state calculations are shown in table 2. When different parameters have been used, reference is made explicitly in the text.

TABLE 2

Parameters used in the ground state and low excited state calculations

	Na^{23}(d, p)Na^{24}	Ni^{58}(d, p)Ni^{59}	Ni^{60}(d, p)Ni^{61}
Neutron well parameters			
r_n (fm)	1.3	1.3	1.3
a_n (fm)	0.7	0.7	0.7
Optical model parameters for deuterons			
U_d (MeV)	50	65	65
W_d (MeV)	15	15	15
r_{od} (fm)	1.5	1.43	1.43
a_d (fm)	0.6	0.6	0.5
Optical model parameters for protons			
U_p (MeV)	45	45	45
W_p (MeV)	8	8	8
r_{op} (fm)	1.3	1.3	1.3
a_p (fm)	0.6	0.6	0.5
Coulomb parameters			
r_{cd} (fm)	1.3	1.3	1.3
r_{cp} (fm)	1.3	1.3	1.3

3. Results for the Na^{23} (d, p) Na^{24} reaction

The experimental results for this reaction, which has a ground state transition Q-value of 4.731 MeV, were obtained with 8.9 MeV deuterons. In fig. 1 are shown the proton angular distributions to the ground and first excited states of ^{24}Na. These are both $l = 2$ transitions and the DWBA calculations obtained using the parameters in table 2 are shown in comparison with the Butler theory curves calculated using the Gamow-Critchfield radius of 5.2 fm. A striking feature is the satisfactory fit of the DWBA curves to the forward part of both experimental distributions. This rise in the cross-section at 0° seems to be a well established feature of $l = 2$ transitions to nuclei in this mass region. It is evident in the reactions Mg^{24}(d, p)Mg^{25}, Si^{28}(d, p)Si^{29} and

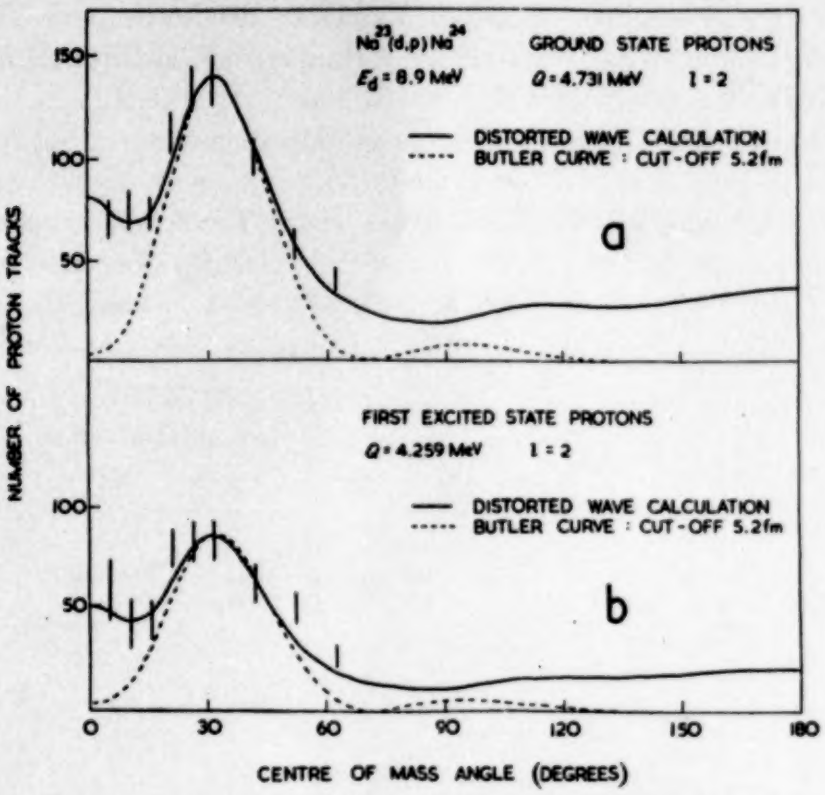
$Na^{23}(d,p)Na^{24}$ GROUND STATE PROTONS
E_d = 8.9 MeV Q = 4.731 MeV l = 2
DISTORTED WAVE CALCULATION
BUTLER CURVE : CUT-OFF 5.2fm
a
FIRST EXCITED STATE PROTONS
Q = 4.259 MeV l = 2
DISTORTED WAVE CALCULATION
BUTLER CURVE : CUT-OFF 5.2fm
b
NUMBER OF PROTON TRACKS
CENTRE OF MASS ANGLE (DEGREES)

Fig. 1. Angular distributions of ground state and first excited state protons from the reaction $Na^{23}(d, p)Na^{24}$. The parameters used in the distorted wave calculation are given in table 2.

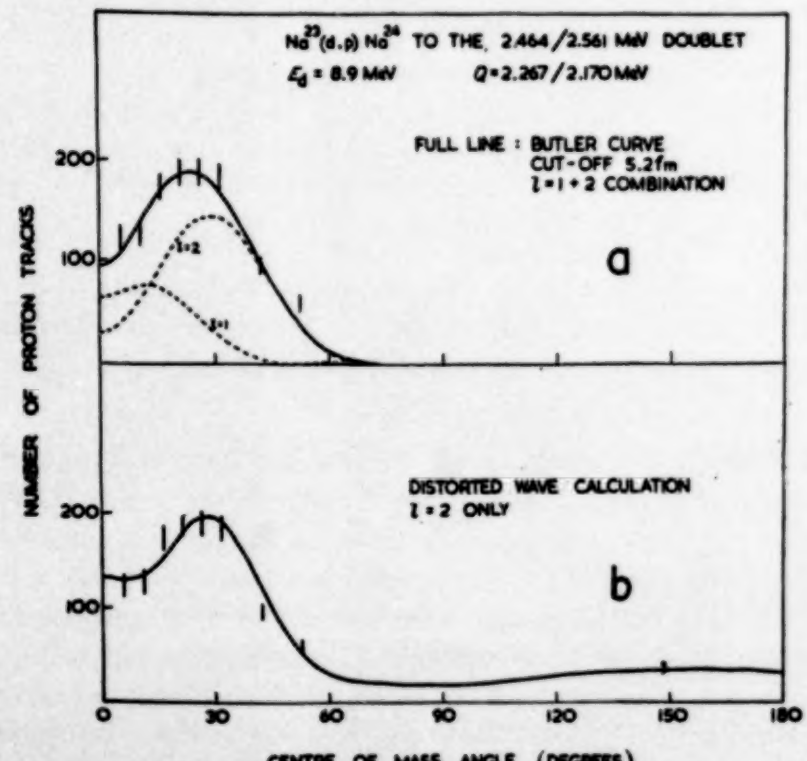
$Na^{23}(d,p)Na^{24}$ TO THE 2.464/2.561 MeV DOUBLET
E_d = 8.9 MeV Q = 2.267/2.170 MeV
FULL LINE : BUTLER CURVE
CUT-OFF 5.2fm
l = 1 + 2 COMBINATION
a
DISTORTED WAVE CALCULATION
l = 2 ONLY
b
NUMBER OF PROTON TRACKS
CENTRE OF MASS ANGLE (DEGREES)

Fig. 2. Angular distribution of protons corresponding to the 2.464/2.561 MeV doublet in Na^{24}. The parameters used in the distorted wave calculation were $U_p = 46.5$ MeV, $W_p = 7$ MeV together with the other parameters given in table 2.

S^{32}(d, p)S^{33} which exhibit similar $l = 2$ angular distributions [16]). The DWBA curves also go some way towards fitting the experimental points at 50° and 60° which the Butler curves fail to do.

In fig. 2 is shown a proton angular distribution corresponding to a doublet at 2.464 MeV and 2.561 MeV excitation in Na^{24}. This was originally fitted with an $l = 1$ plus $l = 2$ Butler combination as seen in fig. 2. The $l = 1$ component was used in an attempt to explain the forward contribution close to 0°. However, the DWBA calculation for $l = 2$ alone appears to fit this distribution satisfactorily, indicating that either both components of the doublet are due

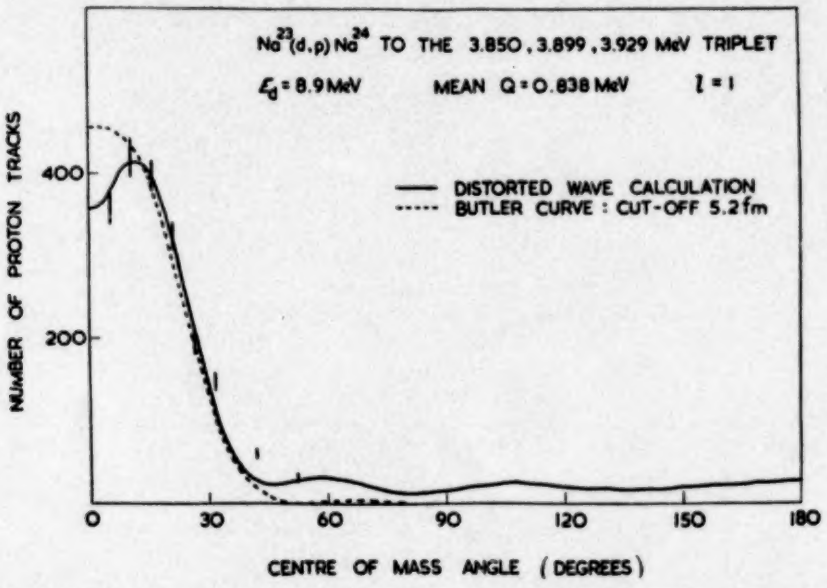

Fig. 3. Angular distribution of protons corresponding to the 3.850, 3.899 and 3.929 MeV triplet in Na^{24}. The parameters used in the distorted wave calculation were $U_p = 47.4$ MeV, $W_p = 6.4$ MeV together with the other parameters given in table 2.

to $l = 2$ transitions or that one is predominantly so. This distorted wave curve was calculated with the same parameters as shown in table 2 except that U_p was increased slightly to 46.5 MeV and U_p was decreased to 7 MeV to take account of the lower proton energy.

Frequently in (d, p) reactions, $l = 1$ peaks are observed for which the experimental points dip down below the $l = 1$ Butler curves. These usually occur for proton groups corresponding to states in the final nucleus with high excitation for which the $l = 1$ Butler curves peak at 0° (ref. [17])). Such a proton group was observed in this reaction on sodium. This group corresponded to three unresolved states at 3.850, 3.899 and 3.929 MeV in Na^{24} and is shown in fig. 3. A distorted wave curve was calculated for this group using values of $U_p = 47.4$ MeV and $W_p = 6.4$ MeV but otherwise the same parameters as in table 2. This is shown in fig. 3 and is seen to fit the dip quite well compared with the Butler curve.

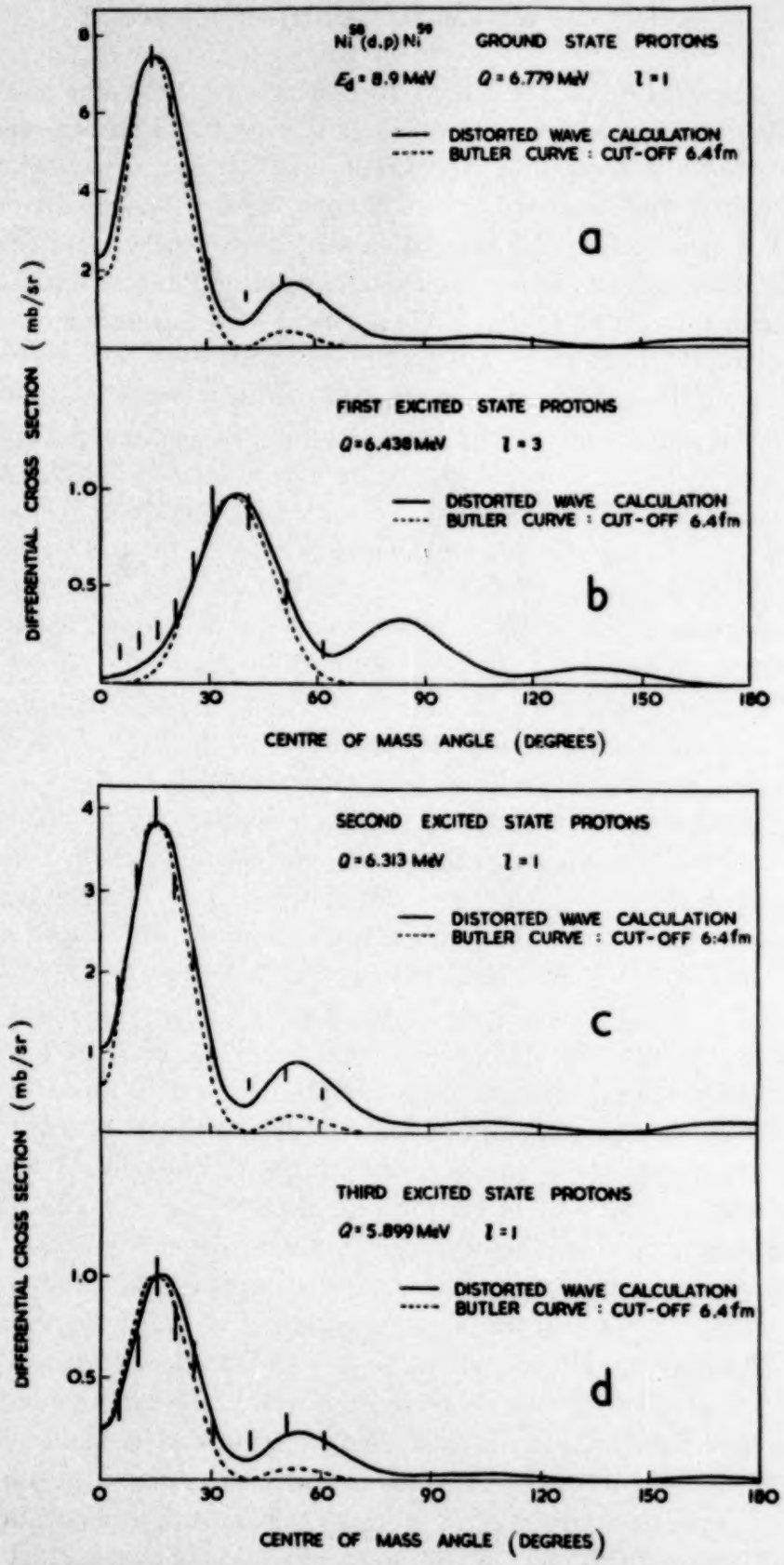
$Ni^{58}(d,p)Ni^{59}$ GROUND STATE PROTONS
E_d = 8.9 MeV Q = 6.779 MeV l = 1
DISTORTED WAVE CALCULATION
BUTLER CURVE : CUT-OFF 6.4fm
a
FIRST EXCITED STATE PROTONS
Q = 6.438 MeV l = 3
DISTORTED WAVE CALCULATION
BUTLER CURVE : CUT-OFF 6.4fm
b
DIFFERENTIAL CROSS SECTION (mb/sr)
CENTRE OF MASS ANGLE (DEGREES)
SECOND EXCITED STATE PROTONS
Q = 6.313 MeV l = 1
DISTORTED WAVE CALCULATION
BUTLER CURVE : CUT-OFF 6.4fm
c
THIRD EXCITED STATE PROTONS
Q = 5.899 MeV l = 1
DISTORTED WAVE CALCULATION
BUTLER CURVE : CUT-OFF 6.4fm
d
DIFFERENTIAL CROSS SECTION (mb/sr)
CENTRE OF MASS ANGLE (DEGREES)

Fig. 4. Angular distributions of protons corresponding to the ground, first, second and third excited states of Ni^{59} in the reaction Ni^{58}(d, p)Ni^{59}. The distorted wave curves were all calculated with the same parameters as given in table 2.

4. Results for the Ni^{58}(d, p)Ni^{59} Reaction

The experimental results for this reaction which has a Q-value of 6.779 MeV, were obtained with 8.9 MeV deuterons [9]). In fig. 4(a) is shown the angular distribution to the ground state of Ni^{59}. This was fitted quite well by the Butler curve calculated with Gamow-Critchfield radius of 6.4 fm. The distorted wave curve also shown in fig. 4(a) was calculated with the parameters given in table 2. This curve gave an improved fit and accounted for most of the secondary peak in the vicinity of 50°. Such secondary peaks are a common occurrence in stripping angular distributions and have been dealt with by some workers in terms of an additional l-value contribution. The method of subtracting a constant background and fitting the remaining secondary peak with that occurring in the Butler curve, has also been used, but is difficult to justify.

The distribution in fig. 4(b) is that corresponding to the first excited state in Ni^{59} at an excitation of 0.341 MeV which is reached by an $l = 3$ transition. Fig. 4(b) shows the $l = 3$ Butler curve and the $l = 3$ distorted wave curve for the same parameters as the ground state distribution. This is the first $l = 3$ distorted wave curve to be reported and illustrates the need for data in the region of the secondary peak near 80°. The remaining two distributions in fig. 4 are for the proton groups corresponding to the levels in Ni^{59} at 0.466 and 0.880 MeV excitation, both of which are reached by $l = 1$ transitions. It can be seen that the experimental peaks are in quite good agreement with the Butler curves calculated with the Gamow-Critchfield radius. The distorted wave curves calculated with the same parameters as previously appear to give better overall agreement. The values of reduced widths obtained by the two theoretical methods are compared in sect. 6.

Fig. 5 illustrates the difficulty encountered when assigning l-values to proton groups corresponding to states at high excitation in the final nucleus. The proton group illustrated corresponds to a state with excitation 5.69 MeV and Q-value 1.09 MeV. This distribution was obtained with 8.9 MeV deuterons. Wilkinson has shown [5, 18]) that for low Q-values the discrimination between l-values is improved and the distortions are expected to be much smaller if a low deuteron energy is used. However, when the accelerator available produces deuterons with a fairly high fixed energy, it becomes necessary to take account of the distortions in the analysis of the results. For the proton group in fig. 5, the experimental resolution was about 70 keV so that the experimental points can be expected to contain some contribution from the competing levels in the vicinity of 5.69 MeV excitation. The identification of the state responsible for the great majority of the intense forward peak was made with the help of a table of proton yields obtained in a high resolution investigation of the reaction by Paris [19]) at angles of 30°, 50° and 70° to the direction of the incident deuteron beam. It can be seen in fig. 5(a) that the experimental points on the peak lie

between the $l = 0$ and $l = 1$ Butler curves calculated with the Gamow-Critchfield radius. These curves can be made to fit the experimental points by using the l-value and radius combinations $l = 0$, $R = 4.0$ fm or $l = 1$, $R = 8.0$ fm as shown in fig. 5(b) but the ambiguity still persists. It had been suspected for some time that the choice of the lower l-value in such circumstances would

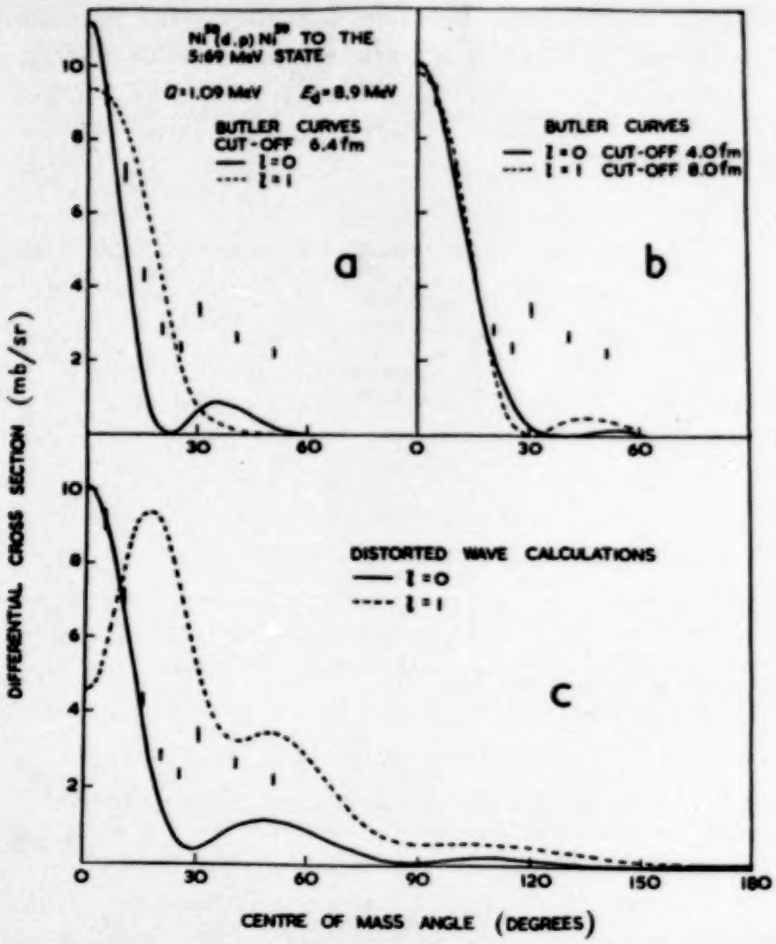

Fig. 5. Angular distribution of protons corresponding to the 5.69 MeV state in Ni^{59}. The distorted wave curves were calculated using $U_p = 48$ MeV and $W_p = 7$ MeV together with the other parameters given in table 2.

be the correct one. This was partly because of the naturally high intensity of $l = 0$ groups compared with $l = 1$ groups, and also because the deviation of these forward peaking experimental groups from the $l = 0$ Butler curves for Gamow-Critchfield radius increased as the Q-value decreased. Such behaviour might be expected to happen on the basis of Coulomb force considerations since as the Q-value decreased, the Coulomb force on the outgoing protons would increase and push the proton angular distributions further out. Whether or not the Coulomb forces actually dominated in a smooth manner the specific-

ally nuclear effects, which tend to move the distribution to smaller angles, was not known. In order to determine this, the $l = 0$ distorted wave calculations were carried out for Q-values of 6.0, 4.0, 2.0, 1.09 and 0.0 MeV using the same parameters as in table 2 for all the Q-values. The curves obtained are shown in fig. 6 normalised to the peak of the $Q = 6$ MeV curve. The increase in the peak width as Q decreases is quite definite and in fig. 5(c) the curve for $Q = 1.09$ MeV is seen to fit the experimental peak quite well indicating $l = 0$ to be the correct assignment. To take account of the proton energy variation the

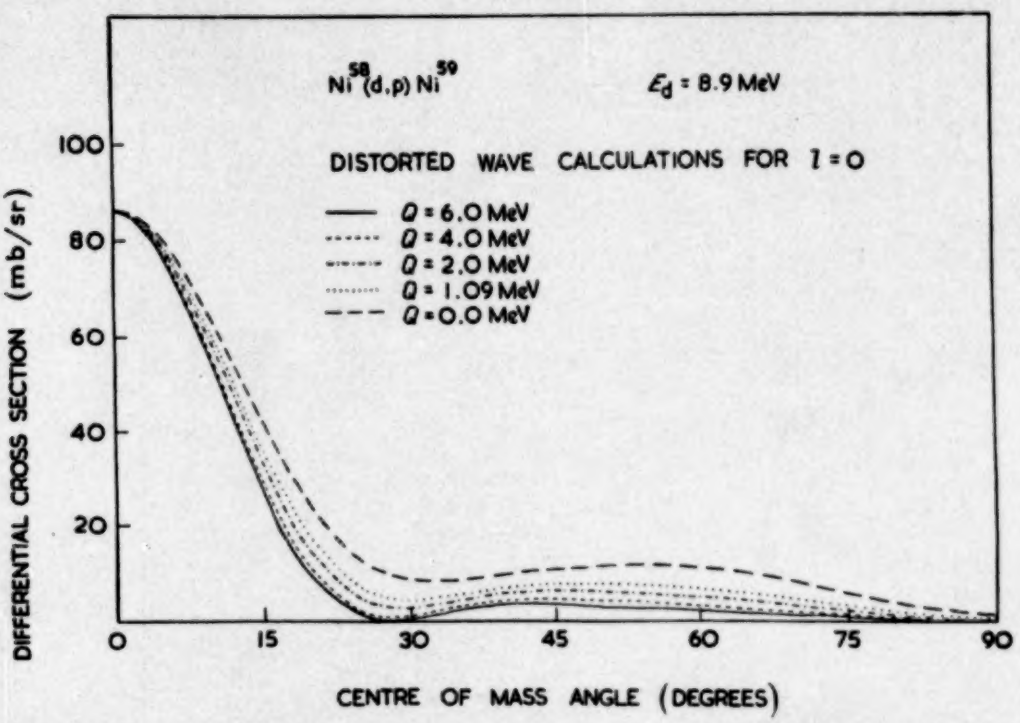

Fig. 6. Theoretical $l = 0$ distorted wave curves for the reaction Ni^{58}(d, p)Ni^{59} at 8.9 MeV deuteron beam energy and with the assumed Q-values of 6.0, 4.0, 2.0, 0.9 and 0.0 MeV.

calculations were repeated allowing U_p to increase and W_p to decrease slowly for curves of decreasing Q-value. Substantially the same results as in fig. 6 were obtained.

5. Results for the Ni^{60}(d, p)Ni^{61} Reaction

The experimental results for this reaction, which has a Q-value of 5.598 MeV were obtained with 8.6 MeV deuterons [9]). The protons corresponding to the ground state and first excited state at 68 keV excitation were not resolved so that the protons corresponding to the second excited state at 0.284 MeV were used for the preliminary fitting procedure. The parameters decided upon are shown in table 2 and the experimental distribution, the Butler $l = 1$ curve for Gamow-Critchfield radius 6.5 fm and the distorted wave $l = 1$ curve are

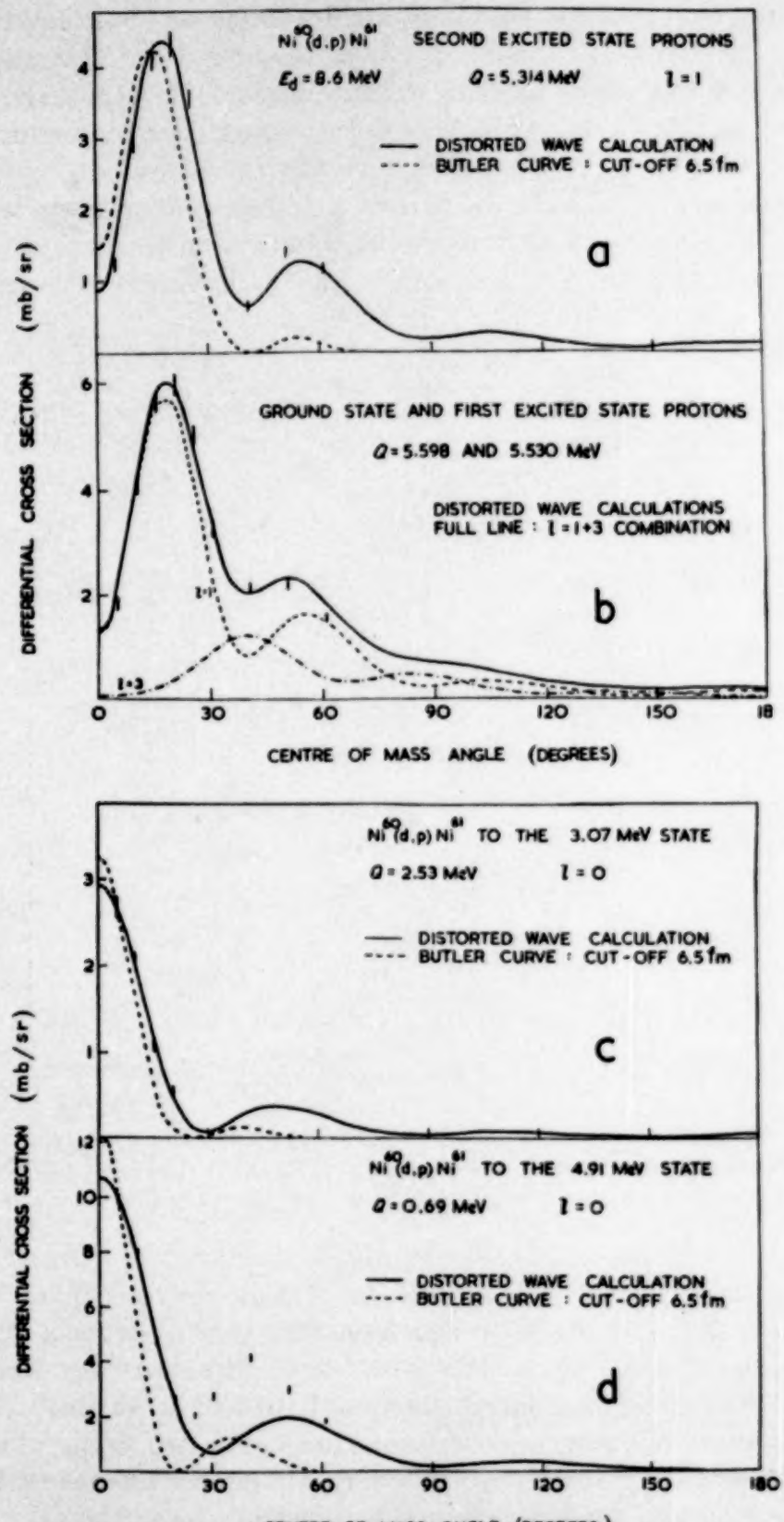
Ni⁶⁰(d,p)Ni⁶¹ SECOND EXCITED STATE PROTONS
E_d = 8.6 MeV
Q = 5.314 MeV
l = 1
DISTORTED WAVE CALCULATION
BUTLER CURVE : CUT-OFF 6.5 fm
a
GROUND STATE AND FIRST EXCITED STATE PROTONS
Q = 5.598 AND 5.530 MeV
DISTORTED WAVE CALCULATIONS
FULL LINE : l = 1+3 COMBINATION
b
DIFFERENTIAL CROSS SECTION (mb/sr)
CENTRE OF MASS ANGLE (DEGREES)
Ni⁶⁰(d,p)Ni⁶¹ TO THE 3.07 MeV STATE
Q = 2.53 MeV
l = 0
DISTORTED WAVE CALCULATION
BUTLER CURVE : CUT-OFF 6.5 fm
c
Ni⁶⁰(d,p)Ni⁶¹ TO THE 4.91 MeV STATE
Q = 0.69 MeV
l = 0
DISTORTED WAVE CALCULATION
BUTLER CURVE : CUT-OFF 6.5 fm
d
DIFFERENTIAL CROSS SECTION (mb/sr)
CENTRE OF MASS ANGLE (DEGREES)

Fig. 7. Proton angular distributions for the reaction $Ni^{60}(d,p)Ni^{61}$ proceeding to the second excited state, the ground and first excited states, the 3.07 MeV state and the 4.91 MeV state in Ni^{61}. The distorted wave curves were calculated with the parameters given in table 2, except in (c) and (d) where the values for U_p and W_p were taken as (c) $U_p = 47$ MeV, $W_p = 7$ MeV, (d) $U_p = 48$ MeV, $W_p = 7$ MeV.

shown in fig. 7(a). It can be seen that at this Q-value of 5.314 MeV the Butler curve does not peak at the same position as the experimental distribution. It can be made to do so by reducing the cut-off radius to 5.1 fm. The distorted wave curve fits the peak very well and also accounts for the secondary peak as in the case of the reaction on Ni^{58} previously considered.

The combined ground state and first excited state proton groups were fitted with an $l = 1$ plus $l = 3$ distorted wave combination as shown in fig. 7(b) using the same parameters as used for the state at 0.284 MeV. This assignment

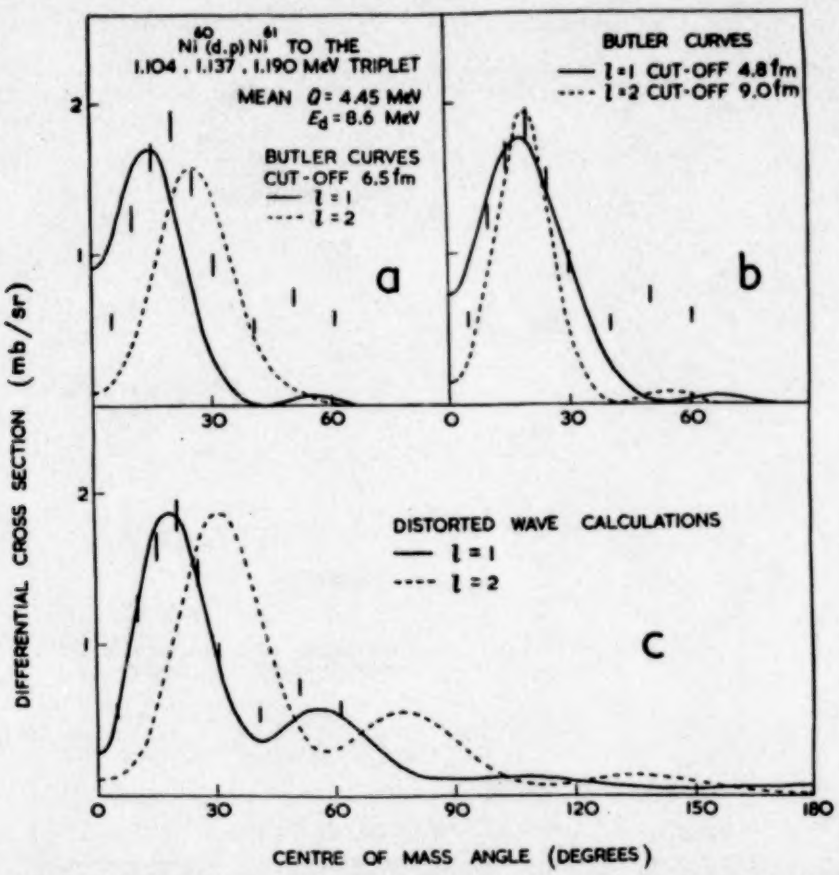

Fig. 8. Angular distribution of protons corresponding to the 1.104, 1.137 and 1.190 MeV triplet in Ni^{61}. The distorted wave curves were calculated using the parameters given in table 2.

is in agreement with Enge and Fisher [20]) who resolved these groups and assigned the $l = 3$ value to the 68 keV level. The proton groups corresponding to the three levels in Ni^{61} at 1.104, 1.137 and 1.190 MeV were observed as one group because of the poor resolution. However, Enge and Fisher have made $l = 1$ assignments to two of these levels, those at 1.104 and 1.190 MeV. They also found the third component to be very weak. Since the two strong components have the same shape we are justified here in considering the observed proton group to be due to a single l-value. This group illustrates the difficulty experienced in deciding between the assignments $l = 1$ and $l = 2$. In fig. 8(a)

the experimental points for this group are shown together with the Butler curves calculated for $l = 1$ and $l = 2$ with Gamow-Critchfield radius of 6.5 fm. It can be seen that the experimental points lie between these two curves. The Butler curves can be made to agree with the experimental peak position by using the l-value and cut-off radius combinations $l = 1$, $R = 4.8$ fm and $l = 2$, $R = 9.0$ fm as is shown in fig. 8(b). The $l = 1$ curve might be thought to give the better fit but the correct assignment is by no means clear. Using the distorted wave $l = 1$ calculation and the same parameters as in table 2 it is seen in fig. 8(c) that the ambiguity is completely removed, and that the correct peak position is predicted. The secondary peak is nearly fitted also.

In figs. 7(c) and 7(d) are shown two angular distributions corresponding to states at 3.07 and 4.91 MeV excitation in the final nucleus Ni^{61}. These strong proton groups were also identified using the tables published by Paris [19]). The 3.07 MeV experimental peak can be seen to be broader than the $l = 0$ Butler theory predicts for the Gamow-Critchfield radius of 6.5 fm. A fit to the forward peak can be obtained by reducing the cut-off radius to 5.1 fm. However, the $l = 0$ distorted wave curve fits the peak satisfactorily for the parameters $U_p = 47$ MeV, $W_p = 7$ MeV and the other values given in table 2 for this reaction. The 4.91 MeV peak can be fitted by the Butler curves for $l = 0$, $R = 3.75$ fm or $l = 1$, $R = 8.0$ fm. The distorted wave $l = 0$ curve fits the experimental points on the peak very well. The only parameter adjustments were to put $U_p = 48$ MeV and $W_p = 7$ MeV. Otherwise the parameters in table 2 were used for this calculations.

6. Reduced Widths

In table 3 the values of the dimensionless reduced widths $(2J+1)\,\theta^2$ obtained from the Butler analysis are compared with the corresponding values of $(2J+1)\,\theta^2_{jl}$ extracted from the distorted wave calculations. In view of the approximations employed in deriving the distorted wave formalism and also the uncertainty in the parameters used in the calculations, no great significance should be attached to the absolute values of $(2J+1)\,\theta^2_{jl}$. However the distorted wave calculations should be fairly reliable for extracting relative reduced widths in cases in which the parameters employed are the same or approximately so. The results have been tabulated for particular l-values and the absolute reduced widths have been converted to relative values in the table by assigning a value of 100 relative units to one strong transition for each l-value. For the six $l = 1$ transitions, the agreement between the relative reduced widths extracted from the Butler and distorted wave theories is very good. This might be expected on the grounds that the states involved lie fairly close together within a Q-value range of about 2.3 MeV. For all the transitions the ingoing deuteron partial waves will be distorted in exactly the same way. At the

TABLE 3

Comparison of the reduced widths obtained from the Butler and distorted wave analyses

Final nucleus	Excitation of final state (MeV)	Q-value of transition (MeV)	l value	Butler analysis			DWBA analysis		
				Cut-off radius	$(2J+1)\theta^2$		$(2J+1)\theta_{sp}^2$		θ_{sp}^2
					absolute	relative	absolute	relative	
Ni^{59}	0.000	6.779	1	6.4	0.035	100	1.61	100	0.40
Ni^{59}	0.466	6.313	1	6.4	0.019	54	0.79	49	
Ni^{59}	0.880	5.899	1	6.4	0.0039	11	0.20	12	
Ni^{61}	0.000	5.598	1	5.7	0.024	69	1.11	69	0.28
Ni^{61}	0.284	5.314	1	5.1	0.019	54	0.82	51	
Ni^{61}	1.104 1.137 1.190	4.45	1	4.8	0.0073	21	0.31	19	
Ni^{59}	5.69	1.09	0	4.0	0.0077	100	0.18	100	0.09
Ni^{61}	3.07	2.53	0	5.1	0.0022	29	0.052	28	0.026
Ni^{61}	4.91	0.69	0	3.75	0.0086	112	0.25	133	0.12
Ni^{59}	0.341	6.438	3	6.4	0.023	100	2.64	100	0.33
Ni^{61}	0.068	5.530	3	5.7	0.037	161	2.87	109	0.48
Na^{24}	0.000	4.731	2	5.2		100		100	
Na^{24}	0.472	4.259	2	5.2		51.5		57	

energies involved the partial waves for the outgoing protons corresponding to each final state will be distorted by approximately similar amounts. For a particular l-value the relative reduced widths obtained from similarly distorted distributions should then be approximately the same as those obtained by comparing undistorted distributions.

In the case of the $l = 0$ and $l = 2$ transitions the agreement between the relative reduced widths is satisfactory, with the possible exception of the values for the $l = 0$ transition to the 4.91 MeV state in Ni^{61}. Since the variation of the Butler reduced width at this Q-value is directly proportional to the low value of the cut-off radius used, the disagreement in this particular case is not too serious.

For the two $l = 3$ transitions the agreement is poor, which is difficult to understand in view of the good agreement obtained for the other l-values. The value of $(2J+1)\ \theta^2$ for the $l = 3$ transition to the 68 keV state in Ni^{61} was found in the original Butler analysis to be 0.060 since there was little contribution from the secondary peak of the $l = 1$ Butler curve to be taken into account. When the distorted wave $l = 3$ curve had been obtained, the Butler $l = 3$ curve was fitted to the same peak cross-section and this yielded the smaller value for $(2J+1)\ \theta^2$ of 0.037.

7. Discussion

The results of this general investigation have shown that greater agreement between theory and experiment can be obtained by the use of distorted wave stripping calculations. In particular the ambiguities in the l-value assignments which sometimes occur when medium heavy nuclei are bombarded with 9 MeV deuterons, can be resolved in favour of the lower l-value by using a distorted wave analysis. This appears to be principally due to the overriding influence of the Coulomb forces in this mass and energy region. The relative reduced widths extracted from Butler and distorted wave calculations for distributions with particular l-values generally appear to be in good agreement.

Whether or not the distorted wave theory in its present form can give a quantitative understanding of the stripping process, cannot be determined from this investigation. In order to test this, the angular distributions of elastically scattered deuterons and protons must be measured at the appropriate energies and from the relevant nuclei, in conjunction with the stripping experiment. This would greatly help in fixing the embarrassingly large number of parameters involved. It might then be possible to interpret the stripping differential cross sections and reduced widths in terms of fractional parentage coefficients. To do this in the present investigation would be rather premature.

The author wishes to express his thanks to Dr. B. Buck and Dr. P. E. Hodgson for permitting him to use their distorted wave stripping programmes. He is also indebted to Dr. B. Buck, Dr. H. C. Newns and Dr. G. Parry for many valuable discussions and to the Staff of the Computing Machine Laboratory at the University of Manchester for their untiring assistance.

References

1) S. T. Butler, Proc. Roy. Soc. A **208** (1951) 559;
A. B. Bhatia, K. Huang, R. Huby and H. C. Newns, Phil. Mag. **43** (1952) 485
2) J. Horowitz and A. M. L. Messiah, J. Phys. et Rad. **14** (1953) 695;
D. Robson, Nuclear Physics **22** (1960) 34;
W. Tobocman and M. H. Kalos, Phys. Rev. **97** (1955) 132
3) W. Tobocman, Phys. Rev. **115** (1959) 98
4) B. Buck and P. E. Hodgson, Phil. Mag. (to be published)
5) D. H. Wilkinson in Proc. Int. Conf. on Nuclear Structure, Kingston, Canada, 1960 (North Holland Publ. Co., Amsterdam, 1960)
6) A. W. Dalton, G. Parry and H. D. Scott, Proc. Phys. Soc. **73** (1959) 677;
A. W. Dalton, A. Kirk, G. Parry and H. D. Scott, Proc. Phys. Soc. **75** (1960) 95
7) G. Gamow and C. L. Critchfield, Theory of the atomic nucleus (Oxford University Press, 1949) p. 11
8) R. Huby, M. Y. Refai and G. R. Satchler, Nuclear Physics **9** (1958) 94
9) A. W. Dalton, G. Parry, H. D. Scott and S. Swierszczewski, Proc. Phys. Soc. **77** (1961) 682
10) M. H. Macfarlane and J. B. French, Rev. Mod. Phys. **32** (1960) 567
11) G. R. Satchler, Nuclear Physics **18** (1961) 110
12) B. Buck, R. N. Maddison and P. E. Hodgson, Phil. Mag. **5** (1960) 1181

13) M. A. Melkanoff, Proc. Int. Conf. on the Nuclear Optical Model, Florida, 1959, p. 207
14) M. A. Melkanoff, J. S. Nodvik, D. S. Saxon and R. D. Woods, Phys. Rev. **106** (1957) 793
15) F. Bjørklund, Proc. Int. Conf. on the Nuclear Optical Model, Florida, 1959, p. 1
16) J. R. Holt and T. N. Marsham, Proc. Phys. Soc. A **66** (1953) 259, 467
17) A. W. Dalton, S. Hinds and G. Parry, Proc. Phys. Soc. A **70** (1957) 586
18) D. H. Wilkinson, Phil. Mag. **3** (1958) 1185
19) C. H. Paris, Massachusetts Institute of Technology, Progress Report of Laboratory for Nuclear Science, May 1959
20) H. A. Enge and R. A. Fisher, Massachusetts Institute of Technology, Progress Report of Laboratory for Nuclear Science, May 1959

4.E

Nuclear Physics **27** (1961) 507—515; © *North-Holland Publishing Co., Amsterdam*

Not to be reproduced by photoprint or microfilm without written permission from the publisher

A STUDY OF BETA-GAMMA DIRECTIONAL CORRELATION IN THE DECAY OF Au^{199}

M. S. EL-NESR † and R. OTHAZ ††

Institute of Physics, University of Uppsala, Uppsala, Sweden

Received 6 March 1961

Abstract: The directional correlation between the 302 keV beta-group and the 158 keV gamma-ray in the decay of Au^{199} has been measured as a function of the energy of the beta-particles. A magnetic lens beta-ray spectrometer was used to select the energy of the beta-rays. Measurements have been made at five beta-energies 89, 127, 164, 187 and 211 keV. Moreover, the directional correlation between the 251 keV beta-group and the 208 keV gamma-ray has been studied. Within the statistical accuracy of the data the correlations are isotropic.

1. Introduction

The decay of Au^{199} (3.14 d half-life) has been the subject of several investigations [1–5]), and the decay scheme is well established (see fig. 1). It was found [6–8])

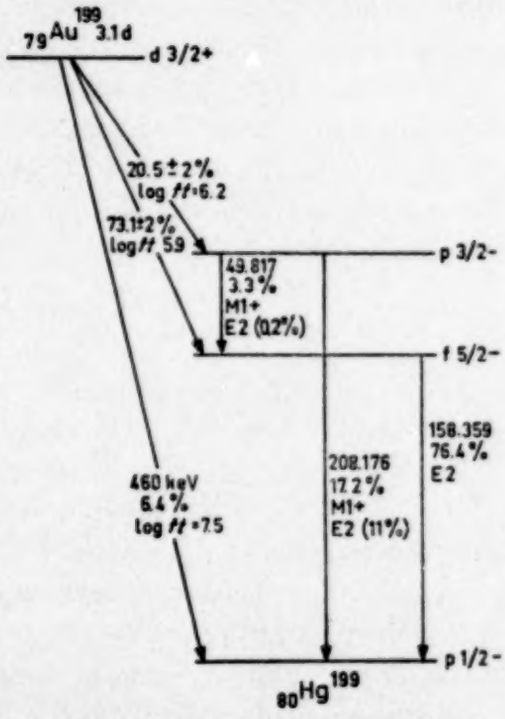

Fig. 1. Decay scheme of Au^{199}

† On leave from the U.A.R. Atomic Energy Commission, Cairo, Egypt

†† On leave from Instituto de Fisica, Facultad de Ciencias Fisicomatematicas, La Plata, Argentina

that the beta-decay of Au^{199} proceeds through three branches to the Hg^{199} levels with maximum energies of 251, 302 and 460 keV. The relative intensities of these beta-branches were determined [8, 9]) as 20.5 ± 2 %, 73.1 ± 2 % and 6.4 %, respectively. Bell *et al.* [7]) found that all the beta-branches have an allowed shape. According to the theory of beta-gamma angular correlation proposed by Falkoff and Uhlenbeck [10]), there would be no angular correlation to be expected when the beta-transition is allowed. Since the beta rays of Au^{199} followed by gamma transitions in Hg^{199} are classified as $d_{\frac{3}{2}} \rightarrow f_{\frac{5}{2}}$ and $d_{\frac{3}{2}} \rightarrow p_{\frac{3}{2}}$ transitions they should be of the first forbidden non unique type. Consequently the beta-gamma directional correlation is expected to have an anisotropic pattern.

2. Source Preparation

The Au^{199} activity was produced by irradiating pure platinum metal in the R1 reactor in Stockholm in a flux of 10^{12} n/cm^2 · sec for about 5 days. The target was divided in two parts, one of which was subjected to chemical separation by means of solvent extractions [11]), and the separated activity deposited onto an Al foil of thickness ≈ 0.67 mg/cm^2. The remaining half of the activity (Pt target) was placed in a special apparatus, to be described elsewhere [12]) and the gold fraction separated and deposited directly onto an Al foil of the thickness previously mentioned. This latter method, unfortunately, produced only weak samples because of the poor cooling efficiency of the collecting foil. However, it has proved possible to measure with such sources, which apart from being weak were of far better quality than those prepared chemically. The diameters of the sources used were 3—5 mm. The measurements were carried out with 4 different sources of the same mean thickness of approximately 30 μg/cm^2, in order to reveal a possible anisotropy due to a non-uniformity of the source.

3. Equipment

The beta-gamma directional correlation measurements were performed with a magnetic long lens spectrometer adapted for correlation experiments [13]). The experimental setup, as shown in fig. 2, was a beta-ray spectrometer and a 5.08 cm $\times$ 5.08 cm NaI(Tl) scintillation detector for the gamma-rays. The NaI(Tl) crystal was optically coupled to RCA6810-A photomultiplier tube. The spectrometer baffle was set so that the momentum resolution $\Delta p/p$ was about 3 %. With this baffle setting the transmission of the spectrometer for electrons was about 1.8 % for the 4 mm source diameter. The beta-particles were detected by a plastic crystal which was coupled to RCA6810-A photomultiplier tube through a light guide. A typical electron-spectrum is shown in fig. 3.

A fast-slow coincidence circuit with an effective resolving time of 2.5×10^{-8} sec was used in the experiments. To ensure that the experimental arrangement

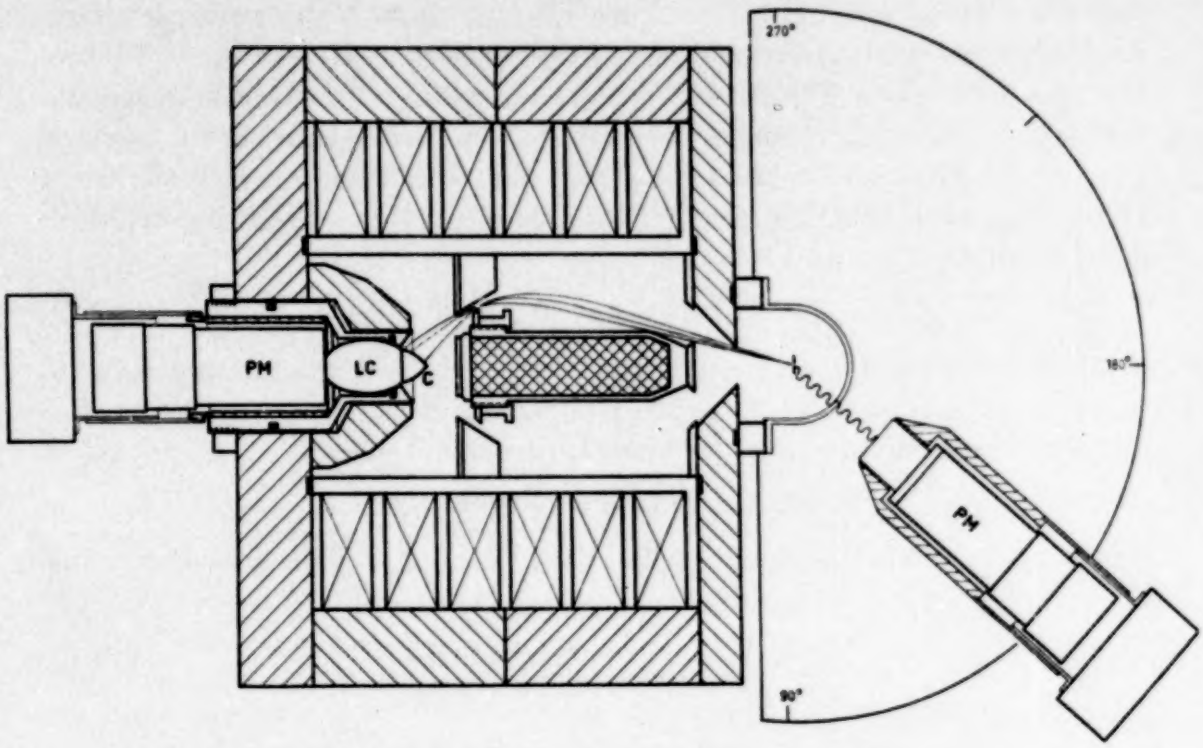

Fig. 2. Electron-gamma angular correlation spectrometer

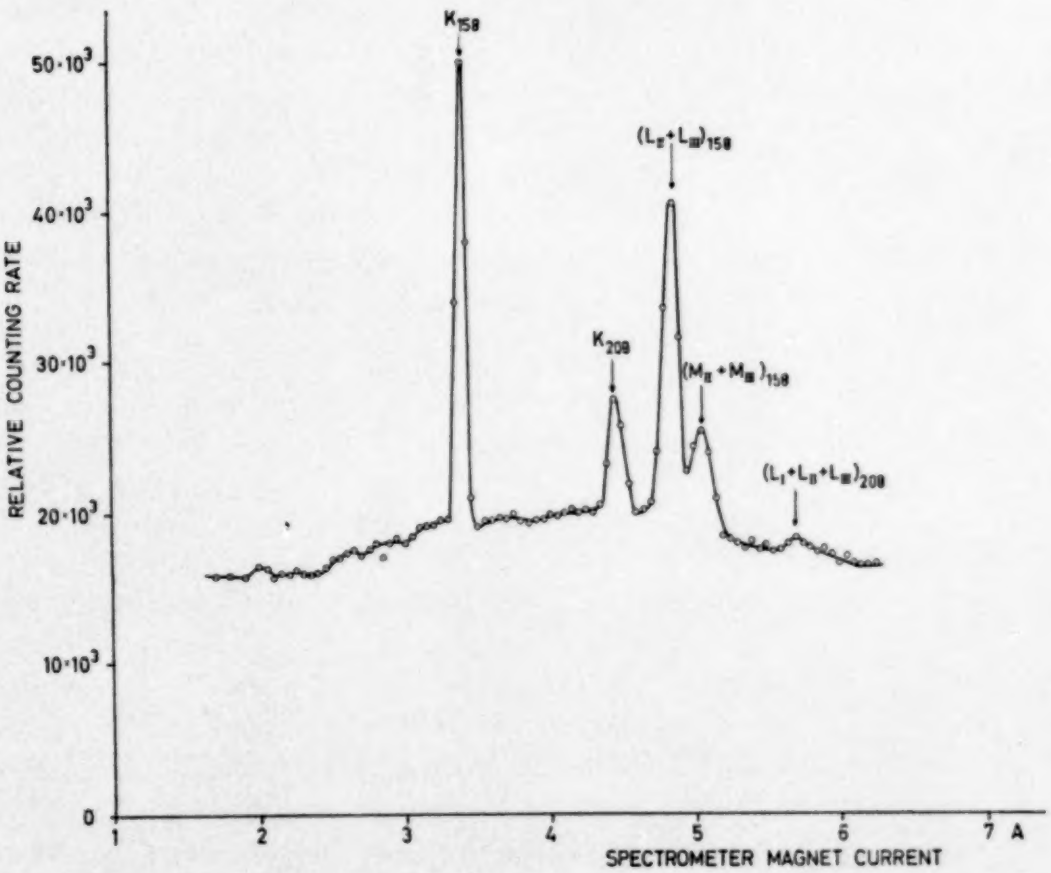

Fig. 3. Beta-spectrum of Au^{199}

did not introduce an anisotropic correlation, tests have been done on Co^{60}. The radiations emitted in the decay of Co^{60} to Ni^{60} are well known [14]) to have isotropic correlations. The gamma-channel was adjusted to accept both gamma-rays. The magnetic spectrometer was adjusted on the maximum of the beta-ray spectrum (i.e. E_β is about 127.5 keV). The result obtained for the A_2 coefficient in the angular correlation function $W(\theta) = \sum_\nu A_\nu P_\nu(\cos\theta)$ after corrections for the finite solid angles is

$$A_2 \text{ (corrected)} = -0.001 \pm 0.011.$$

For further check, the correlation between the 134 keV gamma-ray and the K-conversion electrons of the 165 keV gamma-ray in Hg^{197m} was measured. The activity was evaporated on Ag backing. The result obtained for A_2 (corrected) is

$$A_2 \text{ (corrected)} = +0.19 \pm 0.02.$$

This result is in good agreement with that measured previously by Pettersson *et al.* [15]).

4. Experimental Details

The gold source was first centered with respect to the magnetic spectrometer, then the centre of rotation of the gamma-detector was carefully adjusted to

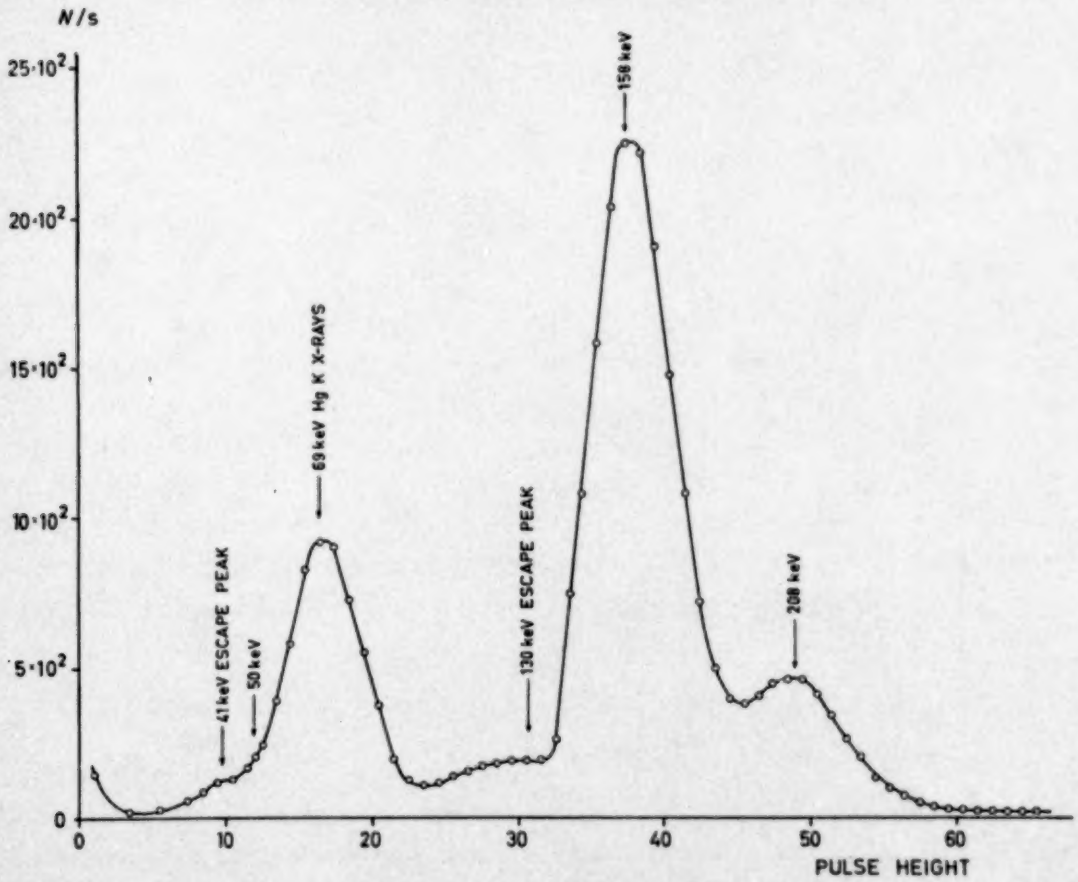

Fig. 4. γ-spectrum of Au^{199}

coincide with the centre of the source. A scintillation spectra obtained in the gamma-channel is shown in fig. 4. The resolution was 17 % for the 158 keV gamma-ray of Au^{199}. The differential discriminator of the gamma-channel was adjusted to a position corresponding to the gamma-line of interest (i.e. 158 or 208 keV). The window width was adjusted to correspond to the approximate width of this line at half-maximum. When the γ-channel had been adjusted to accept e.g. the 158 keV γ-ray, the single counting rates at the 90°, 180° and 270° positions were found to be equal within 0.02 %. The remaining differences in gamma-counting rates were corrected by normalization. The influence of the magnetic field on the PM-tube of gamma-detector was shown to be negligible as was the influence of the iron shield of the γ-detector on the beta counting rates. Coincidences were recorded between

a) beta-particles of five different energies from the 302-keV beta group and the 158 keV gamma-ray, and
b) beta-particles of two different energies from the 251 keV beta-group and the 208 keV gamma-ray,

with the gamma detector setting at 90°, 180° and 270° with respect to the spectrometer axis. In the case a), measurements have been made at five beta-energies 89, 127, 164, 187 and 211 keV. In the case b), two beta-energies were selected 112 and 164 keV. The energy setting on the beta-spectrum was varied randomly. At each energy over 100 000 real coincidences were taken at both 90°+270° and 180°. The real coincidence rates were calculated from the equation

$$R = N_T - 2\tau N_\gamma N_\beta, \tag{1}$$

where N_T is the total number of coincidences, N_γ and N_β are the gamma- and beta-single counting rates and 2τ is the resolving time. The real coincidence rates were normalized by dividing by the two single counting rates N_γ and N_β. This method provided sufficient correction for source centering and any slight drift in the single counting rates. No asymetry between 90° and 270° was observed. The resolving time of the coincidence circuit was measured several times and found to be very constant over long periods of time. No dependence of 2τ on beta energy was observed. Chance coincidences were measured from time to time. The ratio of true/chance coincidences exceeded 10 at all energies.

5. Corrections Applied to the Experimental Data

5.1. GEOMETRICAL CORRECTIONS

For the geometry used in the experiments the correction for the finite solid angles is important. The correction for the finite size of the gamma detector was calculated using the formulae given by Lawson and Frauenfelder[16]). For the beta-

spectrometer the finite aperture angle correction factor was calculated by means of special "P_2-baffle" experiment to be described elsewhere [13]). The corrected A_2 coefficient in the correlation function can be written as

$$A_2 \text{ (corrected)} = \frac{1}{S_2^{\gamma}} \frac{1}{S_2^{e^-}} A_2 \text{ (uncorrected)}, \tag{2}$$

where S_2^{γ} is the correction for the finite solid angle of the gamma-detector and $S_2^{e^-}$ is the correction for the finite solid angle of the beta-spectrometer.

5.2. CORRECTION FOR THE DECAY

The procedure of rotating the gamma-detector made decay-corrections unnecessary.

5.3. EXTRA-NUCLEAR FIELD EFFECTS

The life-time of the 158 keV level [7]) is 2.4×10^{-9} sec and for the 208 keV level [17]) it is 6×10^{-11} sec. In our results discussed below we assumed that there is no attenuation on the β-γ correlation due to interaction with extra-nuclear fields [18]).

5.4. INNER BREMSSTRAHLUNG EFFECT

Inner bremsstrahlung of high energy beta-ray may give rise to a photon associated with a beta-particle having the remaining energy. This would cause a coincidence and may simulate a β-γ correlation if the energies are appropriate. The relative number of inner bremsstrahlung photons per beta-decay is quite small. Besides, the angular correlation of inner bremsstrahlung-beta as observed by Novey [19]), is strongly peaked around 30° and falls off sharply and there is no inner bremsstrahlung at the angle 180° to the betas. Since the maximum beta-ray energy in Au^{199} decay is 460 keV, the contribution of the I.B.-beta anisotropy in the measured correlation can be considered very small, and it is very much less than the errors of our anisotropy measurements. The measured directional anisotropy A was calculated from coincidence data at 90°, 180° and 270° using the expression

$$A = \frac{\sum C(180) - \sum [C(90)+C(270)]}{\sum [C(90)+C(270)]}. \tag{3}$$

The spin sequences of the cascades in question are the following:

302 keV beta — 158 keV gamma: $\frac{3}{2}-\frac{5}{2}-\frac{1}{2}$,

251 keV beta — 208 keV gamma: $\frac{3}{2}-\frac{3}{2}-\frac{1}{2}$.

Thus it is theoretically possible to have an A_4 term, but the fact that the correlation gives very small anistropy it is justified to neglect the A_4 term. Therefore, the uncorrected A_2 coefficient is given by

$$A_2 \text{ (uncorrected)} = \frac{2A}{A+3}. \tag{4}$$

5.5 SCATTERING

Precaution was taken in order to reduce the scattering of electrons as well as of gamma-rays. Thus evaporated thin sources were used. Further, the mechanical construction of the spectrometer and detectors made the scattering of gamma-rays into the gamma-detector negligible.

6. Results

6.1. DIRECTIONAL CORRELATION BETWEEN THE 302 keV BETA-GROUP AND THE 158 keV γ-RAY

The directional correlation between the 302 keV beta-group and the 158 keV gamma-ray has been measured as a function of the energy of the beta-particles. Fig. 5. is a plot of the experimental corrected anisotropy A_2 (E_β)

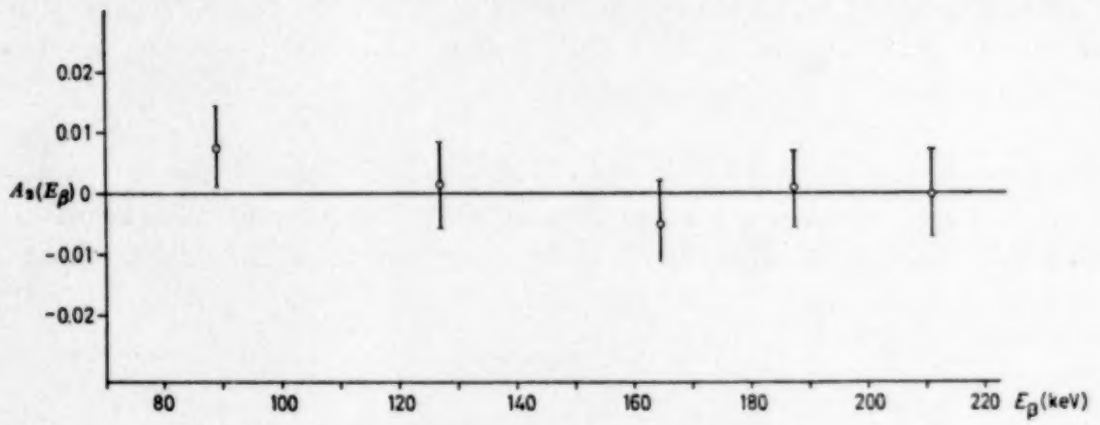

Fig. 5. Beta-gamma anisotropy in Au^{199}

versus the beta-energy in keV. The errors shown are the statistical errors. It is evident that the beta-gamma directional correlation is isotropic. This result is in agreement with that reported previously [5]).

6.2. THE DIFFERENTIAL CORRELATION BETWEEN THE 251 keV BETA-GROUP AND THE 208 keV GAMMA-RAY

The β-γ directional correlation between the 208 keV γ-ray and the 251 keV beta-group feeding it has been studied at energies 112 and 164 keV. Both correlations were isotropic.

At 112 keV beta-energy, the value of the A_2 coefficient after correction for the finite solid angles is

$$A_2 = -0.002 \pm 0.007.$$

At 164 keV beta-energy, the value of A_2 (corrected) is

$$A_2 = -0.003 \pm 0.006.$$

The authors could not proceed with the correlation experiment for lower beta-energy settings because of the low coincidence counting rate observed. In addition the correlations for further beta-energies do not add more information since the correlations were isotropic.

7. Conclusion

The authors have studied experimentally the directional correlation of the beta-decay of Au^{199} and following gamma transitions in Hg^{199}. The angular correlations were investigated for two beta-groups and, within each group, for several beta-energies, and found to be isotropic in all cases. Since these transitions have been classified as $d_{\frac{3}{2}} \rightarrow f_{\frac{5}{2}}$ and $d_{\frac{3}{2}} \rightarrow p_{\frac{3}{2}}$ transitions, they should be of the first forbidden non-unique type. According to the recent theory proposed by Kotani and Ross [21]) they are expected to be anisotropic and the anisotropy should be proportional to p^2/W. It was surprising that no trace of anisotropy could be found. It is possible that the effects are too small to show up in the experiment.

The authors are greatly indebted to Professor Kai Siegbahn for his encouragement and stimulating interest in this work. Grateful thanks are due to Fil. Lic. B. G. Pettersson for his helpful suggestions and discussions.

References

1) E. McMillan, M. Kamen and R. Ruben, Phys. Rev. **52** (1937) 375
2) C. E. Mandeville, M. V. Scherb and W. B. Keighton, Phys. Rev. **74** (1948) 601
3) J. L. Meems and F. Maienschein, Phys. Rev. **76** (1949) 328
4) L. A. Beach, C. L. Peacock and R. G. Wilkinson, Phys. Rev. **76** (1949) 1585;
R. D. Hill, Phys. Rev. **79** (1950) 413
5) K. Siegbahn, Arkiv Fysik, **4** (1952) 223
6) P. M. Sherk and R. D. Hill, Phys. Rev. **83** (1951) 1097
7) R. E. Bell, R. L. Graham and H. E. Petch, Can. J. Phys. **30** (1952) 35
8) S. K. Haynes and W. T. Achor, J. Phys. radium **16** (1955) 635
9) G. Bäckström, O. Bergman and J. Burde Nuclear Physics **7** (1958) 263
10) D. L. Falkoff and G. E. Uhlenbeck, Phys. Rev. **79** (1950) 334
11) Wilkinson and Hicks, ed. W. Meinke. Chemical Procedures used in Bombardment Work at Berkeley, URCL-432;
W. Parker Nucl. Instr. and Methods **5** (1959) 142
12) W. Parker, (to be published)
13) T. R. Gerholm, R. Othaz and M. S. El-Nesr, Arkiv Fysik, to be published
14) R. M. Steffen in Proc. Rehovoth Conf. on Nuclear Structure, ed. by H. J. Lipkin (North-Holland Publ. Co., Amsterdam, 1958);
R. M. Steffen, Phys. Rev. Lett. **3** (1959) 277

15) B. G. Pettersson, J. Thun and T. R. Gerholm, Nuclear Physics **24** (1961) 223
16) J. S. Lawson, Jr, and H. Frauenfelder, Phys. Rev. **91** (1953) 649
17) R. L. Graham, R. E. Bell, L. Yaffe and J. S. Geiger, Phys. Rev. **99** (1955) 1646
18) A. Abragam and R. V. Pound, Phys. Rev. **92** (1953) 943
19) T. B. Novey, Phys. Rev. **89** (1953) 672
20) H. Frauenfelder, in Beta- and gamma-Ray spectroscopy, ed. by K. Siegbahn -(North-Holland Publishing Co., Amsterdam, 1955) Ch 19: Ann. Rev. Nuclear Sci. **2** (1953) 129
21) T. Kotani and M. Ross, Phys. Rev. Letters **1** (1958) 140;
T. Kotani and M. Ross, Prog. Theor. Phys. **20**, No. 5 (1958) 643;
T. Kotani and M. Ross, Phys. Rev. **113** (1959) 622; and
T. Kotani, Phys. Rev. **114** (1959) 795

1.E.1:
4.E

Nuclear Physics **27** (1961) 516—528; © *North-Holland Publishing Co., Amsterdam*
Not to be reproduced by photoprint or microfilm without written permission from the publisher

DECAY OF Er^{172} AND Tm^{172}

P. G. HANSEN, O. J. JENSEN and K. WILSKY
Chemistry Department, Research Establishment Risø, Denmark

Received 7 April 1961

Abstract: The isotopes Er^{172} and Tm^{172} were produced by double n-capture in Er^{170} and isolated by ion exchange chemistry. The radiations were studied mainly by scintillation methods and coincidence techniques. A tentative decay scheme for Er^{172} is given. The Tm^{172} decay scheme includes levels at 79, 260, 1170, 1467, 1550 and 1609 keV. The main β-groups have the following energies (log *ft* values are given in parentheses) 1920 keV (8.9), 1840 (8.7), 1660 (10.0) 740 (7.9), 450 (6.8) and 310 (6.5). The β-decay to the ground state rotational band shows that Tm^{172} must have spin and parity 2−. This assignment is confirmed from a more detailed consideration of the β-transition probabilities. The single particle configuration for Tm^{172} is discussed.

1. Introduction

The isotope Tm^{172} was first reported by Folger *et al.* [1]). In a subsequent investigation by Nethaway *et al.* [2]), Tm^{172} was found to be the daughter of (49.8 ± 1)h Er^{172} (half life from milking experiments). The Tm^{172} half life was (63.6 ± 0.3) h and the β-end point was at 1.5 MeV (absorption measurements). γ-rays at 0.076, 0.18, 0.40, 1.09, 1.44 and 1.79 MeV were reported. Recently the decay schemes of both isotopes have been studied by Helmer and Burson [3]) who obtained results that are in satisfactory agreement with those presented in the following.

It was felt that an investigation of the two nuclei would be of interest, especially since the level structures of Tm^{172} and Er^{172} might reveal features of interest in connection with the study of nuclear properties in the region of deformed nuclei. It turned out that a detailed description was only possible for the Tm^{172} decay because of lack of detailed information on the Er^{172} radiations. Consequently the main emphasis is on features pertinent to the former decay scheme.

Further information [4, 5]) on the Yb^{172} levels is available from the decay of Lu^{172} and from Coulomb excitation.

2. Experimental Technique

Approximately 1.5 mg samples of enriched Er^{170} as the oxide (87.3 %, obtained from Isotopes Division, Oak Ridge National Laboratory, U.S.A.) were irradiated for 5 d in the 10^{14} n/cm^2 · sec flux of the vertical facility in the DR2

reactor. Er^{172} was formed from n-capture in 7.8 Er^{171} and Tm^{172} was formed through β-decay of the Er-activity and through neutron capture in 680 d Tm^{171}. After a cooling period of 2 d the sample was dissolved in hydrochloric acid and erbium was precipitated with concentrated hydrofluoric acid. The ErF_3 was dissolved in H_3BO_3—HNO_3 and erbium hydroxide separated with ammonia. The $Er(OH)_3$ was taken up in a small excess of HCl and the rare earths were separated on a cation exchange column with α-hydroxy isobutyric acid as the eluant [6, 7]). The resin was Dowex 50 × 12 graded to a settling rate in water of 2 to 4 mm/min. The Tm^{172} source prepared in this way contained large amounts of Tm^{171} and was used for experiments involving only high energy γ, e.g. the measurements with the three-crystal pair-spectrometer. Sources of high radiochemical purity were prepared by milking followed by still another ion exchange separation. Samples for γ-ray spectrometry were placed inside 2 mm thick polyethylene tubes, sources for β-ray work were prepared by a micro-column method [8]) or by electroplating onto thin (1 mg/cm^2) nickel foils.

The γ-ray spectrometry was performed with 7.6 cm diam. × 7.6 cm thick NaI(Tl) crystals coupled to EMI-9578B tubes. The high energy γ-rays were studied in more detail by means of a three-crystal pair-spectrometer-similar to the spectrometers described by Mann *et al.* [9]) and by Alburger and Toppel [10]). The spectrometer used a 5.1 cm diam. × 5.1 cm thick NaI crystal as the central crystal and two 7.6 cm × 7.6 cm crystals in the sides. The side crystals were shielded from direct radiation and fed into a conventional fast-slow coincidence circuit ($2\tau = 10^{-7}$ sec) which gave an output only when the side crystals simultaneously detected a 511 keV gamma ray (channel width 10 %). This signal was used to gate a multichannel-analyzer. It should be noted that since the larger part of the counting rate in the side crystals is due to scattered photons from the central crystal a fast triple coincidence demand would hardly mean any essential improvement.

The γ-γ coincidence work was done using the fast-slow coincidence circuit and a multichannel-analyzer. The resolving time was selected as 3×10^{-7} sec in order to insure quantitative detection of the low energy radiations. The detectors were two 7.6 cm diam. × 7.6 cm thick crystals. From the geometry and from published efficiency data for this crystal size [11]) the coincidence experiments could be interpreted quantitatively, that is, in terms of a coincidence efficiency expressing the frequency of the coincident event relative to the frequency of the selected event. Experiments on β-γ coincidence were carried out analogously with a 3.8 cm diam. × 2.5 cm thick anthracene crystal or a well-type plastic scintillator [12]) as the β-detector.

Two multichannel-analyzers were used during the investigation, namely a Philips 99 channel analyzer and a T.M.C. 256 channel analyzer.

3. Experimental Data

3.1. THE ISOTOPE Er^{172}

The Er fraction from the ion exchange separations contained the following activities: 9.4 d Er^{169} from neutron capture in the 9.0 % Er^{168}, 7.8 h Er^{171} from n-capture in 87.3 % Er^{170} and Er^{172} from double n-capture. Since Er^{169} emits no electromagnetic radiation it was possible to look for γ-rays from Er^{172} as soon as the 7.8 h activity had decayed.

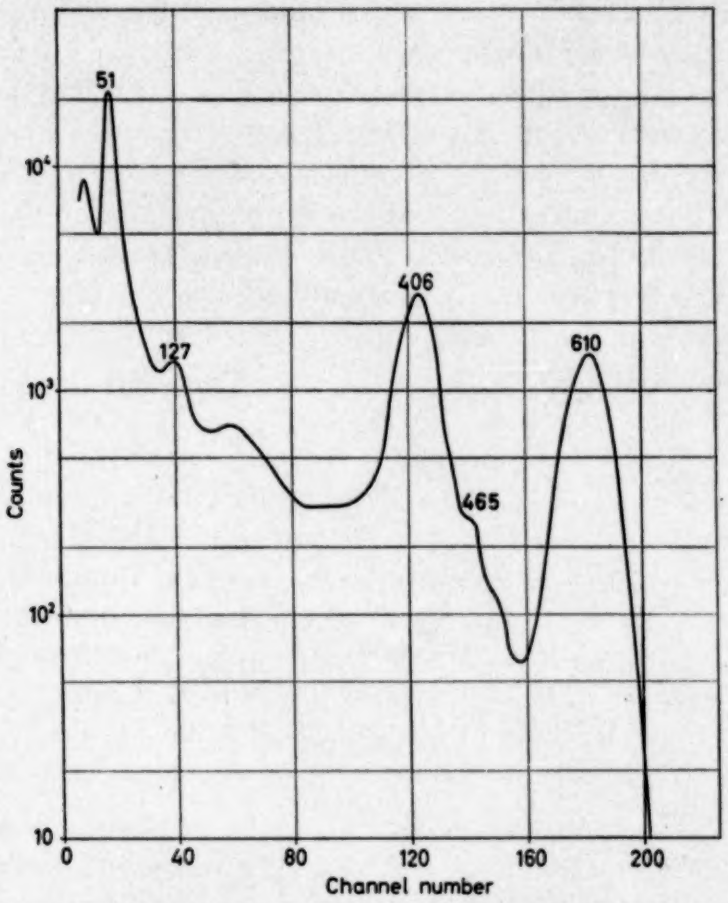

Fig. 1. The γ-spectrum of Er^{172} measured with a 7.6 diam. × 7.6 cm NaI crystal.

The γ-ray spectrum is shown in fig. 1 and the corresponding energies and relative intensities are given in table 1. The line designated K-X was measured with better resolution in a xenon filled proportional counter, and was resolved into the K_α and K_β X-rays of thulium. The half life of the 400-600 keV rays was followed over a period of 2 weeks, and was found to be (49.5 ± 0.5) in agreement with the result of Nethaway *et al.* [2]). This proves the assignment of these lines to Er^{172}.

Growth of the high energy γ-rays from Tm^{172} was observed in the erbium. The growth and decay rate was well in agreement with the assumption of a 50 h mother activity. This mixed spectrum could be used for a normalization of the

Er^{172} and Tm^{172} intensities to each other. Since the Tm intensities are known to an absolute scale (see fig. 7), the Er^{172} intensities given in table 1 also represent absolute intensities.

TABLE 1

Energies and intensities of γ-rays from the decay of Er^{172}

Energy keV	Intensity [a]) %	Coincidence relationships
K–X	7.2	K–X, 406
127	0.25	
406	31	K–X, 127 and $\beta(E_{max}$ 380)
465	12	
610	38	$\beta(E_{max}$ 290) Not coinc. with γ

[a]) The intensities are fundamentally relative intensities, but have been normalized to the (absolute) Tm^{172} intensities from the growth and decay characteristics. The intensities are believed to be accurate within ± 30 %.

Measurements of γ-γ and β-γ coincidences were performed. Since the presence of large amounts of Er^{169} prevented singles β-spectroscopy on Er^{172} the latter technique formed the only way to obtain information on the β-energies in this decay. The β-energies were measured in a hollow plastic scintillator in coincidence with γ-rays selected in a 7.6 cm diam. $\times$ 7.6 cm crystal. The results of all coincidence measurements are summarized in table 1.

Relatively little can be said about the Er^{172} decay scheme from the data available. Intensity and energy considerations make it seem plausible that levels at 406, 610 and probably 465 and 533 keV exist. The Q value for the β decay is around 900 keV. This tentative decay scheme is shown in fig. 7.

3.2. THE ISOTOPE Tm^{172}

3.2.1. Singles spectra

The γ-spectrum of Tm^{172} is shown on fig. 2. The spectrum contains γ-rays of 50 (K X-ray), 79, 181, 909, 1092 keV and an unresolved group of 1400–1600 keV. The half life of all γ-rays above 1000 keV was followed for a period of 2 weeks. The half life was found to be 63.5 ± 0.5 h in agreement with the value of 63.6 ± 0.3 h found by Nethaway *et al.* [2]). The γ-ray intensities obtained from the singles spectrum are listed in table 2. The high energy group was resolved in the three crystal pair-spectrometer and turned out to be composed mainly of lines with the energies 1390, 1465, 1528 and 1610 keV. The existence of the weak line at 1290 keV was confirmed in coincidence experiments. The three crystal spectrum is shown on fig. 3, intensities are given in table 2.

The β-spectrum of Tm^{172} was measured with the six-gap magnetic spectrometer at the Institute for Theoretical Physics in Copenhagen [13]). A pure, but

weak source was prepared (mounted on 200 $\mu g/cm^2$ Al-backing). The spectrum was scanned with six gaps at 1.3 % resolution. The Kurie plot is shown on

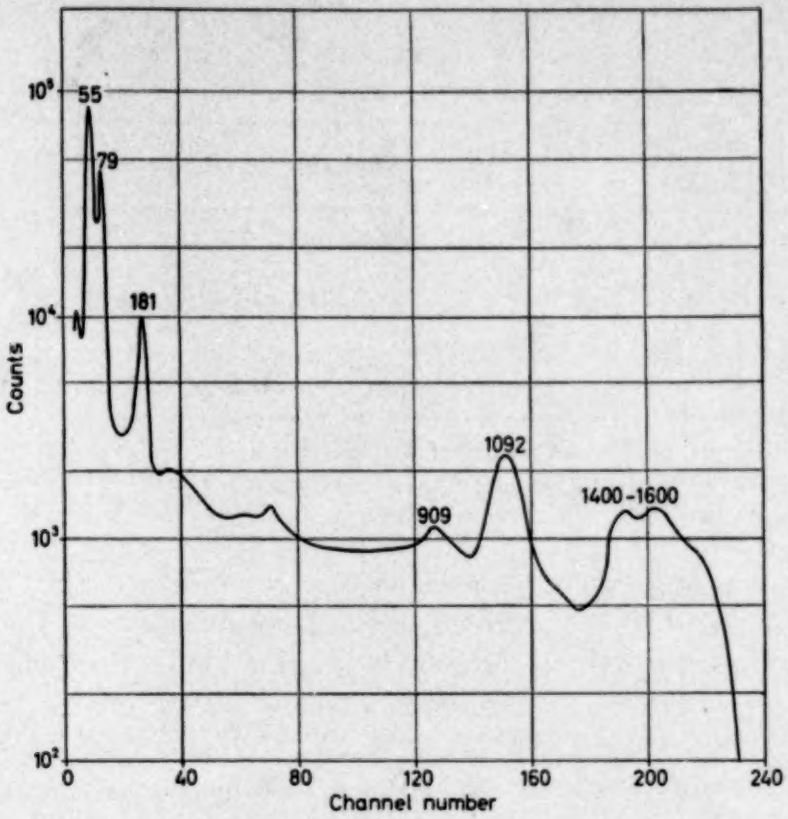

Fig. 2. The γ-spectrum of Tm^{172} measured with a 7.6 cm diam. × 7.6 cm NaI crystal.

TABLE 2

Energies and intensities of γ-rays from the decay of Tm^{172}

Three-crystal pair-spectrometer		7.6 cm × 7.6 cm NaI crystal		Transition intensity [a])
E_γ keV	Intensity %	E_γ keV	Intensity %	%
		K–X	10.9	
		79	6.8	68
		181	2.1	2.8
		909±10	1.4	1.4
		1092±10	7.4	7.4
1290±10	0.7			0.7
1390± 7	6.6			6.6
1565± 7	7.3	1400 to	25.2	7.3
1528± 7	5.6	1600		5.6
1610± 7	5.0			5.0

[a]) The intensities are fundamentally relative intensities, but have been normalized (see fig. 7 and sect. 4) to express absolute intensities in % of all β-decays. The intensities are believed to be accurate within ±20 %.

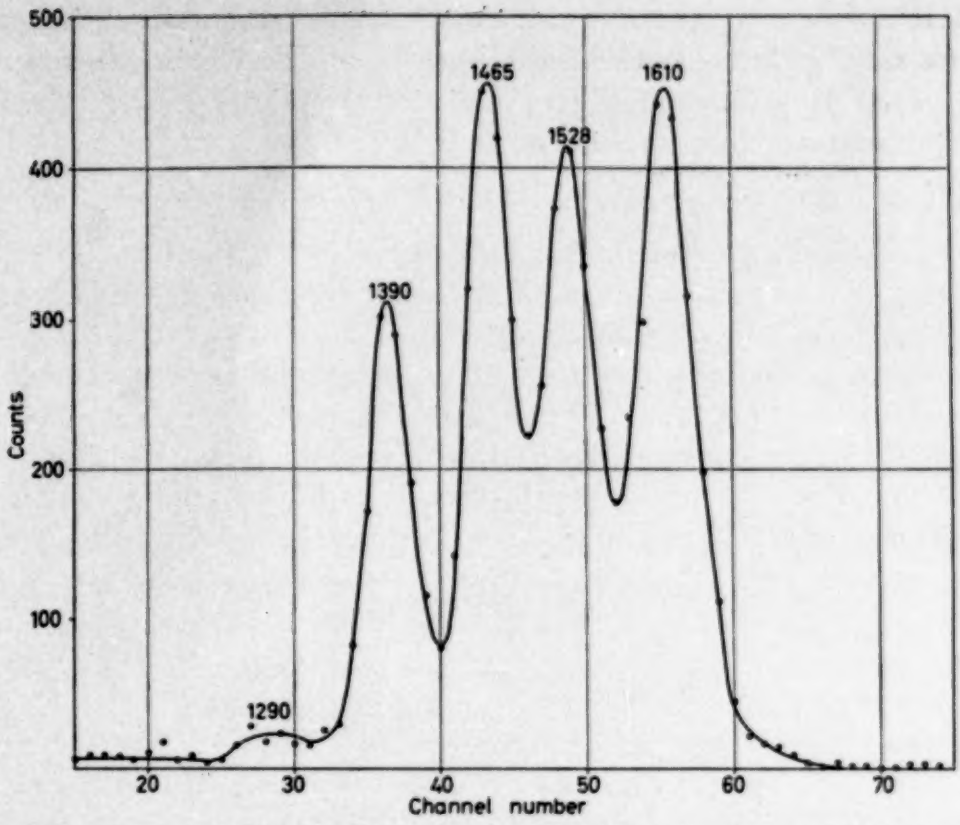

Fig. 3. High energy γ-rays from Tm^{172} measured with the three-crystal pair-spectrometer. The spectrum was measured over a period of 1000 min. The energy calibration was performed with a mixed source of Co^{60}, Tm^{172} and Y^{88}, using the 1172, 1333 and 1840 keV lines as the calibration points.

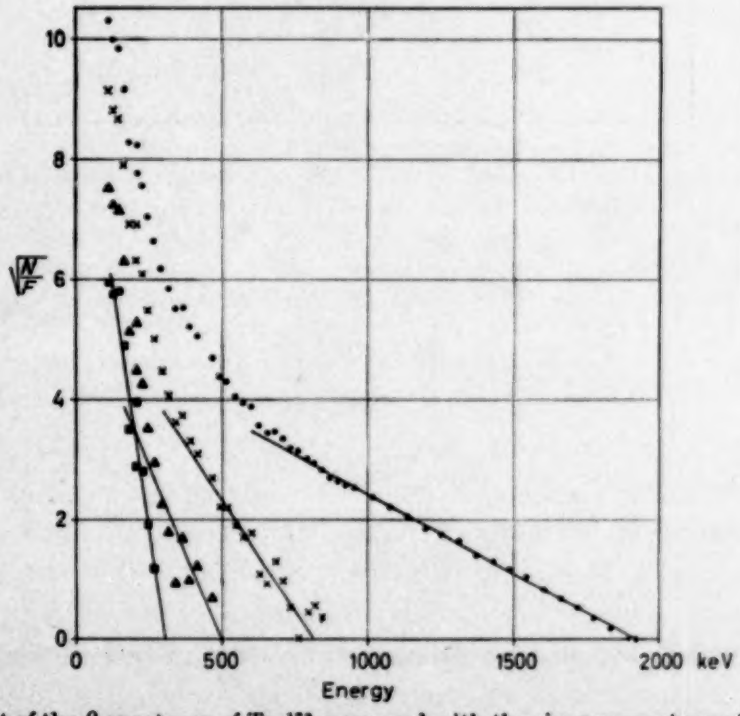

Fig. 4. Kurie plot of the β-spectrum of Tm^{172} measured with the six gap spectrometer. This analysis yields four groups with endpoints 1920 keV (58 %), 810 keV (19 %), 500 keV (9 %) and 300 keV (14 %). The high energy group is known from coincidence experiments to be a composite of three β-groups, presumably with α-type shape. A comparison with data from γ-singles spectra and coincidence experiments is made in sect. 4.

fig. 4. It is shown later that the high energy β form a composite of three groups feeding states at 79 and 260 keV. These groups prosumably have α-type shape. Because of this and because of poor statistics, the β-intensities obtained from the γ-intensities are considered more accurate.

3.2.2. Coincidence experiments

The γ-γ coincidence experiments were carried out with all major γ-rays in the decay. Most measurements took place in a 90° geometry with a lead anti-scattering shield. The experiment with the 79 keV ray was repeated in a 180° geometry. Coincidences with the Compton background were subtracted in the experiments with 79 and 181 keV by setting the channel away from the photopeak. In the coincidence experiments with the high energy γ-rays the situation was more complex, and it was felt that little could be learned from a more detailed analysis of the coincidence efficiencies. The data obtained in the γ-γ experiments are summarized in table 3. Typical coincidence spectra are shown on fig. 5.

TABLE 3

Results of $\gamma-\gamma$ coincidence experiments on Tm^{173}

Selected event keV	Coincident event (Coincidence frequencies [a]) in % are given in parentheses)
79 [b]	(K–X), 181 (4.7), 909, 1092 (14.2), 1390 (11.3) 1528 (9.8)
181 [b]	(K–X), 79 (120), 909 (45), 1210 (5), 1290 (10) 1350 (5)
909 [c]	(K–X), 79 (91), 181 (27)
1092 [c]	(K–X), 79 (108), 181 (2.5)
1250 [c]	(K–X), 79 (68), 181 (15.3)
1400 [c]	(K–X), 79 (85), 181 (2.4)
1500 [c]	(K–X), 79 (78)

[a]) The coincidence frequencies express the probability that the coincident transition will occur in conjunction with the selected event. Thus corrections for internal conversion of the observed γ-transitions have been included. The coincidence frequencies are believed to be accurate within ± 20 %.

[b]) The coincident spectra have been corrected for contributions from the underlying Compton distribution. The coincidence frequencies therefore represent true values based on the selected event.

[c]) The coincidence frequencies refer to a 100 keV broad channel centred at the selected energy. Thus these coincidence frequencies represent merely an average value characteristic for this setting (see fig. 2).

The β-γ coincidences were performed to establish the position of the major β-transitions observed in the Kurie plot. Using the 3.8 cm diam. $\times$ 2.5 cm thick anthracene crystal as the β-detector it was established that the 79 keV transition was coincident with β-rays with endpoint at 1900 keV, the 1100 keV γ with β of about 700 keV and the 1400–1600 keV group with β of about 360 keV.

A special experiment was performed to investigate which states in the ground state rotational band were fed directly in the β-decay. The β-side of the fast-

slow coincidence circuit was set to accept only pulses corresponding to β with more than 1 MeV energy, and the coincident γ-spectrum was recorded. The β-counter was now covered with 1.14 g/cm^2 lucite and the resulting coincidence spectrum was subtracted. Fig. 6 shows the uncorrected and the corrected

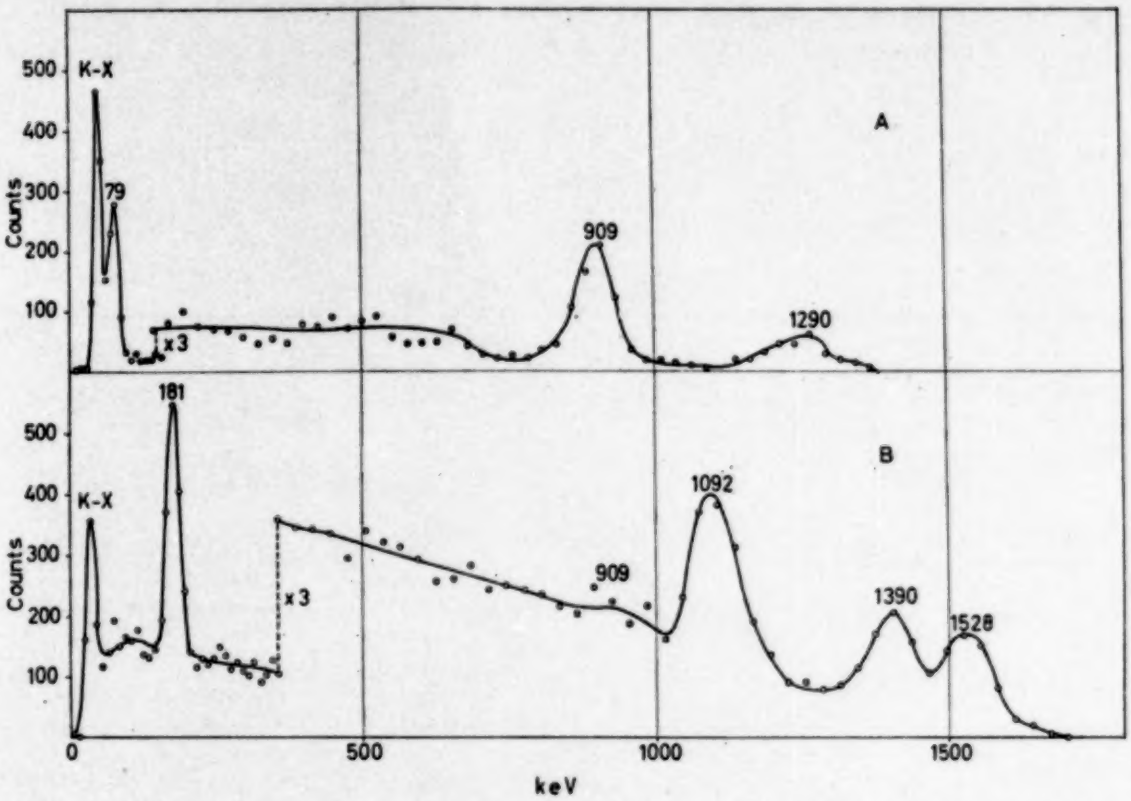

Fig. 5. (A) γ-rays in coincidence with the 181 keV transition. (B) γ-rays in coincidence with the 79 keV transition. The spectra have been corrected for coincidences with the underlying Compton distribution.

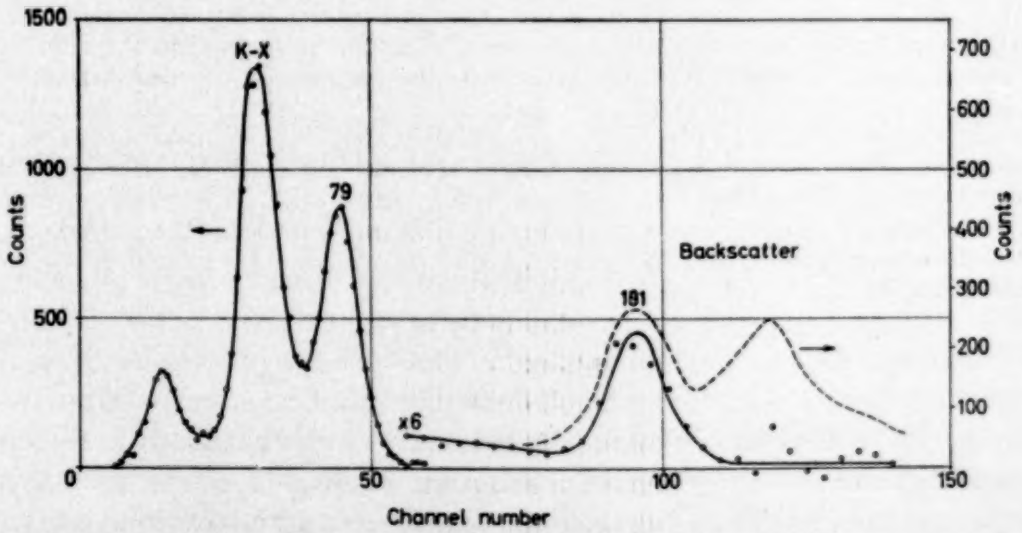

Fig. 6. The γ-spectrum in coincidence with β-particles of more than 1 MeV energy uncorrected (dotted) and corrected for backscatter and γ—γ coincidences. Counting time 50 min. See text (sect. 3.2.2.) for details of measurement.

spectrum. As could be expected the uncorrected spectrum contains a considerable contribution from hard γ scattered in the anthracene crystal. It is seen that the hard β are coincident only with the 79 and 181 keV transitions. The coincidence efficiencies (table 4) obviously correspond to the fraction of *recorded* β coincident with the two γ-rays. To get the coincidence efficiency for the β-groups a correction for detection efficiency is needed. These corrections were obtained from a computation of the fraction of β with energy above 1.00 MeV for β with end-point 1.92 MeV, (1.92-0.08) MeV and (1.92-0.26) MeV assuming allowed shape. The resulting fractions and the fractional intensities of the three hard β-groups are given in table 4. It is obvious that in this treatment

TABLE 4

Results of β–γ coincidence experiments on Tm^{170} and Tm^{172}

Nucleide	Bias in β-channel keV	Coincident event keV	Coincidence efficiency [a] %	Corresponding β end-point keV	Fraction of β above bias [b]	Branching ratio %
Tm^{170}	300	84	21.8	884	0.309	24.7
		(nil)	(78.2)	968	0.363	75.3
	600	84	18.7	884	0.0621	26.5
		(nil)	(81.3)	968	0.0975	73.5
Tm^{172}	1000	181	1.26	1660	0.166	1.86
		79	61.9	1840	0.236	62.9
		(nil)	(38.1)	1920	0.265	35.3

[a]) The coincidence efficiency includes corrections for internal conversion

[b]) This calculation assumes allowed shape and energy independent detection efficiency for the β-groups.

corrections for the energy dependent response function of the anthracene crystal (bias at 1 MeV) has been neglected. One would, however, expect that the errors to first order would cancel when the three β-groups are compared. As an experimental test of the reliability of this technique the same experiment was performed with a source of 129 d Tm^{170}. Two bias settings in the β-side were used, and it is seen from the results (table 4) that the corrected values are both in good agreement with the accepted value of $(24.0 \pm 2.1)\%$ found by Graham *et al.* [14]). It can therefore be concluded that the technique is of a satisfactory accuracy. The high energy β-rays from Tm^{172} populate the levels at 0, 79 and 260 keV in the following intensities: $(35 \pm 6)\%$, $(63 \pm 6)\%$ and $(1.9 \pm 0.2)\%$.

4. The Decay Scheme of Tm^{172}

Levels at 78.7 and 260.2 keV in Yb^{172} have been established [4]) in the decay of Lu^{172}. The 79 and 181 keV transitions observed in the present investigation correspond to transitions between these levels. This is confirmed from a) intensity considerations, b) β-γ coincidence experiments and c) the E2 multipole orders inferred from the K-X to γ ratio for the two rays (see fig. 5).

The four γ-rays in the 1400-1600 keV group correspond to 2 pairs of rays separated by approximately 80 keV. This suggests levels in Yb^{172} at 1467 and 1609 keV decaying to the ground state and first excited state. This assumption is confirmed from the γ-γ coincidence data, where only the 1390 and 1528 keV rays are seen in coincidence with the 79 keV transition.

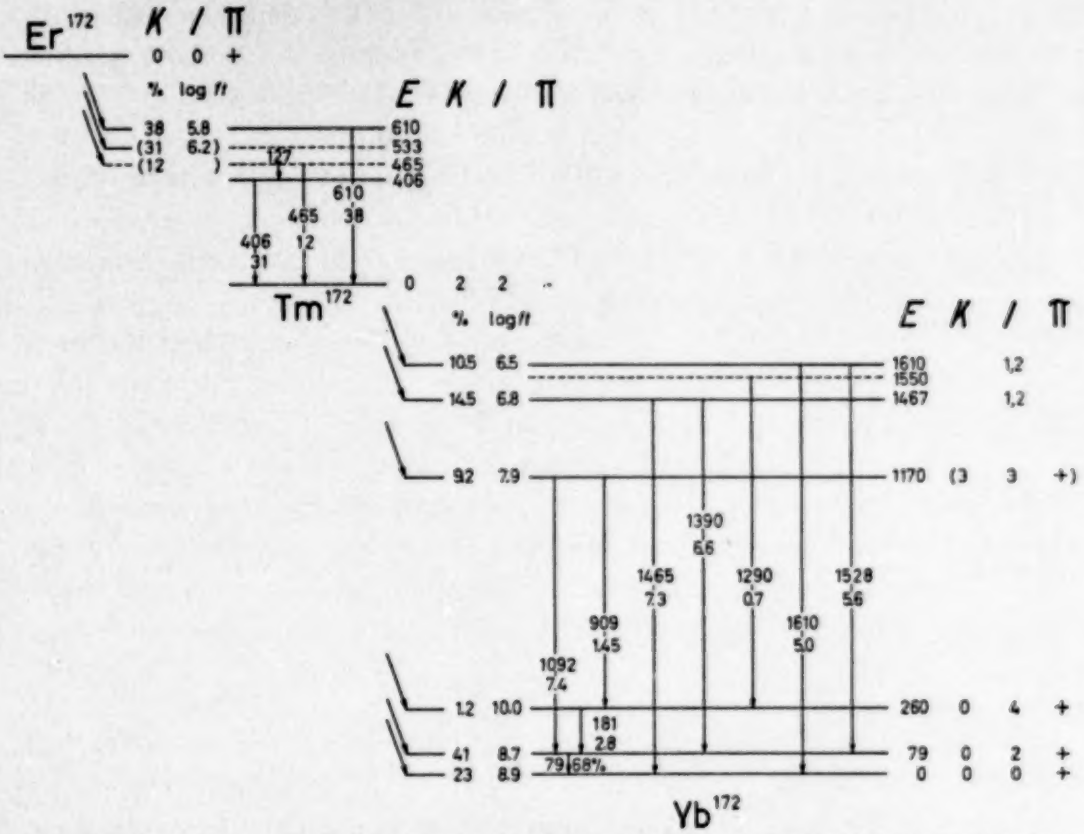

Fig. 7. The decay schemes of Er^{172} (tentative) and Tm^{172}. Energies in keV and intensities in per cent are given for the transitions.

The transitions of 1092 and 909 keV suggest a level at 1170 keV decaying to the 79 and 260 keV states in agreement with the fact that both γ-rays are observed in coincidence with the 79, but only the 915 is coincident with the 181.

Evidence for the presence of weaker transitions is available from the spectrum of γ-rays coincident with the 181 keV γ (see fig. 5 and table 3). The coincident transitions are centred around 1300 keV and account for approximately 0.7 % of all β-decays. The weak line at 1290 keV in the pair spectrum may correspond to this transition and suggests the existence of a level at 1550 keV. With the sensitivity of the methods used in the present investigation other transitions of similar intensity cannot be excluded.

A decay scheme constructed from this information is given in fig. 7. The γ-ray intensities quoted are those obtained from the singles spectra. The intensities of the β-groups can be found from the γ-intensities and from the β-γ coincidence data given in table 4.

The data available allow the following number of cross-checks to be made:

a) The intensities of γ-rays feeding the 79 keV level can be computed from the intensity of the 79 and the measured coincidence efficiencies. One finds (singles values are given in parentheses): 181 keV 3.2 % (2.8 %), 1092 keV 9.6 % (7.4 %), 1390 7.7 % (6.6 %) and 1528 keV 6.7 % (5.6 %). The systematic deviation of 10 % to 20 % is not outside our experimental errors.

b) Analogously the intensities of the γ-rays feeding the 260 keV state can be estimated from coincidence data: 909 keV 1.26 % (1.45 %), 1210 keV 0.14 %, 1290 keV 0 28 % (0.7 %) and 1350 keV 0.14 %.

c) The intensity of the β-branch feeding the 260 keV state can be obtained from the fraction of 181-decays unaccounted for by coincident γ. This fraction (35 %) corresponds to 1.0 % of all transitions. From the β-γ coincidence experiment a value of 1.2 % was deduced.

d) Furthermore the division of the major β-groups found from the Fermi-analysis must be consistent with the values inferred from γ-ray and coincidence data. The results are (see figs. 4 and 7) 58 % (65 %), 19 % (9.2 %), 9 % (14.5 %) and 14 % (10.5 %). In view of the possible sources of error in this Fermi-analysis the results must be considered in satisfactory agreement.

Considering the arguments leading to the Tm^{172} decay scheme given in fig. 7 and the various checks made possible by the quantitative coincidence experiments it can safely be concluded that the decay scheme represents the main features of the Tm^{172} decay.

5. Discussion

The levels at 79 and 260 keV obviously correspond to the first and second excited states of the ground state rotational band. For the 1170 keV level spin 3 seems a likely assignment since the level decays to the 79 keV 2+ state and the 260 keV 4+ state. Spin 2 appears to be excluded since no cross-over to the ground state is observed. It is natural to assume that this state is identical to the state observed by Wilson and Pool [5]) in the decay of Lu^{172}, where an Yb^{172} level at 1172 keV was observed and assigned $K = 3$, $I = 3$ and even parity on the basis of the position of the level as the ground state of a band decaying primarily through the rotational states to the presumed 3+ state. The branching ratio measured by Wilson and Pool for the decay of this state (5.5) is within the experimental errors identical to the ratio 5.1 obtained in the present investigation. The interpretation of the 1170 keV state as a γ-vibrational state ($K = 2$) would seem plausible from the ratio of the reduced transition probabilities (0.47 assuming pure E2, theoretical without rotation-vibration corrections 0.40). Tm^{172} has, however, been shown to have $I = 2$ and in case the 1170 keV level is assigned as the 3+ state of the γ-vibrational band it would be hard to explain why the corresponding 2+ state has not been observed.

The β-decay to the ground state rotational band is of special interest since the 0+, 2+ and 4+ states are populated. The log ft values are respectively 8.9, 8.7 and 10.0. This is consistent only with the assignment of spin 2 and odd parity for Tm^{172} and the assignment unique first forbidden for the β-transitions.

The relative β-decay transition probabilities for the decay to the members of the ground state rotational band can be expressed as a ratio of geometrical factors [15]). This provides a further test of the interpretation given above. The experimentally obtained reduced transition probabilities for the decay to the 0, 2 and 4 states are $(0.44 \pm 0.12) : 1 : (0.053 \pm 0.007)$ (the reduced transition probabilities have been taken as $(f_1 t)^{-1}$, where $f_1 t$ is the reduced half life for a first forbidden unique transition)†. The corresponding theoretical ratios for $K_1 = 2$, $I_1 = 2$, $L = 2$ and $K_f = 0$, $I_f = 0{,}2$ and 4 are 0.70 : 1 : 0.05. The discrepancy between the experimental and theoretical results can hardly be considered outside the experimental errors.

The ground state for Tm^{172} is a combination of an odd neutron and an odd proton state, where the orbitals are expected to be those known from the neighbouring odd mass nuclei [16]). Empirical coupling rules for predicting the resulting ground state spin have been given by Gallagher and Moszkowski [17]). The odd proton in Tm^{172} is presumably characterized by the Nilsson state [16]) $\frac{1}{2}+[411]$ (ground state in Tm^{169} and Tm^{171}). The 103rd neutron is most likely to be $\frac{5}{2}-[512]$ (ground state [16]) in Er^{171}, Yb^{173} snd Hf^{175}). One then obtains a predicted ground state spin of 2 and odd parity for Tm^{172}. This is well in agreement with the experimental evidence.

It is known that selection rules based upon the asymptotic quantum numbers play an important role for the β and γ transition probabilities [18]). These selection rules demand for a first forbidden β-transition with α type shape $\Delta K = 2$, $\Delta N = 1$, $\Delta n_z = 0$ and $\Delta \Lambda = 1$. The β-decay of Tm^{172} to the ground state of Yb^{172} corresponds to the conversion of a $\frac{5}{2}-[512]$ neutron into a $\frac{1}{2}+[411]$ proton. It is seen that the change in asymptotic quantum numbers is that demanded for a unique first forbidden transition.

The same single particle transformation has previously been observed in the β-decay of Er^{171} where a β-branch to the $\frac{1}{2}+$ and $\frac{3}{2}+$ states of the Tm^{171} ground state rotational band has been observed. The log ft in this decay is 8.6 or greater. This agrees with the values obtained in the present investigation.

The authors are indebted to Dr. K. O Nielsen of the DR2 reactor, who provided the high neutron flux so essential for this research, and to Mr. K. Heydorn for arranging the numerous irradiations. We wish to thank Mr. O. B. Nielsen of the Institute for Theoretical Physics, Copenhagen for loan of the six-gap spectrometer. Most of the electronics used in this investigation was

† See *Note added in proof* at the end of this paper

designed and built in the Risø Electronics Department, and was put at our disposal by the department head, Mr. G. K. Frølich Hansen, to whom our best thanks are due.

Note added in proof: The recent publication by Orth and Dropesky [19]) presents results on the decay schemes for Er^{172} and Tm^{172} that are on the whole well in agreement with our data. The β-branching ratios, however, differ widely from those given above, whereas we agree as to order of magnitude with Helmer and Burson [3]). The corresponding results are: $(2.25 \pm 0.85) : 1 : (0.27 \pm 0.14)$ [ref. [19])], and $(0.56 \pm 0.37) : 1 : (0.041 \pm 0.035)$ [ref. [3])].

References

1) R. L. Folger, P. C. Stevenson and G. T. Seaborg, UCRL-1195 rev (1951)
2) D. R. Nethaway, M. C. Michel and W. E. Nervik, Phys. Rev. **103** (1956) 147
3) R. G. Helmer and S. B. Burson, Bull. Am. Phys. Soc. **6** (1961) 72, ANL-6270 (1961)
4) J. W. Mihelich, B. Harmatz and T. H. Handley, Phys. Rev. **108** (1957) 989
5) R. G. Wilson and M. L. Pool, Phys. Rev. **118** (1960) 1067
6) S. G. Thompson, B. G. Harvey, G. R. Choppin and G. T. Seaborg, J. Am. Chem. Soc. **76** (1954) 6229
7) G. R. Choppin and R. I. Silva, J. Inorg. Nucl. Chem. **3** (1956) 153
8) S. Bjørnholm, O. B. Nielsen and R. K. Sheline, Nature **178** (1956) 1110
9) L. G. Mann, W. E. Meyerhof and H. I. West, Jr., Phys. Rev. **92** (1953) 1481
10) D. E. Alburger and B. J. Toppel, Phys. Rev. **100** (1955) 1357
11) R. L. Heath, IDO-16408 (1957)
12) D. G. Gardner and W. W. Meinke, Int. J. Applied Radiation and Isotopes **3** (1958) 232
13) O. B. Nielsen and O. Kofoed-Hansen, Mat. Fys. Medd. Dan. Vid. Selsk. **29**, No. 6 (1955)
14) R. L. Graham, J. L. Wolfson and R. E. Bell, Can. J. Phys. **30** (1952) 459
15) G. Alaga, K. Alder, A. Bohr and B. R. Mottelson, Mat. Fys. Medd. Dan. Vid. Selsk. **29**, No. 9 (1955)
16) B. R. Mottelson and S. G. Nilsson, Mat. Fys. Skr. Dan. Vid. Selsk. **1**, No. 8 (1959)
17) C. J. Gallagher and S. A. Moszkowski, Phys. Rev. **111** (1958) 1282
18) G. Alaga, Nuclear Physics **4** (1957) 625
19) C. J. Orth and B. J. Dropesky, Phys. Rev. **122** (1961) 1295

NORTH-HOLLAND BOOKS

Just out

Elements of Hamiltonian Mechanics

by D. TER HAAR

University Reader in Theoretical Physics
and Fellow of Magdalen College, Oxford

CONTENTS:

1. Newtonian mechanics
2. The Lagrangian equations of motion
3. Small vibrations
4. Dynamics of rigid bodies
5. The canonical equations of motion
6. Hamilton-Jacobi theory
7. Perturbation theory
8. Continuous systems

Bibliography - Problems

This book is based upon a course of lectures given to final year undergraduates and first year graduate students at Oxford University. The emphasis and the selection of subject matter differs in a number of points from those in existing modern text-books. The main differences are in the way constraints are introduced by freezing in of degrees of freedom, and in the discussion of classical perturbation theory.

6 x 9'' 196 pp. Gld. 20.— (40s.)

NORTH-HOLLAND PUBLISHING COMPANY
P. O. BOX 103 - AMSTERDAM

Distributor for U.S.A.: Interscience Publishers, Inc. — New York

NORTH-HOLLAND BOOKS

QUANTUM MECHANICS

Just out

VOL. I

by ALBERT MESSIAH (Centre d'Etudes Nucléaires de Saclay)

translated from the French by G. M. Temmer (Florida State University, Tallahassee)

6×9" 520 pp. Gld. 50.- (100s.)

CONTENTS VOL. I. *The formalism and its interpretation.* Origins of the Quantum Theory. Matter waves and the Schrödinger equation. One dimensional quantum systems. Statistical interpretation of the wave-corpuscle duality and uncertainty relations. The development of the formalism of Wave Mechanics and its interpretation. Classical approximation and WKB method The general formalism of Quantum Theory: A) Mathematical framework. B) Description of physical phenomena. — *Simple systems.* Solution of the Schrödinger equation by separation of variables. Central force field. Scattering problems. Central force field and the method of phase shifts. Coulomb interaction. Harmonic oscillator. — *Appendices:* «δ function» and distributions. Special functions and related formulae.

". . . . the reviewer would like to recommend the book to students taking a beginner's course in quantum mechanics, to teachers for broadening the scope of such courses, and also to research workers in understanding the principles and methods of quantum mechanics and for acquiring the necessary knowledge for an understanding of the advanced parts of the field."

(PHYSICS TODAY on the original French Edition)

VOLUME II in preparation

Ask your bookseller or

NORTH-HOLLAND PUBLISHING COMPANY

P.O. BOX 103—AMSTERDAM

Distributor for U.S.A.: Interscience Publishers, Inc. — New York